FOURIER TRANSFORM INFRARED SPECTROSCOPIC CHARACTERISATION OF BIOMOLECULES

MICHAEL JACKSON

Department of Protein and Molecular Biology,
Royal Free Hospital School of Medicine,
Rowland Hill St.,
London

Submitted in fulfilment of the requirements for the degree of Doctor of Philosophy for the University of London, 1990

ABSTRACT

Fourier transform infrared (FTIR) spectroscopy has been applied to the characterisation of structural changes in a range in biological molecules.

The polymorphic phase behaviour of non-hydroxy fatty acid galactocerebrosides was shown to be the result of extensive rearrangements of the headgroup hydrogen bonding network. Formation of a metastable cerebroside form upon rapid cooling was shown to be due to dehydration of the lipid. Polymorphism was abolished by cholesterol and DPPC at levels normally found in myelin.

The temperature dependence of the secondary structure of a range of proteins was investigated. It was demonstrated that several predominantly α-helical proteins partialy unfolded at 70-80^{o}C forming intermolecular β-sheet structures. This behaviour was demonstrated for globular, fibrous and membrane proteins. Addition of Ca^{++} to α-helical Ca^{++}-binding proteins prevented unfolding of the helices.

Calmodulin, parvalbumin and troponin C were shown to exhibit FTIR spectra in H_2O characteristic of helical/disordered proteins. Deuteration resulted in significant shifts of the amide absorption to wavelengths consistent with disorganised structures, in contrast to CD spectroscopic studies which suggested a helical structure. Disruption of protein-solvent interactions with glycerol increased the frequency of the amide I band for parvalbumin. It was suggested that the unusual frequency of the amide I band in $^{2}H_2O$ is related to the high degree of protein-solvent interaction in these proteins conferred by their open structures.

Examination of the FTIR spectra of the Ca^{++}-ATPase of sarcoplasmic reticulum under conditions known to stabilise the protein in a variety of conformational substates indicated no significant changes in secondary structure during the catalytic cycle. This result was confirmed by curve fitting analysis of the FTIR data. A number of flaws became apparent in this analysis, the most important being the assumption that all secondary structures have equal molar absorptivities. Studies on polylysine showed this not to be so.

ACKNOWLEDGEMENTS

There are many people without whose kindness, friendship and generosity this work would never have been completed.

I would like to thank the Wellcome Trust for financial support during the course of this work.

I would particularly like to thank Christine Hall, Trevor Boyd and Laks Sinha for sharing their expertise and Dr. David Lee and Dr. David Johnston for introductions to FTIR spectroscopy and calorimetry.

I would like to thank Dr. Peter Bayley, Dr. Stephen Martin (National Institute for Medical Research, London) Prof. Juan-Camillo Gomez-Fernandez and Dr. Jose Villalain (University of Murcia, Spain) for their collaboration in the work presented in Chapter 5 and Chapter 6.

Special thanks go to Dr. Gerald Davies, Dr. Parvez Haris and Dorian Kennedy of this department for their collaboration and many useful discussions on most aspects of this work.

Finally, I would like to express admiration and gratitude to my supervisor, Prof. Dennis Chapman, for his continued support, encouragement and much needed spelling lessons.

ABBREVIATIONS USED

ATP	ADENOSINE TRIPHOSPHATE
BSA	BOVINE SERUM ALBUMIN
Cam	CALMODULIN
CD	CIRCULAR DICHROISM
DMPC	DIMYRISTOYL PHOSPHATIDYLCHOLINE
DPPC	DIPALMITOYL PHOSPHATIDYLCHOLINE
DPPE	DIPALMITOYL PHOSPAHATIDYLETHANOLAMINE
DSC	DIFFERENTIAL SCANNING CALORIMETRY
DSPC	DISTEROYL PHOSPHATIDYLCHOLINE
EGTA	ETHYLENE GLYCOL TETRA-ACETIC ACID
EMR	ELECTROMAGNETIC RADIATION
ESR	ELECTRON SPIN RESONANCE
ER	ENDOPLASMIC RETICULUM
FTIR	FOURIER TRANSFORM INFRARED
IR	INFRARED
NMR	NUCLEAR MAGNETIC RESONANCE
PAGE	POLYACRYLAMIDE GEL ELECTROPHORESIS
PC	PHOSPHATIDYLCHOLINE
PE	PHOSPHATIDYLETHANOLAMINE
PI	PHOSPHATIDYLINOSOITOL
PS	PHOSPHATIDYLSERINE
SNR	SIGNAL-TO-NOISE RATIO
SR	SARCOPLASMIC RETICULUM
T_m	TEMPERATURE OF THE MAIN PHASE TRANSITION IN PHOSPHOLIPIDS

TnC	TROPONIN C
TNP-ATP	TRINITROPHENYL-ADENOSINE TRIPHOSPHATE
UV	ULTRA-VIOLET

TABLE OF CONTENTS

INDEX TO FIGURES

INDEX TO TABLES

CHAPTER 1

BIOPHYSICAL MEASUREMENT TECHNIQUES

1.1 INTRODUCTION

A number of biophysical techniques are available for the structural analysis of biological membranes, lipids and proteins. Of these, X-ray diffraction, circular dichroism (CD), Raman, infrared, nuclear magnetic resonance (NMR) and fluorescence spectroscopy are the most popular. As results obtained from many of these techniques will be mentioned in this work it would seem appropriate to give a brief outline of each technique at this point. Special attention will be given to the technique of Fourier transform infrared spectroscopy, as results obtained using this technique will form the basis of this work.

Many biophysical measurement techniques have their basis in the interaction of electromagnetic radiation (EMR) with the material under investigation. The nature of the interaction is determined by the energy of the photons, that is, the wavelength of the EMR. The electromagnetic spectrum is illustrated schematically in Fig. 1.1 together with the absorption/emission processes involving EMR from each region of the spectrum.

Figure 1.1: The electromagnetic spectrum and interaction of EMR with matter.

DEPARTMENT OF PROTEIN AND MOLECULAR BIOLOGY

Have been asked by Mike Jackson to pass this on to you.

With Compliments

Christine Hall

Royal Free Hospital School of Medicine (University of London)
Rowland Hill Street London NW3 2PF Telephone 01-794 0500

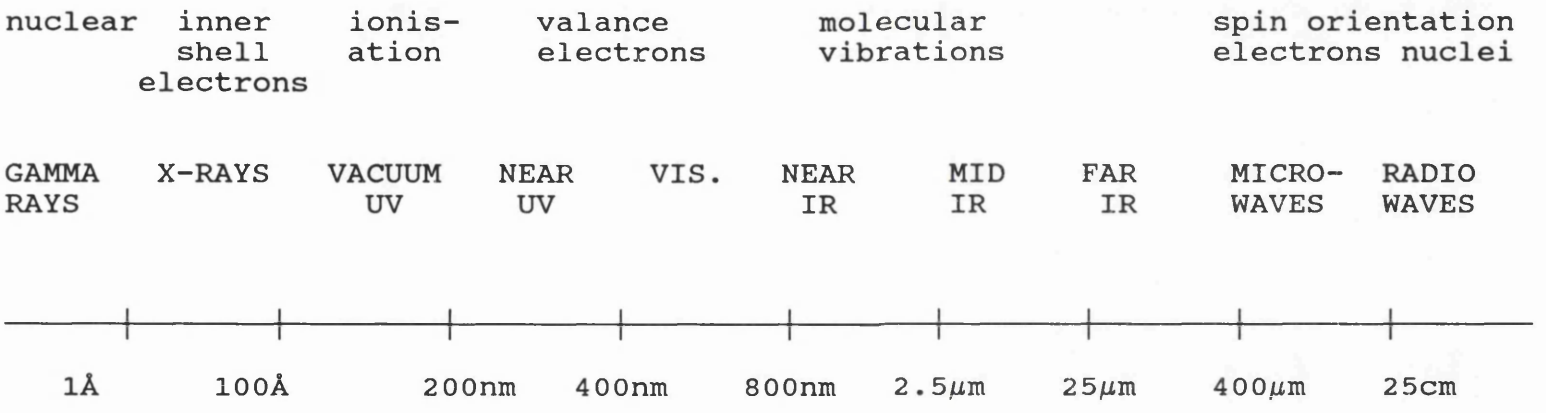

1.2. X-Ray Diffraction

If the material to be analysed is available in crystalline form, X-ray diffraction is the technique of choice for structural characterisation. Every atom in a crystal scatters an incident X-ray beam in all directions. As these atoms are arranged in a regular, repetitive manner, constructive and destructive interference occurs. From the Bragg equation:

$$m = 2d\sin\theta \qquad 1.1$$

m = order of diffraction,
= wavelength of the incident X-ray beam
d = spacing between atomic planes in the crystal lattice
θ = angle of diffraction of the X-ray beam

we can see that when atoms lie exactly on a crystal plane, maximum constructive interference will occur as the waves are in phase. Similarly, maximum destructive interference occurs when atoms are located exactly midway between planes. Atoms at intermediate positions result in either constructive or destructive interference dependent upon position, although this effect is submaximal.

The extent to which an atom scatters the X-ray beam is dependent upon the number of electrons it possesses. We can see therefore that the position of a diffracted X-ray beam

depends upon the wavelength of the incident radiation and the size and shape of the unit cell, while the intensity of the scattered X-rays is also dependent upon the type of atoms present and their position within the unit cell. By considering the intensity and position of the diffracted radiation it is therefore possible to deduce the nature and position of the atoms within the unit cell.

X-ray diffraction does of course require the production of relatively large, good quality crystals, which for many proteins is not possible . This is particularly so for membrane proteins, where the bipolar nature of the environment (partly located within the hydrophobic lipid matrix and partly extending into the cytoplasm/extracellular fluids) has rendered crystallisation impossible in all but a few cases (Deisenhofer, 1985; Allen et al 1987). Where crystallisation has been achieved, this has often necessitated the use of non-physiological conditions to produced the crystals, such as high concentrations of ammonium sulphate, organic solvents or enzymatic digestion to produce crystallisable fragments. The relevance of the final conformation of proteins treated in this manner to the native state is questionable. Indeed, many spectroscopists are of the opinion that crystal structures, even without proteolysis etc. may not completely reflect the native state of the protein.

However, a wide range of proteins have now been

crystallised and their crystal structures described in some detail. An advantage to the X-ray diffraction method is that quantitative estimates of the various secondary structures can readily be obtained. Again, care must be taken in evaluating this data, as it is not always a straight forward procedure to determine, for example where an α-helix ends and a strand of β-sheet begins. Thus, conflicting results can be obtained using various analytical methods (Dev, 1987).

1.3. NUCLEAR MAGNETIC RESONANCE SPECTROSCOPY

Measurement of the absorption of electromagnetic radiation by spinning atomic nuclei forms the basis of NMR spectroscopy. All nuclei carry a net positive charge. Many nuclei also posses angular momentum, i.e. they spin. Such spinning nuclei will have a magnetic moment and when placed in a magnetic field of strength H_o the magnetic moment precesses, inclined to H_o at a constant angle θ. For many nuclei relevant to biological studies (e.g. ^{1}H, ^{13}C, ^{31}P) only two orientations (or **spin states**) are possible. Transition between the two states can be induced by electromagnetic radiation whose energy is equal to the difference in energy between the two states. For a given type of nucleus, the magnetic moment is constant and all nuclei of this type will be excited by EMR of the same frequency. However, all nuclei are shielded to a greater or lesser extent by their electronic environment and a spectrum

of absorption peaks occurs, each nucleus having a characteristic position dependent upon its environment.

The major source of information relating to protein structure is the nuclear Overhauser effect (NOE). The NOE arises from dipolar cross-relaxation between protons and is decreased as the distance between protons is increased, becoming to weak to measure at 5Å. It is therefore possible to calculate the distance between protons (if this is less than 5Å). Together with the ability to estimate dihedral angles, this allows secondary structure determinations to be made for small proteins using NMR spectroscopy.

Nuclei in the higher energy state may relax to the lower energy state by loss of energy to their neighbours. The rate of relaxation may be determined by NMR spectroscopy and provides valuable information relating to the mobility of the segment of the molecule containing the nuclei being studied.

1.4. CIRCULAR DICHROISM SPECTROSCOPY

Natural light consists of a large number of electromagnetic waves propagated in all directions from a source. It is possible to produce radiation propagated in only one plane; this is plane polarised light. Circularly polarised light consists of electromagnetic radiation in which the electrical component (and so the magnetic component) spirals around the direction of propagation in either a clockwise (dextrorotatory, or **d**) direction or an

anti-clockwise (levorotatory or **l**) direction. Plane polarised light can be thought of as consisting of two circularly polarised rays, one **d** and one **l**, of equal amplitude.

If plane polarised light is passed through an optically active medium it is possible for one of the circularly polarised components to be slowed down. The result will be that the plane of the plane polarised light is rotated slightly, the angle of rotation being half the phase difference between the two components.

Within an absorption band, the molar absorptivity for **l** and **d** components differs, resulting in the circularly polarised light becoming elliptically polarised. This is termed circular dichroism. The circular dichroism spectra of proteins are sensitive to the polypeptide backbone conformation, particularly the secondary structure. In fact, the CD spectrum of a protein of known conformation is generally close to that expected from an average of α-helical, β-sheet and disordered spectra weighted according to their occurrence within the protein.

CD spectroscopy has been used for many years for the structural analysis of proteins, and has some advantages over X-ray diffraction and NMR spectroscopy. Thus, CD spectra can be recorded from proteins in solution, and size is not a limiting factor. An attractive feature of CD spectroscopy is that, like X-ray diffraction and NMR

spectroscopy, quantitative information is readily obtained from spectra. This is a consequence of protein spectra being a weighted average of α-helical, β-sheet and random absorptions. Direct comparison of spectra of proteins of unknown structure with reference spectra allows quantitation of the secondary structure.

LIght scattering can severely limit the applications of CD spectroscopy to the analysis of membrane suspensions, and the discrimination between β-sheet and turns is not distinct.

1.5. FLUORESCENCE SPECTROSCOPY

Absorption of electromagnetic radiation by molecules can promote electrons from the ground state to vibrational energy levels in an excited electronic state. The electrons may then decay to the lowest vibrational energy level within the excited state by redistribution of energy to other vibrational modes. Relaxation from the lowest vibrational energy state in the excited electronic state to any vibrational energy level within the ground electronic state results in fluorescence, that is emission of EMR of energy equal to the energy difference between the excited electronic state and the vibrational energy level of the ground electronic state.

Fluorescence can be expected in molecules possessing delocalised π-electrons (e.g. aromatic compounds and those containing multiple conjugated double bonds). Fluorescence

is enhanced by factors which decrease the probability of competing processes such as intersystem crossing and collisional heat degradation. Such factors include molecular rigidity and substituents which delocalise the π-electrons ($-NH_2$, $-F$, $-N(CH_3)_2$). Solvents which exhibit strong interactions with the fluorescing molecule decrease or abolish fluorescence by prolonging the lifetime of collisional encounters.

Perhaps the most useful application of fluorescence spectroscopy is the determination of the distance between groups on molecules, where one group is a fluorescent energy donor and the other an acceptor. If the absorption and emission spectra of the donor and receiver overlap, fluorescent light emitted by the donor will be absorbed by the acceptor species. The efficiency of this process varies with the sixth power of the distance between the groups. The distance between two fluorescent groups can therefore be calculated.

It is readily apparent that fluorescence spectroscopy has great potential in the structural analysis of lipids and proteins, as it can provide important information concerning molecular rigidity , solvent exposure and distances between sites on molecules. Furthermore, as fluorescing molecules absorb and emit EMR at different wavelengths, emission is measured against an effectively zero background, allowing extremely high sensitivity. However, a prerequisite of the

technique is the presence of a fluorescing group within the system being studied. In many cases fluorescent probes must be introduced into the system which may distort the structure.

1.6. RAMAN SPECTROSCOPY

When monochromatic radiation is scattered by a molecule,a small proportion of the scattered radiation has a different frequency to the incident radiation, a phenomenon known as the Raman effect.

The Raman effect arises when a beam of radiation passes through a sample which contains molecules which are able to undergo a change in molecular polarisability as they vibrate. When a photon is absorbed by a vibrating bond which shows this change in the polarisability of the bond, three things may happen. Firstly, the photon may be absorbed and promote the molecule to what is termed a " virtual excited state". The molecule then returns to its ground state rapidly (10^{-12} s) with the emission of a photon of the same energy and frequency as the incident radiation. This is termed Rayleigh scattering. Secondly, the molecule may absorb the photon, be raised to a virtual excited state and return to an excited vibrational state rather than the ground state. This results in the emission of a photon of lower energy and frequency than the incident radiation and produces what is termed a Stokes line. Finally, the molecule may absorb the photon from an excited vibrational state and

decay to the ground state. The emitted photon has a greater energy and frequency than the incident radiation. This produces an anti-Stokes line. As most molecules will be in the ground rather than an excited state, the stokes line is more intense than the anti-stokes line.

The frequency of a Raman absorption will be determined by the nature of the bond, solvent and intermolecular interactions. Raman spectroscopy can therefore be used to study protein secondary structure and the structure of lipid bilayers.

Raman spectroscopy has many problems associated with its use. The major flaw with respect to the analysis of proteins is the poor signal to noise ratio generally obtained. This is partly a consequence of the number of molecules in a solution which will exhibit Raman scattering, which under normal circumstances is very low. This problem can be overcome by co-adding scans. However, it is not unusual to record spectra for a period of 12 hours and still have an inadequate signal to noise ratio. Secondly, background fluorescence may swamp the Raman signal and provide little if any useful information.

1.7. DIFFERENTIAL SCANNING CALORIMETRY

Differential scanning calorimetry is not, in contrast to the other techniques described here, a spectroscopic technique. Rather DSC has its basis in the measurement of the absorption and emission of heat by a sample relative to

a standard. Basically, differential scanning calorimeters consist of two compartments, a sample compartment and a reference compartment. Into the sample compartment, the material under investigation is placed in a sealed pan of a suitable material (often aluminium or stainless steel). The reference compartment contains an empty pan, or sometimes a water filled pan if hydrated systems are being investigated. The sample compartment is then heated (or cooled) at a known rate and the energy required to keep the heat/energy flow into the reference compartment identical to that into the sample compartment calculated (hence the differential of the title).

Thermal transitions in the material being investigated result in the need for either the input or removal of excess energy from the reference pan to maintain the equilibrium condition. Thus, a record of the heat/energy flow of the reference compartment gives information relating to the phase behaviour of the material. The commonest uses of DSC in biology are the study of phase behaviour of natural and artificial membranes and thermal transitions (denaturation) in proteins.

1.8.FOURIER TRANSFORM INFRARED SPECTROSCOPY

1.8.1. INTRODUCTION

Infrared spectroscopy has been used for structural characterisation for many years by organic chemists. However its applications to biological materials is a more recent

development. The earliest infrared studies of biological materials were hampered by the necessity of making spectroscopic measurements in aqueous media to gain meaningful results. Clearly structural information gained from materials in organic solvents or the dry state have little, if any, relevance to the native state of the material. The strong absorption of water in the mid-infrared region of the spectrum (Fig. 1.2) necessitated the use of high concentrations and low pathlengths. These problems could partly be overcome by the use of deuterium oxide (^2H_2O) as a solvent, which has less absorption in the regions generally of interest to biologists (see Fig 1.2).

Many early studies of proteins and polypeptides were undertaken in ^2H_2O buffers (Susi et al 1967), and these experiments allowed empirical correlations between infrared spectra and structure to be drawn. A major advance in the field came with the development of microprocessor controlled spectrometers, allowing the development of digital subtraction routines (Koenig and Tabb, 1980). The next major advances came with the development of the Fourier transform method of infrared spectroscopy and so-called resolution enhancement techniques (Kauppinen et al 1981; Tooke, 1988), both of which are discussed in more detail below. These developments produced a technique which could be applied to the study of biological molecules in their native environments at relatively low concentrations, in a short

Figure 1.2: The infrared spectrum of H_2O (solid line) and ^2H_2O (broken line)

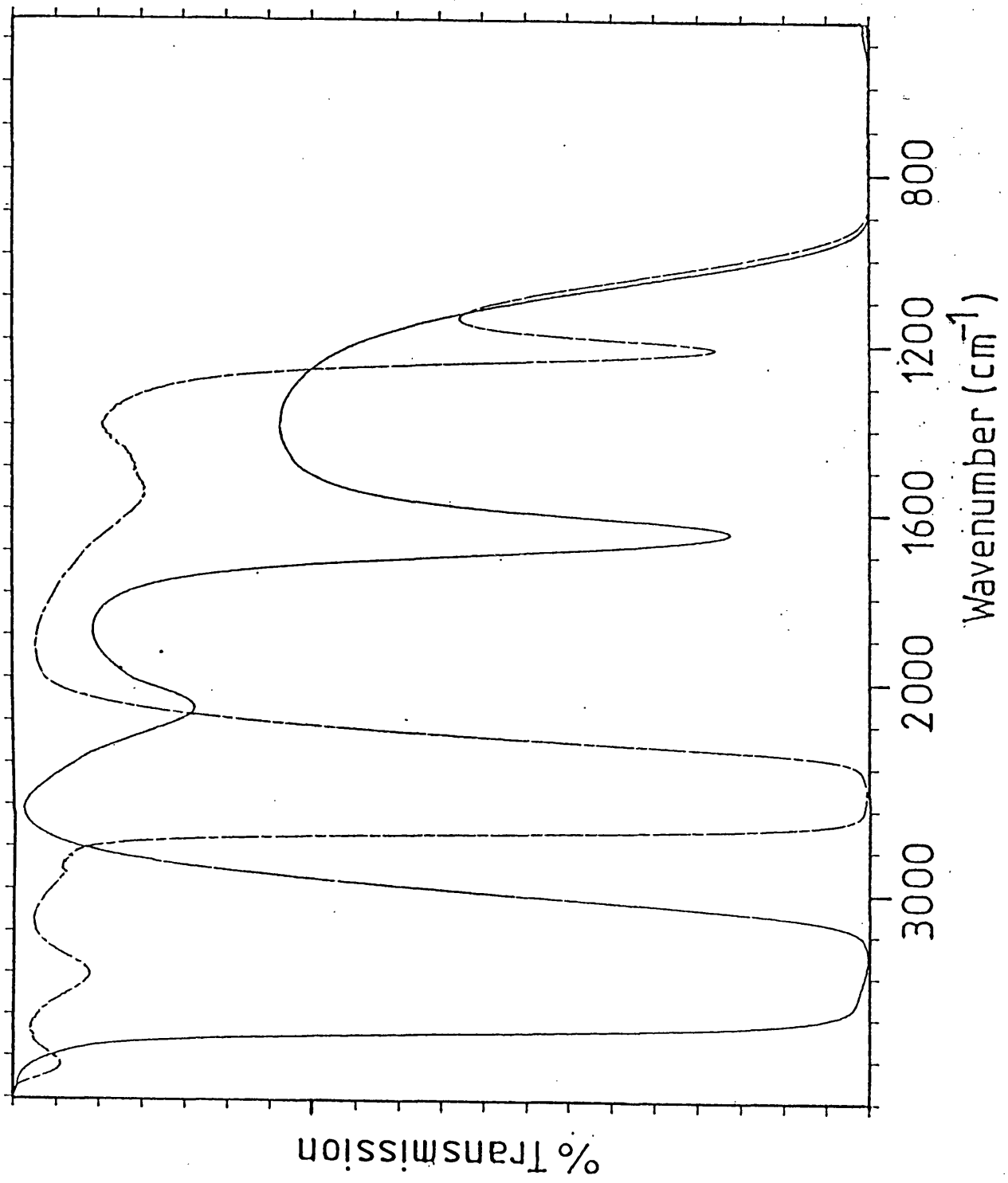
% Transmission
3000
2000
1600
1200
800
Wavenumber (cm⁻¹)

space of time with an excellent signal-to-noise ratio.

1.8.2. THEORY OF ABSORPTION OF INFRARED RADIATION

The position of a non-linear molecule in space can be described by three Cartesian coordinates for each atom, requiring 3N coordinates to describe the whole molecule. Of these, 3N-6 coordinates, or degrees of freedom, describe molecular vibrations of the molecule. Thus, a non-linear molecule has 3N-6 fundamental or normal modes of vibration. Whether a normal mode of vibration is infrared active or not depends upon the nature of the molecule. For a vibration to be infrared active it must result in a change in the dipole moment of the molecule. Consider the HCl molecule, a simple linear species. This molecule has a permanent dipole, with the H atom relatively positive charged and the Cl atom relatively negative. When the molecule undergoes a stretching vibration, the centre of the dipole moment is changed and this vibration in infrared active. On the other hand, the symmetric stretching vibration of CO_2 is not infrared active. The centre of the dipole moment is not altered by the symmetric stretch. However, the asymmetric stretching vibration of CO_2 does result in a change in the dipole moment and thus is infrared active.

1.8.2. INSTRUMENTATION

FTIR spectroscopy relies upon the processes of interferometry and Fourier transformation for its speed and sensitivity. Most interferometers used in commercial FTIR

spectrometers today are based upon the Michelson interferometer (Michelson, 1891). The simplest form of the Michelson interferometer is shown in figure 1.3. It consists of two mutually perpendicular mirrors, one of which moves in a direction perpendicular to its plane. Between the two mirrors is a beamsplitter, usually made from KBr. The beamsplitter reflects part of the incident radiation (a) to the fixed mirror and transmits the remaining radiation (b) to the moving mirror. An ideal beamsplitter reflects and transmits 50% of IR radiation. After reflection from the two mirrors, the radiation (the reflected radiation is labelled a' and b' in figure 1.3) recombines at the beamsplitter (a'+b'), from where it is reflected to the detector. The intensity of the recombined beam, and so the detector output, varies with the position of the moving mirror. The simplest way to describe the variation of the detector output is to examine what happens when the incident radiation is monochromatic.

When the two mirrors are equidistant from the beamsplitter, the IR beams recombine and constructive interference results. The detector output is at a maximum at this point as a and b are in phase. As a pathlength difference is introduced between the two beams by moving mirror the two beams become out of phase and destructive interference occurs when the beams are recombined at the

FIGURE 1.3: Schematic representation of the Michelson interferometer (see text for further details)

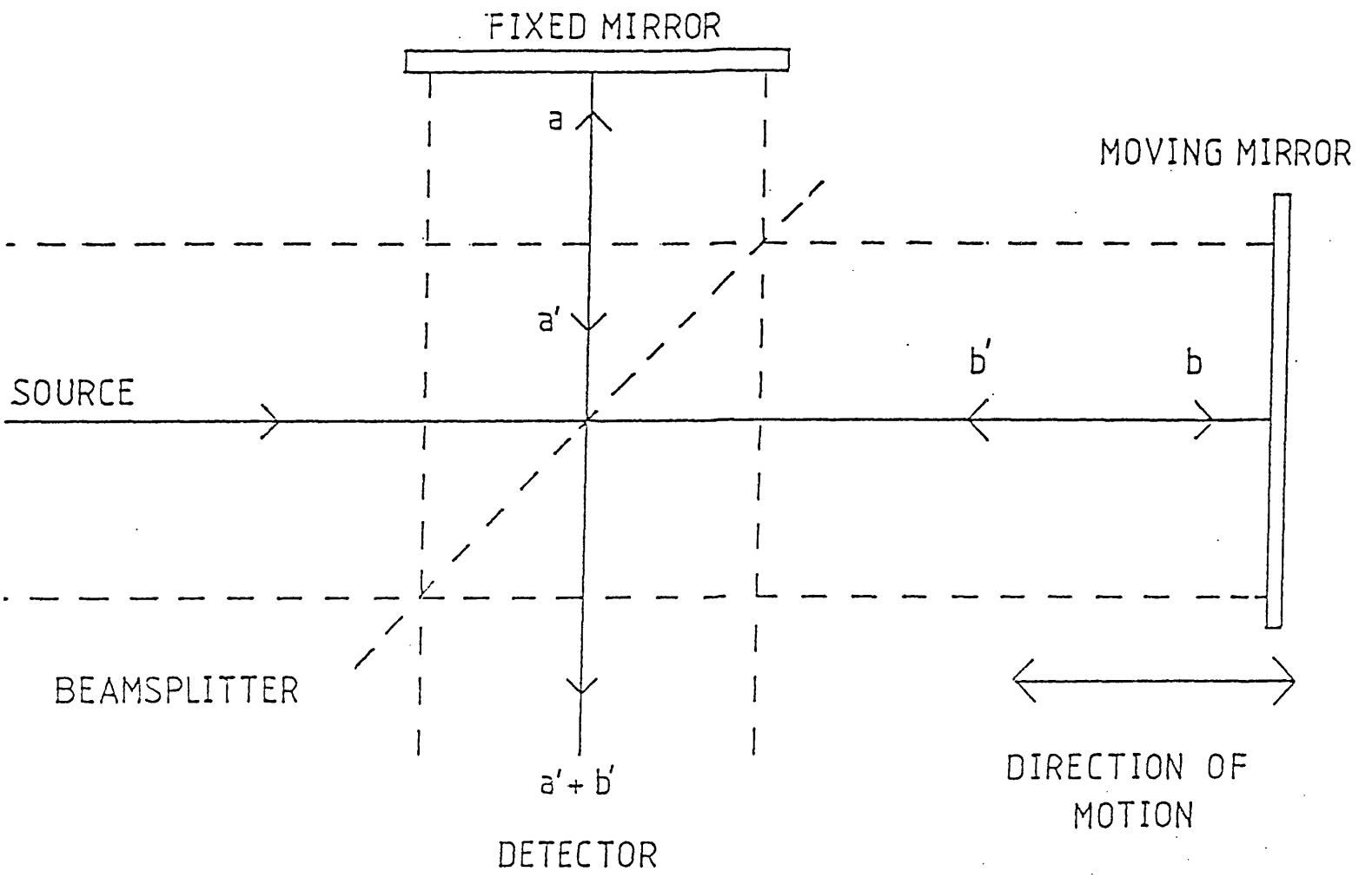
FIXED MIRROR
a
MOVING MIRROR
a'
b'
b
SOURCE
BEAMSPLITTER
a' + b'
DETECTOR
DIRECTION OF
MOTION

beamsplitter. This destructive interference will be at a maximum when the pathlength difference is equal to $\lambda/2$. Further mirror movement results in an increase in the detector output until at a pathlength difference equal to the beams are once again in phase and the output is at a maximum once again. Thus, the detector output varies sinusoidaly with constant velocity motion of mirror.

The intensity of the ir beam measured by the detector is given the symbol $I'(\delta)$, and the detector output for a mirror retardation d is given by equation 1.1:

$$I'(\delta) = 0.5\ I(v)\ \{\ 1 + \text{Cos}\ 2\ \pi\ v\ \delta\ \} \qquad 1.1$$

δ = mirror retardation

v = frequency in wavenumbers (cm^{-1})

I(v) = source intensity

Thus $I'(\delta)$ comprises a constant component (0.5I(v)) and a modulated component (0.5I(v) Cos 2 π v δ), which varies with the position of the mirror. This latter component is generally referred to as the interferogram, $I(\delta)$. A number of factors can affect the magnitude of the detector output, such as variable frequency responses of amplifiers and variation in the response characteristics of the detector with v. Thus the expression describing the interferogram must be modified to account for this variation, and yields equation 1.2:

$$I(\delta) = B(v) \text{ Cos } 2 \pi v \delta \qquad 1.2$$

where B(v) is the source intensity at wavenumber v.

The frequency of the radiation can be calculated by the process of Fourier transformation. $I(\delta)$ is the cosine Fourier transform of B(v), and the cosine Fourier transform of $I(\delta)$ yields the frequency of the radiation. Alternatively, examination of the interferogram for a monochromatic source allows direct measurement of the frequency of the incident radiation, which is equal to the frequency of the sinusoidal output of the detector.

For a polychromatic source, the interferogram is the sum of the individual interferograms for each frequency of ir radiation present. Thus, it is not possible to directly measure the frequencies present, Fourier transformation of the interferogram is required to generate the spectrum.

1.8.4. Advantages of FTIR spectroscopy

Fourier transform infrared spectroscopy produces spectra of much higher signal-to-noise ratio in a greatly reduced data collection interval when compared to dispersive infrared spectroscopy for spectra at the same resolution recorded over the same spectral range. The enhanced signal to noise ratio is a direct consequence of the use of an interferometer as compared to a diffraction grating or prism. In dispersive IR spectrometers, IR radiation is effectively monochromated by the grating or prism before

transmission to the sample, and each wavelength in the spectral region of interest must be sampled individually. This is both time consuming and drastically reduces the optical throughput of the system. With the use of an interferometer no monochromation is required and all wavelengths are scanned simultaneously, thus reducing the time required for data acquisition and increasing the optical throughput.

1.8.5. DERIVATIVE AND DECONVOLUTION ROUTINES

The amide bands, and many other spectroscopically useful bands, are often broad, composite bands from which little information can be obtained. A number of mathematical routines have recently been developed to increase the separation of the overlapping bands in such absorptions (Kauppinen et al 1981; Took 1984). Of these, derivative and deconvolution routines are the most frequently used.

1.8.5.1. FOURIER DECONVOLUTION

Any spectral band can be expressed as the convolution of a line shape with a line position. This can be achieved in either the wavenumber or Fourier domains. For the case of a spectrum with infinite resolution, in the wavenumber domain convolution of a Lorentzian band shape with a Dirac delta function at wavenumber v produces a Lorentzian band at v. The operation in the Fourier domain which results in convolution in the wavenumber domain is a vector product.

The vector product of the Fourier transform of the Lorentzian (a decaying exponential, whose rate of decay is determined by the width of the band) and the transform of a Dirac delta function (a cosine, whose period is determined by the position, v, of the function), yields a decaying cosine. The inverse Fourier transform of this produces a Lorentzian at v.

Deconvolution is the opposite of this procedure, that is a spectral line or a composite band has a line shape deconvolved from it to yield positional data. This is acheived by the multiplication of the transform of the line or band with an increasing exponential. If the rate of increase of the exponential matches the rate of decrease of the decaying cosine, the result is a cosine whose period is determined by the frequency of the line. At infinite resolution the transform of this cosine would be a Dirac delta function. However, as the resolution is not infinite, the cosine is truncated. The transform of this truncated cosine is a sinc function, which is wider than the Dirac delta function but narrower than the original band. Thus, deconvolution results in band narrowing.

It is important to realise that the sinc function has associated with it quite strong side lobes which will cause distortions in deconvolved spectra. These can be removed by calculating the vector product of the truncated cosine and an apodisation function such as a $sinc^2$ or Besel function.

This will be a gradually decaying cosine, the inverse transform of which will be a triangular function rather than a sinc funtion. This triangular function will be broader than the sinc function but still narrower than the original band and have minimal side lobes.

The $sinc^2$, Besel and other such functions also have the desirable characteristic of going to zero. This property is of value in eliminating noise. When the transformed spectrum multiplied by the icreasing exponential, a side effect is that the noise present in every spectrum will increase exponentialy, until at some point the noise will be greater than the amplitude of the cosine. If the apodisation function is chosen so as to go to zero at this point, this noise will be eliminated . Thus, apodisation functions are also smoothing functions. Preliminary smoothing can be achieved by the correct choice of instrumental resolution. If the resolution is chosen such that as much of the measured interferogram as possible is non-zero, then noise contributions will be kept to a minimum.

The complete deconvolution procedure can be summarised as follows. The Fourier transform of the spectrum, which will be the sum of a number of exponentialy decreasing cosines, is multiplied by a range of exponentials, of progresively greater rates of increase (corresponding to progressively broader bands). When the rate of increase corresponds to a band width greater than the broadest band

in the spectrum, side lobes begin to appear (see Fig. 1.4). The width should then be slightly reduced. The apodisation/smoothing function is then adjusted to a point where the level of noise is acceptable. This will correspond to the point where the function decays to zero and the exponentialy increasing noise is greater than the amplitude of the truncated cosine. The end result will be significantly narrower bands with minimal contributions from side lobes and noise.

1.8.5.2. SECOND AND FOURTH DERIVATIVE SPECTRA

Derivative spectra can be calculated either in the Fourier domain or directly from the infrared spectrum. The relationship between and infrared spectrum E(v) and its Fourier transform I(t) can be written as:

$$E(v) = \int_{-\infty}^{\infty} I(t)\exp(i2\pi t)\delta t \qquad 1.3$$

The second derivative can therefore be expressed as:

$$\delta_2 E(v) / \delta v^2 = \int_{-\infty}^{\infty} (i2\pi t)^2 I(x)\exp(i2\pi vt)\delta t \qquad 1.4$$

Thus, the complex transform of the second derivative of the spectrum is the vector product of the complex transform of the spectrum and a weighting function, $-4\pi^2t^2$. For fourth derivative spectra, this function is $16\pi^4t^4$.

An alternative calculation of derivative spectra

FIGURE 1.4: Deconvolution of chymotrypsinogen; a) difference spectrum b) under deconvolution (F=1.5 W=16) c) over deconvolution (F=2.5 W=16) d) correct deconvolution (F=2.0 W=16)

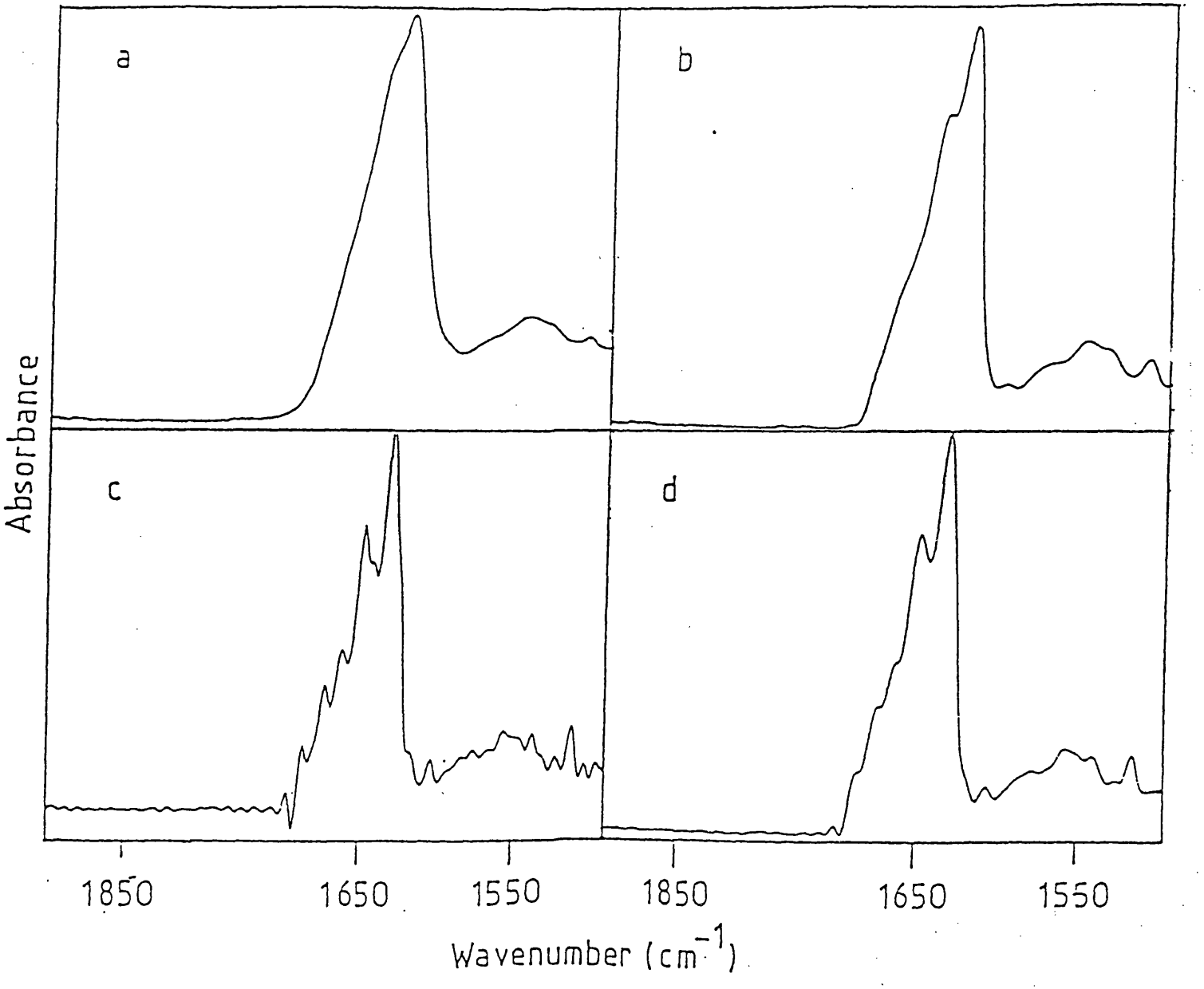
a
b
c
d
Absorbance
1850
1650
1550
1850
1650
1550
Wavenumber (cm^{-1})

requires measurement of the rate of change of the gradient of the infrared absorption bands directly from the spectrum. In this case, the "resolution" and noise limits of the spectrum are determined by selecting the separation of data points between which the gradient is to be calculated. The rate at which the gradient changes is the second derivative of the spectrum. To calculate the fourth derivative, this procedure is applied to the second derivative spectrum. In this way, any inflections on the absorption bands due to overlapping components are enhanced.

This latter procedure is the one commonly used in this work.

1.8.5.3. LIMITATIONS OF DECONVOLUTION AND DERIVATION

Both deconvolution and derivative techniques enhance the noise present in a spectrum, although with FTIR instrumentation noise is generally not a problem. Deconvolution and derivative techniques are equally sensitive to noise. Both methods also distort the original line shape, width and height.

Derivative spectra suffer from the presence of side lobes near major bands in the spectrum, which may mask overlapping bands. It is common practise to apply both techniques to spectra, and only assign peaks seen in both deconvoluted and derivative spectra.

1.8.6. BIOLOGICALLY IMPORTANT VIBRATIONS

A number of infrared active vibrations are of use to biological spectroscopists. These vibrations will be discussed briefly below.

1.8.6.1LIPID VIBRATIONS

Many groups within lipid molecules are infrared active. The CH_2 groups of the acyl chains show a series of stretching, wagging, bending and rocking vibrations (Fig. 1.5). Strong absorptions arising from the ester C=O groups of phospholipids are also seen (see Table 1-I).

Lipid molecules are known to exists in several polymorphic forms and infrared spectroscopic analysis of the above bands has been extensively used to characterise these forms (Asher and Levin 1977, Cameron et al 1980, Cortijo and Chapman 1981). The main endothermic phase transition in phospholipids has been shown to be accompanied by abrupt changes in the frequency and bandwidths of the CH_2 stretching vibrations of the acyl chains. As the transition temperature is approached the bandwidth and frequency both increase. As found in DSC experiments, the structural changes associated with the phase transition in phospholipid bilayers occurs over a narrow temperature range, typically $1\text{-}2^{o}C$.

The C=O groups in the intermediate region of lipid molecules are also sensitive to phase. Deconvolution and

FIGURE 1.5: Normal vibrations of the CH_2 groups of lipid acyl chains.

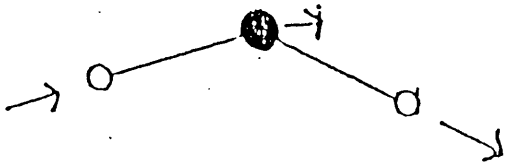

Asymmetric stretching

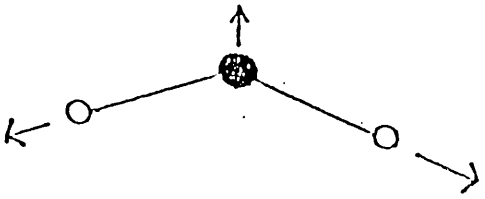

Symmetric stretching

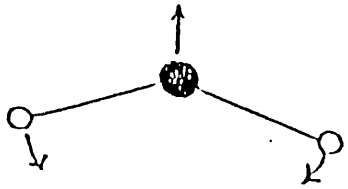

Scissoring

Wagging

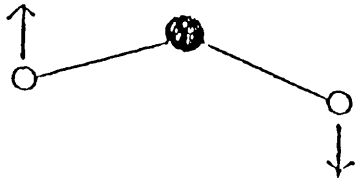

Twisting

Rocking

Table 1-I: Major infrared active vibrations of lipids.

BAND POSITION	ASSIGNMENT
	ACYL CHAINS
2956	CH_3 ASYMMETRIC STRETCH
2920	CH_2 ASYMMETRIC STRETCH
2870	CH_3 SYMMETRIC STRETCH
2850	CH_2 SYMMETRIC STRETCH
1470	CH_2 BENDING/SCISSORING
1380	CH_2 SYMMETRIC DEFORMATION
1380-1190	CH_2 WAGGING BAND PROGRESSION
1150-700	CH_2 ROCKING BAND PROGRESSION
	HEADGROUPS
3050	CH_3 ASYMMETRIC STRETCH OF $N(CH_3)_3$
1740-20	C=O STRETCH FORM ESTERS
1490	CH_3 ASYMMETRIC BEND OF $N(CH_3)_3$
1405	CH_3 SYMMETRIC BEND OF $N(CH_3)_3$
1250	O=P=O ASYMMETRIC STRETCH
1200-1000	C-O STRETCH
1170	C-O FROM ESTERS
1085	O=P=O SYMMETRIC STRETCH
1070	C-O FROM ESTERS
1040	C-N STRETCH
900-800	P-O STRETCH
800	C-N STRETCH

derivative routines demonstrate that the band arising from the C=O stretching vibration is actually a composite band. It has been suggested (Bush et al., 1980) that these absorptions could be assigned to the sn-1 (1743cm^{-1}) and sn-2 (1728cm^{-1}) C=O groups. However, recent ^{18}O substitution experiments (Blume et al., 1988) suggest that the composite band is due to absorptions arising from C=O groups hydrated to different extents, the lower frequency band being the more hydrated.

As the phase transition is approached, a decrease in the frequency of the composite C=O absorption can be demonstrated. Band narrowing techniques show this to be due to an increase in absorbance at 1728cm^{-1}, consistent with increased hydration of the headgroup at the phase transition.

It is apparent that infrared spectroscopy provides a powerful accompaniment to DSC for analysis of the phase behaviour of lipids, and this will form the basis of the work presented in Chapter 3 of this thesis.

1.8.6.2. PROTEIN VIBRATIONS

The most important infrared-active vibrations arising from proteins are the amide vibrations. In all, nine amide vibrations have been described and they are summarised in table 1-II . Each of these amide vibrations arises from the peptide bonds in the protein backbone. The most useful of

AMIDE VIBRATION	FREQUENCY	ASSIGNMENT
A	3300	N-H (s)
B	3100	N-H (s)
I	1680-1600	C=O (s) (80%) N-H (b) (10%) C-N (s) (10%)
II	1580-1480	N-H (b) (60%) C-N (s) (40%)
III	1300-1230	C-N (s) (30%) N-H (b) (30%) C=O (s) (10%) O=C-N (b) (10%)
IV	770-626	O=C-N (b) (40%) OTHER (60%)
V	800-640	N-H (b)
VI	605-540	C=O (b)
VII	200	C-N (t)

Table 1-II: Assignment of amide vibrations. b=bending s=stretching t=torsion

the amide vibrations for biological purposes are the amide I and II vibrations. The amide I vibration cannot be attributed to any one molecular vibration, but is a composite vibration (Miyazawa 1960) arising primarily from the C=O stretch (80%) with a weak coupling from the C-N stretch (10%) and N-H bend (10%). The amide II vibration on the other hand arises predominantly from the bending of the peptide N-H groups.

As the amide I vibration is predominantly due to C=O stretching vibrations, it is very sensitive to the degree and strength of hydrogen bonding involving C=O groups. As each discrete protein secondary structure is associated with a unique hydrogen bonding pattern, the position of the amide I vibrational absorption may be expected to vary with secondary structure. This has indeed been shown to be the case. As early as 1960 Elliot and Ambrose drew empirical correlations between the position of the amide I maximum and the secondary structures believed to be present in a protein. Since this pioneering study a large body of information has been presented correlating infrared amide I frequencies with polypeptide and protein structure. Significant contributions in this area have been made by Chapman and co-workers (Jackson et al., 1990a and references therein), Mantsch and co-workers (Surewitzc and Mantsch 1990 and references therein) and Susi and Byler (Susi and Byler 1986 and references therein).

From the FTIR spectroscopy studies carried out to date, a number of general points have emerged.

1) Helical membrane proteins in H_2O and ^2H_2O solution typically absorb at 1656-58cm^{-1}, while soluble proteins absorb at 1648-56cm^{-1}. This is presumably related to the hydrophobic membrane environment, which will decrease protein-water interactions in membrane proteins an increase the amide I maximum.

2) β-sheet secondary structures exhibit absorptions in the range 1628-40cm^{-1}, with a minor component at around 1680-90cm^{-1}.

3) Most membrane proteins studied to date have little β-sheet as deduced from FTIR spectra. The exception to this is matrix porin from **Rhodobacter capsulatus** which is almost completely β- sheet (Haris et al 1989).

4) Unordered polypeptide chains absorb in the same region of the spectrum as α-helices in H_2O, but this absorption is shifted to 1644cm^{-1} upon deuteration.

The amide II vibration is not as well studied as the amide I vibration, and the position of the amide II band can only be poorly correlated with protein structure. However, as the amide II vibration is predominantly a N-H bending vibration, it is highly sensitive to isotopic substitution. Thus, the amide II band can provide valuable information concerning solvent accessibility of the protein.

1.8.7. EXPERIMENTAL CONSIDERATIONS

1.8.7.1. Sampling techniques

Measurement of FTIR spectra is often a routine procedure and many methods of spectral measurement now exist. Only those used in the present work will be described here.

Aqueous samples are placed between a pair of infrared transparent windows, often made from CaF_2, separated by a tin or teflon spacer. The thickness of the spacer, and so the pathlength, is determined by the material being studied and the solvent used. Spectra of proteins dissolved or suspended in H_2O cannot be recorded at pathlengths greater than 12μm due to the strength of the H-O-H absorption in the region 1800-1400cm^{-1}, which masks the main protein absorption band. Dissolution in ^2H_2O allows the use of longer pathlengths (and so lower concentrations) as the ^2H-O-^2H absorption is found some 400cm^{-1} lower (see Fig. 1.2).

Solid samples can be analysed dispersed in an infrared transparent material such as KBr. In such techniques, the material to be analysed is ground with dry KBr to a final concentration of 1% w/v. The sample/KBr mixture is then placed between two stainless steel plates and placed in a press under a pressure of approximately 10 tonnes for 10 minutes. This produces a transparent disc which can be mounted in the spectrometer and analysed.

1.8.7.2. Water vapour absorptions

A major problem in recording infrared spectra of materials which absorb in the region 2000-1400cm^{-1} is the presence of intense absorptions from water vapour in this region of the spectrum (Fig. 1.6). This is particularly a problem if band narrowing techniques such as deconvolution or second derivative are to be used, as these techniques greatly enhance such sharp bands. The presence of water vapour can therefore lead to distortion of spectra. In this work, all spectra were recorded using a stream of dried, compressed air or nitrogen to purge the spectrometer.

FIGURE 1.6:Background spectrum recorded with no purge (solid line) and after 5 minutes of purging with nitrogen (broken line).

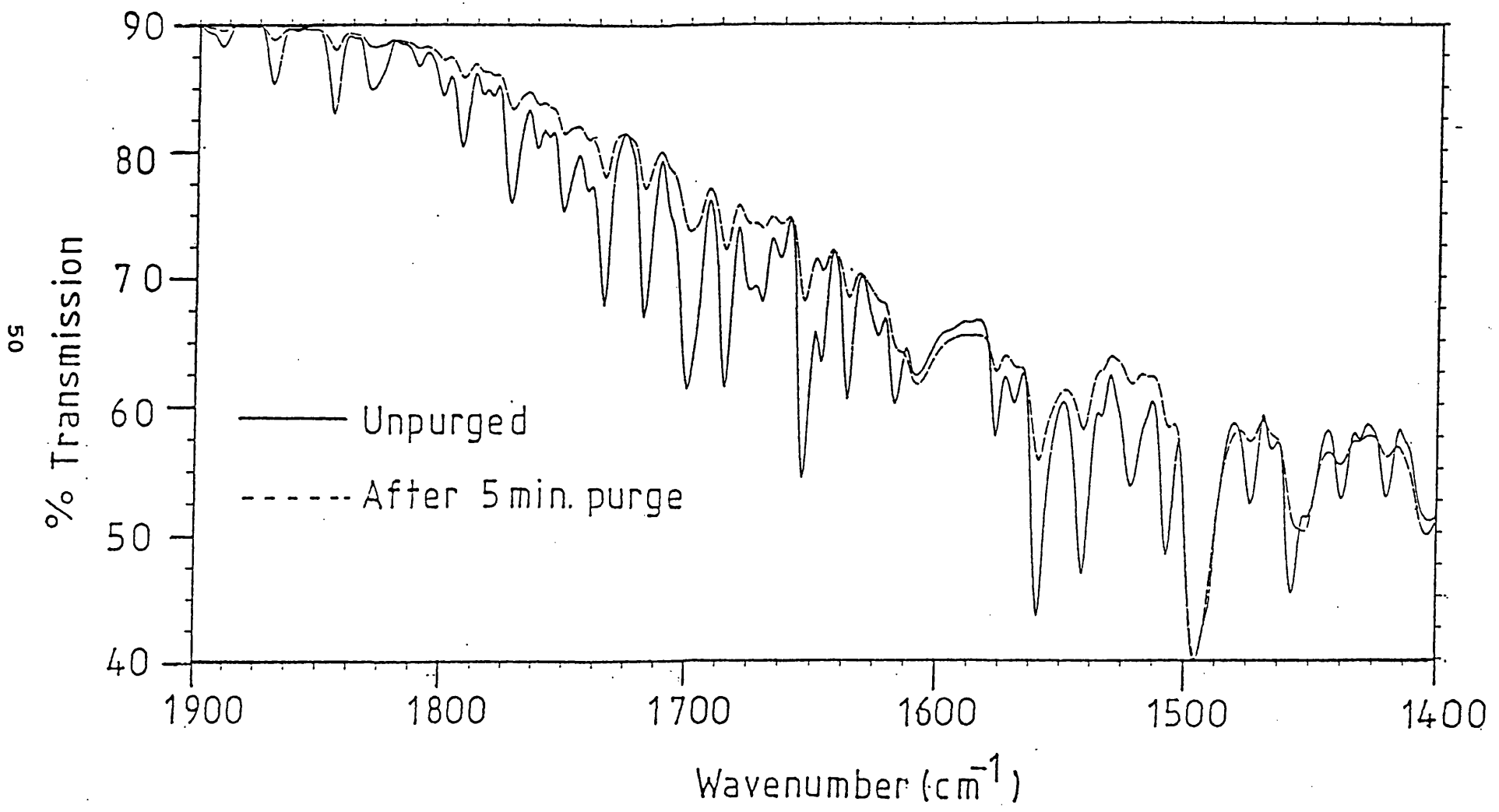
90
80
70
60
50
40
% Transmission
Unpurged
After 5 min. purge
1900
1800
1700
1600
1500
1400
Wavenumber (cm⁻¹)

1.9. SUMMARY

Many sophisticated measurement techniques are currently being applied to the structural characterisation of biological materials and their assemblies. Each of these techniques has its own advantages and disadvantages, and which technique is chosen for a particular series of measurements is determined in the light of this.

While X-ray crystallography still remains the technique of choice, it has associated problems. The major hurdle for analysis of proteins is the production of crystals, which is often not possible or requires severe, non-physiological conditions.

NMR spectroscopy is regarded by many as the best second choice. However, 2-D NMR cannot be performed on proteins of molecular weight greater than 15,000 due to line broadening effects.

Circular dichroism spectroscopy is not limited by the size of the molecule being studied. However, light scattering can severely limit the techniques application to membrane suspensions.

Fluorescence spectroscopy can be applied to molecules of any size and also to membranes. However, the information produced is limited, and requires the presence of a fluorescing chromophore, which may have to be artificially introduced into the system. Such manipulations may perturb the system under investigation.

Raman spectroscopy is not limited by size, light scattering, or a requirement for perturbing probes. However, it does have the drawback of generally producing spectra with a poor SNR. This precludes the use of resolution enhancement techniques without considerable data smoothing.

FTIR spectroscopy is not limited by size, light scattering or SNR. However, sample concentrations are considerably higher than for many other of the techniques discussed above, and aggregation phenomena must be born in mind when the technique is used. Furthermore, assignment of the important protein amide I bands is far from complete, and structural characterisation of proteins by this method still requires caution. However, for the systems investigated in this work, FTIR spectroscopy is by far the most generally applicable. It is the only technique discussed here which is readily applicable to the study of glycolipids, small Ca^{++}-binding proteins, large blood proteins and membrane proteins.

CHAPTER 2

PROPERTIES OF BIOLOGICAL MOLECULES

2.1 INTRODUCTION

Biophysical investigations of molecular structure and architecture are of fundamental importance in the study of the molecular basis of life. Enormous advances have been made in the last fifty years, including an understanding of many of the central metabolic processes in man (Krebs and Johnson 1937), elucidation of the structure and mechanism of replication of DNA (Watson and Crick 1953a,1953b), crystallisation and structural characterisation of a range of proteins (Kendrew 1957, Deisenhofer et al 1985), elucidation of the molecular basis of a number of diseases (Perutz and Lehman 1968) and an understanding of many of the physical and functional properties of biological membranes (Singer and Nicholson 1972).

Many of these advances would have been impossible without the extensive range of biophysical measurement techniques which have been developed. These techniques have given us unprecedented insight at the molecular level into a vast range of fundamental processes, and the ever increasing sophistication of instrumentation holds out the prospect of even greater advances in the future. In this chapter, the fundamental properties of a selection of biological molecules will be outlined, including the nature of lipids and proteins, lipid assemblies and biological membranes. This information will form the basis for the characterisation of the functional properties of a range of

lipids and proteins in subsequent chapters, using a range of biophysical measurement techniques.

2.2 PROTEINS

2.2.1 PROTEIN STRUCTURE

Proteins are heteropolymers derived predominantly from 20 commonly occurring amino acids. The sequence of amino acids in the polymeric chain is termed the primary structure of the protein. Unlike many chemical polymers, proteins are not simply extended chains, rather they are highly folded, globular structures. The manner in which the protein chain folds upon itself is termed the secondary structure of the protein. The secondary structure of proteins is dictated by the primary structure of the protein (Sanger, 1952; Schroeder, 1968), that is, it is the amino acid composition of the protein which determines how the chain will fold. Folding of the protein is therefore influenced by a number of parameters which affect the physio-chemical characteristics of amino acids, such as the nature of the solvent, temperature and pH (Anfinsen 1973).

A number of well characterised secondary structures are formed by the polypeptide chains within proteins. The first such secondary structure to be described (Pauling et al 1951) was the α-helix (α denoting that it was the first regular structure to be described), based upon experimentally observed bond angles and distances in amino acids and peptides. The α-helix is a tightly coiled rod-like structure stabilised by hydrogen bonds between N-H and C=O groups of the main chain. The C=O groups of each amino acid

are hydrogen bonded the N-H group of the amino acid four residues ahead in the primary sequence. Sequential residues are related by a rise of 1.5Å and a rotation of 100°. This gives 3.6 amino acids per turn of the helix and a pitch of 5.4Å. The sense of α-helices in proteins is always right-handed. Such a structure was first observed in myoglobin seven years after it was postulated on theoretical grounds (Kendrew et al., 1958).

The second periodic structure to be described (Pauling and Corey 1951) was the β-pleated sheet (β denoting that it was the second regular structure to be described). The polypeptide chain in this structure is almost fully extended, rather than coiled. Furthermore, the structure is stabilised by hydrogen bonds between N-H and C=O groups in different polypeptide strands, rather than within the same strand. Such sheets can be either parallel (adjacent strands running in the same direction) or anti-parallel (adjacent strands running in opposite directions).

Reversal of the direction of a polypeptide chain is achieved by including structures known as β-turns in the protein. Such turns are achieved by forming hydrogen bonds between C=O and N-H groups three amino acids apart.

Other, less common secondary structures have recently been described. These include variations on the α-helix such as 3_{10}- and α_{II}-helices, and the type II trans helix exhibited by poly-l-proline and collagen (Miller, 1982). The

STRUCTURE	N	H	H-BONDING
α-HELIX	3.60	1.495	5 → 1
α_{II}-HELIX	3.60	1.5	5 → 1
3_{10}-HELIX	2.99	2.01	4 → 1
3_1-HELIX	3.00	3.10	INTERMOL.

TABLE 1-I: Hydrogen bonding scheme, number of residues per rise (N) and rise (H) per residue for helical secondary structures. Modified from Krimm and Bandekar 1986.

3_{10}- and α_{II}- helical structures differ from the α-helix in the hydrogen bonding pattern, number of residues per turn and the degree of rise per residue (see table 2-I). The type II trans helix is a more unusual structure. This helix motif is adopted by polyproline. No hydrogen bonds stabilise this structure, due to the lack of hydrogen atoms on the nitrogen of the peptide bonds. Instead, steric repulsion between pyrrolidone rings provides the stabilising force. This structure is more open than the α-helix, having a rise of 3.12Å per residue and 3 residues per turn. The connective tissue protein collagen consists of three polypeptide chains in such a conformation, each strand containing numerous proline and hydroxyproline residues. Approximately every third residue in these chains is glycine. The intertwined strands are held together by hydrogen bonds between the N-H groups of glycines and C=O groups of amino acids in other chains.

Much attention has been focused on the occurrence of individual amino acids or small sequences of amino acids within specific secondary structures in attempts to correlate amino acid composition with structure. The weighted average occurrence of àmino acids in the more common protein secondary structures is listed in Table 2-II. As this table shows, very few amino acids show a preference for a particular secondary structure. Exceptions to this general rule are Pro and Gly which disrupt helices,

AMINO ACID	P_α	P_β	P_t
Ala	1.29	0.90	0.78
Arg	0.96	0.99	0.88
Asn	0.90	0.76	1.28
Asp	1.04	0.72	1.41
Cys	1.11	0.74	0.80
Gln	1.27	0.80	0.97
Glu	1.44	0.75	1.00
Gly	0.56	0.92	1.64
His	1.22	1.08	0.69
Ile	0.97	1.45	0.51
Leu	1.30	1.02	0.59
Lys	1.23	0.77	0.96
Met	1.47	0.97	0.39
Phe	1.07	1.32	0.58
Pro	0.52	0.64	1.91
Ser	0.82	0.95	1.33
Thr	0.82	1.21	1.03
Trp	0.99	1.14	0.75
Tyr	0.72	1.25	1.05
Val	0.91	1.49	0.47

TABLE 2-II: Weighted average occurrence of amino acids in α-helices (P_α), β-sheet (P_β) and turns (P_t) calculated from 32 proteins. A value of 1 indicates no preference (from Creighton, 1984). .paand Val, Met Ile and Leu which are

not prevalent in reverse turns. It seems that the actual sequence, not the composition of the chain, determines the way the chain folds.

2.2.2 CLASSIFICATION OF PROTEINS

Proteins can be divided into two broad categories, depending upon where they are located within an organism. Proteins found in the cytoplasm or body fluids are generally highly water soluble, often highly charged species. Such proteins are termed soluble proteins. The second major class of proteins are those associated with membranes. Such proteins are generally referred to as membrane proteins.

Water soluble proteins can be divided into two subclasses, globular and fibrous proteins. The vast majority of water soluble proteins are in fact globular in nature, being composed of a number of domains which interact with each other to give a specific tertiary structure which is often compact in nature. Examples of such proteins include haemoglobin and albumin. Fibrous proteins, on the other hand are as their name implies extended molecules, often having mechanical functions. Such proteins include collagen and spectrin. The distinction between these classes is somewhat arbitrary, as many fibrous proteins contain globular domains, for example fibrinogen.

Membrane proteins can also be subdivided into two subclasses, intrinsic and extrinsic membrane proteins. Intrinsic membrane proteins are highly hydrophobic in

nature,and are deeply embedded within the lipid matrix of the membrane and cannot be removed without the use of detergents. Such proteins include ion transporting ATPases, ion channels and metabolite transporting proteins. Extrinsic membrane proteins are loosely held at the membrane (either interior or exterior) surface, and can readily be removed in most cases by alterations in the pH or ionic strength of the surrounding medium. Extrinsic proteins are held at the surface by electrostatic interactions between charged amino acids and charged groups on lipids. Relatively little, if any, penetration of the bilayer occurs.

2.3 LIPIDS

Membrane lipids are amphipathic molecules (i.e. contain both polar and nonpolar segments) and as such are insoluble in water. They account for approximately 50% of a typical cell membrane, and a membrane area of 1um x 1um contains approximately 5×10^6 lipid molecules.

2.3.1 CLASSES OF LIPIDS

There are three major classes of lipid in biological membranes; phospholipids, glycolipids and sterols. Of these, phospholipids are the most abundant. Phospholipids are derived from either a glycerol or a sphingosine backbone. Phospholipids derived from glycerol are termed phosphoglycerides, and the only phospholipid found in biological membranes which is not a phosphoglyceride is sphingomyelin, a lipid based on sphingosine.

The fatty acid chains in phospholipids and glycolipids generally contain an even number of carbon atoms, between 14 and 24, with 16 and 18 carbon chains being the most common. The fatty acid chains may be either saturated or unsaturated, and the configuration of the double bond in unsaturated chains is almost always cis. In most phospholipids and glycolipids, one fatty acid chain is saturated and one unsaturated. In animal membranes, the acyl chains are never branched.

In a typical phosphoglyceride, the fatty acid chains are esterified to the C-1 and C-2 carbon atoms of glycerol. Phosphoric acid is esterified to C-3. The phosphate group is then esterified to the hydroxyl group of an alcohol to produce the commonly occurring phosphoglycerides. This alcohol may be choline (forming a phoshatidylcholine or PC), ethanolamine (forming a phosphatidylethanolamine or PE), inositol (forming a phosphatidylinositol or PI) or serine (forming a phosphatidylserine or PS). The structure of a range of phospholipids are shown in fig 2.1.

Sphingomyelin is the only phospholipid in biological membranes which is not based upon a glycerol backbone. Instead, the backbone is the amino alcohol sphingosine. The amino group of the sphingosine chain is linked to a fatty acid by an amide bond and the hydroxyl group of the sphingosine is esterified to phosphoric acid. Choline is esterified to the phosphoric acid.

FIGURE 2.1: Structure and nomenclature of phospholipids.

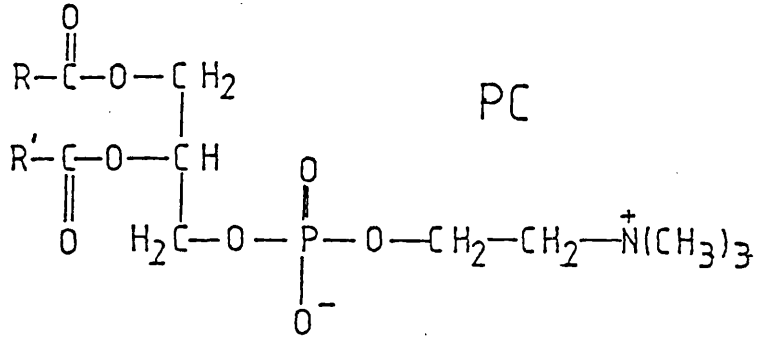

PC

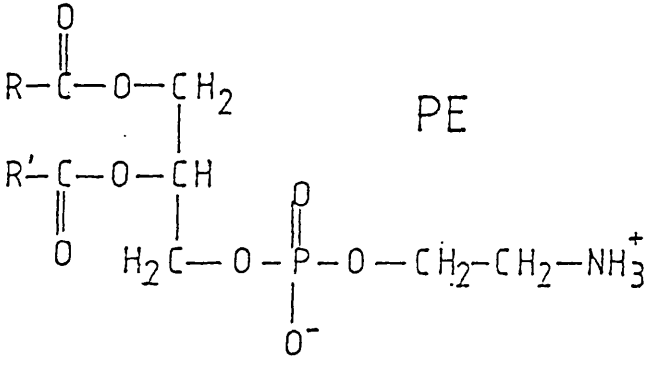

PE

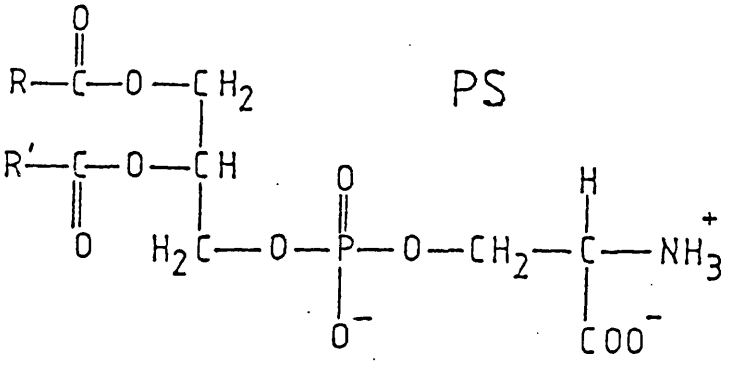

PS

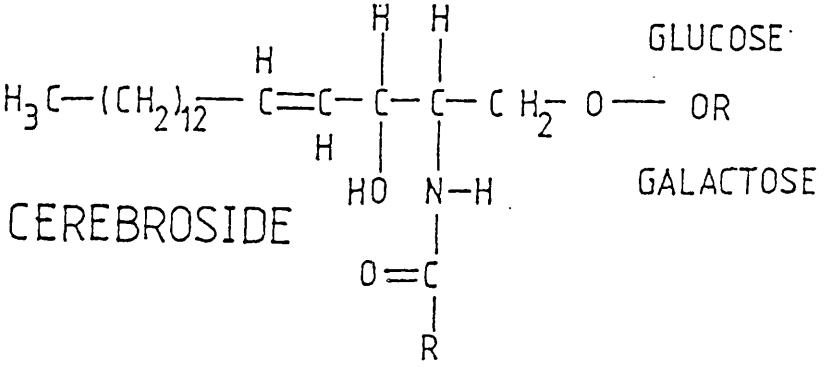

CEREBROSIDE

Glycolipids are also found in most biological membranes, although often in very small amounts. These lipids are related to sphingomyelin in that they contain a fatty acid linked via an amide bond to sphingosine. In glycolipids however the primary hydroxyl group is esterified not to phosphoryl choline but to one or more carbohydrate residues. The simplest glycolipids are cerebrosides, where the carbohydrate headgroup is either one glucose (glucocerebrosides) or one galactose (galactocerebrosides) residue. More complex glycolipids such as gangliosides may have up to seven carbohydrate residues.

Finally, sterols play an important part in biological membranes. The most abundant sterol in membranes is cholesterol, which is characteristically abundant in plasma membranes but present in only small amounts in the membranes of organelles.

Most cell membranes contain a vast range of chemically distinct lipids (150-200) within the frame work of the three subclasses discussed above, due to variation in the headgroups and fatty acid composition of the chains. In view of the enormous range of biological processes which occur in membrane of even the simplest of cells, this complexity is perhaps not surprising. More surprising is that many subcellular organelles have equally complex membranes. As these organelles have highly specialised functions to perform, it may be thought that the membrane itself would

have a more specialised/homogeneous composition. However, it should be born in mind that the physical and chemical characteristics of the numerous lipid species may have only subtle effects on the bilayer. It therefore makes sense from a purely economic point of view to incorporate any lipids available within the membrane, within limits.

2.3.2 ASSEMBLIES OF LIPIDS

When placed in an aqueous environment, amphipathic molecules such as lipids show a tendency to aggregate, with the hydrophobic regions of the molecules clustered together and the hydrophilic sections interacting with water. This can result in the formation of two distinct types of structure. Firstly, the molecules may aggregate to produce a micelle (see fig 2.2a) with the non-polar regions forming a hydrophobic core and the polar regions exposed to the water. Alternatively, a bilayer structure may be formed (fig. 2.2b) with the non polar regions of two layers of amphiphile being sandwiched between the polar regions. This second type of structure, which is the basis of all biological membranes, is formed by most phospholipids and glycolipids in aqueous environments. Thus, membrane formation is a self-assembly process.

The bilayer structure is stabilised by a range of non-covalent forces. Firstly there are Van der Vaal's interactions between adjacent hydrocarbon chains which

FIGURE 2.2: Structure of lipid assemblies in aqueous dispersion a) micelle, b) bilayer.

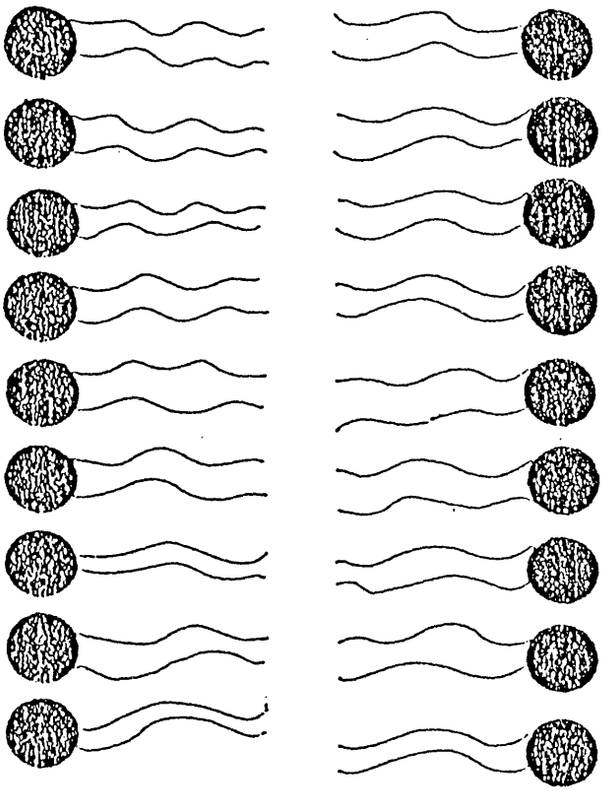

(b)

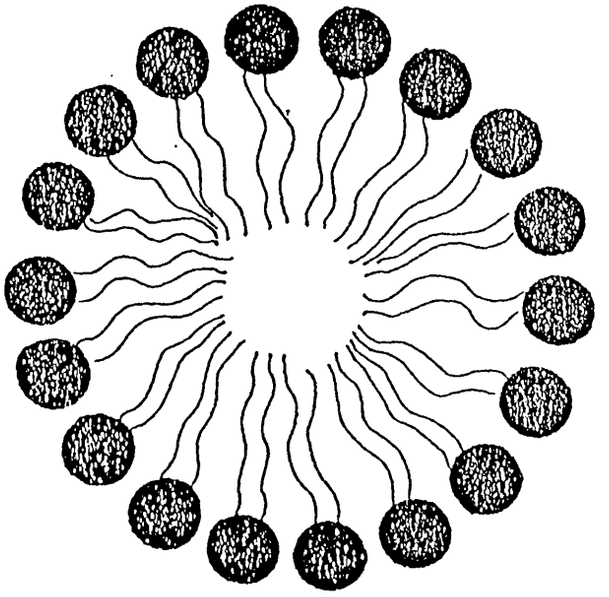

(a)

favours close packing of acyl chains. Secondly, electrostatic interactions occur between polar headgroups. Finally, inter-head group hydrogen bonding is important in further enhancing stability. These factors lead to three important consequences:

1) Lipid bilayers tend to be extensive (up to 10^7 Å).
2) Lipid bilayers tend to close in upon themselves, that is, there are no exposed hydrocarbon chains
3) Lipid bilayers are self-sealing

Lipid bilayers are not static structures. Rapid diffusion of molecules in the plane of the bilayer occurs at all temperatures above the phase transition of the component lipid. This rate of diffusion ($10^{-8}cm^2s^{-1}$) means that it is possible for a lipid molecule to diffuse the entire length of a bacterial cell in about 1 second. Transfer of lipid molecules from one side of a bilayer to the other is, on the other hand, a much slower process, occurring approximately once every two weeks.

2.3.3 PHASE TRANSITIONS AND MEMBRANE FLUIDITY

It has been known for many years that biological membranes are fluid, rather than static structures. Data supporting a fluid lipid matrix has been obtained from a range of techniques, including NMR (Chapman and Salsbury, 1966; Oldfield et al., 1972) and IR (Cameron et al., 1980; Cortijo and Chapman, 1981) spectroscopy and calorimetry (Chapman et al., 1969). Calorimetric thermograms indicate a

highly cooperative major phase transition in hydrated lipid bilayers and biomembranes (Chapman et al., 1969; Steim et al., 1969). Below this transition, little motion of the acyl chains of the lipid components is detected, suggesting a highly ordered gel-like state. Above the major transition a large degree of molecular motion is apparent from NMR and IR studies. The nature of this phase transition and the effect of membrane composition upon it have been the focus of intense research for decades.

It is now clear that at the temperature of the main phase transition, denoted by T_m, a number of important changes occur in lipid bilayers. Thus the acyl chains show an increase in the proportion of gauche conformers (Cameron et al., 1980; Snyder et al., 1982). As the bilayer is subject to close packing of the acyl chains, the introduction of one such distortion into the bilayer disrupts the chain packing allowing further distortions to be made. Thus the phase transition is a highly cooperative event, occurring over a very narrow temperature range (typically 1-2^{o}C). This rotational disorder is most marked at the ends of the acyl chains (Chapman and Salsbury, 1966).

The temperature of the phase transition and the enthalpy change associated with it are markedly dependent upon the headgroup, length of the acyl chains and degree of unsaturation (Chapman et al., 1967, see table 2-III). Long acyl chains increase the Van der Waals interactions between

LIPID	COMPOSITION	H (KCAL.MOL^{-1})	T_M(°C)
DMPC	14:0	6.26	23.7
DPPC	16:0	9.69	41.7
DPPE	16:0	8.0	63.0
DSPC	18:0	10.84	58.2
DOPC	18:1	7.6	-22.0

TABLE 2-III: Effect of headgroup, chain length and unsaturation upon transition temperatures (T_m) and enthalpy changes (H)

neighbouring lipid molecules and each CH_2 group adds 0.5kcal/mol to the enthalpy change of the transition. The introduction of a double bond into a chain disrupts the chain packing, causing a decrease in T_m and the enthalpy of the transition.

The fluidity of the bilayer can therefore be modulated by subtle variations in the fatty acid composition of the component lipids, a technique employed by many bacteria (Miller and Koshland , 1977) and protozoa (Dickens and Thompson, 1982) to maintain a fluid membrane. Furthermore, by having a complex mixture of lipids with a less ordered packing arrangement than a simple mixture (or a single lipid) the T_m of the bilayer is reduced.

Many molecules within biological membranes have profound effects upon membrane fluidity. As mentioned earlier, cholesterol plays a significant role in the control of membrane fluidity in animals. Addition of cholesterol to bilayers causes a marked decrease in T_m and the enthalpy change of the transition, and causes a decrease in the cooperativity of the transition. This is a result of the disruption of the close packing of the lipid molecules as cholesterol intercalates between them (Ladbrooke et al., 1968). This disruption allows an increase in the molecular motion of the acyl chains with a concomitant increase in the proportion of gauche conformers within the bilayer (Oldfield and Chapman 1972). On the other hand above the phase

transition temperature of the bilayer cholesterol sterically blocks rotational movements, and decrease the proportion of gauche conformers. Thus, cholesterol serves to maintain membrane fluidity within certain limits.

2.4 BIOLOGICAL MEMBRANES

It has long been recognised that the lipid bilayer is the basic unit of biological membranes. This was inferred when it was demonstrated that the area occupied by a total lipid extract from an erythrocyte was equal to twice the surface area of the cell (Gorter and Grendel, 1925). Thus, the lipid must form a bilayer arrangement. The behaviour of the lipid component of biomembranes in forming a bilayer could easily be accounted for by theoretical considerations. However, biological membranes are not composed solely of lipid, but contain significant amounts of protein. In fact in most biological membranes proteins account for 50-70% of the total mass of the membrane (with the exception of myelin which is approximately 80% lipid). It has proved much more difficult to devise a model for biological membranes including both lipid and protein components.

At first, it was suggested that the protein was loosely held at the surface of the bilayer by polar attractions (Danielli and Davson 1935). However,this model does not explain why some proteins are difficult to remove from membranes, to which they appear to be tightly bound. The model was therefore revised. To explain the strength with

which some proteins appeared to be adsorbed to the bilayer, it was suggested that these proteins were "unrolled", the energy normally required to stabilise the secondary and tertiary structures of the proteins would then be available to enhance absorption. Thus, biological membranes were considered to consist of a lipid bilayer, covered by a layer of "unrolled " protein, possibly covered with a layer of globular protein (Davson and Danielli, 1952). This view was supported by the trilaminar appearance of biological membranes in electron micrographs. These electron micrographs were thought to show a lipid bilayer sandwiched between two layers of protein. However, they could equally reflect the hydrophilic-hydrophobic-hydrophilic pattern of the lipid bilayer. In support of this latter interpretation, similar electron micrographs have been produced from artificial lipid bilayers containing no protein.

A number of serious flaws soon became apparent in this model. Firstly, the dimensions of such a membrane would be in excess of those observed for real membranes (70-90 Å). Secondly it is not clear how globular proteins could become unrolled when in contact with the bilayer surface. Thirdly, membrane proteins can be shown to have distinct secondary structure,i.e. they are not unfolded. Fourthly, freeze-fracture electron micrographs suggest the protrusion of many proteins into the hydrophobic core of the lipid bilayer. Finally, on the basis of such a model, it is difficult to

explain such phenomena as facilitated diffusion and active transport.

To explain the rapid rates of diffusion of certain water soluble solutes across membranes, it was suggested that the membrane must contain pores , and these pores must have some selectivity. Such pores must obviously be hydrophilic in nature. It was therefore necessary to explain how hydrophilic regions could be included in the hydrophobic membrane without destroying the membrane. At this time, it had been observed that haemoglobin and possibly other globular proteins could form a lamellar type structure, with hydrophobic and hydrophilic amino acid side chains on opposing sides of the lamellae. This led Danielli (1954) to propose that pores could be gaps in the bilayer lined by proteins in such a lamellar arrangement, with hydrophobic side chains interacting with the lipid acyl chains and hydrophylic chains protruding into a water filled channel. The layer of unrolled protein was replaced by "lamellar" protein inserted into the bilayer such that it interacted with both acyl chains and polar headgroups.

While this model does account for some of the transport characteristics of real membranes, it does not explain the selective permeability of the membrane, and there still remain morphological and energetic objections. A more reasonable postulate is that proteins associated with membranes can be divided into two distinct classes,

intrinsic and extrinsic membrane proteins. It is envisaged that extrinsic membrane proteins are loosely attached to the membrane surface by electrostatic attraction. These proteins are easily removed by pH or salt treatment. The second class of protein, intrinsic membrane proteins were suggested to be amphipathic, having sufficient hydrophobic residues to allow the protein, or at least some portion of it, to be incorporated into the bilayer. Thus, the current model of biological membranes is the so called "fluid mosaic" model postulated by Singer and Nicholson (1972) , in which a fluid lipid matrix supports a mosaic of loosley associated soluble proteins and deeply embedded insoluble proteins (fig. 2.3).

The Singer and Nicholson model of membrane structure is not without discrepancies. It is envisaged in this model that the lipid matrix is a "sea" in which the membrane proteins "float". However, in many membranes proteins exist as semi-crystalline arrays within the bilayer, with extensive protein-protein contacts, a feature not discussed in the Singer and Nicholson model. The lateral diffusion of many membrane protein is controlled by interaction with the cytoskeleton, a network of proteins underlying the cell membrane which are responsible for controlling the shape of cells and regulating the movement of proteins such as receptors within the membrane. Furthermore, bacterial cell membranes can be shown to have discrete patches of highly ordered lipid. Thus, while the basic postulates of the model

FIGURE 2.3: Schematic representation of the Singer and Nicholson "fluid mosaic" model of biomembrane structure. a=peripheral protein b= glycosylated membrane protein c)non-glycosylated membrane protein.

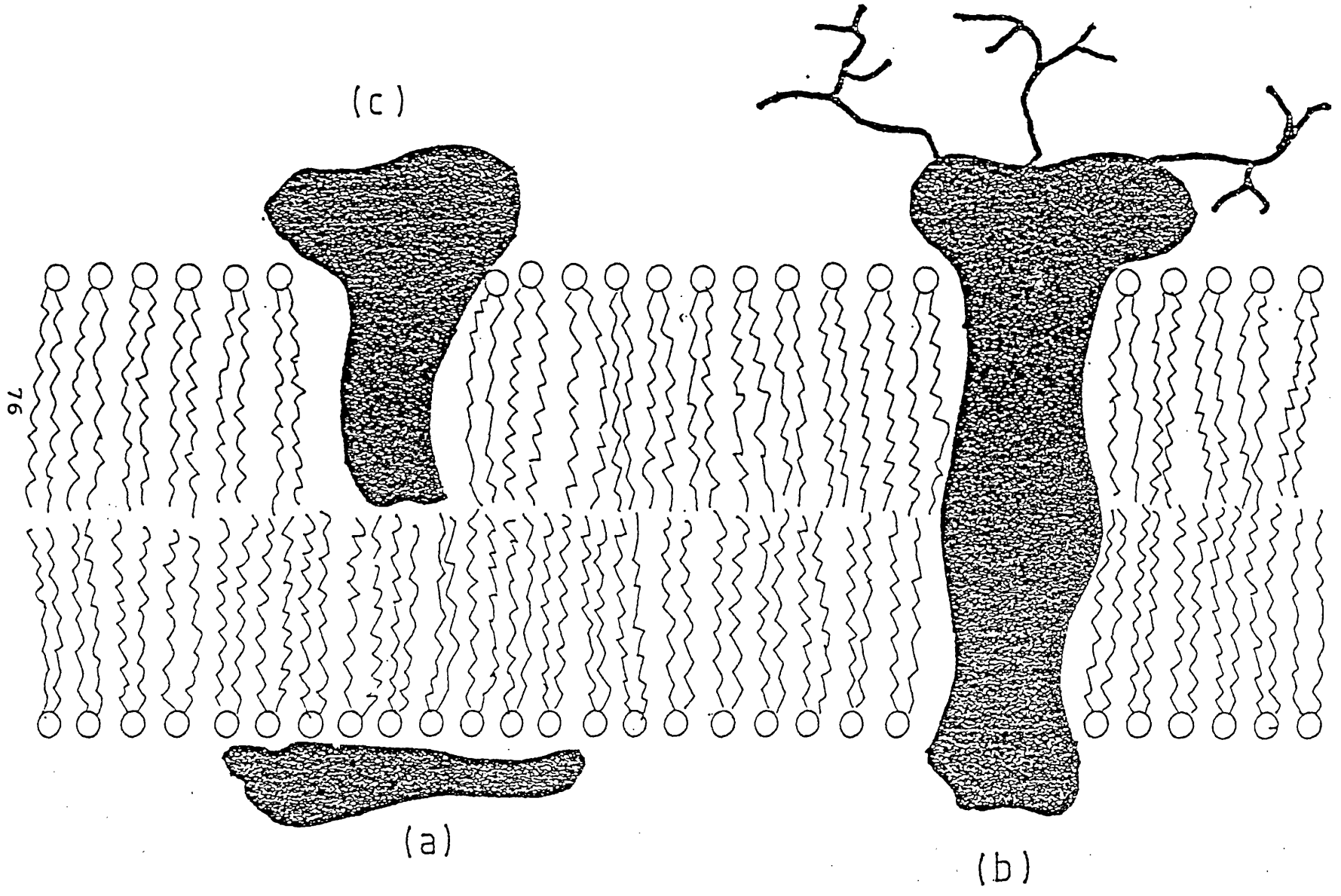
(c)
(a)
(b)

appear to adequately describe many biological membranes, it should be born in mind that areas of order (with respect either to lipids or proteins or both) may exist within the otherwise fluid membrane.

2.5 ASYMMETRY IN BIOLOGICAL MEMBRANES

One of the most intriguing properties of biological membranes is their structural and functional asymmetry, that is, the inner and outer layers of the membrane have different lipid and protein composition. The significance of such an asymmetry in protein composition is readily apparent when we consider the distribution and properties of a protein such as the Na^+/K^+-ATPase. The orientation of this protein within the membrane is such that transports Na^+ out of cells and K^+ into cells, coupled to hydrolysis of ATP at the cytoplasmic face of the membrane. Transport of ions in the opposite directions is not detected, nor is hydrolysis of ATP at the exterior membrane surface. Furthermore, ouabain, a potent inhibitor of this transport system, is only effective if present at the outer membrane surface. Such an absolute asymmetry is a necessary requirement for maximal ion transport, as a random distribution would result in transport in both directions and thus no net ion transfer. Protein asymmetry is maintained by the lack of transmembrane movement of membrane proteins.

Lipid asymmetry also exists in biological membranes. The functional significance of this asymmetry was a puzzle

for many years. It is now becoming clear that this asymmetry plays an important role in a number of processes:

a) one role of lipid asymmetry is the prevention of thrombogenic responses when blood proteins come into contact with erythrocyte cell membranes. Thus it has been repeatedly demonstrated that phosphatidylcholines are haemocompatable, whereas negatively charged lipids such as phosphatodylserines induce blood coagulation. It therefore comes as no surprise to find an absence of PS in the outer layers of biological membranes. The presence of PS in the inner layers of membranes may be thought surprising. Why not simply construct the inner layer with the same composition as the outer layer? The presence of PS in the inner layers of membranes will result in the initiation of a thrombogenic response upon tissue damage as PS is released. The asymmetric distribution of PS in cells not intimately associated with blood remains something of a puzzle.

b) The asymmetric distribution of PI is more readily explained. This lipid is found exclusively in the inner layers of cell membranes. As discussed in chapter 5, PI has an important role as a second messenger in signal transduction. Following binding of some hormones or neurotransmitters to receptors, a membrane associated phospholipase hydrolyses PI to inositol bis phosphate, which then stimulates the cellular response. In such systems, it is an obvious requirement to have the PI at the inner

membrane surface.

c) A further role of lipid asymmetry may be in the maintenance of full enzymatic activity. In this respect, it has been shown in membrane protein reconstitution experiments that many membrane proteins require a specific lipid composition for maximal activity.

2.6 SUMMARY

While the structure and interactions of biological molecules are necessarily complex, many of the fundamental principles governing the structure and interactions have been elucidated. It can be demonstrated that the basis of all biological membranes is the lipid bilayer. The lipid composition of the various membranes within an organism and within a cell can be shown to vary considerably, and this variation is associated with the function of the cell/organelle. Thus, the myelin sheath can be shown to be unusually rich in cerebrosides, a class of lipid with the capacity for forming extensive hydrogen bonding networks across the bilayer surface. Such networks will undoubtedly aid in the " insulating " function of this membrane.

Lipid bilayers provide an effective permeability barrier to water soluble molecules, thus segregating the cell interior from the outside world. This has the disadvantage of disrupting the flow of nutritional materials into and waste products out of the cell. This is overcome by the inclusion of transport proteins within the lipid bilayer. The transport characteristics of these proteins are directly related to their structure, small variations in structure (due to temperature, pH or solvent effects) can impair transport. Similarly, variations in the bilayer environment (i.e. changes in membrane fluidity) drastically alter the function of many membrane proteins.

The structure of proteins, both membrane and water soluble, is a direct result of the sequence of amino acids in the polypeptide chain and the physico-chemical nature of the environment. Subtle variations in amino acid composition, pH or ionic strength can have dramatic effects on the structure of proteins.

The nature of structural changes induced within proteins, lipids and biological membranes are in many cases poorly understood. It will be the aim of this work to characterise structural changes induced within lipids and proteins using the technique of Fourier transform infrared spectroscopy. Particular attention will be devoted to structural changes induced by temperature and ligand binding.

CHAPTER 3

FTIR SPECTROSCOPIC INVESTIGATION OF CEREBROSIDE POLYMORPHISM

3.1 INTRODUCTION

Cerebrosides belong to a class of lipids known as glycosphingolipids. Glycosphingolipids are composed of a sphingosine backbone attached to which is a fatty acid (either hydroxy or non-hydroxy) to form a ceramide. This ceramide then has one or more hexose sugar residues attached to form a glycosphingolipid. In the case of glucocerebrosides, one glucose residue is present, while in galactocerebrosides, a galactose residue is found (see fig 2.1).

Glycosphingolipids are found in most if not all animal cell membranes, although in relatively small amounts. A number of severe pathological states are associated with elevated levels of glycosphingolipids (Krabbe's disease, Gauchers disease, metachromic leucodystrophy). Certain specialised membranes have been shown to contain appreciable amounts of cerebrosides under normal physiological conditions. Such membranes include the myelin sheath of central and peripheral nervous system tissue and the brush border membranes of the kidney and gastrointestinal tract. The function of cerebrosides in such membranes is unclear. However, these membranes have in common the requirement for very carefully controlled permeability characteristics. Cerebrosides may therefore be involved in maintaining a high degree of order, and thus impermeability, within the membrane. The potential for extensive hydrogen bonding

involving the headgroup region of cerebrosides would be important in this respect. Such hydrogen bonding would not only aid in maintaining an efficient permeability barrier but would also confer enhanced stability to membranes exposed to a high degree of mechanical stress, as brush border membranes often are.

Many glycosphingolipids (cerebrosides included) exhibit complex polymorphic phase behaviour. The structure and polymorphism of non-hydroxy (Type II) galactocerebrosides have been the subject of a number of recent studies using differential scanning calorimetry (DSC) (Freire et al 1980, Reed and Shipley 1987), X-ray diffraction (Ruocco et al 1981) and spectroscopy (Skarjune and Oldfield 1982, Lee et al 1986). Upon heating type II galactocerebrosides in excess water, the main endothermic phase transition was observed to occur at 80^{o}C by DSC. Rapid cooling (quenching) of the lipid/water mixture produced two exothermic transitions, and a gel state with an X-ray diffraction pattern identical to that obtained from anhydrous galactocerebrosides (Ruocco et al 1981). Subsequent reheating produces an exothermic transition at 50-60^{o}C prior to the main endothermic transition. The presence of such an exothermic transition indicates conversion of the cerebroside from a high energy, metastable state to a more thermodynamically stable, lower energy state. This conversion can also be shown to occur at room temperature over prolonged periods.

Due to the occurrence of high levels of cerebrosides in myelin and brush border membranes it is important to clarify the molecular basis of cerebroside polymorphism and to attempt to discover how this behaviour is affected by other membrane components.

MATERIALS AND METHODS

Type II bovine brain cerebrosides (98% non-hydroxy, 99% pure), cholesterol (5 (6) - cholesten - 3β - ol, 99% pure) and deuterium oxide (99.8 atom %) were purchased from Sigma, UK. Dipalmitoyl phosphatidylcholine (1,2 - dipalmitoyl - 1 - s n - glycero - 3 -phoshpatidylcholine, DPPC, 99% pure) was purchased from Fluka. All solvents were of spectrophotometric grade, purchased from Aldrich.

Lipid mixtures were prepared as follows. Stock solutions of cerebroside, DPPC and cholesterol were made up in chloroform/methanol solution (2:1). Cerebroside/DPPC and cerebroside/cholesterol dispersions were formed by mixing the appropriate volumes of stock solutions to give the required ratios. The solvent was evaporated under a stream of nitrogen and samples stored under vacuum to remove any final traces of solvent.

Samples for FTIR spectroscopy were prepared as follows. Hydration of samples was achieved by heating lipids and water (ultrapure, final cerebroside concentration 10mg/ml), at 90^{o}C and agitating with a vortex mixer. Metastable samples were produced by quenching the hydrated lipids from 90-0^{o}C in an ice bath. Stable samples were produced by incubating metastable samples for 10-15 minutes at 70^{o}C.

Infrared spectra were recorded on a Perkin-Elmer 1750 Fourier transform infrared spectrometer interfaced to a Perkin-Elmer 7300 data station. For each sample, 50ul was

pippetted between a pair of CaF_2 windows separated by a 6um tin spacer. The cell was mounted in a Beckmann FH-01 thermostated cell holder. Temperature was maintained at 20°C (unless otherwise stated) by a circulating water bath. For each sample 200 scans were recorded at $4cm^{-1}$ resolution and signal averaged. Difference spectra were generated by digital subtraction of a suitable background spectrum. Anhydrous cerebroside spectra were recorded from a KBr disc containing 1% cerebroside by weight.

DSC thermograms were recorded on a Perkin-Elmer DSC-7 at a heating and cooling rate of 2.5°/minute over the range 0-100°C. Lipid mixtures prepared as above were weighed (15-20mg) into stainless steel pans. Each sample was hydrated by introducing excess water into the pans via a microsyringe and the pans sealed. To ensure that the lipid mixtures were homogeneous and at equilibrium each sample was taken through several heating and cooling cycles and left for 24 hours before being scanned.

RESULTS

Differential scanning calorimetry

Calorimetric thermograms of aqueous dispersions of galactocerebroside and galactocerebroside/cholesterol mixtures are presented in Figure 3.1. Upon heating pure galactocerebrosides, the main gel-liquid crystalline phase transition occurred at 79^{o}C with an enthalpy change of 90J/g. Cooling scans exhibited two exothermic transitions at 58.4^{o}C and 36.2^{o}C with enthalpy changes of -26.2J/g and -7.1J/g, respectively, indicating formation of two gel states. A subsequent heating scan showed a distinct exotherm at 51.8^{o}C with an enthalpy change of -12J/g. This was followed by a split endotherm with peaks at 74.8^{o}C and 78.7^{o}C with a combined enthalpy change of 85J/g. Repetition of the heating and cooling cycle produced identical thermograms to those illustrated in Figure3.1a-c.

The addition of 9 mol% cholesterol to galactocerebrosides produced a thermogram essentially the same as that seen for the pure cerebroside upon initial heating. A complex exotherm was produced upon cooling, with a peak at 57.3^{o}C and an enthalpy change of -40J/g. Subsequent heating scans showed the characteristic exotherm, reduced in peak temperature to 41.6^{o}C and broadened considerably but of comparable enthalpy change to that seen for the pure cerebroside. This was again followed by a split endotherm with peaks at 73.6^{o}C and 79^{o}C with a

FIGURE 3.1: DSC thermograms of hydrated type II galactocerebrosides containing (a-c) 0; (d-f) 9; and (g-h) 34 mol% cholesterol. Heating and cooling rate =2.5^{o}C/min.

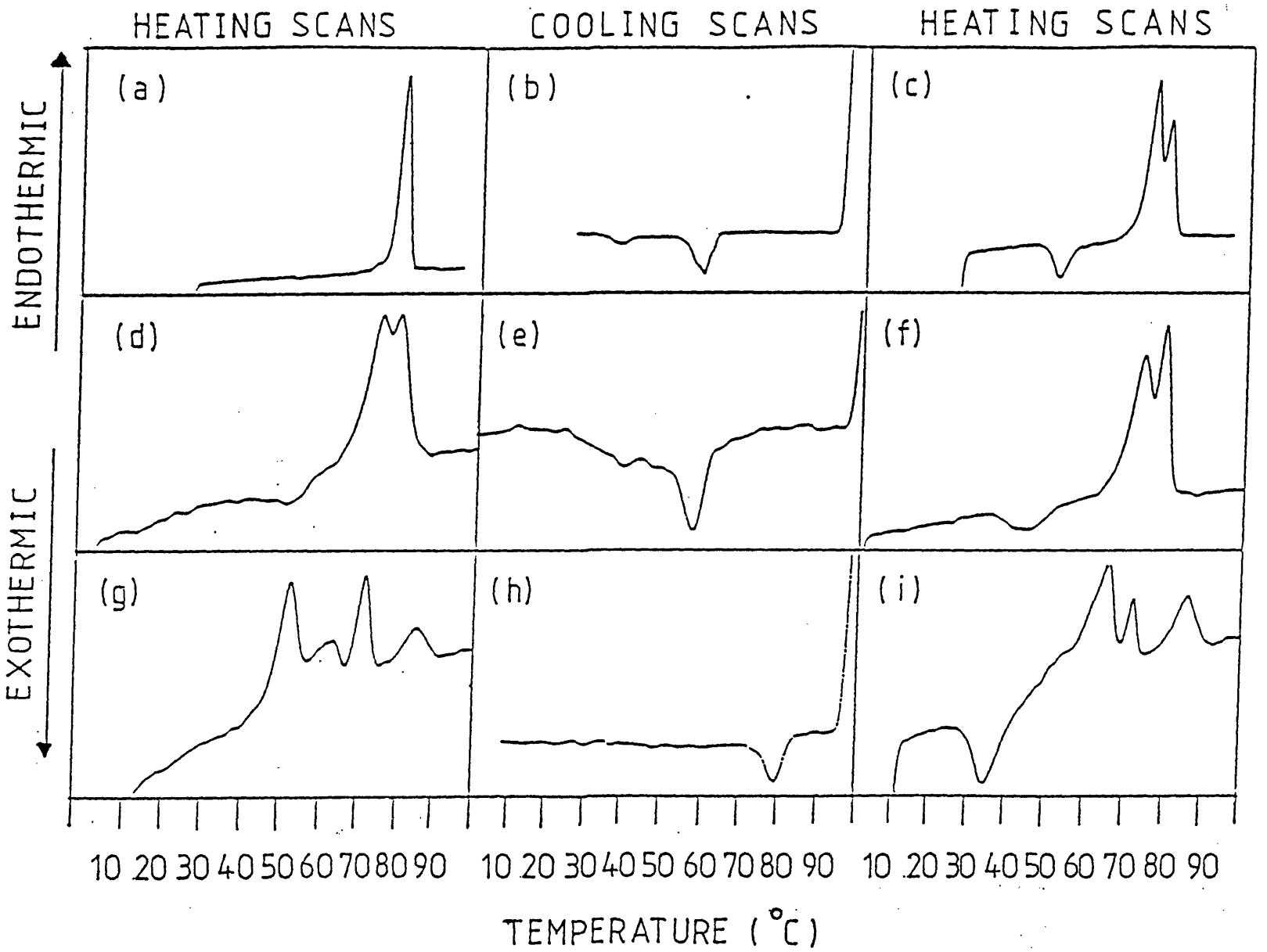
HEATING SCANS
COOLING SCANS
HEATING SCANS
(a)
(b)
(c)
(d)
(e)
(f)
(g)
(h)
(i)
ENDOTHERMIC
EXOTHERMIC
10 20 30 40 50 60 70 80 90
10 20 30 40 50 60 70 80 90
10 20 30 40 50 60 70 80 90
TEMPERATURE (°C)

combined enthalpy change of 70J/g.

Thermograms of cerebrosides with the addition of 34 mol% cholesterol are shown in Figure 3.1g-i. An initial heating scan produced four endothermic transitions, at 53.2°C, 63.5°C, 72°C and 86°C with a combined enthalpy change of 53.3J/g. A cooling scan showed only one exothermic transition, at 80.8°C. Immediate reheating produced an exotherm at 35.6°C followed by three endotherms at 65.7°C, 72.2°C and 86°C.

Figure 3.2 shows the effects of addition of DPPC to cerebroside samples. After addition of 9 mol% DPPC an initial heating scan produced an endotherm at 79.3°C with an enthalpy change of 76.2J/g. Cooling produced an exotherm with a peak at 57.5°C and a shoulder at 55°C. The enthalpy change of this complex endotherm was -32.2J/g. Subsequent heating produced an exotherm centred at 54.5°C with an enthalpy change of -18.6J/g followed by a split endotherm with peaks at 75.3°C and 78.9°C and an enthalpy change of 77.6J/g.

Increasing the DPPC concentration to 34mol% produced the thermograms shown in Figure3.2e-h. The initial heating endotherm was complex, having three transitions at 43.5°C, 54.5°C and 72.3°C with a combined enthalpy change of 51.7J/g. Only one exotherm is seen in cooling scans, at 52.2°C with an enthalpy change of 41.9J/g. Immediate reheating produced a thermogram exhibiting both endothermic

FIGURE 3.2: DSC thermograms of hydrated type II galactocerebrosides containing (a-d) 9; (e-h) 33 and (i-j) 50 mol% DPPC. Heating and cooling rate = 2.5^{o}C/min.

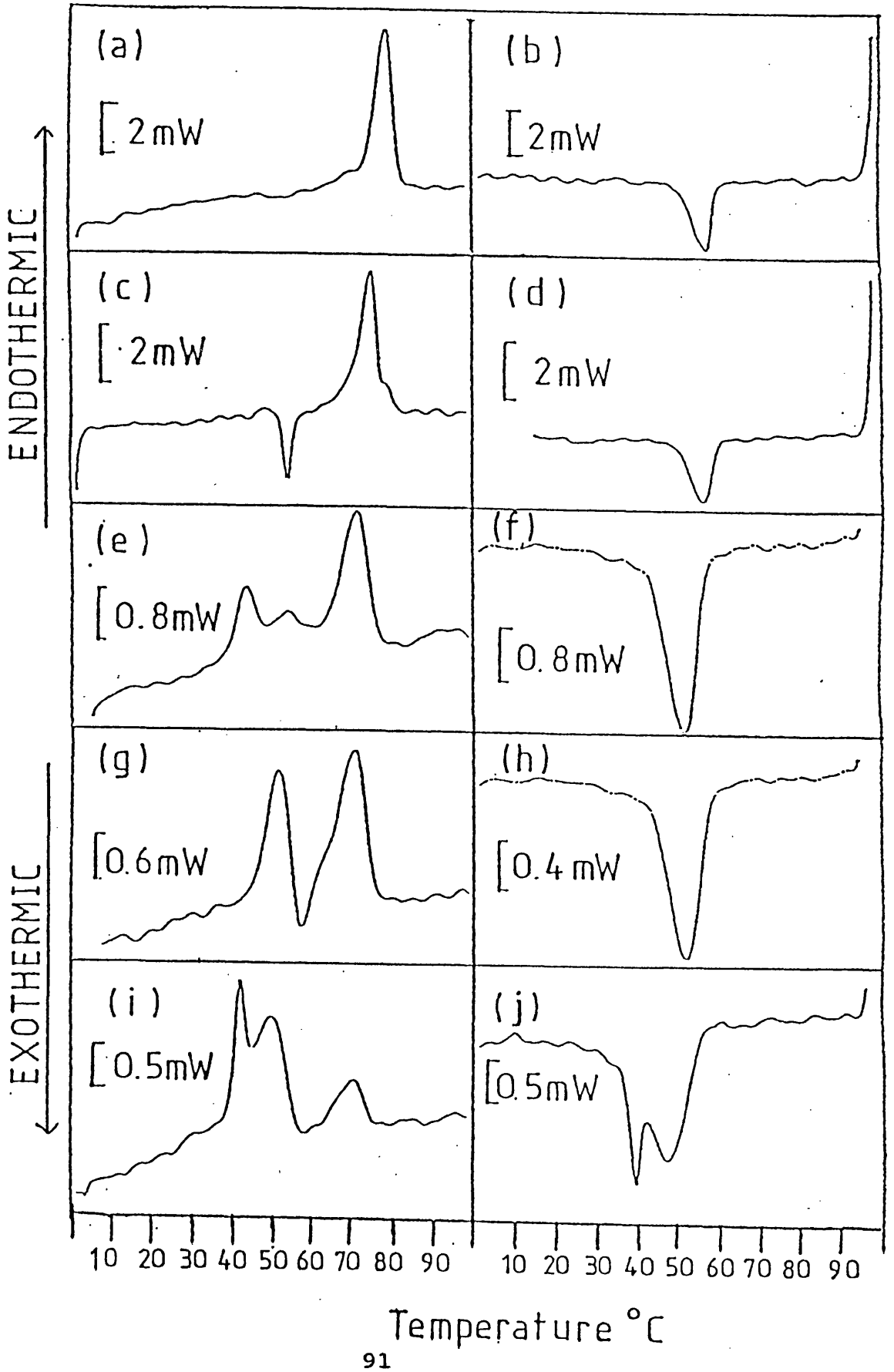
(a)
2mW
(b)
2mW
(c)
2mW
(d)
2mW
(e)
0.8mW
(f)
0.8mW
(g)
0.6mW
(h)
0.4 mW
(i)
0.5mW
(j)
0.5mW
ENDOTHERMIC
EXOTHERMIC
10 20 30 40 50 60 70 80 90
10 20 30 40 50 60 70 80 90
Temperature °C

and exothermic transitions. The peak temperatures of the first endotherm and the exotherm could not be determined due to the overlap of these transitions. Similarly, the enthalpy change of the thermogram could not be determined. The final endotherm had its peak at 71.6^{o}C.

When the DPPC concentration was further elevated to 50 mol% multiple peaks were seen in heating scans. Three endotherms were seen, at 42.9^{o}C, 51.4^{o}C and 70,9^{o}C with a total enthalpy change of 48.6J/g. Cooling produced an exotherm at 49.6^{o}C with a shoulder at 52^{o}C.A further sharp peak was seen at 39.6^{o}C. The combined enthalpy change of these transitions was -43J/g. A subsequent heating and cooling cycle produced identical thermograms to those shown in Figure3.2i-j.

FTIR spectroscopy

Pure galactocerebrosides containing non-hydroxy fatty acids show marked spectral differences between the stable and metastable polymorphs. Figure 3.3 shows difference spectra of metastable and stable bovine brain type II galactocerebrosides in the amide I and II region of the spectrum. In the stable state two amide I bands were observed, at 1616cm^{-1} and 1646cm^{-1}, with an amide II band at 1550cm^{-1}. Quenching the cerebroside suspension in an ice bath resulted in a shift of the amide II band to 1546cm^{-1} and the disappearance of the amide I component at 1616cm^{-1}

FIGURE 3.3: FTIR difference spectra of the amide I and amide II region of type II galactocerebrosides in the metastable (broken line) and stable (solid line) states.

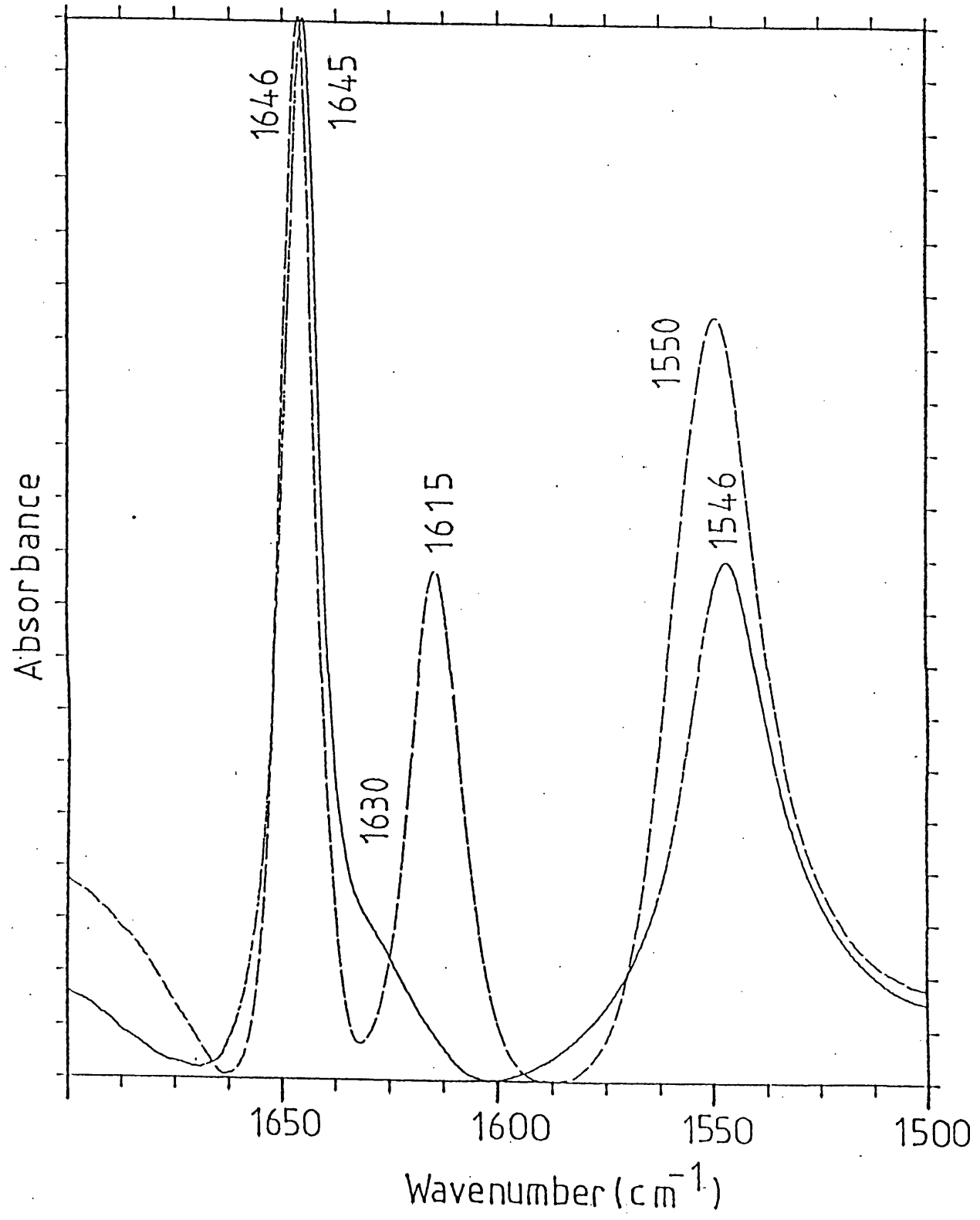
1646
1645
1630
1615
1550
1546
Absorbance
1650
1600
1550
1500
Wavenumber (cm⁻¹)

FIGURE 3.4: FTIR difference spectra of the C-O stretching region of type II galactocerebrosides in the metastable (broken line) and stable (solid line) states.

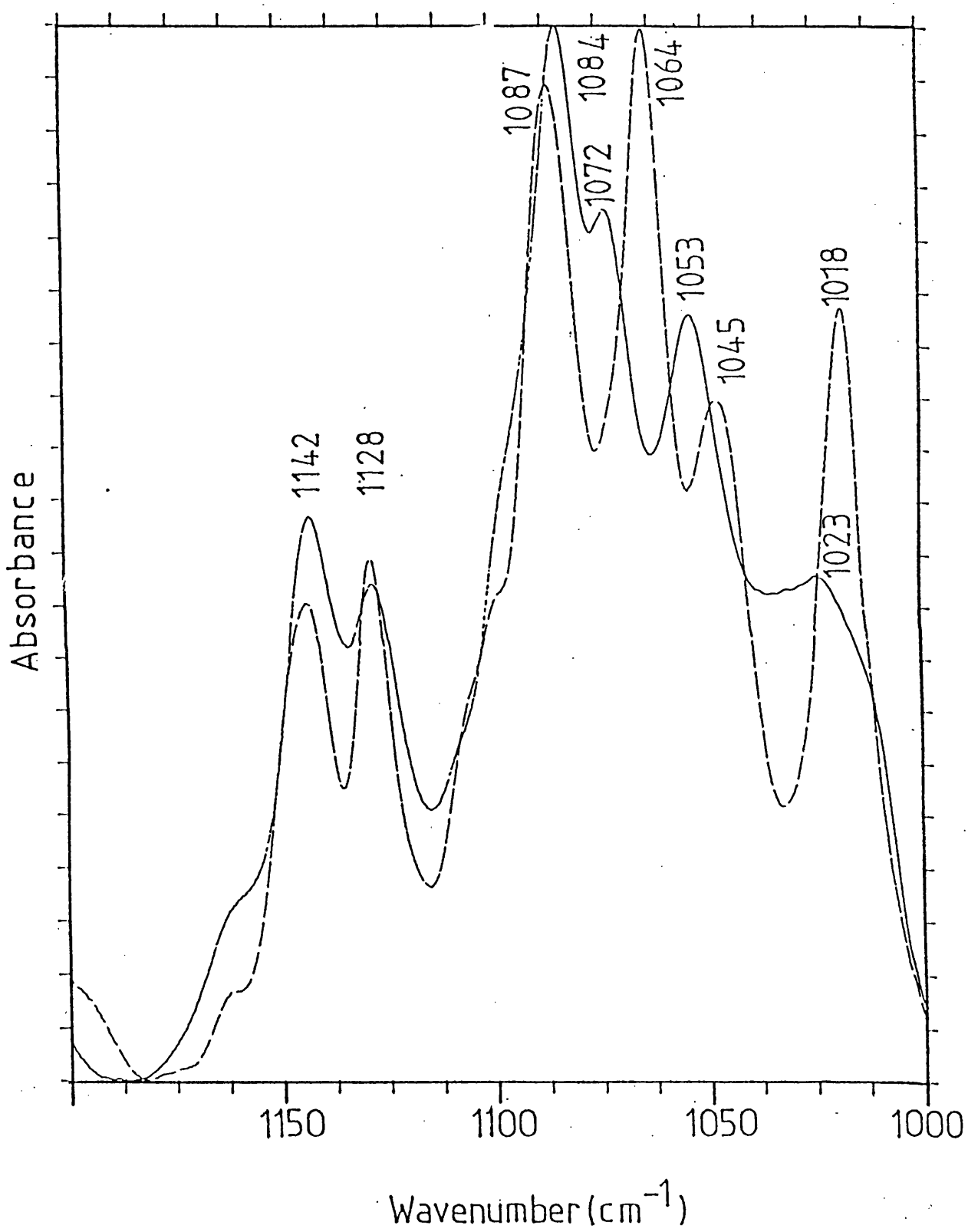
1142
1128
1087
1084
1072
1064
1053
1045
1023
1018
1150
1100
1050
1000
Absorbance
Wavenumber (cm^{-1})

FIGURE 3.5: FTIR specrum of the amide I and amide II region of anhydrous type II galactocerebrosides.

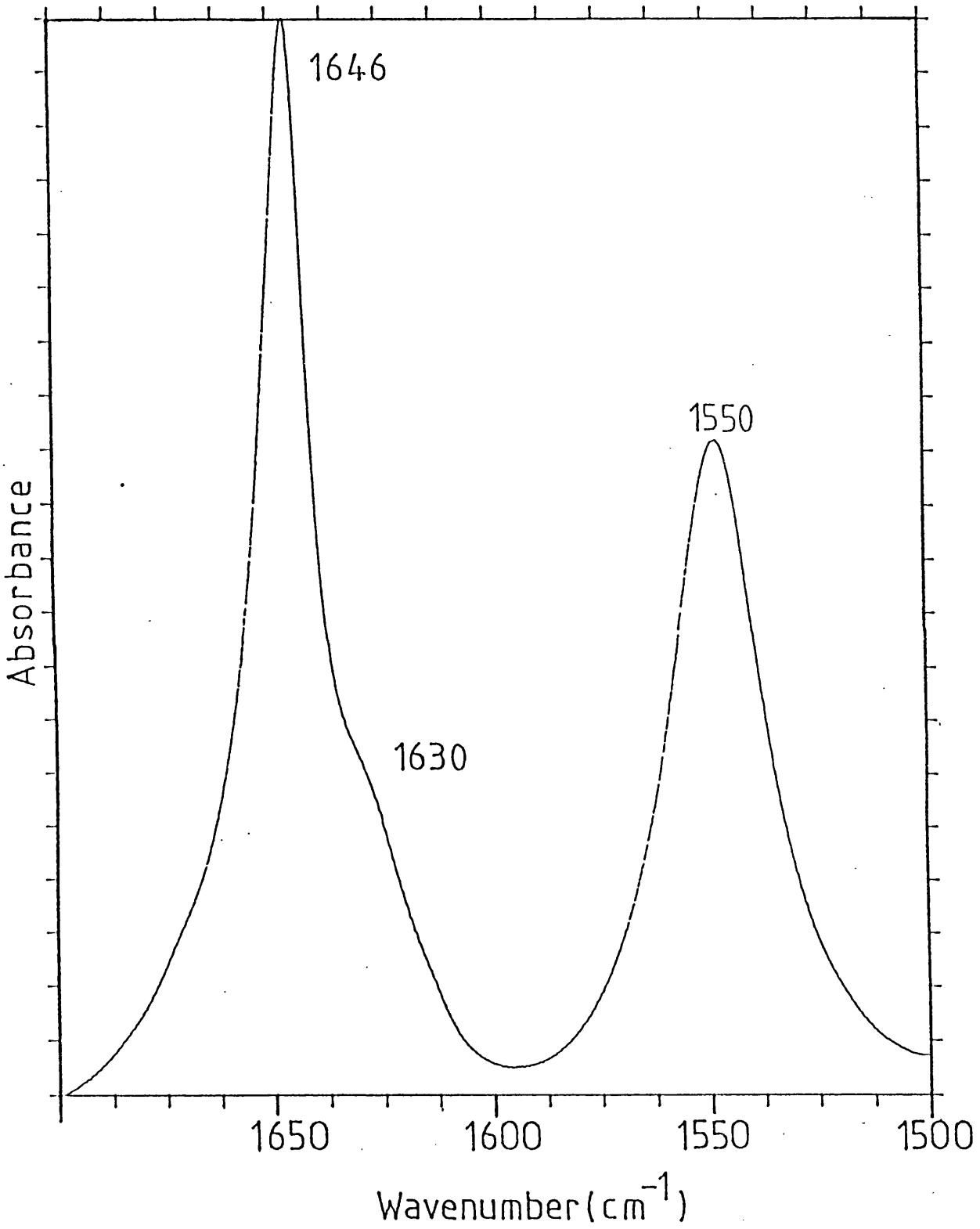
1646
1550
1630
Absorbance
1650
1600
1550
1500
Wavenumber (cm^{-1})

A shoulder at 1630cm^{-1} was observed on the main amide I component.

Spectral differences were also apparent in the region 1200-1000cm^{-1} (Fig. 3.4), associated with stretching of the C-O bonds of the galactose headgroup and sphingosine hydroxyl group. In the stable state, bands are seen at 1142cm^{-1}, 1128cm^{-1}, 1087cm^{-1}, 1064cm^{-1}, 1045cm^{-1} and 1018cm^{-1}. It is not possible to assign these bands to individual C-O groups without a series of isotopic exchange experiments. Upon quenching, bands are seen at 1142cm^{-1}, 1128cm^{-1}, 1084cm^{-1}, 1072cm^{-1}, 1053cm^{-1} and 1023cm^{-1}.

The amide I and II region of FTIR spectra of anhydrous galactocerebrosides are shown in Figure3.5 and 3.6 The amide I maximum was seen at 1646cm^{-1} with a shoulder at 1630cm^{-1}. The amide II band was observed at 1550cm^{-1}. In the C-O stretching region bands were observed at 1142cm^{-1}, 1128cm^{-1}, 1084cm^{-1}, 1072cm^{-1}, 1053cm^{-1} and 1023cm^{-1}.

The infrared spectrum of galactocerebrosides incorporating minor amounts of cholesterol shows significant differences from that of the pure cerebroside (Fig. 3.7). The intense amide I peak seen at 1616cm^{-1} in the stable state was progressively reduced in intensity until at 9 mol% cholesterol only a shoulder at 1628cm^{-1} was seen. In the C-O stretching region (Fig. 3.8) the peak at 1064cm^{-1} in the stable state was also progressively reduced in intensity as the cholesterol content was increased. At 50 mol%

FIGURE 3.6: FTIR spectrum of the C-O stretching region of anhydrous type II galactocerebrosides.

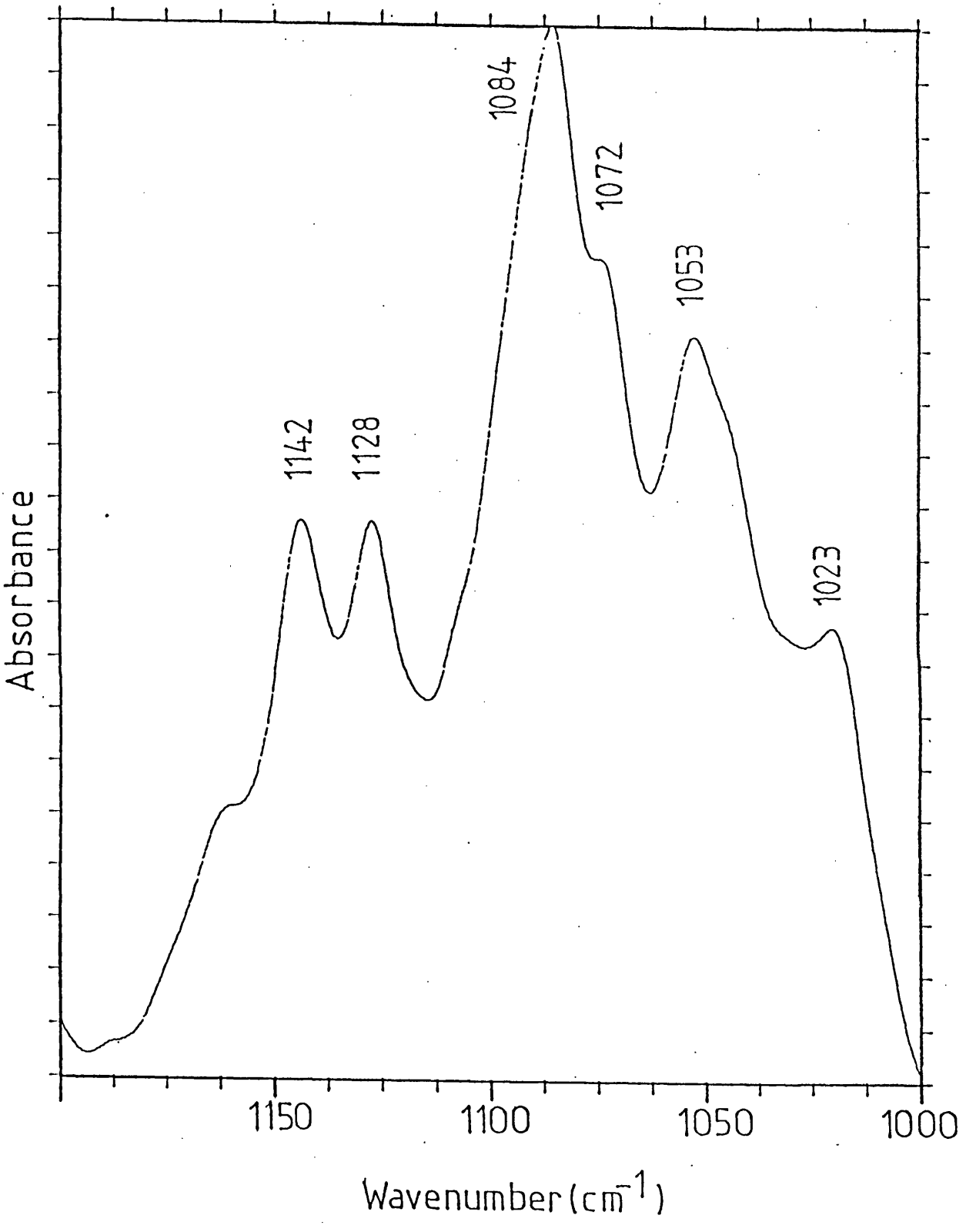
1142
1128
1084
1072
1053
1023
Absorbance
1150
1100
1050
1000
Wavenumber (cm⁻¹)

FIGURE 3.7: FTIR difference spectra of the amide I and amide II region of type II galactocerebrosides in the stable state incorporating 6.25 mol% (solid line) and 9 mol% (broken line) cholesterol.

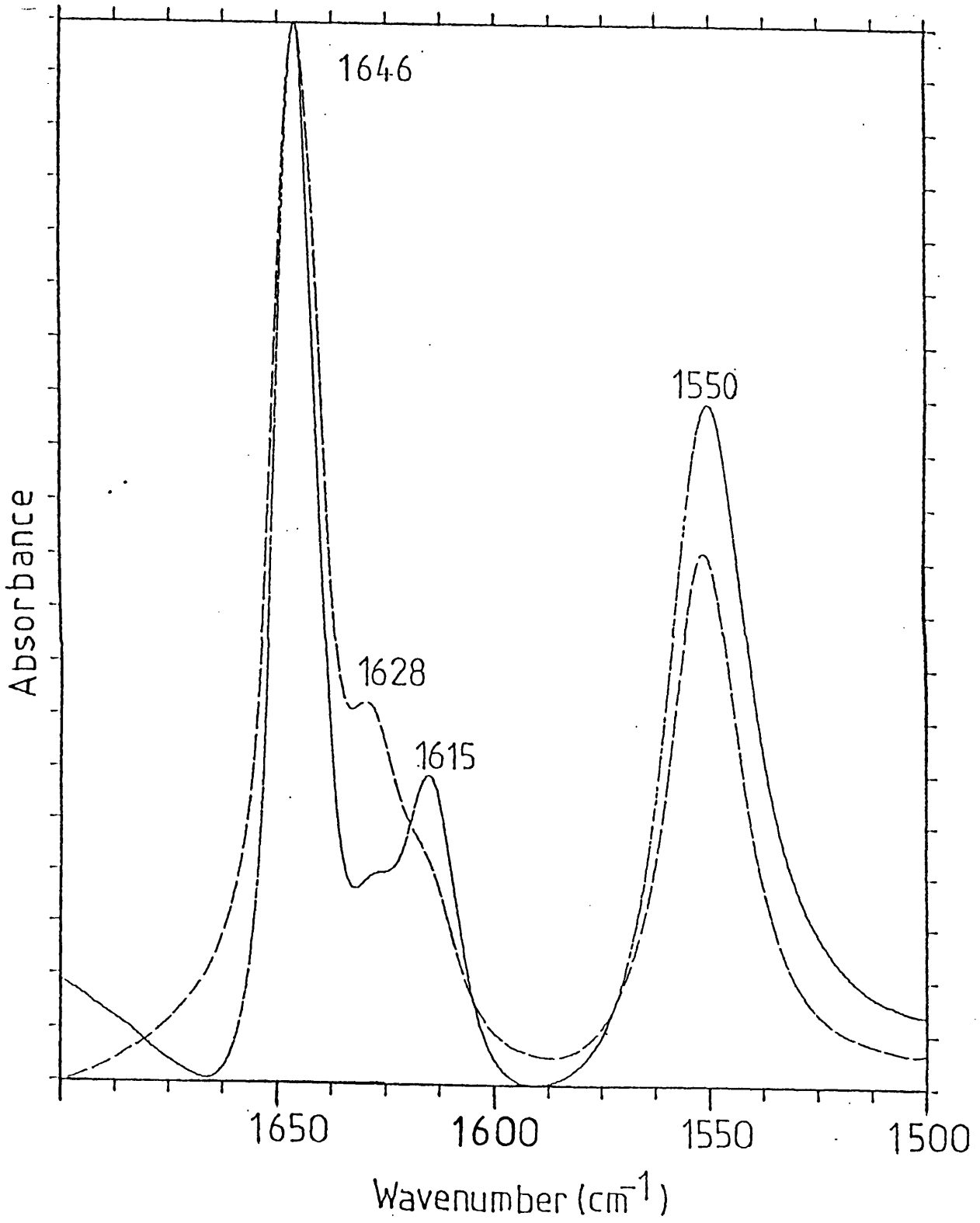
1646
1628
1615
1550
Absorbance
1650
1600
1550
1500
Wavenumber (cm⁻¹)

FIGURE 3.8: FTIR difference spectrum of the C-O stretching region of type II galactocerebrosides in the stable state incorporating 9 mol% cholesterol.

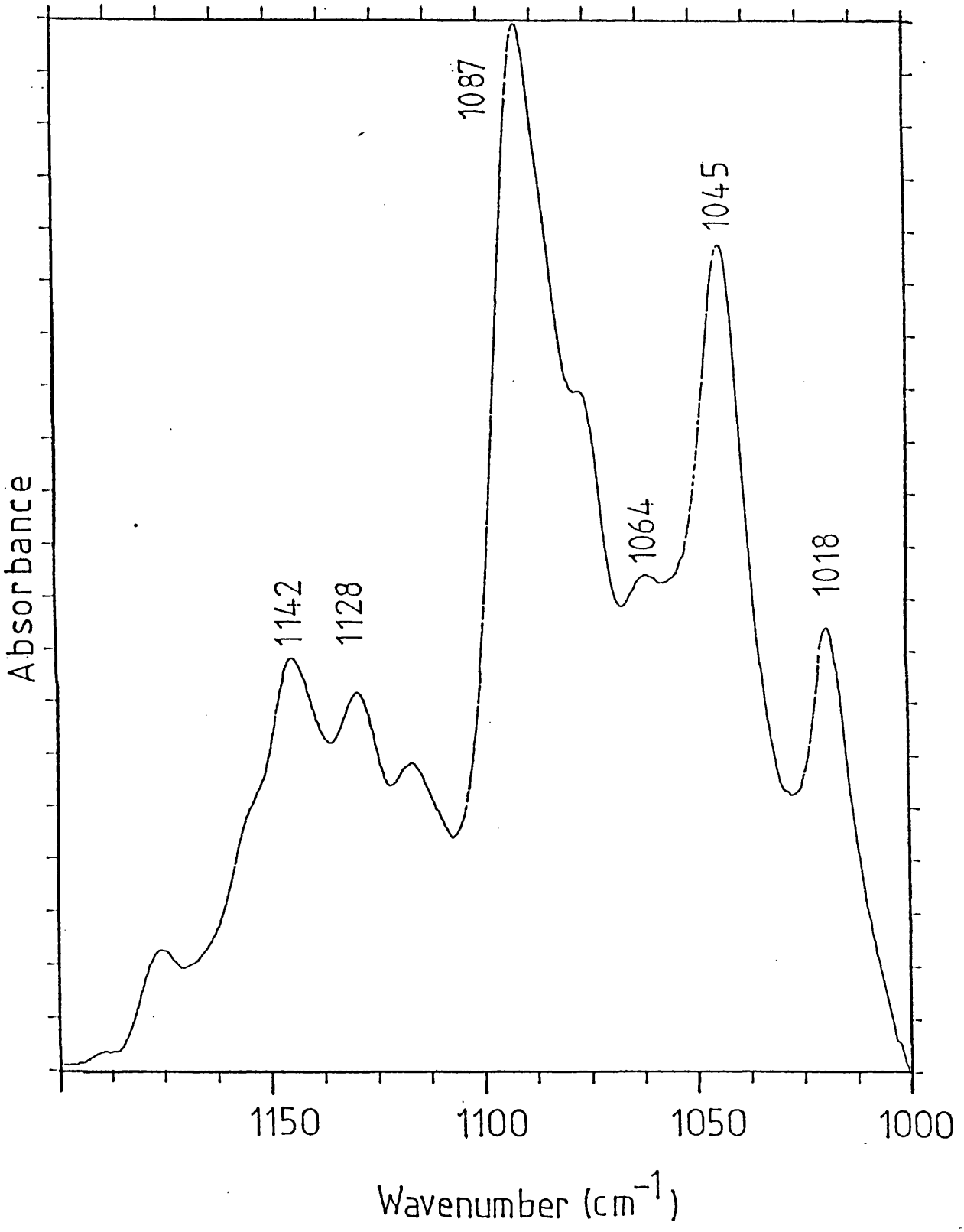
1087
1045
1064
1142
1128
1018
Absorbance
1150
1100
1050
1000
Wavenumber (cm^{-1})

cholesterol, quenched and reheated samples exhibited identical infrared spectra (Fig. 3.9).

The effects of incorporation of DPPC into cerebroside bilayers upon the infrared spectrum are similar to those observed for cholesterol. At 9 mol% DPPC and 33 mol% DPPC the amide I maxima in the stable state are seen at 1646cm^{-1} and 1616cm^{-1} (Fig. 3.10 and Fig. 3.11). At 33 mol% DPPC the peak at 1616cm^{-1} is much reduced in intensity. Quenched samples containing up to 33 mol% DPPC showed an amide I maximum at 1645cm^{-1} with a shoulder at 1630cm^{-1} and an amide II maximum at 1546cm^{-1} . In the presence of 50 mol% DPPC the amide I band at 1616cm^{-1} was no longer observed (not shown). The amide I and II bands were seen at 1646cm^{-1} and 1550cm^{-1} respectively in both quenched and reheated samples at 50 mol% DPPC.

FIGURE 3.9: FTIR difference spectra of the amide I and amide II region of type II galactocerebrosides incorporating 50 mol% cholesterol in a quenched (broken line) and reheated (solid line) sample.

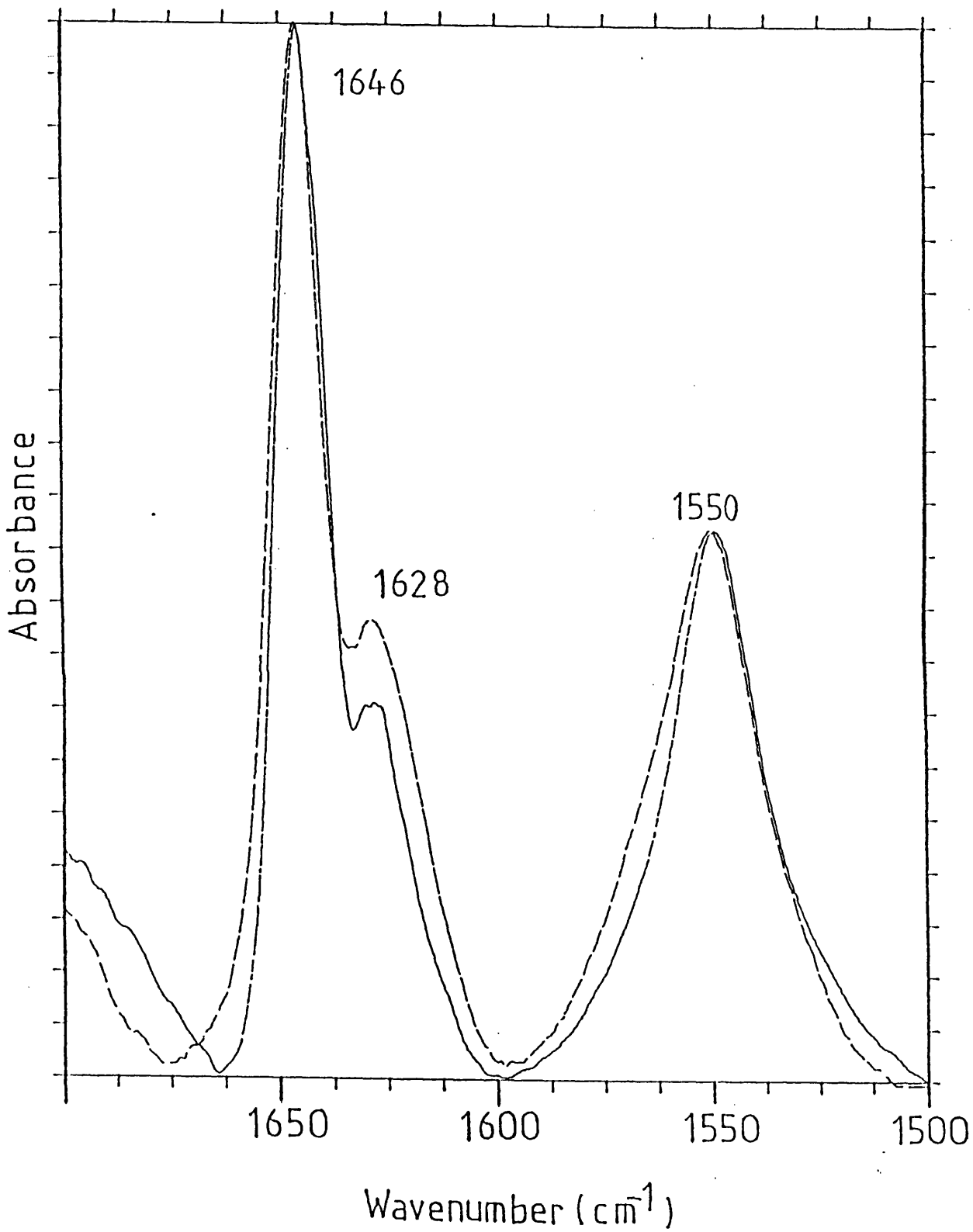
1646
1628
1550
Absorbance
1650
1600
1550
1500
Wavenumber (cm⁻¹)

FIGURE 3.10: FTIR difference spectra of the amide I and amide II region of type II galactocerebrosides incorporating 9 mol% DPPC in a quenched (solid line) and reheated (broken line) sample

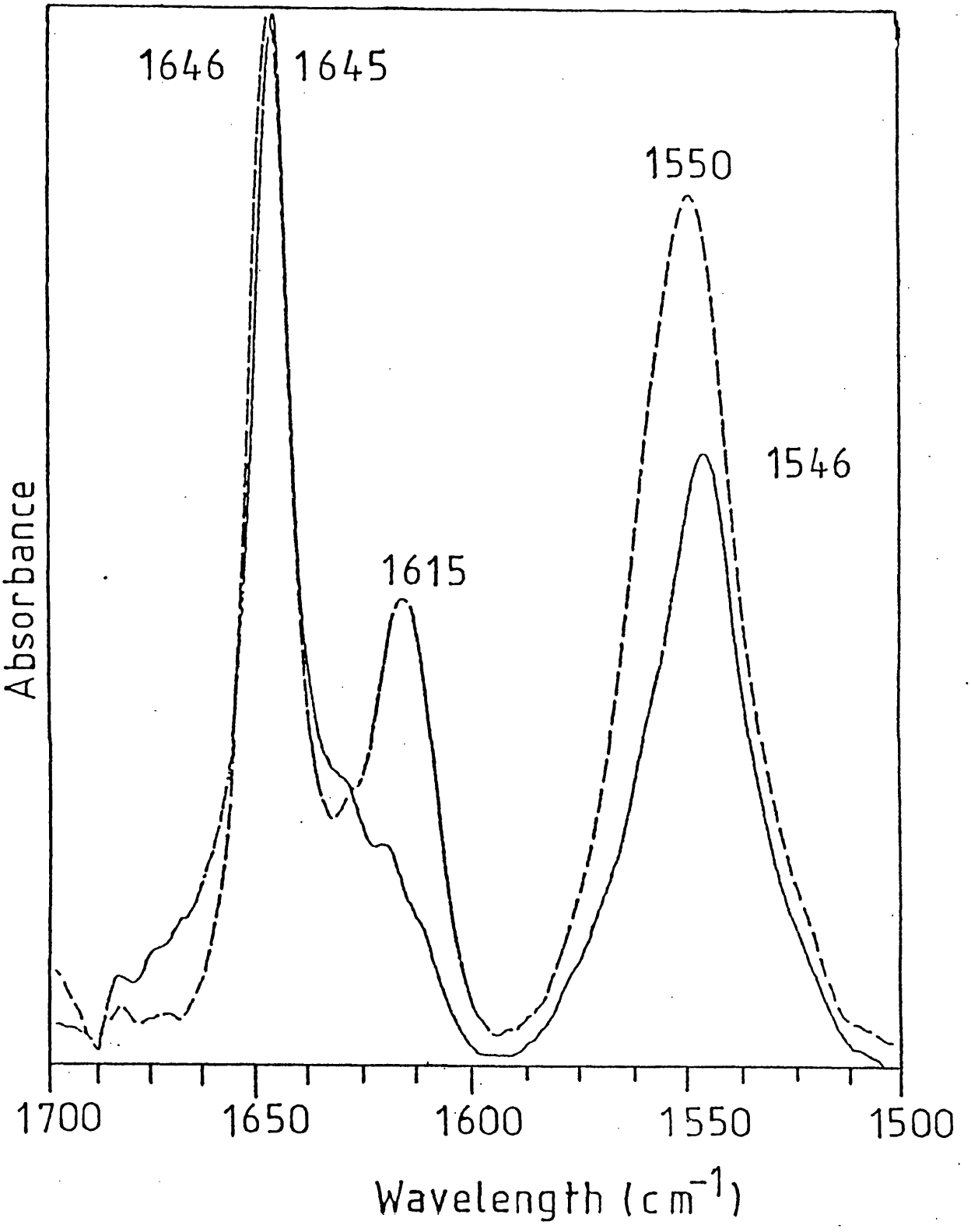
1646
1645
1550
1546
1615
Absorbance
1700
1650
1600
1550
1500
Wavelength (cm^{-1})

FIGURE 3.11: FTIR difference spectra of the amide I and amide II region of type II glactocerebrosides incorporating 33 mol% DPPC in a quenched (solid line) and reheated (broken line) samples.

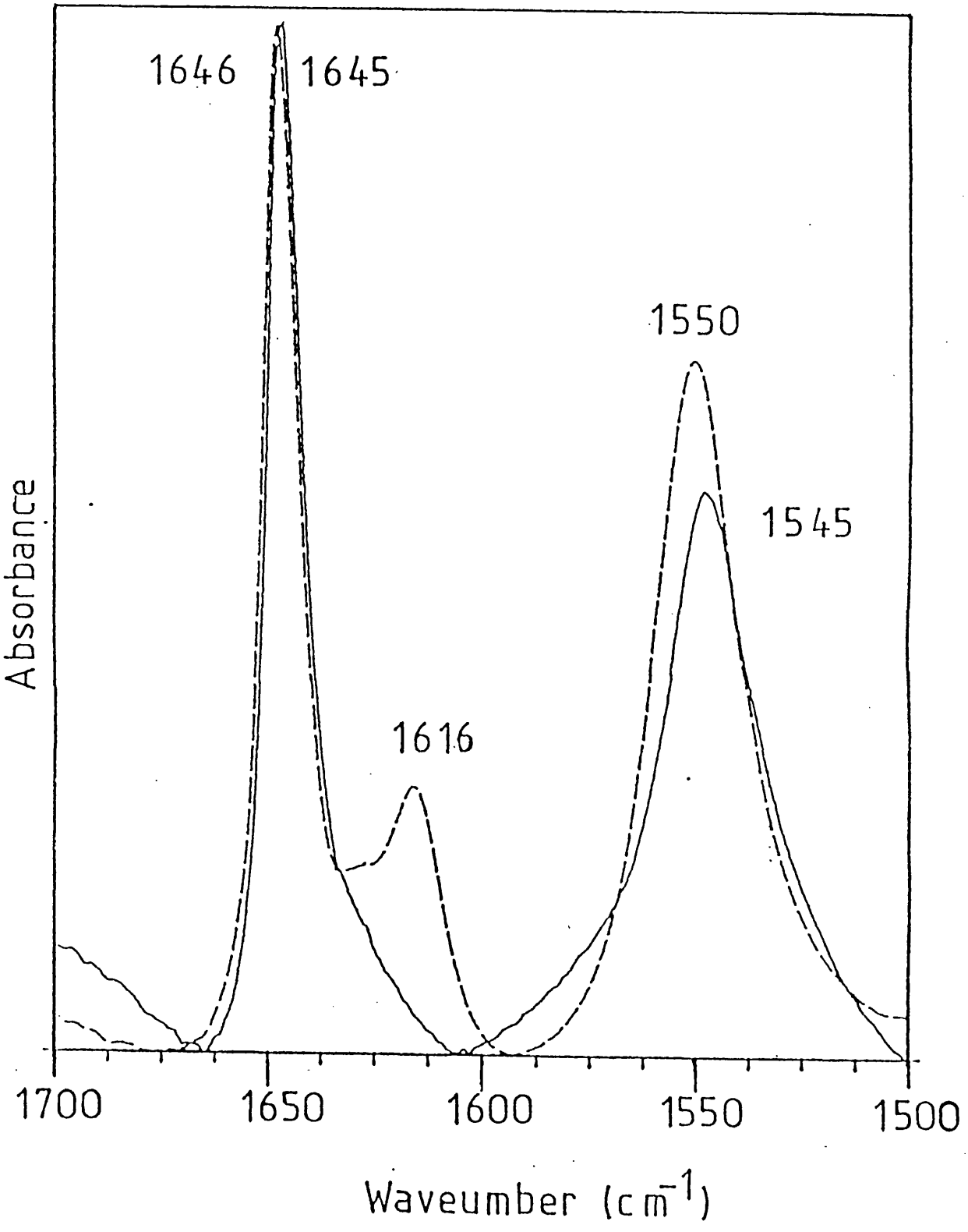
1646
1645
1550
1545
1616
Absorbance
1700
1650
1600
1550
1500
Waveumber (cm⁻¹)

DISCUSSION

Complex polymorphic phase behaviour has been described for a number of glycosphingolipids, including galactocerebrosides (Freire et al 1980,Curatolo 1982, Curatolo 1985). Earlier studies have demonstrated the formation of a metastable cerebroside form in non-hydroxy fatty acid cerebrosides (but not hydroxy fatty acid cerebrosides) upon rapid cooling. The results presented here confirm these findings.

Upon heating type II bovine brain galactcerebrosides in excess water, calorimetric thermograms indicate a gel-liquid crystalline phase transition at 79^{o}C. This is unusually high for such transitions in lipids, and can be related to a high degree of intermolecular hydrogen bonding via the hydroxyl groups of the galactose residues, which imparts great stability to the bilayers. As the bilayer was rapidly cooled two exothermic transitions were recorded, due to the formation of at least two gel states. The discrepancy in the enthalpy changes of the heating and cooling scan (a difference of some 57 J/g) suggests that at least one of these gel states is metastable, that is, has been "frozen" in an unstable, high energy state. Elevation of the temperature to 50-60^{o}C results in the release of the excess energy and conversion of the cerebroside to a more thermodynamically stable state. Marked spectral differences have been described between the metastable and stable

cerebroside forms. Two intense amide I bands were seen in the spectrum of stable galactocerebrosides at 1646cm^{-1} and 1616cm^{-1}.

The presence of two amide I bands in the spectrum of the stable lipid has a number of possible explanations. Firstly, it is possible that one of these bands arises from water of hydration associated with the lipid. However, upon deuteration, both components are shifted to frequencies some 15cm^{-1} lower. Had either of these bands been due to water absorptions it would be found some 400cm^{-1} lower in $^{2}H_2O$ than in H_2O. Furthermore, spectra of stable state cerebrosides are identical at 70^{o}C and 20^{o}C. It can therefore be concluded that neither of these bands is due to water.

Secondly, it has to be remembered that the sphingosine chain in the cerebrosides contain C=C bonds, which absorb in the 1640-1650cm^{-1} region of the spectrum. With this is mind, spectra of di-hydro galactocerebroside were obtained. If one of the amide components is actually due to a C=C absorption, then the spectrum of this material should be simpler than that of type II galactocerebrosides. In fact, the spectrum is much more complex. The appearance of multiple peaks in the spectrum of type II galactocerebrosides is unlikely therefore to arise simply from the presence of a double bond.

As the two absorptions cannot be explained in terms of

water or C=C absorptions, it is reasonable to assume that they are amide absorptions. This suggests the occurrence of two subpopulations of amide C=O groups within the bilayer, the groups giving rise to the band at 1616cm^{-1} being very strongly hydrogen bonded. The absence of this peak in metastable samples suggests a decrease in the degree or strength of hydrogen bonding in this state. Similar changes in hydrogen bonding to the galactose headgroup can be inferred from examination of the C-O stretching region of the spectrum of the two states. Stronger hydrogen bonding in the stable state weakens the C-O bonds and results in a decrease in the frequency of a number of bands associated with this vibration.

Comparison of the spectra of metastable and anhydrous galactocerebrosides is illuminating.In both cases the amide I maximum lacks the distinctive band seen at 1616cm^{-1} in the stable polymorphic form and exhibit only a shoulder at 1630cm^{-1} on the main band. This suggests a similar hydrogen bonding or hydration scheme in the metastable and anhydrous lipid. Examination of the C-O stretching region of the spectra showed this region to be identical in the metastable and anhydrous cerebroside. This data suggests that rapid cooling of the liquid-crystalline phase results in dehydration of the cerebroside headgroups, resulting in a hydrogen bonding pattern similar if not identical to that found in anhydrous cerebrosides. Dehydration of the

galactose headgroup has been suggested on the basis of X-ray diffraction data (Ruocco et al 1981). X-ray diffraction patterns of the metastable and anhydrous cerebroside were found to be identical. Furthermore, hydration of galactocerebrosides in the presence of ethylene glycol results in the formation of a cerebroside form with thermal characteristics intermediate between those of the metastable and stable polymorphs (Curatolo 1985, Miller and Bach 1986). This can be interpreted as the production of a cerebroside form with a reduced hydration sphere as a result of the preferential hydrogen bonding of water to ethylene glycol.

Following the conversion of the metastable cerebroside form to a more stable form, the calorimetric data indicated two high temperature endothermic transitions. The presence of two endotherms can be related to the heterogeneous composition of the type II cerebrosides, which contain cerebrosides of various chain lengths. Such dual peaked endotherms are not described in calorimetric studies of N-palmitoyl galactocerebroside (Curatolo, 1982; Ruocco et al 1983). The two thermal transitions described here presumably reflect the gel-liquid crystalline phase transitions of cerebrosides with different chain lengths.

Addition of small amounts of cholesterol and DPPC to cerebroside bilayers had effects upon thermograms identical to those described previously for lipid mixtures (Ruocco et al 1983, Ruocco and Shipley 1984). In the presence of 9 mol%

cholesterol or DPPC, transitions were broadened and reduced both in peak temperature and enthalpy change. These effects can be related to disruption of the acyl chain packing and disruption of the headgroup/headgroup interactions in the cerebroside bilayers as cholesterol or DPPC molecules intercalate between cerebroside molecules. This reduces the co-operativity of thermal transitions and decreases the energy required to produce the trans/gauche isomerisation associated with the phase transition.

Cooling and reheating still produces thermograms consistent with the production of a metastable state.

The disruption of the cerebroside bilayers caused by the presence of small amounts of cholesterol is also evident from the infrared spectra presented in Figure 3.7. Cholesterol decreases the intensity of the amide I component seen at $1615cm^{-1}$ in the stable state until at 9 mol% cholesterol only a shoulder is apparent at $1628cm^{-1}$. A similar decrease is seen in the C-O stretching band at $1064cm^{-1}$. The simultaneous reduction in the intensity of the bands at $1615cm^{-1}$ and $1064cm^{-1}$ may represent disruption of C=O---H-O-C hydrogen bonds. If this is so, the most likely hydroxyl group to be involved in this hydrogen bonding scheme would be the hydroxyl group on the sphingosine chain, rather than a hydroxyl group associated with the galactose headgroup.

The characteristic shifts in the remaining C-O

stretching vibrations and the amide II peak are still seen upon quenching the samples. This implies that some kind of metastable cerebroside form is still formed under these conditions, in agreement with the DSC data. It must be stressed that this metastable state may not be the same as that produced by quenching of the pure cerebroside.

Similar effects are not observed until much higher concentrations of DPPC. The amide I component seen at 1615cm^{-1} in the stable state is not reduced to a shoulder until the concentration of DPPC is in the region of 50 mol%. A significant reduction in intensity has however occurred by 33 Mol % DPPC.

At 33 mol% cholesterol and DPPC, cerebroside bilayers exhibit very complex thermograms.In each case, the phase separation discussed above becomes even more enhanced. In the presence of 33 mol% cholesterol, an initial heating scan produces four endothermic transitions, the result of phase separation of cerebroside/cholesterol mixtures into four domains, presumably on the basis of cerebroside chain length. The high temperature of the fourth transition suggests that this phase does not contain cholesterol, but pure cerebroside. The peak temperature of this transition is higher than that observed for the pure cerebroside, even when some phase separation is apparent. Presumably, the phase giving rise to this high temperature transition contains cerebrosides with very long acyl chains, which do

not completely separate from shorter chain lengths and so give rise to lower temperature transitions in the pure lipid.

This cerebroside phase separates almost immediately upon cooling. The enthalpy change associated with this transition is very low, suggesting that only a small fraction of the cerebroside solidifies at this temperature. The remainder of the cerebroside solidifies still mixed with the cholesterol in a transition/transitions with reduced co-operativity such that no enthalpy change can be detected.

Reheating produces the characteristic exotherm, followed by multiple phase transitions due to phase separation on the basis of chain length as discussed above.

Similarly, 33 mol% DPPC produces phase separation into a number of cerebroside/ DPPC domains. As with 33 mol% cholesterol, at 33 mol% DPPC evidence of metastability is still evident. Thus reheating thermograms still show the characteristic exotherm and rearrangement of the cerebroside headgroup can be inferred from the FTIR spectra.

At 50 mol% cholesterol and DPPC, thermograms (Figure 3.2 and Johnston and Chapman, 1988) and FTIR spectra exhibit no features characteristic of formation of a metastable state. No rearrangement of the hydrogen bond network is apparent and no exothermic transitions are seen in reheating thermograms.

3.5 SUMMARY

The results presented in this chapter are in general agreement with other studies of cerebroside polymorphism (Freire et al 1980; Ruocco et al 1983). Rapid cooling of non-hydroxy fatty acid galactocerebrosides from above the phase transition temperature " freezes " the cerebroside in a metastable, high energy state. Conversion to the thermodynamically stable state occurs slowly at room temperature or in a rapid, cooperative manner at 50-60^{o}C. Conversion to the stable state is accompanied by the release of excess energy.

The metastable cerebroside state has an infrared spectrum which is markedly different to that of the stable form. The spectral differences have previously been suggested to arise from a rearrangement of the hydrogen bonding network involving the cerebroside headgroup (Lee et al 1986). The metastable cerebroside form has an infrared spectrum which exhibits striking similarities to the anhydrous material, suggesting that this hydrogen bond rearrangement is a result of a dehydration/rehydration cycle. Such a possible basis for cerebroside polymorphism has been suggested on the basis of X-ray diffraction and DSC studies (Ruocco et al.,1980; Curatolo, 1985; Miller and Bach, 1986)

Thermograms of cerebroside, cerebroside/cholesterol and cerebroside/DPPC mixtures indicate formation of multiple

domains. Such phase separation has not previously been described for pure cerebrosides. This separation is presumably related to the heterogeneous nature of the type II cerebrosides used in this study and may be a function of chain length, degree of unsaturation and/or position of the double bond in unsaturated chains.

As previously described, (Ruocco et al., 1983; Ruocco and Shipley, 1984) cholesterol and DPPC progressively broadened and decreased the enthalpy of transitions in thermograms. These changes were accompanied by changes in the infrared spectrum indicative of disruption of inter-cerebroside hydrogen bonding.

Metastability was still observed in cerebroside/cholesterol and cerebroside/DPPC dispersions until the cholesterol or DPPC content reached 50 mol%, at which point no rearrangement of the hydrogen bonding network or characteristic heating exotherm were seen.

FTIR spectroscopy has been shown to be a powerful accompaniment to the more often used technique of differential scanning calorimetry for studying lipid polymorphism. Whilst both techniques provide information concerning the onset and peak temperatures of lipid phase transitions, FTIR spectroscopy has the added advantage of giving information concerning hydrogen bonding of lipid headgroups, so allowing a more complete description of the molecular events underlying lipid phase transitions and

lipid polymorphism.

CHAPTER 4

FTIR SPECTROSCOPIC STUDIES OF CONFORMATIONAL TRANSITIONS IN POLYPEPTIDES

4.1:INTRODUCTION

Polypeptides have been used as potential models for protein structure for a number of years due to their ease of synthesis and relatively simple composition. One of the most widely used homopolypeptides for structural studies has been poly-L-lysine. Early work using circular dichroism spectroscopy showed that it was possible to convert poly-L-lysine to a number of conformations by adjustment of the pH of the solution (Townend et al 1966, Tiffany and Krimm 1969, Epand et al 1974). Thus, at pH 7.9 polylysine was observed to adopt an unordered configuration. Elevation of the pH to 10.8 induced a helical structure within the polypeptide. Further raising the pH to 11.5 followed by heating at 60^{o}C converted helical polylysine into a β-sheet form.

There has been considerable debate as to the exact structure adopted by the polypeptide chain at pH 7.9, with a number of authors suggesting that some degree of local order exists within the polypeptide chains (Tiffany and Krimm 1969). The similarity between circular dichroism spectra of polylysine at ph 7.6 and polyglycine II led Tiffany and Krimm to suggest that under these conditions polylysine contained regions of 3_1 helical structure. Proton magnetic resonance studies contradicted this proposal, suggesting no long or short range order exists in the polypeptide chain.

The conformational transitions discussed above were later shown to be accompanied by marked changes in the

infrared spectrum (Susi et al., 1967). However, these spectra were recorded in ^2H_2O using relatively crude instrumentation and very little data processing. The advent of FTIR spectroscopy and the development of digital subtraction routines allowed the study of biological materials in H_2O (Koenig and Tabb 1980). However, much of the early infrared work has yet to be repeated using the more sophisticated instrumentation and data handling techniques now available. The dependence of polypeptide conformation upon chain length has also yet to be fully investigated. The application of derivative and deconvolution routines may provide valuable information concerning the structure of these polypeptides.

The ease of interconversion of polylysine between its various structural forms provides a convenient model system for investigation of effects of variation in secondary structure upon such parameters as molar absorptivity. This is a problem currently assuming great importance in the structural analysis of proteins in view of the increasing application of curve fitting routines to the quantitative estimation of protein secondary structure content from infrared spectra (Byler and Susi 1986, Surewicz et al 1987, Yang et al 1987, Villalain et al 1989). Such routines use the positional information obtained from derivative and deconvolution spectra to generate a synthetic spectrum which matches the experimental spectrum by variation of bandwidths

and heights. The area of each component band in the analysis relative to the total area of the amide I band is taken to be a direct measure of the percentage of secondary structure giving rise to this band in the protein. An important assumption in this type of analysis is that each secondary structure has the same molar absorptivity. This assumption will be evaluated in this chapter.

This study was undertaken in collaboration with Dr. Parvez Haris of this department.

4.2 MATERIALS AND METHODS

Deuterium oxide (98 atom %), deuterium chloride (40% solution in ^2H_2O), sodium deuteroxide (40% solution in ^2H_2O), poly-l-lysine (molecular weight as determined by viscometry= 3,300, 24,000 and 271,00, all 98% pure) and poly-l-glutamate (molecular weight = 43,000) were purchased from Sigma Chemicals. Infrared spectra were recorded on a Perkin-Elmer 1750 FTIR spectrometer continuously purged with dry air.

Samples were injected into a sealed cell (Specac Ltd.) with constant path length (50um). Temperature was maintained with a circulating water bath. For each sample 100 scans were recorded at 20^oC and signal averaged at a resolution of 4cm^{-1}. Difference spectra were generated by digital subtraction of a spectrum of D_2O recorded under the same conditions as the sample spectra.

Samples were prepared for infrared red spectroscopy as follows. Poly-l-lysine was dissolved in D_2O to give a 2% solution by weight, with the pD (pD = pH meter reading) adjusted to 8.3 with NaOD. The pD of the solution was adjusted to 11.2 and spectra recorded. The solution was adjusted to pD 11.9, heated at 60^oC for 30 minutes, cooled to 20^oC and spectra recorded. For comparison purposes spectra of poly-glutamate (2% by weight) were recorded at pD 7 and 4.3.

The integrated area the amide I maximum in each

conformation of the polypeptide at a range of concentrations was calculated using the AREA routine supplied with the Perkin Elmer data Station.

RESULTS

Figure 4.1a shows the difference spectrum of poly-lysine (MW =24,000) in D_2O at pD 8.3. A broad band contour with band maximum at 1644cm^{-1} is seen. Application of second derivative routines reveals the presence of two bands, at 1666cm^{-1} and 1641cm^{-1} (fig. 4.1b). Spectra obtained in H_2O exhibited bands at 1677cm^{-1}, 1648cm^{-1} and around 1620cm^{-1}. A band due to carboxylate groups at the C-terminus of the polypeptide chain is seen at 1590cm^{-1}. This band is reduced in intensity as chain length is increased.

The difference spectrum of poly-lysine (MW=3,300) recorded at pD 11.2 is shown in Figure 4.2a. The amide I maximum is observed at 1638cm^{-1}. Higher molecular weight polymers also gave a band maximum at 1638cm^{-1}. Second derivative analysis of poly-lysine of molecular weight 3,300 (Fig 4.2b) reveals the presence of two bands, at 1662cm^{-1} and 1638cm^{-1}. The band seen at 1590cm^{-1} is from the carboxylate groups at the C-terminus of the helices. This is reduced in relative intensity as the polymer weight is increased. When the polypeptide molecular weight is increased to 24,000, bands are observed at 1670cm^{-1}, 1638cm^{-1} and 1623cm^{-1} with a shoulder at 1644cm^{-1} (Fig.4.3a). Further increase of the molecular weight of the polypeptide to 271,000 (fig 4.4b) gives rise to bands at 1670cm^{-1}, 1644cm^{-1}, 1638cm^{-1} and 1623cm^{-1} .

Figures 4.4a and 4.4b show the difference and

FIGURE 4.1: FTIR difference (a) and second derivative (b) spectra of polylysine (M_r =24,000) recorded at pD 8.3. Factor=13

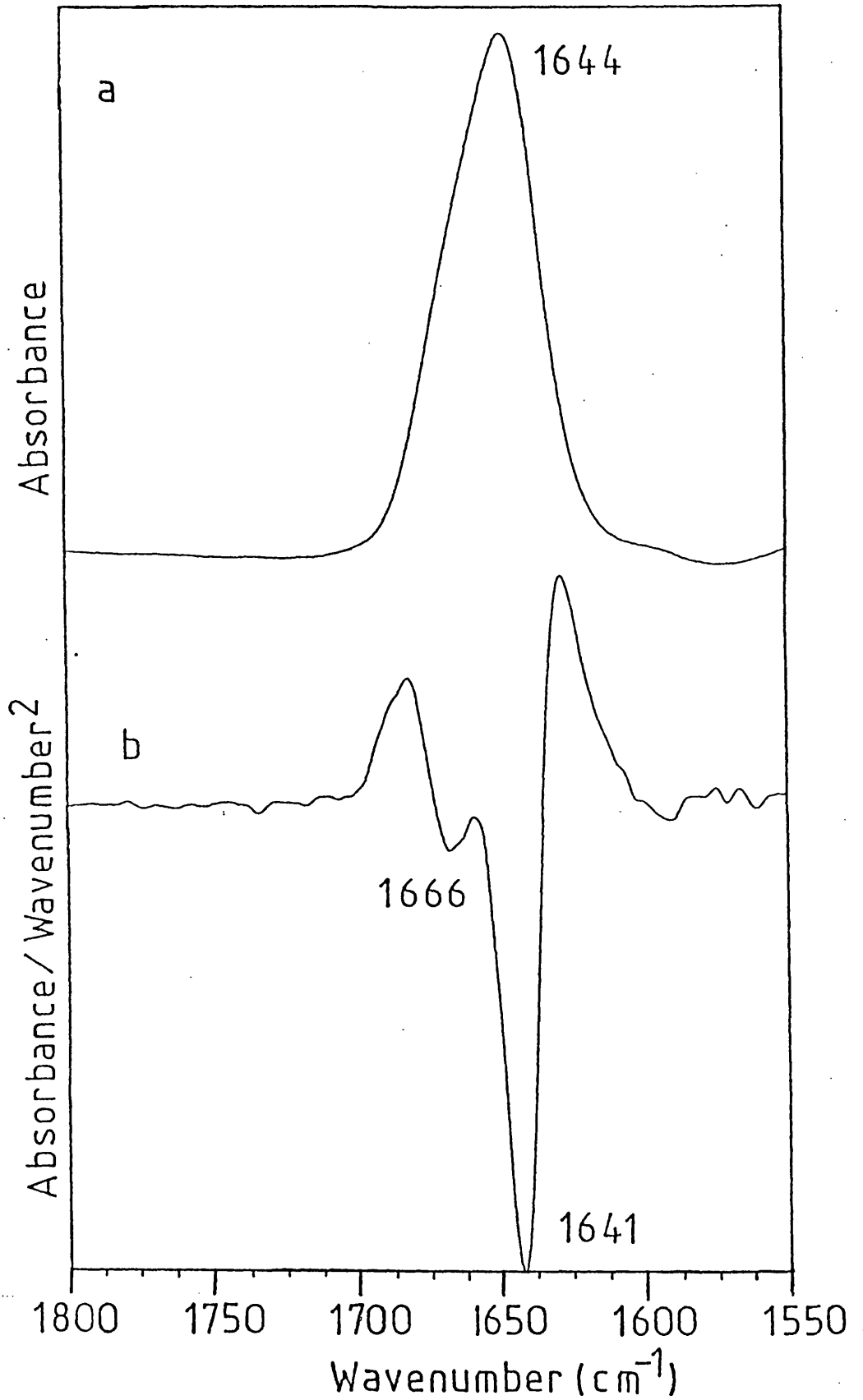
a
1644
Absorbance
b
1666
1641
Absorbance / Wavenumber^2
1800
1750
1700
1650
1600
1550
Wavenumber (cm^{-1})

FIGURE 4.2: FTIR difference (a) and second derivative (b) spectra of polylysine (M_r =3,300) pD 11.2. Factor=13

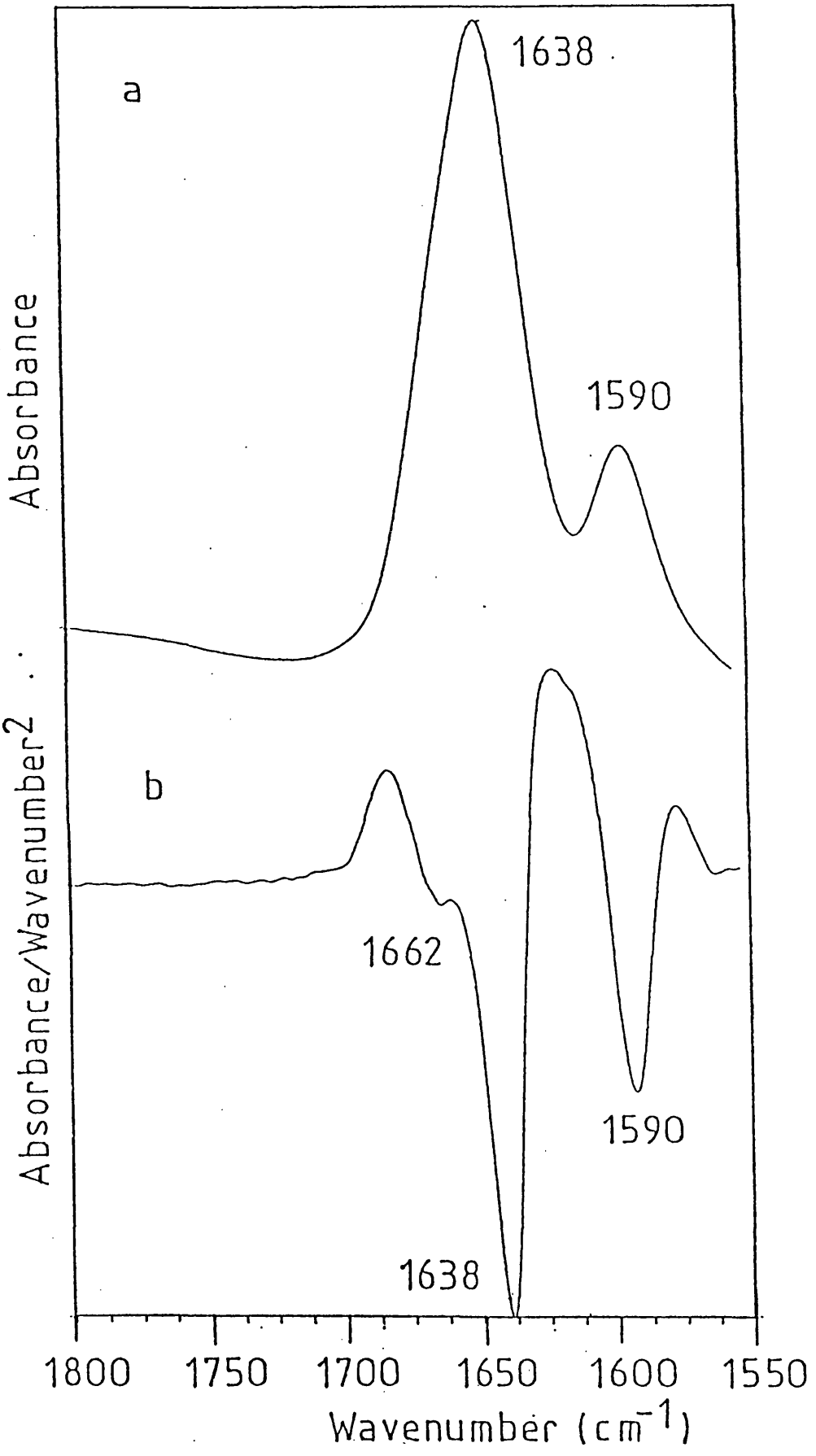
a
1638
1590
Absorbance
b
1662
1590
1638
Absorbance/Wavenumber2
1800
1750
1700
1650
1600
1550
Wavenumber (cm-1)

FIGURE 4.3: FTIR second derivative spectra of polylysine recorded at pD 11.2 (a) M_r =24,000 (b) M_r =210,000. Factor=13

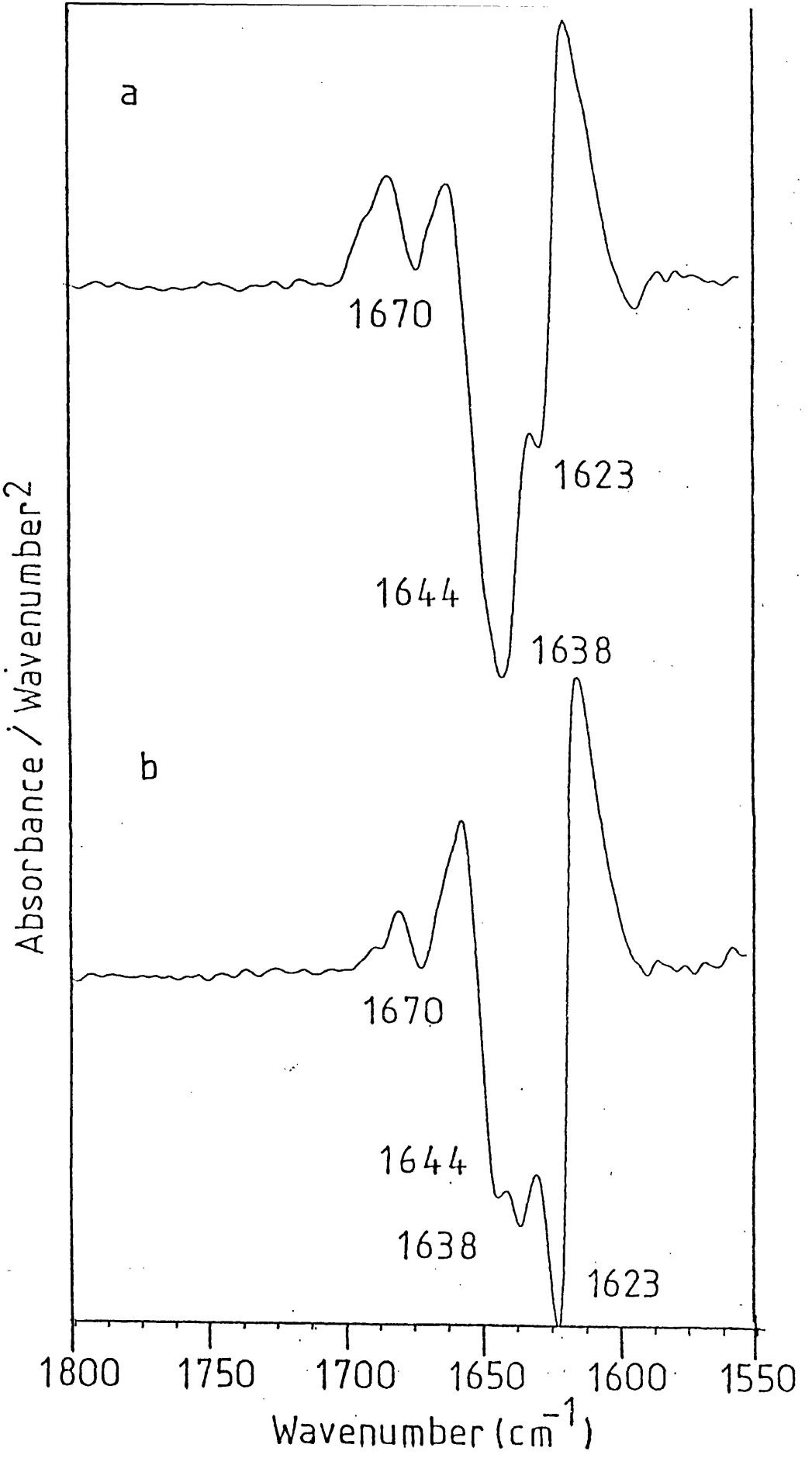
a
1670
1623
1644
1638
b
1670
1644
1638
1623
Absorbance / Wavenumber^2
1800
1750
1700
1650
1600
1550
Wavenumber (cm^{-1})

second derivative spectra of poly-lysine (MW =24,000) in D_2O at pD 11.9 after 30 minutes at 60°C. Further heating does not alter the spectrum. In the difference spectrum, two bands are observed at 1680cm^{-1} and 1610cm^{-1} The low frequency band is asymmetric suggesting the presence of an additional component between 1630-40cm^{-1}. Second derivative analysis reveals only two bands at 1680cm^{-1} and 1610cm^{-1}. Even after extensive heating and further elevation of the pD, the lowest molecular weight poly-lysine gave a spectrum identical to that shown in Figure 4.2a and so had not converted to β-sheet.The polypeptide of molecular weight 271,000 converted to β-sheet spontaneously upon increasing the pD to 11.9 and required no heating (difference and derivative spectra identical to fig 4.5)

The second derivative spectra of poly-glutamate are shown in Figure 4.5. At pD 7 (Fig. 4.5a) two bands are seen, at 1670cm^{-1} and 1644cm^{-1}. A band which we assign to ionised carboxylate side chains is seen at 1565cm^{-1}. A decrease in the pD to 4.3 gives a spectrum with bands at 1673cm^{-1}, 1651cm^{-1}, 1642cm^{-1} and 1623cm^{-1}. A group of bands assigned to unionised carboxylic acid side chains occur in the region 1740-1700cm^{-1}.

The area of the amide I band for poly-lysine a 2% solution of molecular weight 24,000 was calculated for the spectrum recorded at each pD using the AREA routine supplied with the Perkin-Elmer data station. This was not possible

FIGURE 4.4: FTIR difference (a) and second derivative (b) spectra of polylysine (M_r =24,000) pD 11.2 after heating at 60^{o}C for 10 minutes. Factor=13

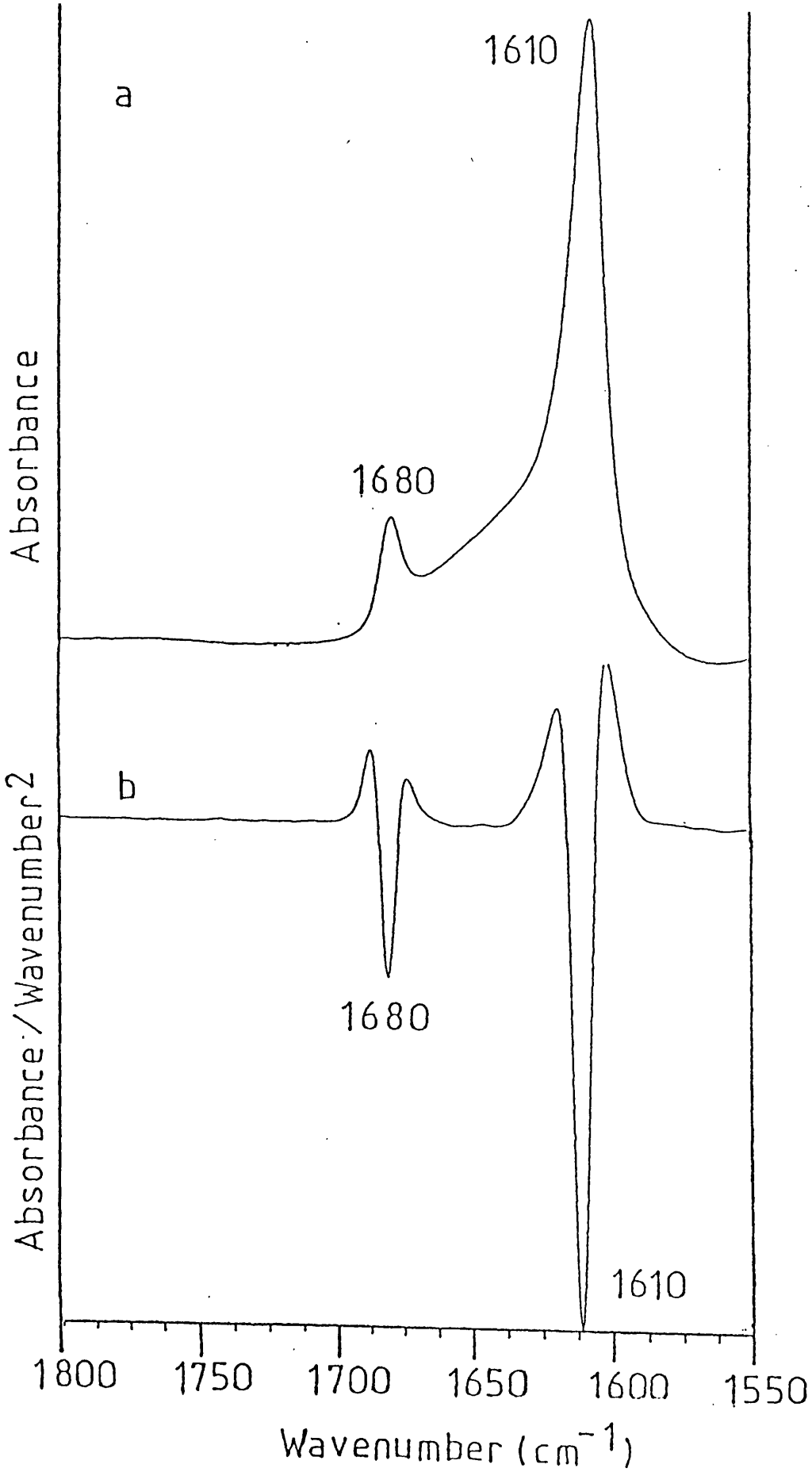
a
1610
1680
Absorbance
b
1680
1610
Absorbance / Wavenumber^2
1800
1750
1700
1650
1600
1550
Wavenumber (cm^{-1})

FIGURE 4.5: FTIR second derivative spectra of polyglutamate recorded at (a) pD 7 and (b) pD 4.3. Factor=13

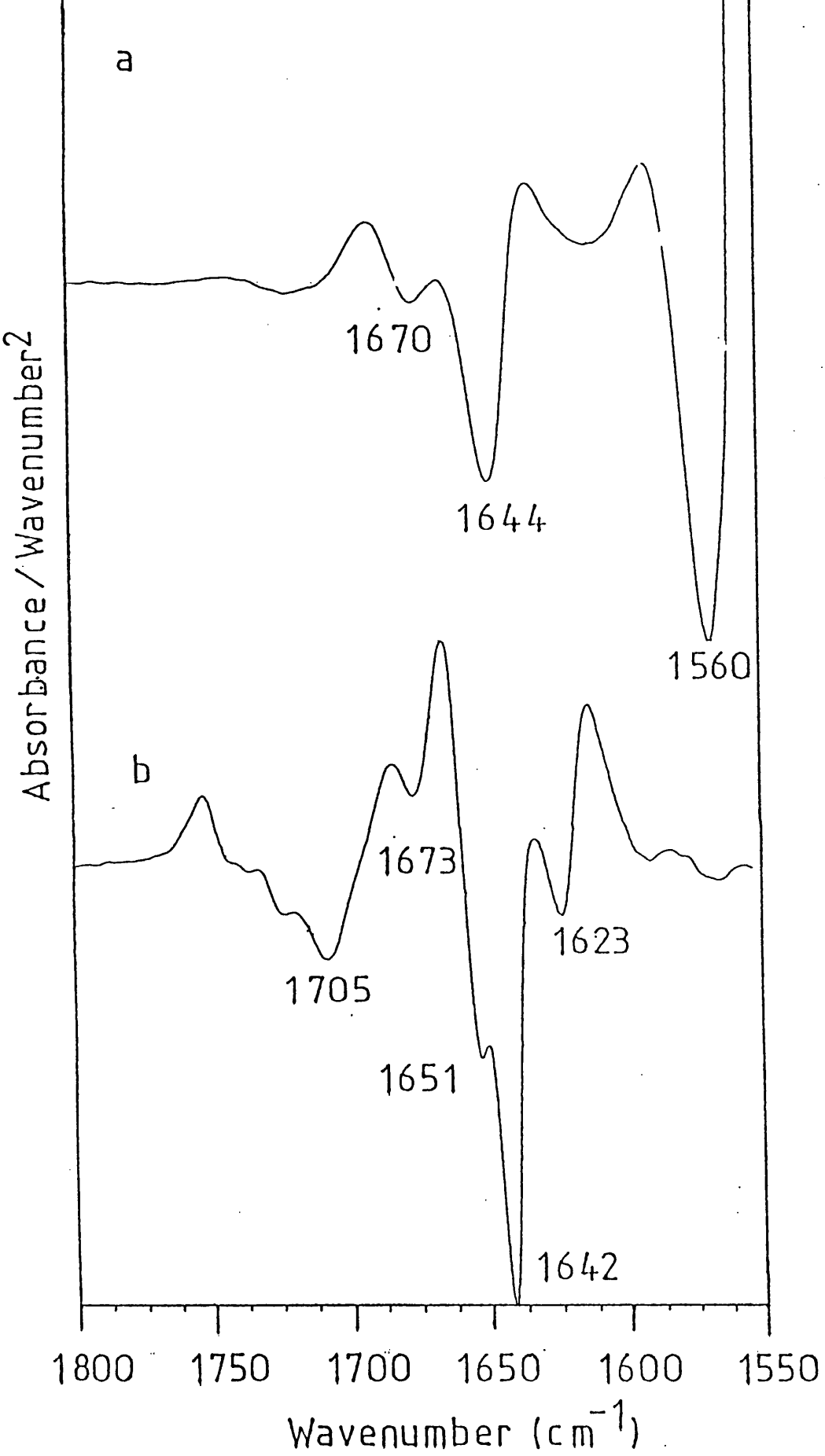
a
1670
1644
1560
b
1673
1705
1623
1651
1642
Absorbance / Wavenumber2
1800
1750
1700
1650
1600
1550
Wavenumber (cm-1)

for poly-glutamate due to the presence of the strong absorptions from the glutamate side chains. The results of these calculations are presented in Table I, normalised to values for the random conformation to account for any variation in pathlength and concentration in repeat experiments. The integrated area of the amide I band is the product of path length (l) molar absorptivity (ε) and concentration (c) in accordance with the Beer-Lambert law:

$$\text{ABSORBANCE} = \varepsilon lc \qquad (4.1)$$

As the pathlength and concentration are identical for each sample, this value is proportional to the molar absorptivity (ε). Thus any change in the integrated absorbance can be used to assess changes in molar absorptivity of the different structures.

Comparison of the integrated absorbances (table 4-I) indicates that random poly-lysine has a lower molar absorptivity (by about 13%) than α-helical poly-lysine, which in turn has a molar absorptivity 18% lower than that of β-sheet poly-lysine. Similar changes were observed in experiments conducted with 1% and 0.5% polylysine solutions.

STRUCTURE	AREA
RANDOM	1.0
α-HELIX	1.13 ± 0.04
β-SHEET	1.31 ± 0.11

TABLE 4-I: Integrated area of the amide I band of 2% solutions of poly-lysine in D_2O in random, helical and β-sheet forms. Results are the mean of 4 observations normalised to the random conformation.

DISCUSSION

Previous CD studies (Townend et al 1966, Tiffany and Krimm 1969, Epand et al 1974) with poly-lysine have shown that a variation in pH can induce different conformational states of the polypeptide. The FTIR spectroscopic results presented here show that as the pD is varied marked spectral changes occur.

Under conditions reported to favour the formation of a random structure the absorbance spectrum of poly-lysine in D_2O exhibits a strong absorption at $1644cm^{-1}$. However with the calculation of the second derivative the broad band contour is resolved into two components (see Figure 4.1b). The main band at $1641cm^{-1}$ can be assigned to the presence of random structures, but the assignment of the band at $1666cm^{-1}$ is uncertain. An examination of the derivative spectrum of poly-glutamate under conditions considered to favour the production of a random structure (Townend et al 1966) shows two bands at similar frequencies. One possible conclusion from this is that the random structure of this polypeptide is characterised by two bands.

However an alternative explanation is that some kind of additional ordered structure is present in the system at this pD. Both turns and 3_{10} helices have been reported to absorb in this spectral range (Krimm and Bandekar 1986, Yasui et al 1986, Kennedy et al manuscript in preparation). Some workers have suggested, based upon a) Raman band

widths, b) the difference in amide I maxima in Raman and infrared spectra and c) comparison of the effects upon CD spectra of various salts and the incorporation of D-amino acids into the polypeptide chain (Painter and Koenig, 1976) that the random chains of poly-lysine and poly-glutamate are interrupted by regions of extended or 3_1 helices. However the amide I maximum of polyglycine II (which exists as a left handed 3_1 helix) has been observed at 1644cm^{-1}. It is therefore difficult to imagine a band at 1666cm^{-1} in the spectrum of polylysine arising from regions of 3_1 helix within the polypeptide chain.

Under conditions which are reported to favour the formation of a helical structure as deduced from CD spectroscopy (Townend et al 1966, Tiffany and Krimm 1969) the FTIR difference spectrum shows an amide I maximum at 1638cm^{-1}. This amide I band maximum is at a lower frequency than the amide I band usually associated with proteins known from X-ray diffraction to contain α-helical structures (1650-1657cm^{-1}). It may be suggested that this may reflect the presence of an unusual helical structure e.g. α_{II} or 3_{10} type structures. However, proteins and peptides which contain such unusual helical structures have been shown by Dorian Kennedy working in this laboratory in conjunction with Professor Claudio Toniollo in Padua and on the basis of theoretical studies (Krimm and Bandekar 1986) to show significantly higher amide I maxima (1660-1666cm^{-1}).

The rather low band frequency observed with polylysine may reflect a higher degree of regularity in polylysine helices as compared to α-helical structures in proteins, allowing stronger hydrogen bonds to be formed in the polypeptide. Furthermore, the heterogeneous amino acid composition of a protein is likely to disrupt the inter and intrachain coupling which occurs with homopolypeptides. Homopolypeptides such as polylysine may also be significantly more hydrated than a protein thereby causing a decrease in the amide I frequency. The effect of hydration upon the amide I maximum is discussed in more detail in chapter 5.

Upon increasing the polylysine molecular weight from 3,300 to 24,000 numerous bands become apparent in spectra enhanced by the use of derivative routines (Figure 4.3). There are a number of potential explanations for these additional bands which need discussing:

i) It is possible that an equilibrium exists between polypeptide chains in a random and helical structure (or that an equilibrium between random and helical structures exists within the chains). However, none of the additional bands seen in Figure 4.3 coincide with bands which are seen in the spectrum of the random polypeptide (see Figure 4.1).

ii) An equilibrium occurs between the polypeptide chains in the β-sheet conformation and α-helical conformation (or such an equilibrium exists within the chains). However,(see

figure 4.4), the frequencies characteristic of the β-sheet conformation do not correspond to the additional bands which are observed in Figure 4.3.

iii) The additional bands are due to turns. It is known that turns can produce bands at 1670cm^{-1} and 1623cm^{-1}. However turns are sterically demanding and it is unlikely that poly-lysine can form such structures.

iv) The additional bands arise from helical structures of slightly different hydrogen bonding characteristics, possibly due to disruption of the hydrogen bonding in regions of the chain which become folded or twisted as the chain becomes longer or the result of variations in the interactions of the side chains with the helix.

It is the latter explanation which seems most likely.

From CD spectroscopy the formation of β-sheet poly-lysine is known to be induced by elevation of the pD to 11.9 followed by heating (Townend et al 1966, Tiffany and Krimm 1969, Epand et al 1974). However conversion from the helical to β-sheet conformation appears to be very dependent upon chain length. In this study the poly-lysine of shortest chain length shows no conversion even after prolonged heat treatment, while the longest chain length poly-lysine showed spontaneous conversion upon elevation of the pD even without heating. Unfolding of α-helices will be favoured by an increase in the length of the polypeptide chain which decreases the stability of the helix. This is a result of

bending an twisting of the helix, weakening the hydrogen bonds. The short polypeptide chains used in this study will therefore form very stable helices which cannot be unfolded under the conditions described here.

Under conditions reported to favour the β-sheet conformation the difference and second derivative spectra of β-sheet poly-lysine show only two bands. However inspection of the difference spectrum reveals an asymmetry in the component at 1610cm^{-1}. This suggests the presence of a further band near 1630-1640cm^{-1}. Probably due to the intensity and narrowness of the main component second derivative and deconvolution routines are unable to resolve this band. It is interesting to note that in an earlier study of polypeptides and proteins in the β-sheet conformation, analysis of the amide I band by curve fitting produced good agreement between synthetic and experimental curves for β-sheet poly-lysine by including a band at 1638cm^{-1} in the calculations (Chirgadze et al., 1973). The occurrence of a band in this position may be due to the presence of a range of chain lengths in our samples, this band arising from a small amount of low molecular weight polypeptide which does not convert to the β-sheet conformation.

As with the α-helical conformation of polylysine, the band frequencies observed in the spectra of "β-sheet" polylysine vary significantly from the frequency reported

for predominantly β-sheet proteins such as concanavalin A, ribonuclease A, immunoglobulin G and chymotrypsin (Alvarez et al 1987; Haris et al 1986a) . Again, this may reflect the homogeneous composition of the polypeptide. However, it is also possible that the unusual frequency of these bands is a result of the formation of an atypical β-sheet structure. The increased viscosity and turbidity of polylysine solutions under these experimental conditions suggests the possibility of aggregation. Thus, the unusual frequency of these bands is discussed in terms of intermolecular hydrogen bonding in chapter 7. It is envisaged that as the state of ionisation of the side chains changes and the temperature is increased, the helical structures become unstable and unfold. Intermolecular hydrogen bonds are then formed between neighbouring polypeptide chains, forming an intermolecular β-sheet.

The ease of interconversion of polylysine between its various structural forms provides a convenient model for assessing the effects of structural variation upon such parameters as molar absorptivity. In most curve fitting routines applied to the quantitative analysis of protein secondary structure the area of each computed band in the analysis is taken to be a direct quantitative measure of the structure giving rise to this band, with each secondary structure having equal molar absorptivity. Empirical observations have tended to support this view, with good

agreement being observed for a number of water soluble proteins (Byler and Susi, 1986) between quantitative data obtained from FTIR spectroscopy and results from X-ray diffraction of single crystals. The calculations presented here (Table 4-I) show a variation in integrated area with structural change which can be related to a change in molar absorptivity. Upon transition from a random to a helical conformation a 13% increase in area/molar absorptivity is noted. A previous infrared study of poly-lysine suggested a large increase (about 50%) in molar absorptivity upon conversion from α-helix to β-sheet (Chirgadze et al 1973). In the present study we observe an increase only of the order of 18%. The reason for this discrepancy is not clear. Since this work was completed, a similar study (Mantsch and Casal, 1989) has been published, corroborating the trend observed here.

The molar absorptivity of various secondary structures needs to be born in mind when quantitative analysis of protein secondary structure is made using this spectroscopic approach.

CONCLUSIONS

The application of IR spectroscopy to the study of conformational transitions in polypeptides has been extended in this chapter. Under conditions which were believed to induce only one type of secondary structure in polylysine and polyglutamate chains, derivative analysis revealed the presence of numerous bands.

For helical polypeptides the number of bands seen in derivative spectra was markedly dependent upon chain length. As the chain length increased, so the number of bands increased. This was attributed to the introduction of distortions within the helix induced by twisting and bending as the chain becomes progressively longer.

The β-sheet conformation of polylysine was characterised by two sharp bands at frequencies somewhat different from those seen in proteins known to contain β-sheet structures. This finding can be explained on the basis of the production of an intermolecular β-sheet, due to the unfolding of the helices and hydrogen bond formation between neighbouring strands. This structure could not be induced shortest chain length polylysine. This is presumably the result of the greater stability of the shorter helical segments; as the helix becomes twisted as bent upon increasing the chain length, so the hydrogen bonding scheme will be disrupted and the helix destabilised, allowing unfolding at elevated temperatures.

Calculation of the area of the amide I band for each conformation of polylysine yielded significant variations with secondary structure. This variation must be a result of a change in the molar absorptivity of the protein as the conformation is altered, as the pathlength of the cell and concentration of the solutions was identical within each experiment. This result contradicts the empirical correlations established between infrared secondary structure calculations and X-ray diffraction structures (Byler and Susi, 1986), but has been confirmed independently by Mantsch and Casal (1989). Such changes in molar absorptivity render curve fitting routines inadequate for the quantitative analysis of protein secondary structure by infrared spectroscopy.

CHAPTER 5

SOLUTION CONFORMATION OF PARVALBUMIN, CALMODULIN AND TROPONIN C DETERMINED BY FTIR AND CD SPECTROSCOPY

5.1.INTRODUCTION

Ca^{++} ions represent one of the most important and widespread physiological triggers and are involved in processes as diverse as fertilisation (Tyler, 1941; Metz and Morroy 1985), cell growth (Metcalfe et al., 1986), endocytosis and exocytosis (Rubin, 1982; Baker and Knight, 1986), muscular contraction (Ebashi et al., 1969), blood coagulation (Esnouf, 1985), intermediate metabolism (Case, 1980; Picton et al., 1981) and mediation of hormone and neurotransmitter release and action (Mauger et al., 1985).

Many of the physiological effects of Ca^{++} are mediated (via binding to target proteins such as calmodulin) following stimulation of cells by hormones or neurotransmitter (Rasmussen and Barrett, 1988). With reference to Figure 5.1, this can be achieved in two ways. The simplest, and quickest, way to induce a Ca^{++} initiated response is to open specific Ca^{++} channels in response to ligand binding. Ca^{++} then diffuses into the cell down a large (x10,000) concentration gradient. This then forms a cytoplasmic Ca^{++} pool available for interaction with target proteins such as calmodulin, producing a rapid, transient response. Alternatively, ligand binding to receptors may result in the activation of a membrane associated phosholipase C, which hydrolyses membrane phosphatidyl inositol bis-phosphate to (1,4,5)-inositol trisphosphate.

FIGURE 5.1: Generation of the Ca^{++} transient.

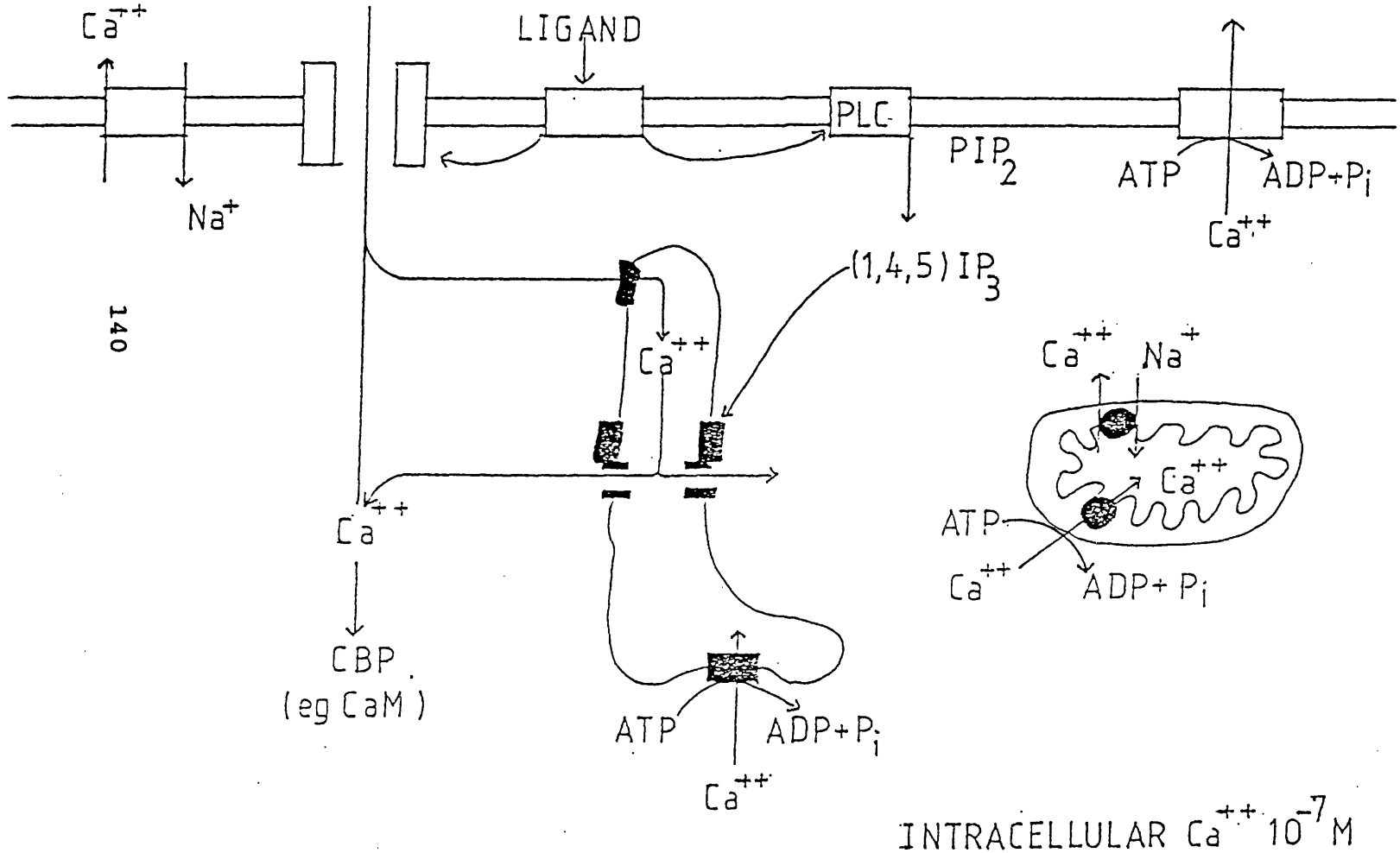
EXTRACELLULAR Ca^{++} 10^{-3}M
Ca^{++}
Na^{+}
LIGAND
PLC
PIP_2
ATP
ADP+P_i
Ca^{++}
(1,4,5) IP_3
Ca^{++}
Ca^{++}
Na^{+}
Ca^{++}
ATP
Ca^{++}
ADP+ P_i
Ca^{++}
CBP
(eg CaM)
ATP
ADP+P_i
Ca^{++}
INTRACELLULAR Ca^{++} 10^{-7}M

This substance is a potent stimulator of Ca^{++} release from storage sites within the endoplasmic reticulum. This Ca^{++} is then available for interaction with target proteins. Responses initiated via this second mechanism are slower and more prolonged.

Of the many cytosolic proteins targeted by Ca^{++} the EF-hand proteins are by far the most widely studied (Kretsinger and Nockolds, 1973; Kretsinger 1980, Babu et al., 1985; Hertzberg and James, 1985; Chiba and Mori, 1989). These are a homologous family of evolutionally related proteins containing the helix-loop-helix or EF-hand supersecondary structure. The first EF-hand protein to be crystallised and its structure described using X-ray diffraction was the Ca^{++} chelating protein parvalbumin (Kretsinger and Nockolds, 1973; Moews and Kretsinger, 1975). Parvalbumin was shown to consist of six helical segments labelled A-F, helices A and B, C and D and E and F separated by loops containing some 12 amino acids, many of which are acidic and are involved in Ca^{++} coordination (see Fig. 5.2). The helices are oriented approximately perpendicular to each other. The C-D and E-F loops (but not the A-B loop) each bind one Ca^{++} ion. The E helix, EF loop and F helix resemble the extended forefinger, clenched middle finger and extended thumb of a right hand and this is the structural motif referred to as the EF-hand. The CD and EF hands are held in

FIGURE 5.2: The E-F hand structural motif

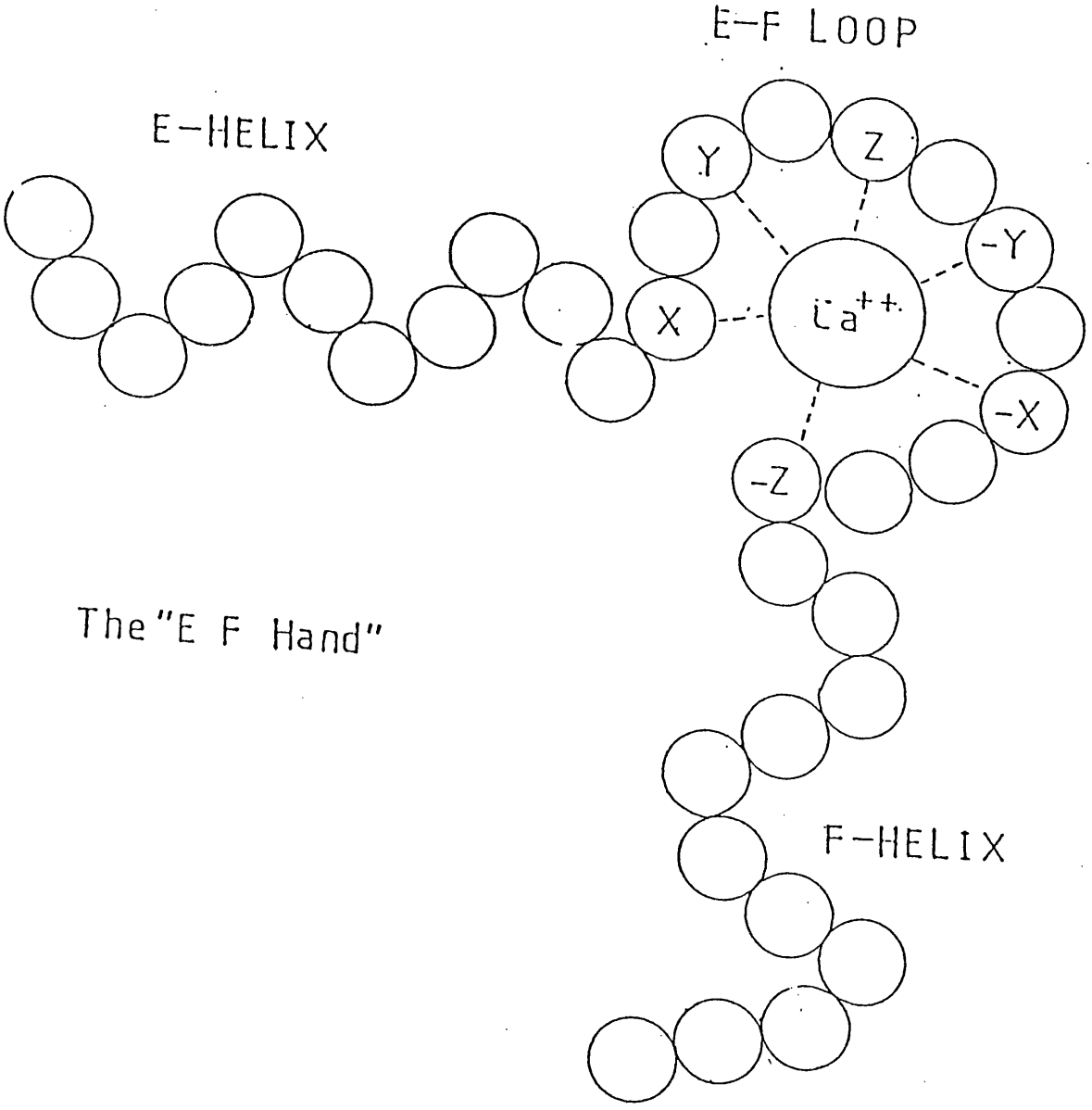

The "E F Hand"

the correct orientation by two β-sheet hydrogen bonds between isoleucine-97 and isoleucine-58 and leucine-77 and lysine 64.

Subsequent to the elucidation of the crystal structure of parvalbumin, a range of proteins were suggested to contain the EF-hand domain, primarily on the basis of amino acid sequence homologies. These proteins include troponin C (Collins et al., 1973; Weeds and McLachlan, 1974), calmodulin (Dedman et al., 1978) and intestinal calcium binding protein (Hoffman et al., 1977). The highest degree of homology is seen between parvalbumin, calmodulun and troponin C. Sequence homology with ICBP is limited to the Ca^{++} -binding domains (Kretsinger, 1980).

Troponin C contains 162 amino acids and is one of three proteins, together with troponin I and troponin T, which make up the troponin complex in skeletal and cardiac muscle. The troponin complex plays a vital role in the regulation of muscular contraction and it is troponin C which confers the Ca^{++} sensitivity to the contractile process (Weber and Murray, 1973). In the resting muscle fibre, troponin I is tightly bound to actin and troponin T to tropomyosin. Tropomyosin covers the myosin binding sites on the actin filaments. Ca^{++} binding to troponin C weakens binding of troponin I to actin, allowing lateral movement of the troponin-tropomyosin complex, thus revealing the myosin

binding sites on the actin filaments and allowing the interactions necessary for generation of tension.

X-ray diffraction analysis of crystals of troponin C (Hertzberg and James, 1986) indicates an elongated dumbbell shaped molecule, some 70Å in length, two globular domains being separated by an eight turn α-helix. The globular domains each contain two helix-loop-helix structural motifs, The AB, CD (NH_3^+ terminus) EF and GH (COO^- terminus) hands. Only the EF and GH hands bound Ca^{++} in the crystals studied.

X-ray diffraction data for calmodulin, a multi-function regulatory protein of 124 amino acids (MW 17,000) indicates a structure remarkably similar to that obtained for troponin C. Seven helical structures are seen , labelled I-VII (Babu et al., 1985; Babu et al., 1988). As in troponin C, four Ca^{++} binding domains of the EF-hand type are seen, pairs of domains being separated by a seven turn α-helical linking region. the length of the calmodulin molecule is somewhat less than the troponin C molecule, at 65Å. The Ca^{++} binding loops 1 and 4 are similar to those in parvalbumin but loops 2 and 3 differ in that they share helix IV.

Although detailed X-ray diffraction data is available for a number of EF-hand proteins, this data relates to a static, Ca^{++} loaded structure. Crystallographic data cannot provide information concerning the native, non-Ca^{++} loaded state,the effects of Ca^{++} upon the secondary structure of

the protein, or information relating to the effects of Ca^{++} on protein stability. Such studies rely on spectroscopic techniques, which can probe the conformation of proteins in an aqueous environment in the presence and absence of Ca^{++}. A number of these spectroscopic techniques have recently been applied to the study of EF-hand proteins, including fluorescence (Baudier et al., 1986), CD (Closset and Gerday, 1975) and FTIR spectroscopy (Haris et al., 1987, Trewhella et al., 1989).

In general, agreement between the spectroscopic techniques has been good. A predominantly helical structure is proposed for all EF-hand proteins studied in the Ca^{++} loaded state, in agreement with X-ray diffraction data. Removal of Ca^{++} leads to a decrease in the proportion of helical structures within the molecule.

Discrepancies between X-ray diffraction results and other techniques have recently been reported. Thus, Heidorn and Trewhella (1988) reported X-ray solution scattering data for parvalbumin and troponin C which was inconsistent with the available X-ray diffraction data for these proteins. While the general dimensions of the globular domains were similar in crystals and in aqueous solution, the centres of mass of the domains were found to be 5Å closer in solution and the distance of closest approach reduced by 10Å. This suggests the possibility of a bend in the helical linking

segments.

FTIR spectroscopic studies of calmodulin (Haris et al., 1987; Trewhella et al., 1989) and troponin C (Haris et al., 1987) have demonstrated an unusual feature of the infrared spectrum of these proteins, namely a markedly lower amide I maximum in ^2H_2O solutions than has previously been observed for predominantly α-helical proteins. This has been attributed to the presence of an unusual type of helical structure (Trewhella et al., 1989).

The infrared spectra of parvalbumin, calmodulin and troponin C are investigated in this chapter. The discrepancy between FTIR spectroscopy and other techniques with respect to the structure of EF-hand proteins will be investigated.

This work was undertaken in collaboration with Dr. Parvez Haris of this department and Dr. S. R. Martin and Dr. P. Bayley of N.I.M.R., Mill Hill, London.

5.2. MATERIALS AND METHODS

Parvalbumin and ^2H_2O were purchased from Sigma. Calmodulin and troponin C were the generous gifts of Prof. Sarzala Gabriella.

Samples were prepared for infrared spectroscopy as follows. Protein solutions (0.25-2.0% w/v) were prepared in ^2H_2O or H_2O buffers containing either 5mM Ca^{++} or 5mM EGTA, 200mM phosphate, and the pD (or pH) adjusted to 5.5, 7.5 or 9.5. Approximately 40μl of each sample was placed between a pair of CaF_2 windows separated by a 50μm tin spacer. The windows were mounted in a Beckman FH-01 cell holder and temperature maintained at 20^{o}C or 70^{o}C by a circulating water jacket. For each sample 100 scans were recorded at a resolution of 4cm^{-1} and signal averaged. Difference spectra were generated by the digital subtraction of the appropriate buffer spectrum.

Circular dichroism measurements were performed by Drs. Stephen Martin and Peter Bayley at the National Institute for Medical Research, Mill Hill, London. Spectra were recorded on a Jasco 600 CD spectrometer at concentrations ranging from 0.02-2.0% w/v, in H_2O and ^2H_2O buffers.

5.3 RESULTS

5.3.1.FTIR spectroscopy

5.3.1.1. EFFECT OF pH UPON INFRARED SPECTRA RECORDED IN H_2O

The difference spectrum of parvalbumin and calmodulin in H_2O, 5mM EGTA, pH 5.5 are shown in Figure 5.3. The amide I maximum was observed at 1654cm^{-1} for parvalbumin and 1653cm^{-1} for calmodulin. Deconvolution (Fig. 5.4) and second derivative analysis of the amide I band of both proteins revealed the presence of further bands, situated at 1670cm^{-1} and 1630cm^{-1} for parvalbumin and 1676cm^{-1}, 1666cm^{-1} and 1632cm^{-1} for calmodulin. Similar spectra were obtained at pD 7.5 and 9.5 (not shown).

5.3.1.2. EFFECT OF pD UPON INFRARED SPECTRA RECORDED IN ^2H_2O

The spectrum obtained 15 minutes after dissolution of parvalbumin in ^2H_2O, pD 5.5 in the presence of 5mM EGTA is shown in Figure 5.5. The amide I maximum is now seen at 1651cm^{-1}, with the amide II band much reduced in intensity. In deconvolved spectra (Fig. 5.6a), the major amide absorption is seen at 1650cm^{-1}. Further bands are seen at 1632cm^{-1} and 1666cm^{-1}. A shoulder is apparent at 1644cm^{-1}. Similar spectra were obtained at pD 7.5 (Fig. 5.6b).

Upon elevation of the pD to 9.5, spectra recorded 15 minutes after dissolution exhibited an amide I maximum in difference spectra at 1644cm^{-1}. Deconvolution analysis (Fig. 5.6c) revealed the presence of a major component at 1644cm^{-1}

FIGURE 5.3: FTIR difference spectra of parvalbumin (solid line) and calmodulin (broken line) in 5mM EGTA, pH 5.5, 20^{o}C

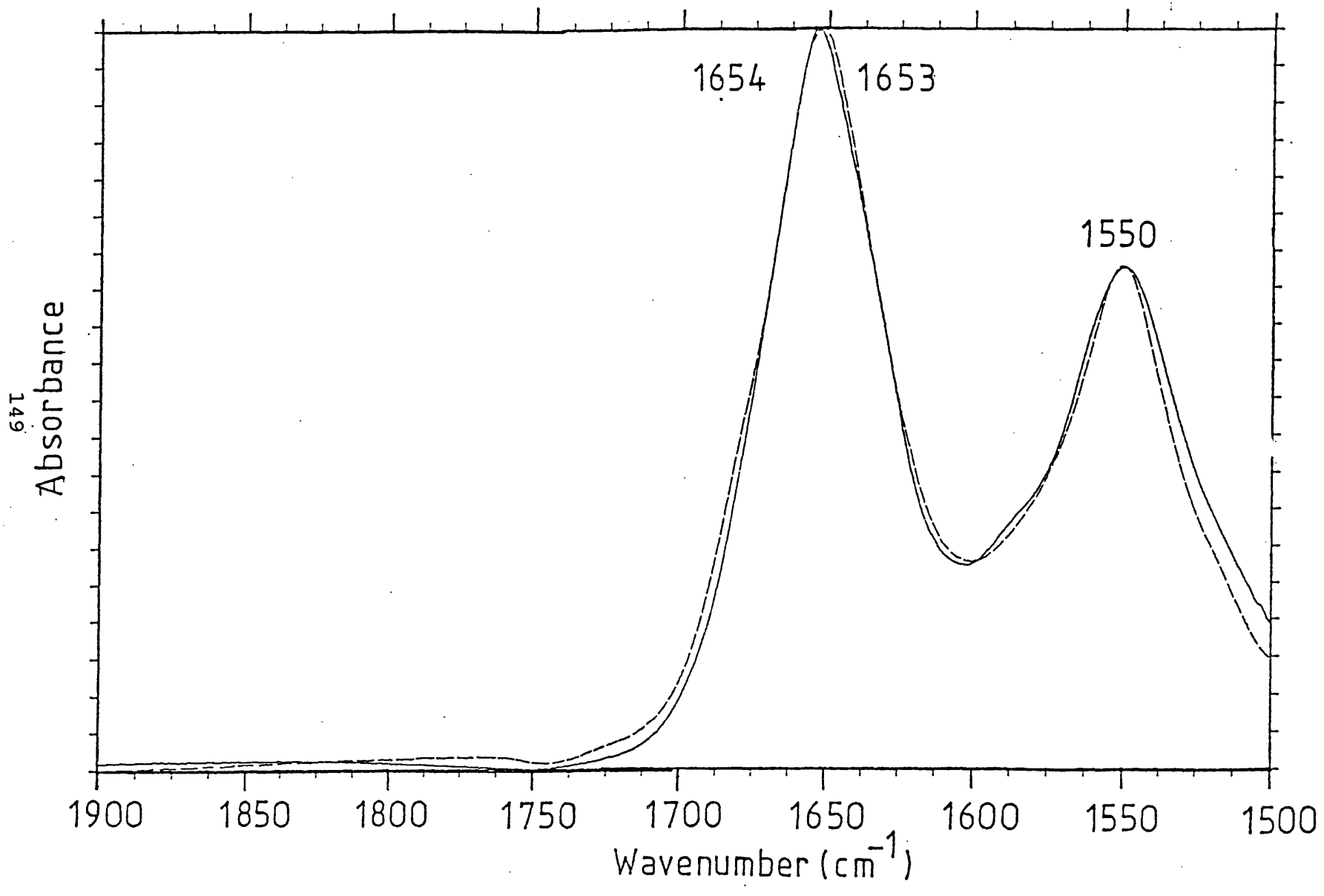
1654
1653
1550
Absorbance
149
1900
1850
1800
1750
1700
1650
1600
1550
1500
Wavenumber (cm^{-1})

FIGURE 5.4: Deconvolved (F=2.5 W=16) spectrum of parvalbumin (a) and calmodulin (b) in 5mM EGTA, pH 5.5, 20^{o}C

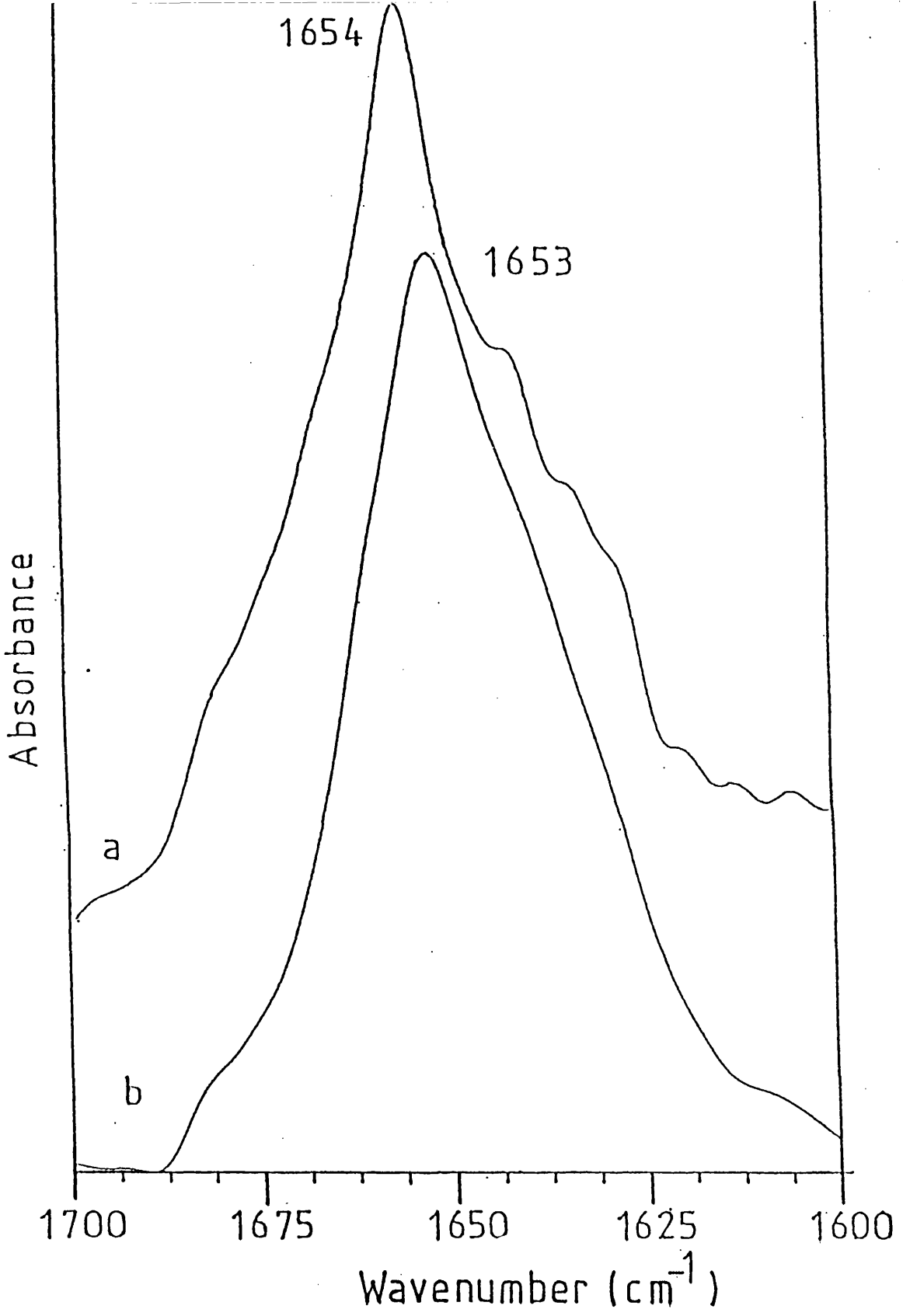
1654
1653
Absorbance
a
b
1700
1675
1650
1625
1600
Wavenumber (cm^{-1})

FIGURE 5.5: Difference spectra of parvalbumin (solid line) and calmodulin (broken line) in ^2H_2O recorded 15 minutes after dissolution

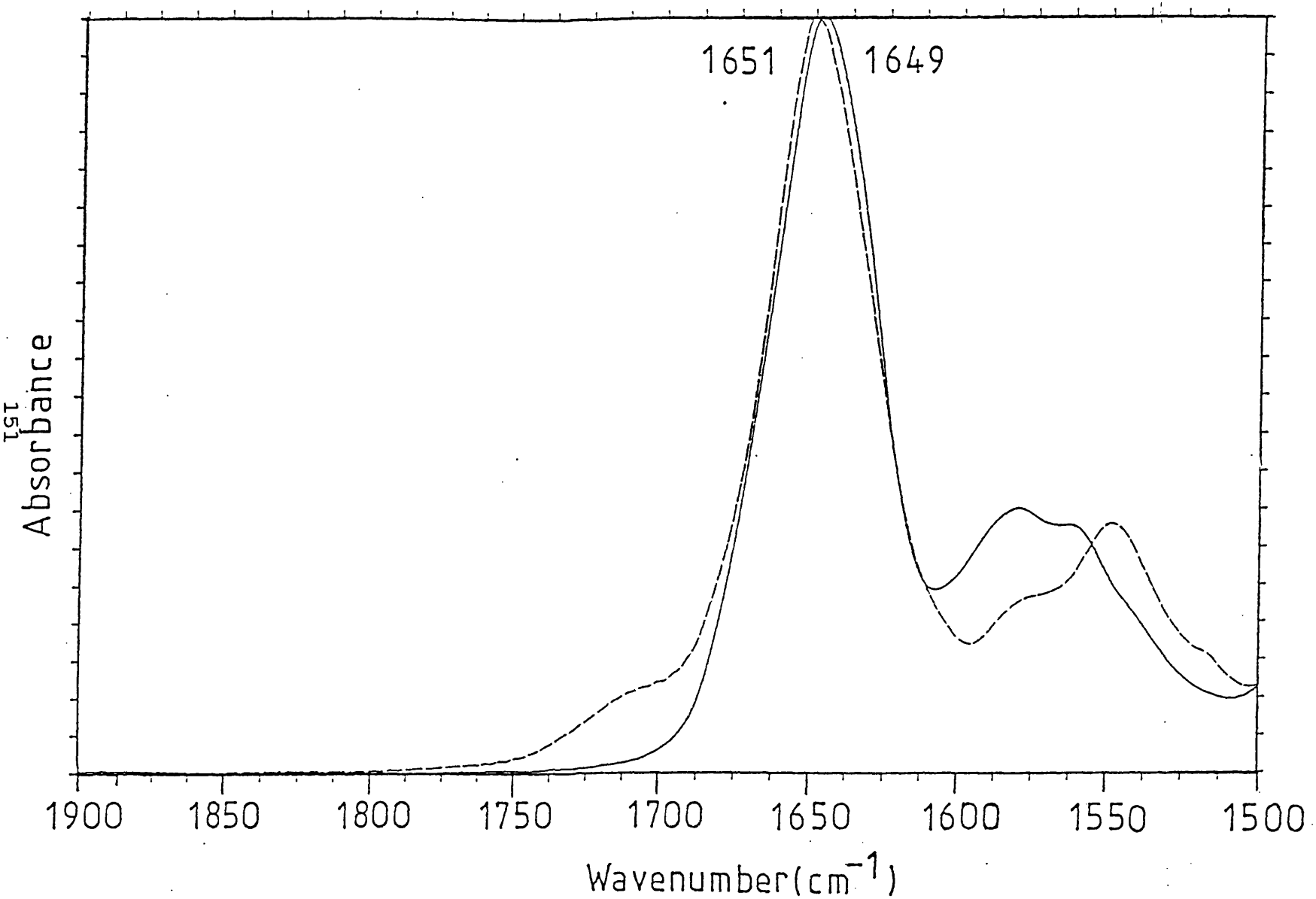
1651
1649
Absorbance
151
1900
1850
1800
1750
1700
1650
1600
1550
1500
Wavenumber(cm^{-1})

FIGURE 5.6: Deconvolved (F=2.5 W=16) spectra of parvalbumin recorded at pD 5.5 (a), pD 7.5 (b), pD 9.5 (c) and pD 5.5 48hrs after dissolution (d) in 5mM EGTA, 20^{o}C.

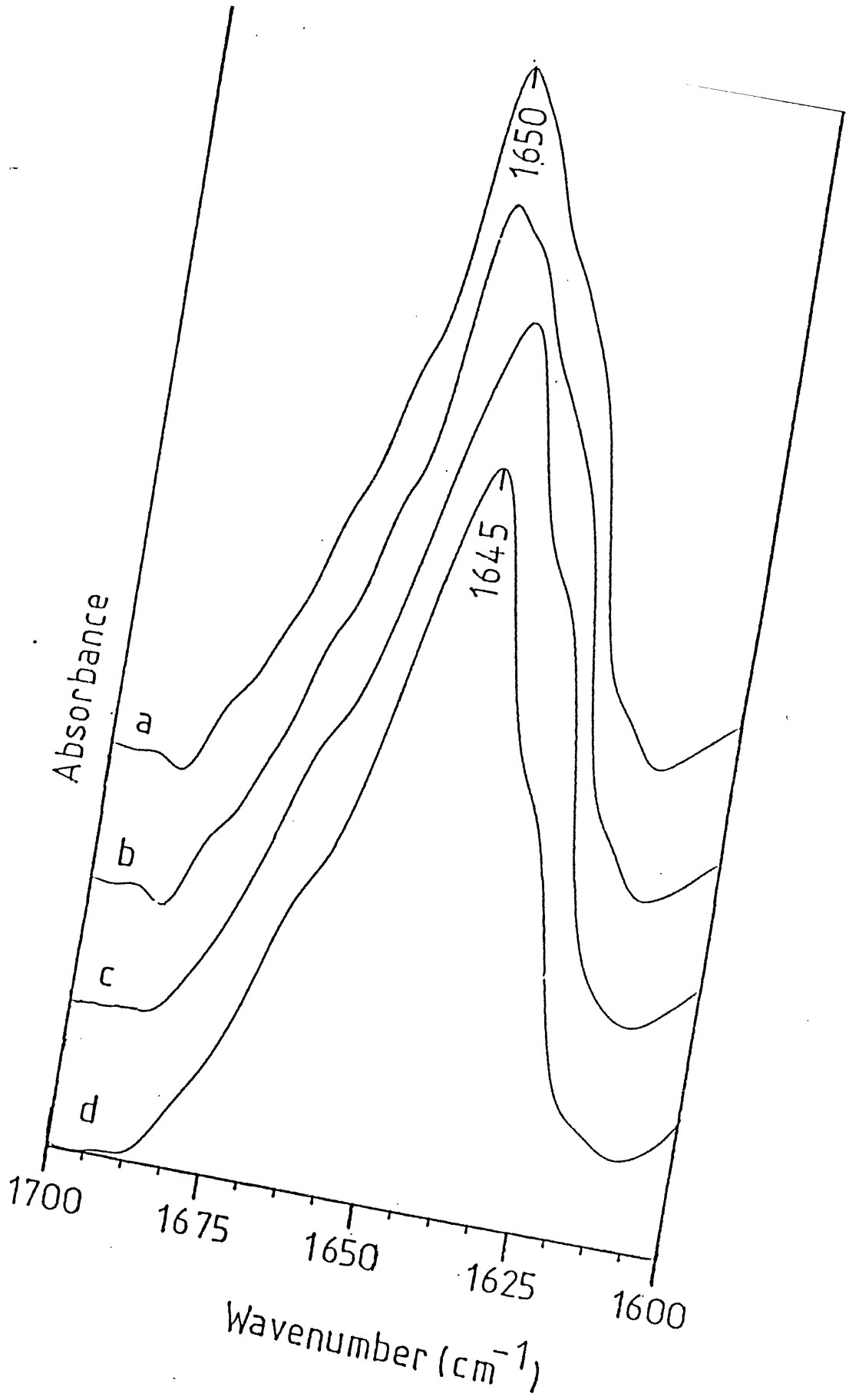
Absorbance
a
b
c
d
1650
1645
1700
1675
1650
1625
1600
Wavenumber (cm⁻¹)

with minor absorption at 1666cm^{-1} and 1632cm^{-1}. No residual amide II band was apparent.

The deconvolved spectrum of parvalbumin recorded at pD 5.5 in 5mM EGTA 24 hours after dissolution is shown in Figure 5.6d. The major absorption occurs at 1644cm^{-1} with minor bands at 1666cm^{-1} and 1632cm^{-1}. Identical spectra were obtained at pD 7.5 and 9.5 24 hours after dissolution. Similar spectra were recorded for calmodulin and troponin C after extended deuteration, with a major amide I absorption at 1644cm^{-1}.

5.3.1.3. EFFECT OF Ca^{++} UPON THE INFRARED SPECTRUM

In the presence of 5mM Ca^{++} spectra of parvalbumin, calmodulin and troponin C in H_2O are identical to those recorded in 5mM EGTA. In ^2H_2O addition of 5mM Ca^{++} to protein solutions results in a retarded rate of hydrogen-deuterium exchange. Spectra of parvalbumin recorded immediately after dissolution exhibit an amide I maximum at 1649cm^{-1} (see Fig. 5.7a) at all pD values. After extended exposure to ^2H_2O (72 hours) the amide I maximum at all pD values is observed at 1645cm^{-1} (Fig. 5.7b) Similar behaviour was observed for calmodulin and troponin C.

5.3.1.4. EFFECT OF TEMPERATURE UPON THE INFRARED SPECTRUM

The effects of temperature upon the infrared spectrum of parvalbumin are shown in Figure 5.8. At 70^{o}C in the absence of Ca^{++} the amide I maxima of parvalbumin, was

FIGURE 5.7: Deconvolved spectrum of parvalbumin in 5mM Ca^{++}, pD 5.5, 20^{o}C a) 15 minutes b) 72 hours after dissolution (F=2.5 W=16).

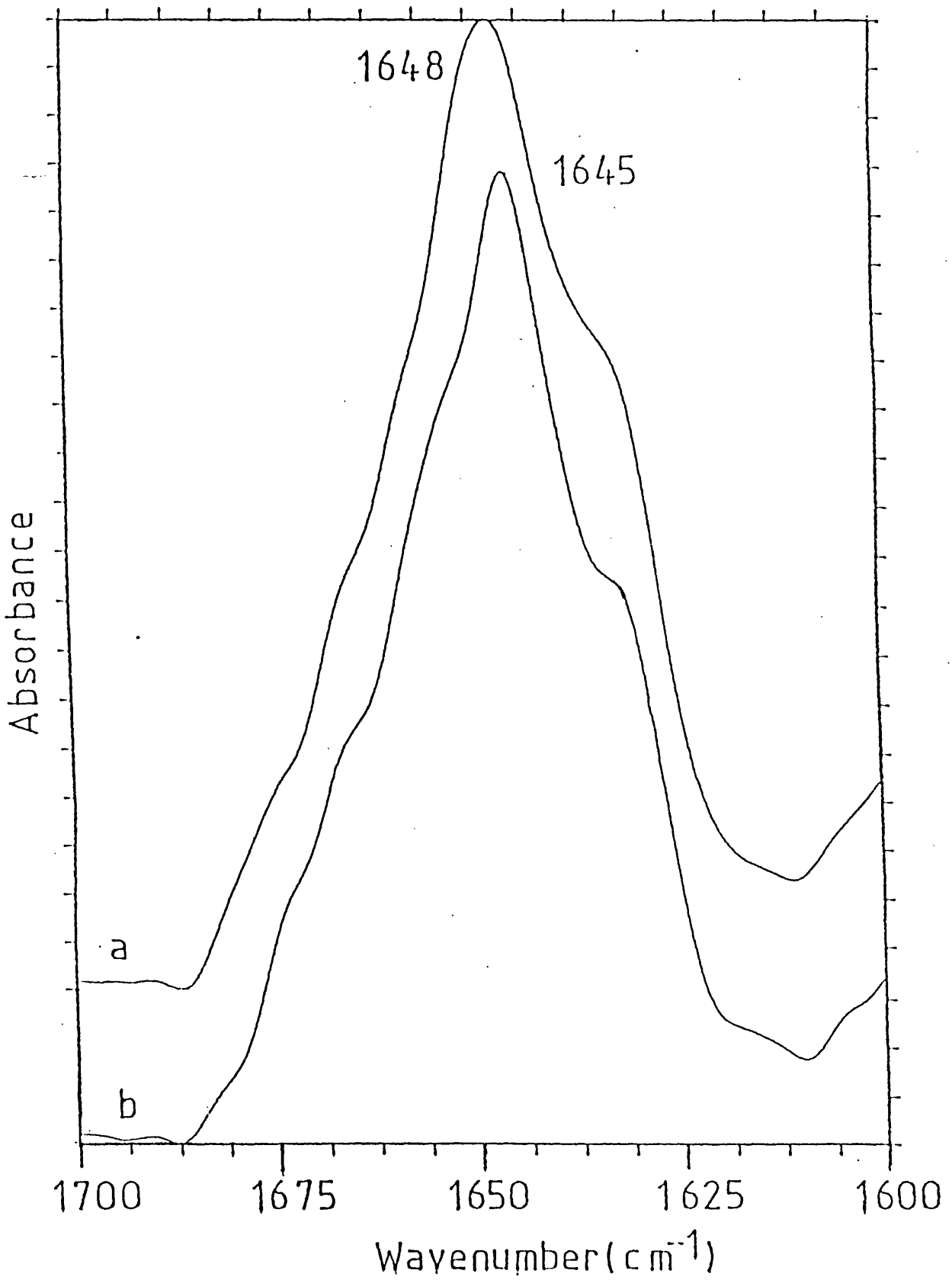
1648
1645
a
b
Absorbance
1700
1675
1650
1625
1600
Wavenumber (cm⁻¹)

FIGURE 5.8: Difference (solid line) and deconvolved (broken line) spectrum of parvalbumin at 70^{o}C pD 7.5, 5mM EGTA. F=2.5 W=16

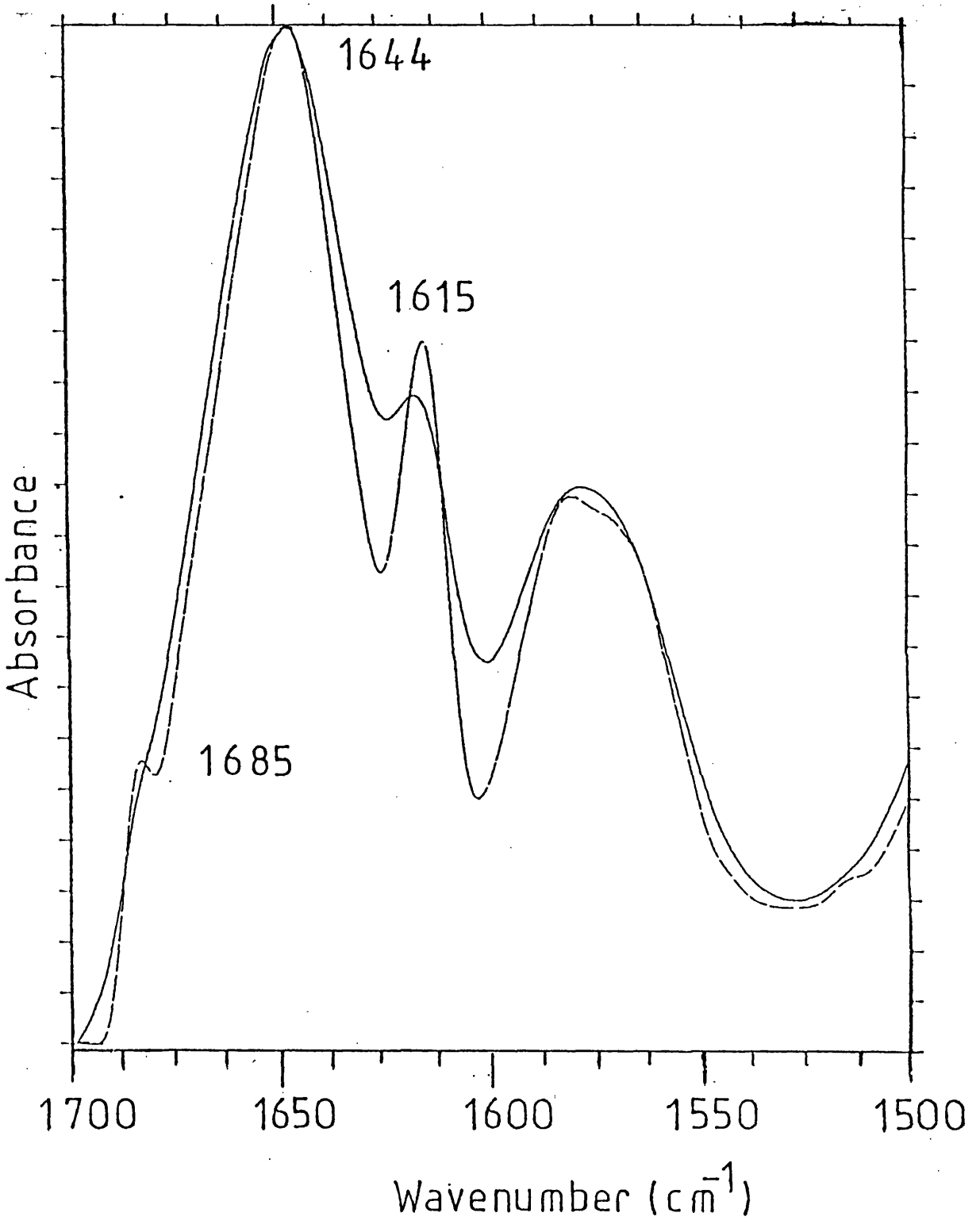
1644
1615
1685
Absorbance
1700
1650
1600
1550
1500
Wavenumber (cm⁻¹)

FIGURE 5.9: Difference spectra of parvalbumin generated by subtraction of a spectrum recorded after 30 seconds at 70^{o}C from spectra recorded after (a) 1 minute, (b) 5 minutes and (c) 30minutes at 70^{o}C.

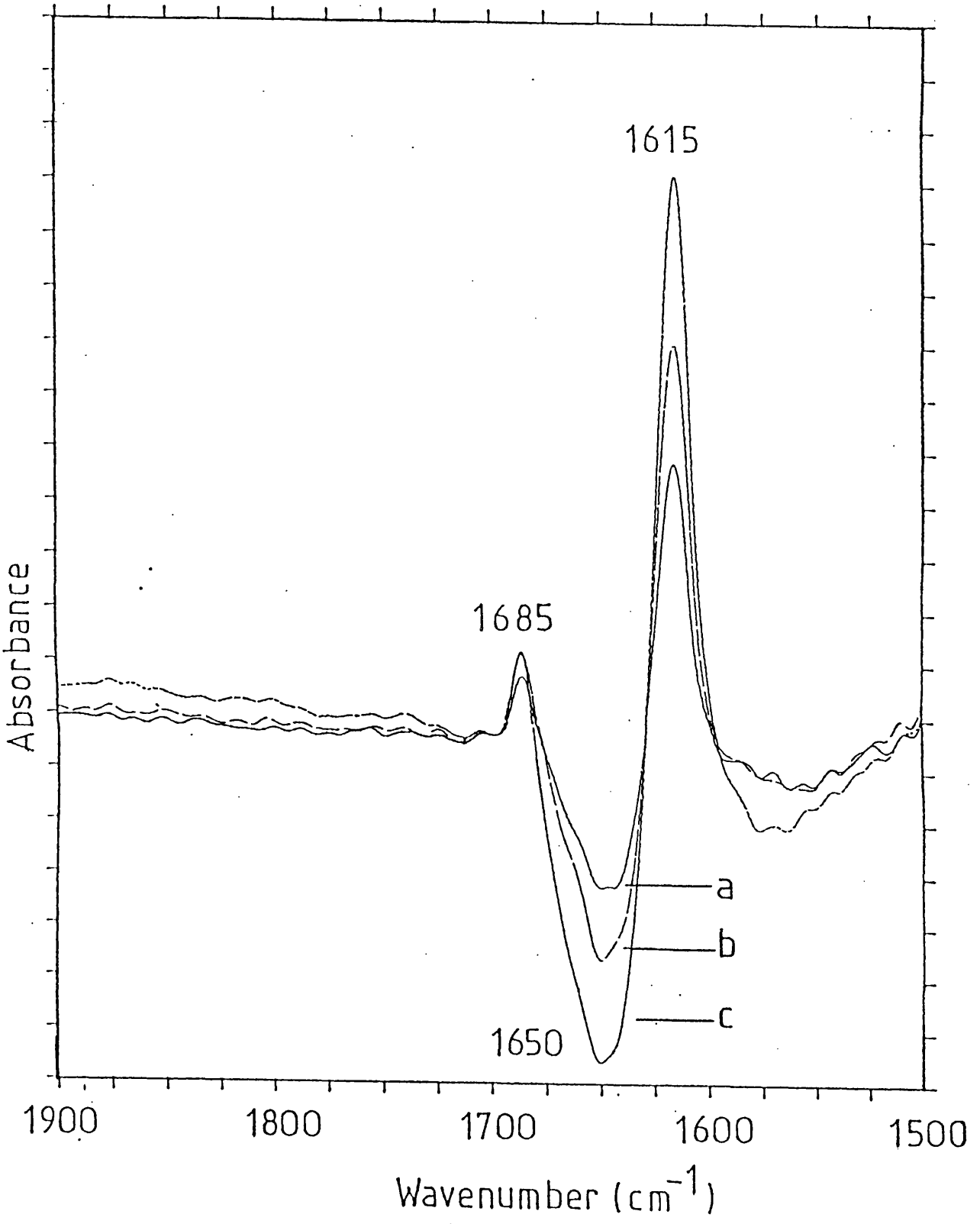
1615
1685
1650
a
b
c
Absorbance
1900
1800
1700
1600
1500
Wavenumber (cm^{-1})

observed at 1644cm^{-1}. In the difference spectrum, two strong shoulders are apparent at 1615cm^{-1} and 1685cm^{-1}. Deconvolution and second derivative analysis reveal the presence of an intense absorption at 1615cm^{-1} and a weaker band at 1685cm^{-1} in addition to the main component at 1644cm^{-1}.

The time dependence of these changes is illustrated in Figure 5.9. Subtraction of a spectrum of parvalbumin recorded after 30 seconds at 70^{o}C from spectra recorded after 1, 5 and 45 minutes at 70^{o}C reveals progressive increase in intensity at 1615cm^{-1} and 1685cm^{-1} and a progressive decrease in intensity at 1650cm^{-1}.

In the presence of 5mM Ca^{++} spectra of parvalbumin, and calmodulin recorded in $^{2}H_{2}O$ at 70^{o}C were similar to those recorded at 20^{o}C.

5.3.1.5. EFFECT OF CONCENTRATION UPON THE INFRARED SPECTRUM

FTIR spectra of parvalbumin were obtained at a range of concentrations (0.25-2.5% w/v). Difference, deconvolved and derivative spectra were found to be unaffected by variations in the concentration of the protein.

5.3.1.6. EFFECT OF GLYCEROL UPON THE INFRARED SPECTRUM

The difference spectrum of parvalbumin recorded in the presence of 60% (v/v) deuterated glycerol is shown in Figure 5.10. An increase in the amide I maximum to 1646cm^{-1} is seen

FIGURE 5.10: Difference spectra of parvalbumin in the presence of 60% w/v deuterated glycerol, pD 5.5 (broken line) and in $^{2}H_{2}O$, pD 5.5 (solid line)

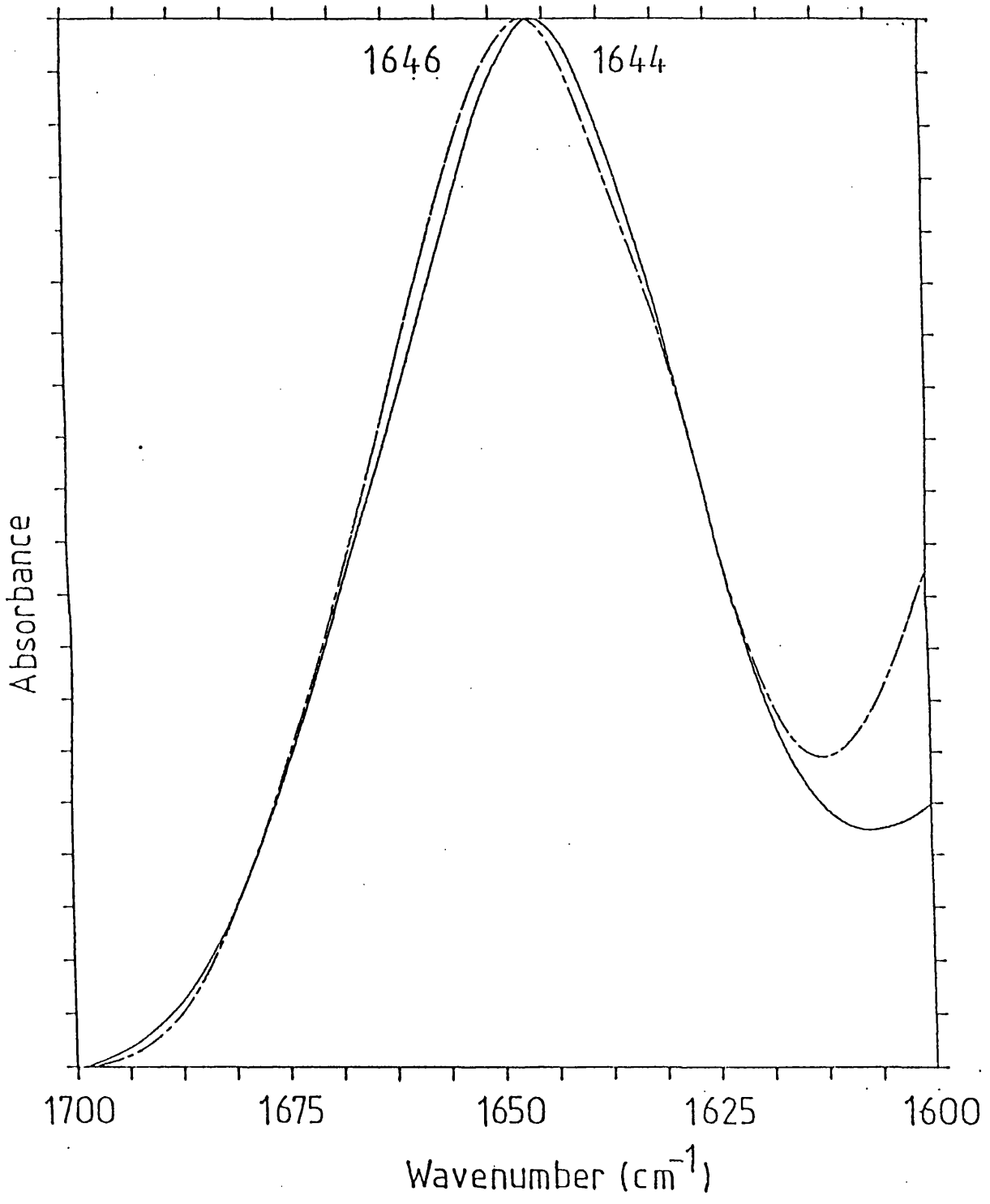
1646
1644
Absorbance
1700
1675
1650
1625
1600
Wavenumber (cm⁻¹)

FIGURE 5.11: Second derivative spectra of parvalbumin in the presence (broken line) and absence (solid line) of 60% w/v deuterated glycerol. Factor=13

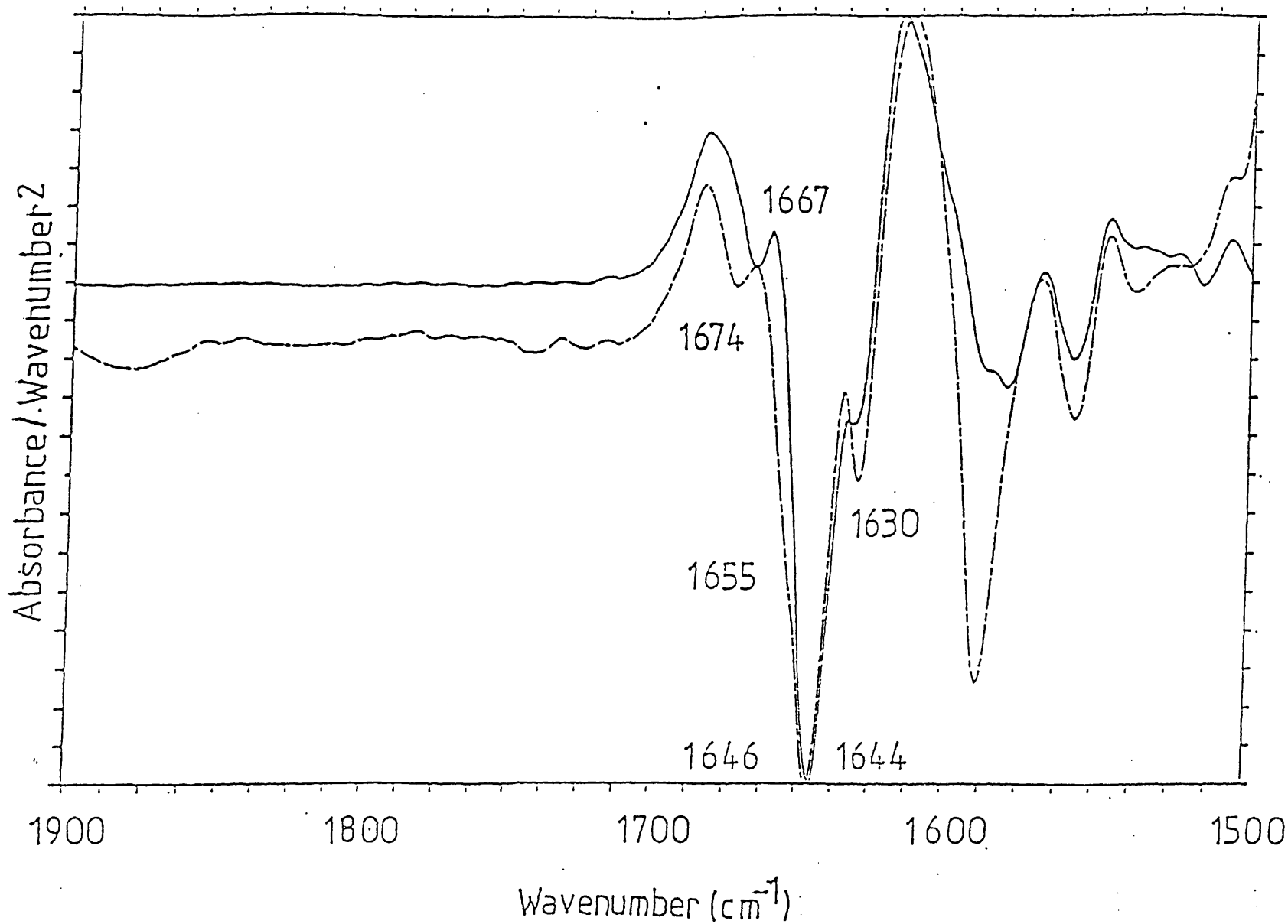
Absorbance / Wavenumber 2
1667
1674
1630
1655
1646
1644
1900
1800
1700
1600
1500
Wavenumber (cm⁻¹)

as compared to the fully exchanged protein in the absence of glycerol. Furthermore, a considerable shift in absorbance from low to high wavenumbers is apparent. Second derivative analysis reveals the presence of a strong shoulder at 1657cm^{-1} on the major absorption band (Fig. 5.11). Fourth derivative analysis results in the production of a discrete band at this frequency (not shown).

5.3.2CIRCULAR DICHROISM SPECTROSCOPY

The circular dichroism spectra of parvalbumin recorded in H_2O at pH 5.5, 7.5, and 9.5 are shown in Figure 5.12. A bilobed spectrum was recorded at all three pH values, with minima at 210nm and 220nm.

CD spectra recorded in ^2H_2O at pD 5.5, 7.5 and 9.5 were identical to those obtained in H_2O (not shown). Cd spectra of parvalbumin recorded at a range of concentrations (0.02%-2% w/v) at pH 5.5-9.5 were identical in form, varying only in intensity. In all cases, a bilobed spectrum with minima at 210nm and 220nm was recorded.

In the presence of 60% (w/v) glycerol, the CD spectrum of parvalbumin was identical to those previously recorded (Fig. 5.13). This spectrum was characterised by a bilobed appearance, with minima at 210nm and 220nm.

FIGURE 5.12: CD spectra of parvalbumin recorded at pH 5.5, 7.5 and 9.5, in 5mM EGTA.

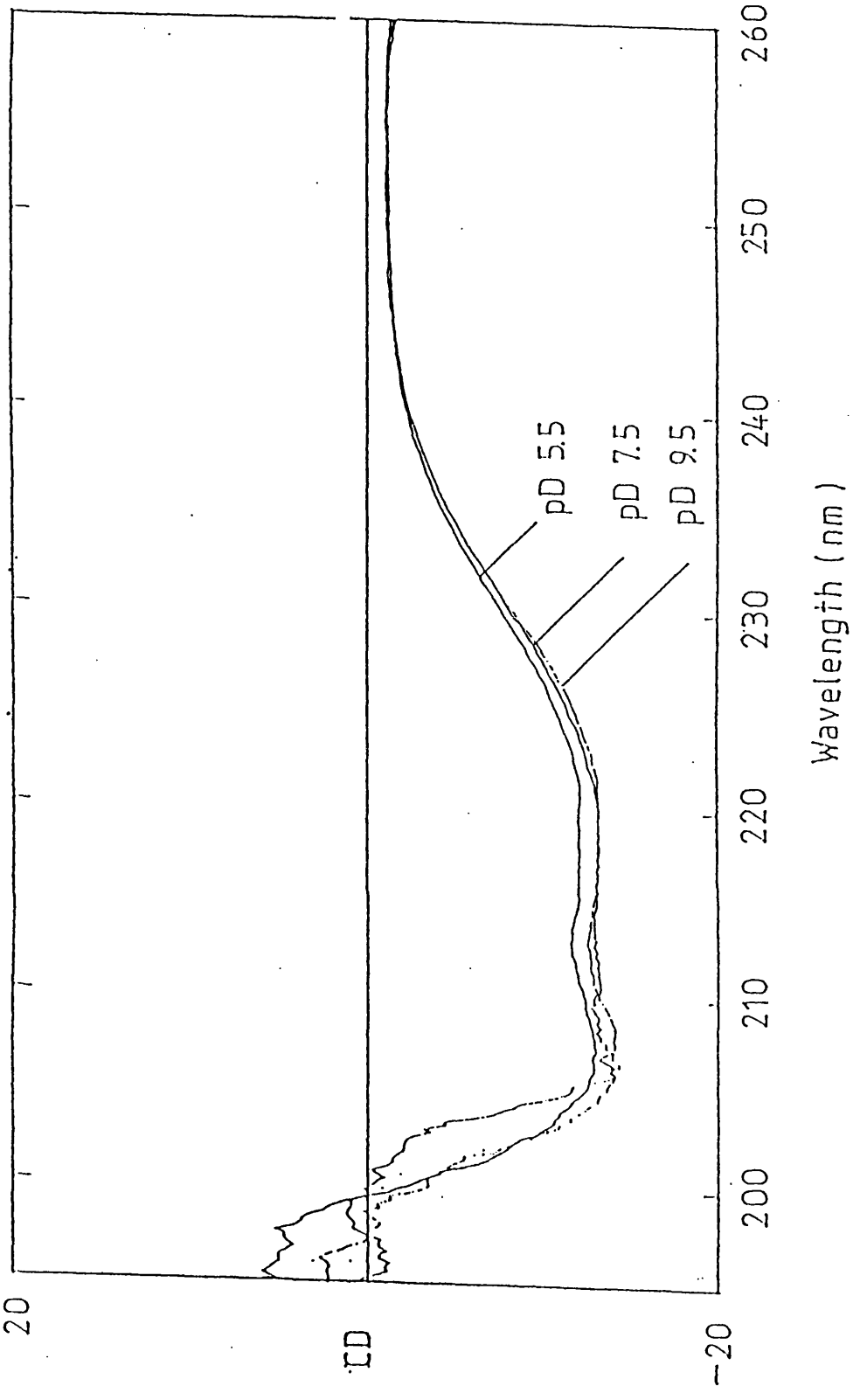
20
CD
-20
200
210
220
230
240
250
260
Wavelength (nm)
pD 5.5
pD 7.5
pD 9.5

FIGURE 5.13: CD spectrum of parvalbumin in 60% w/v glycerol.

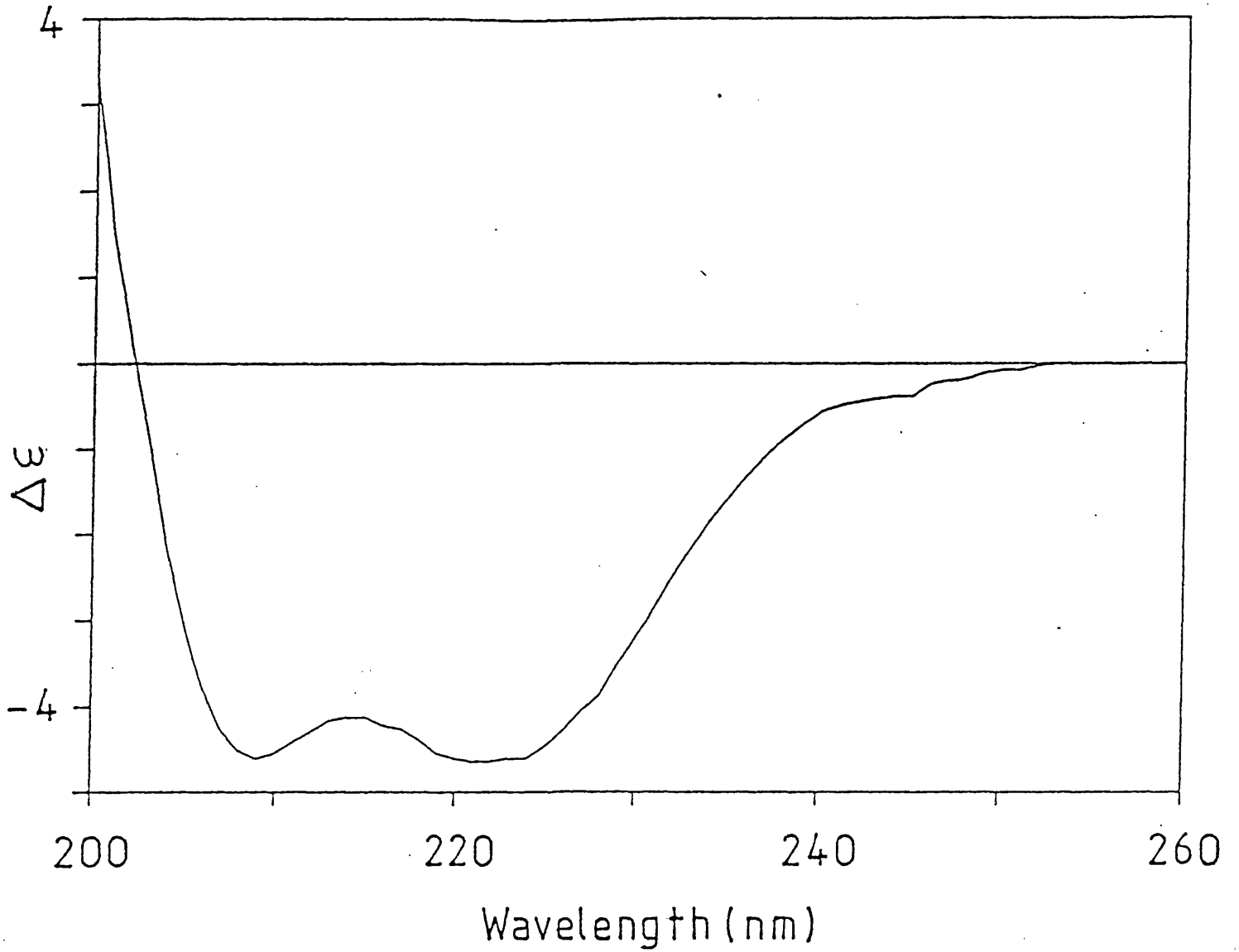
4
Δε
-4
200
220
240
260
Wavelength (nm)

5.4 DISCUSSION

The secondary structures of parvalbumin, calmodulin and troponin C are well established from X-ray diffraction studies (Kretsinger and Nockolds,1973; Moews and Kretsinger, 1975; Babu et al., 1985; Hertzberg and James, 1985). All three proteins are considered to be predominantly α-helical in structure, with small amounts of β-sheet.

Examination of the FTIR spectrum of each protein recorded in H_2O in the presence of Ca^{++} suggests a similar conformation in solution and crystals. For all three proteins, the amide I was found to occur at frequencies consistent with a predominantly α-helical structure. It should however be borne in mind that absorptions from unordered polypeptide chains have been shown to occur at similar positions to those arising from α-helices. Quantitative estimation (Dr. David Lee, personal communication) of the secondary structure of parvalbumin, calmodulin and troponin C using factor analysis confirmed the assignment of the band at 1654-56cm^{-1} to α-helices. This technique quantitates the individual secondary structures based on comparisons with a bank of reference spectra of proteins whose crystal structure have been described (Lee et al., 1990). Excellent agreement was found between the factor analysis and X-ray diffraction estimates of secondary structure for parvalbumin and calmodulin, both sets of

results indicating proteins with 60-70% of amino acids involved in α-helical secondary structures.Circular dichroism spectra of parvalbumin were also fully consistent with this protein having a predominantly helical structure.

In contrast to the studies of Trewhella at al (1989) no evidence for the presence of distorted helical secondary structures was found. The presence of such structures would be expected, on both theoretical (Krimm and Bandekar 1985) and experimental (Yasui et al., 1987; Kennedy et al., manuscript in preparation) grounds to result in an amide I maximum significantly higher than that seen for α-helical proteins. This is clearly not seen.

Minor bands in deconvolved and second derivative spectra at 1628-30cm^{-1} and 1660-80cm^{-1} can be attributed to the presence of β-sheet and turns. Again, good agreement between X-ray diffraction and factor analysis analysis was found, both techniques suggesting 10-15% of the amino acids being involved in β-sheet secondary structures (Dr. David Lee, personal communication).

Removal of Ca^{++} from parvalbumin, calmodulin and troponin C had no significant effects upon the second derivative or deconvolved spectra recorded in H_2O. Spectra were still characteristic of a highly helical protein.

The initial experiments conducted in this study were all carried out at pH 5.5, the pH of the crystalisation

medium. Such a low pH is non-physiological and may induce a conformation significantly different to that adopted at physiological pH (7.4). Analysis of FTIR spectra of parvalbumin, calmodulin and troponin C at pH values ranging from 5.5-9.5 revealed no dependence of the structures upon pH, indicating that the structures adopted at pH 5.5 are similar, if not identical to that adopted at more physiological values

Small amounts of unordered polypeptide chain are known to be present in the structures of parvalbumin, calmodulin and troponin C. Such structures will not be easily identified in FTIR spectra recorded in H_2O as in this solvent absorptions from α-helices and random polypeptide chains can be shown to overlap. Deuterium substitution experiments are now routinely employed in the FTIR spectroscopic analysis of protein secondary structure to separate the overlapping absorptions from helical and unordered polypeptide chains. Following deuteration, the absorption arising from the rapidly exchanging unordered segments is shifted to 1644-46cm^{-1}, while deuterated α-helices can be shown to absorb in the region 1648-55cm^{-1} for water soluble proteins.

Upon immediate dissolution of parvalbumin, troponin C and calmodulin in ^2H_2O at pD 5.5 in the presence of 5mM Ca^{++}, the amide I maximum suggests a predominantly helical

structure. The strength of the absorption arising from carboxylate groups of acidic amino acids is such that it is not possible to accurately assess the intensity of the residual amide II band in order to estimate the extent to which the protein has been deuterated. However, from the relatively weak nature of the shoulder on the band at 1570-80cm^{-1} the protein appears to be highly deuterated. In view of the high degree of solvent exposure conferred by the very open structure of these proteins, this is not surprising.

Deconvolution and derivative analysis revealed a shoulder on the major band, at around 1644cm^{-1}, suggesting the presence of small amounts of unordered polypeptide chains within the protein. The presence of only a minor component representing the residual amide II component confirmed the extensive deuteration of the proteins. Similar results were obtained at pD 7.5.

Elevation of the pD to 9.5 produced spectra characteristic of highly disorganised proteins, with an amide I maximum in difference, deconvolved and derivative spectra at 1644cm^{-1} for all three proteins. Complete deuteration has occurred as demonstrated by the lack of any amide II absorption. Extended exposure of paravalbumin, calmodulin and troponin C to ^2H_2O also resulted in spectra characteristic of a disordered protein and complete deuteration. These results are in contradiction to those

obtained in our CD spectroscopic experiments, in which spectra at all ph values indicated a predominantly α-helical protein.

An amide I band maximum at 1644cm^{-1} is inconsistent with a predominantly α-helical protein. A number of possible explanations for the low frequency of the amide I maxima exist. An unusual feature of these proteins is the complete deuteration that occurs after extended exposure to solvent or high pD. Complete deuteration of proteins is generally only achieved after prolonged exposure (many days or even weeks) to the solvent or incubation at elevated temperatures. It may therefore be argued that the unusual features of the FTIR spectra of these proteins reflects this complete deuteration. However, we have obtained spectra of fully deuterated ribonuclease A and S (Haris et al., 1986a), bovine serum albumin and myoglobin and found no unusual features in the spectra.

A second explanation for this low amide I absorption would be that elevation of the pD and prolonged standing of the proteins induces aggregation, which promotes denaturation. Aggregation is almost certain to occur at the protein concentrations required for FTIR spectroscopy. To assess the effects of aggregation upon the structure of the proteins, CD and FTIR spectra were recorded at a range of pD values and concentrations immediately and 24 hours after

dissolution. In all cases, a dichotomy between CD and FTIR spectra recorded at identical concentrations was apparent, FTIR spectra suggesting a disordered protein structure, and CD spectroscopic results suggesting a predominantly α-helical protein. It would therefore appear that aggregation has little, if any effect upon the FTIR spectra.

While variations in the structure of parvalbumin with concentration and pD can now be ruled out, the discrepancy between the FTIR and CD spectra remains. How can FTIR spectra indicating a disordered protein and CD spectra indicating a predominantly α-helical protein be rationalised?

From the X-ray diffraction data, these proteins have in common a very open structure, with the consequence that the peptide bonds are likely to be very highly solvated. In particular, calmodulin and troponin C have a long, highly exposed helical linking segment (Babu et al., 1985, Hertzberg and James, 1985). It is possible that such unusually open structures may be responsible for the abnormal infrared spectra. With this in mind, spectra of parvalbumin were obtained in the presence of deuterated glycerol to assess the effects of hydration upon the position of the amide I maximum.

It is immediately apparent from the difference spectra of parvalbumin recorded in the presence of 60% (w/v) that a

considerable shift in absorbance to higher frequencies has occurred, together with a reproducible increase in amide I frequency. In the second derivative spectrum a shoulder is apparent at 1657cm^{-1}. As glycerol would be expected to compete with the protein C=O groups to hydrogen bond to water, this result can be interpreted as a decrease in the interaction of the protein with water producing an increase in amide I frequency. It is interesting to note in this context that the shoulder that appears at 1657cm^{-1} in the presence of glycerol is at the position absorptions from α-helices in membrane proteins are characteristically seen. Such helices would be expected to have only minimal interactions with water as they are embedded within the hydrophobic membrane. Structural changes in the protein induced by glycerol can be ruled out as CD spectra recorded in the presence of 60% glycerol were identical to those of the pure protein.

If the increased solvation of these proteins as compared to other water soluble proteins is the cause of the unusual spectroscopic behaviour, then it may be expected that an abnormal amide I maximum would be seen in H_2O as well as in ^2H_2O, which is not the case. It has been observed that for simple amides such as propionamide, the position of the amide I maximum is markedly dependent upon the water content when water/dioxane mixtures are used as solvent

(Kobayashi and Kobayashi, 1980). Similarly, a marked dependence upon ^2H_2O content was seen when ^2H_2O/dioxane mixtures were used as solvent. However, for similar $H_2O/^2H_2O$ contents, the magnitude of the shift was always some 50% greater when the mixture contained ^2H_2O, a result which suggested that the hydrating effect of ^2H_2O is greater than that of H_2O. The unusually low amide I frequency of parvalbumin, calmodulin and troponin C in ^2H_2O may therefore be a consequence of a high degree of solvent accessibility, an unusual spectrum only being recorded in this solvent due to the greater hydrating ability of ^2H_2O compared to H_2O.

The thermal behaviour of calmodulin and parvalbumin in the presence and absence of Ca^{++} has been investigated. In the absence of Ca^{++} elevation of the temperature to 70^oC resulted in the production of two new bands in the infrared spectrum. The position and narrowness of these bands is such that they resemble those associated with anti-parallel β-sheet structures. However, examination of the spectra of predominantly β-sheet proteins such as ribonuleases (Haris et al., 1986a) and concanavalin A (Alvarez et al., 1987, Chapter 7) show bands which are normally associated with this secondary structure to occur in the region 1630-40cm^{-1}. The occurrence of a band at 1616cm^{-1} in spectra of calmodulin and parvalbumin recorded at 70^oC cannot therefore be attributed to the occurrence of standard β-sheet

structures. We have observed this phenomenon in a range of α-helical proteins and have attributed it to the formation of an intermolecular β-sheet upon unfolding of regions of the proteins (Jackson et al., 1990b and Chapter 7).

The unfolding of the proteins to form this intermolecular structure is a gradual process as illustrated in Figure 5.8. Difference spectra generated by the subtraction of a reference spectrum (obtained immediately the temperature was raised to 70^{o}C) from spectra obtained after progressively longer exposure to high temperatures show a gradual increase in absorption at 1685cm^{-1} and 1616cm^{-1}. The formation of this new structure is at the expense of helical regions of the protein, as indicated by a decrease in absorption at 1650cm^{-1}.

In the presence of 5mM Ca^{++} the stability of the protein is significantly enhanced. After extended incubation at 70^{o}C no new bands are apparent in the spectra.

5.5 SUMMARY

The secondary structure of parvalbumin, troponin C and calmodulin are well established from X-ray diffraction work. The FTIR spectra recorded in H_2O and presented here are qualitatively and quantitatively similar to those obtained with X-ray diffraction and CD spectroscopic studies.

Recent infrared studies have suggested that the helical structures present in these proteins were not the standard α-helix, but some kind of distorted structure. The evidence for this was an unusually low amide I frequency for calmodulin and parvalbumin in ^2H_2O solution.

The results presented in this chapter suggests that the helical structures present in these proteins are not significantly distorted, for two reasons. Firstly, distorted helical structures have weaker hydrogen bonds than the standard α-helix, and so would be expected to absorb at a higher, rather than a lower frequency. Secondly, distorted helical structures would absorb at an unusual frequency in H_2O solutions, which is not the case for the proteins studied here.

The low frequency of the infrared absorption has been shown to be unrelated to any possible denaturation phenomena associated with the high concentration of protein used in FTIR experiments, as FTIR spectra recorded at various concentrations were identical. These spectra were always

characterised by an abnormally low amide I maximum, while CD spectra recorded at the same concentrations (from the same stock solutions) always suggested a helical structure.

The addition of glycerol to the protein solutions resulted in a significant shift of absorbance to higher wavenumbers, a result consistent with dehydration of the protein. Thus, the unusually low amide I frequency seen in the FTIR spectra of EF hand proteins in ^2H_2O solution can be reinterpreted on the basis of an increased hydration of the protein due to their exposed structures, without the necessity of postulating unusual secondary structures. The unusual amide I frequency is only apparent in ^2H_2O due to the greater hydrating effect of ^2H_2O compared to H_2O.

Thermal denaturation of the proteins was observed in samples incubated at 70^oC in the absence of Ca^{++}. This denaturation results in the formation of an intermolecular β-sheet arrangement and is prevented by the presence of Ca^{++}.

CHAPTER 6

FTIR SPECTROSCOPIC STUDIES OF CONFORMATIONAL TRANSITIONS IN THE Ca-ATPase OF SARCOPLASMIC RETICULUM ASSOCIATED WITH Ca^{++} TRANSLOCATION

6.1 INTRODUCTION

Muscle contraction is initiated by an efflux of Ca^{++} from the sarcoplasmic reticulum, which then binds to troponin C in the cytoplasm. Conformational changes in the troponin complex result in the exposure of actin binding sites on the myosin filaments. Cross-linking of actin and myosin result in the generation of tension. Binding of Ca^{++} is therefore of fundamental importance in the contractile process. Equally important is the removal of Ca^{++} from the region of the contractile elements, so allowing relaxation. This is the function of the Ca^{++}-ATPase of sarcoplasmic reticulum (EC.3.6.1.38). This enzyme catalyzes the transport of two moles of Ca^{++} ions across the sarcoplasmic reticulum membrane coupled to the hydrolysis of one mole of ATP (see Inesi, 1985 for a review).

The Ca^{++}-ATPase of sarcoplasmic reticulum is the most widely studied ion transporting system. The primary structure of the protein has recently been deduced from it's cDNA sequence and from this data predictions of the secondary structure have been made (MacLennan et al., 1985). Approximately 40% of the protein was predicted to be in a helical configuration, situated within the lipid bilayer. The remainder of the protein was postulated to exist as turn and sheet elements. The nucleotide binding regions and phosphorylation sites were predicted to exist as β-sheet and

FIGURE 6.1: Schematic representation of the structure of the Ca^{++}-ATPase of sarcoplasmic reticulum (modified from Brandl et al 1986). S indicates a helix forming part of the stalk region, m a membrane spanning helix. β indicates regions of β-sheet. NBD= nucleotide binding domain.PD=phosphorylation domain. TD= transduction domain.

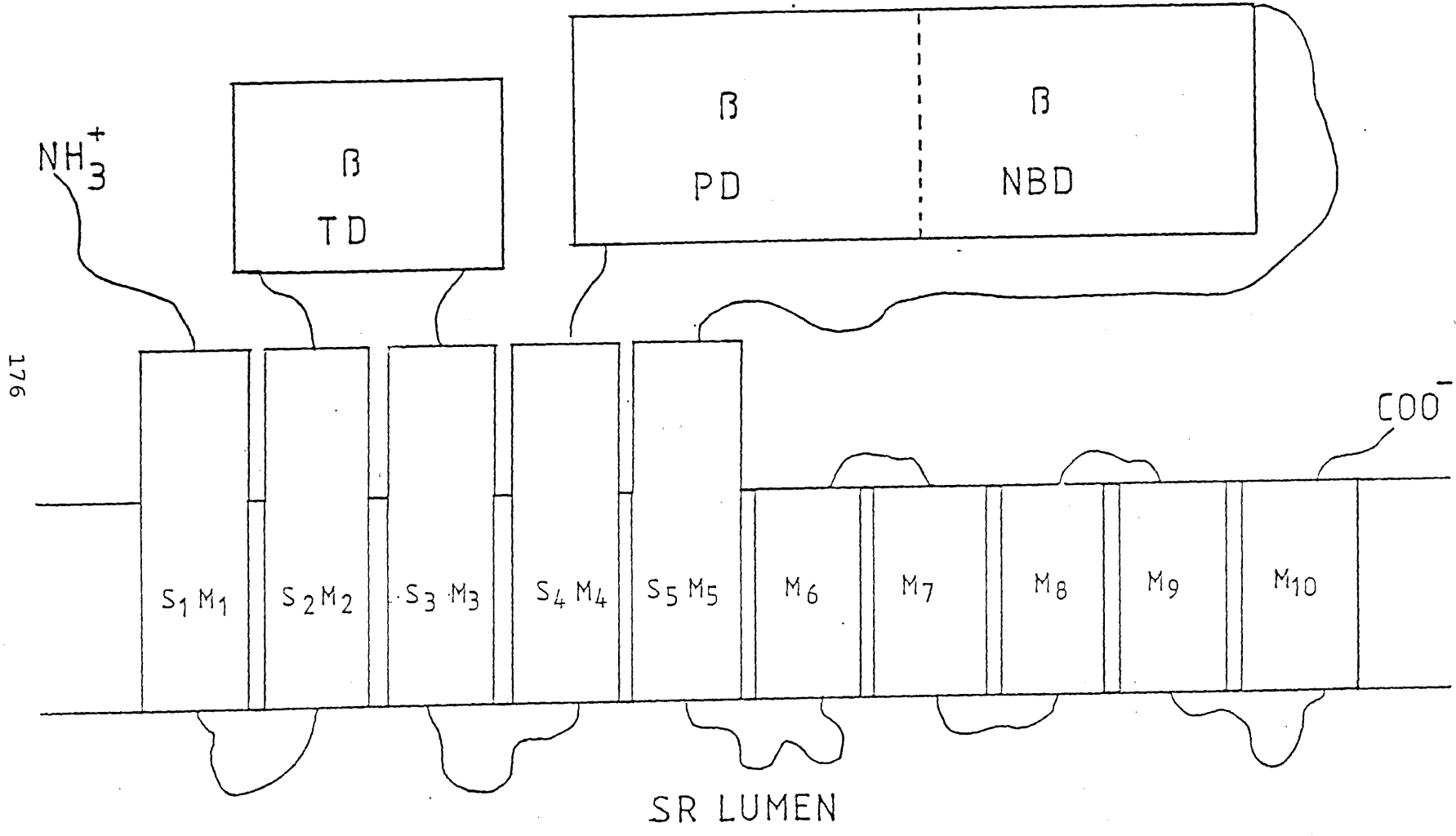
NH3+
ß
TD
ß
PD
ß
NBD
COO−
S1 M1
S2 M2
S3 M3
S4 M4
S5 M5
M6
M7
M8
M9
M10
SR LUMEN

176

be connected by a transduction domain, also in the β-sheet configuration (see figure 6.1) . Electron microscopy (Taylor et al., 1986) and neutron diffraction data (Blasie et al., 1985) also suggest that approximately 40% of the protein is situated in the bilayer. Circular dichroism (Csermely et al., 1987), FTIR (Cortijo et al., 1982, Lee et al., 1985, Arrondo et al., 1988) and Raman spectroscopy (Lippert et al., 1981) all indicate a predominately α-helical structure with significant contributions from β-sheet elements.

The regions of the protein responsible for binding of the two Ca^{++} ions have been cautiously identified using site directed mutagenesis (Clarke et al., 1989). Replacement of 20 negatively charged amino acids in the stalk region of the model proposed by MacLennan et al., (1985) had no effect upon transport, ruling out the stalk region as the binding domain. However, replacement of either Glu309, Glu771, Asp790, Thr799, Asp800 or Glu 908 abolished Ca^{++} transport. The Ca^{++} binding sites within the Ca^{++}-ATPase therefore appear to involve helices M_4, M_5, M_6 and M_8.

During the ATP-dependant transport cycle, the Ca^{++}-ATPase undergoes a series of conformational transitions, characterised by different affinities for Ca^{++}, ATP and other ligands (Inesi, 1985). The transport cycle of the Ca^{++}-ATPase is illustrated schematically in figure 6.2.

FIGURE 6.2: Schematic representation of the catalytic cycle of the Ca^{++}-ATPase of sarcoplasmic reticulum.

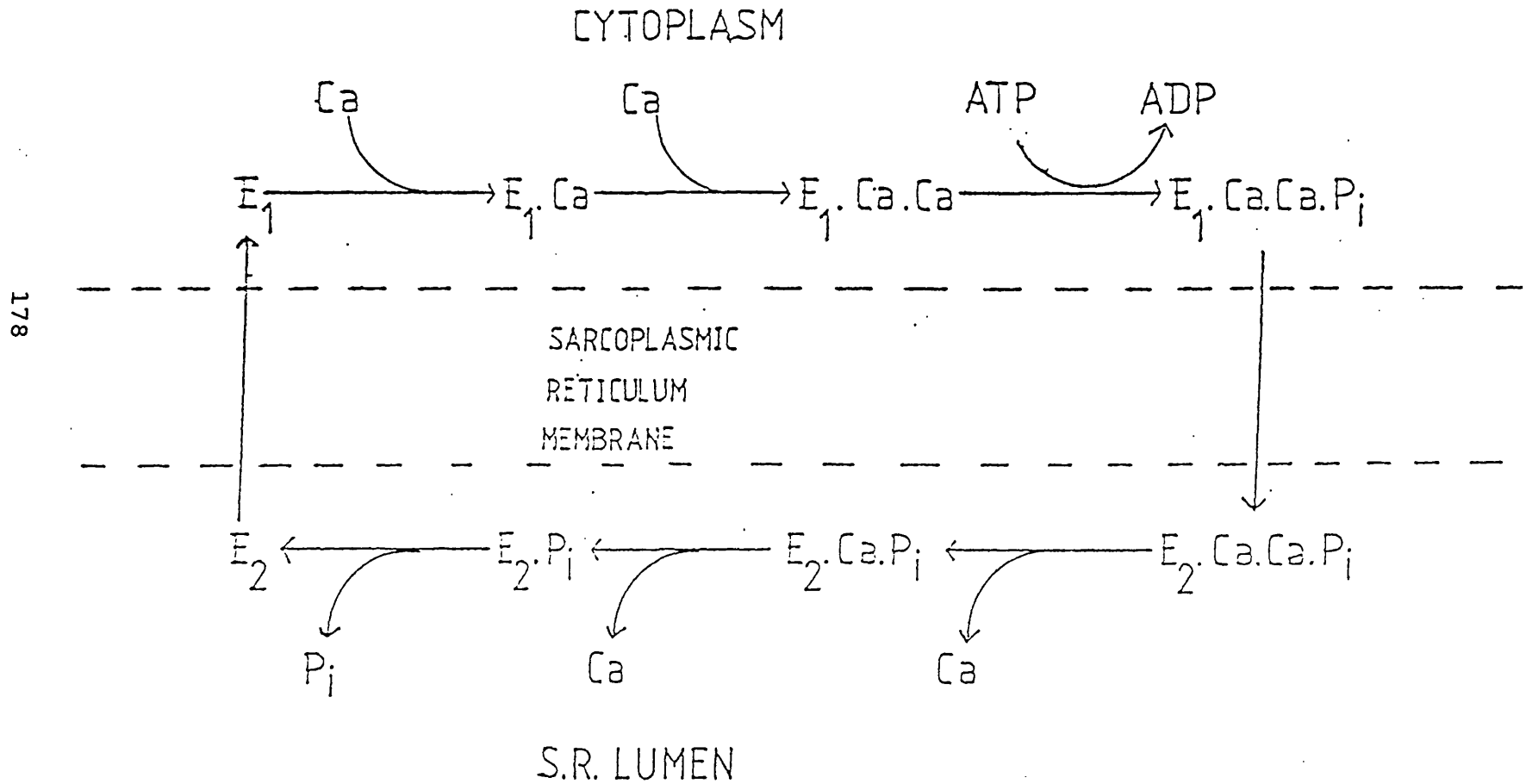
CYTOPLASM
Ca
Ca
ATP
ADP
E1
E1. Ca
E1. Ca. Ca
E1. Ca. Ca. Pi
SARCOPLASMIC
RETICULUM
MEMBRANE
E2
E2. Pi
E2. Ca. Pi
E2. Ca. Ca. Pi
Pi
Ca
Ca
S.R. LUMEN

Cooperative binding of two Ca^{++} ions is followed by phosphorylation of the protein by ATP. The phosphorylated protein then undergoes a conformational change of some nature, with the result that the Ca^{++} ions are now exposed to the sarcoplasmic reticulum lumen. In this configuration the ATPase loses its affinity for Ca^{++} and Ca^{++} is released into the lumen. The protein is then de-phosphorylated and returns to the resting , high Ca^{++} affinity state.

A complete understanding of the conformational changes associated with catalytic activity is obviously required for a full understanding of the physical basis of Ca^{++} translocation. To attempt to follow such conformational changes it is necessary to use physical techniques which can give information concerning the spatial arrangement of the protein. To this end a variety of spectroscopic techniques have been applied to the study of the Ca^{++}-ATPase. However, no clear picture has yet emerged. Fluorescence studies indicated definite changes in protein structure upon Ca^{++} translocation (Watanabe and Inesi, 1982). Similarly, laser Raman spectroscopy (Lippert et al., 1981) has demonstrated a decrease in helical structures associated with translocation. A recent FTIR study (Arrondo et al., 1987) found the opposite to be true, that is, new helical structures were formed. A number of CD studies (Csermely et al., 1987) have found no major change in secondary structure

upon translocation. These discrepancies are possibly due in part to the use of different preparations in the various studies, some authors using purified preparations of sarcoplasmic reticulum membranes (Arrondo et al., 1987) while others have used the purified Ca^{++}-ATPase (Nakamoto and Inesi 1986).

It is apparent that clarification of the structural basis of Ca^{++} transport across the sarcoplasmic reticulum membrane is required. To this end a comprehensive study was undertaken in collaboration with Dr. Jose Villalain and Prof. Juan C. Gomez-Fernandez of the University of Murcia to describe any conformational changes associated with Ca^{++} translocation in both SR and the purified Ca^{++}-ATPase in both qualitative and quantitative terms.

6.2 MATERIALS AND METHODS

Deuterium oxide (99.8 atom%), ATP and phosphoenol pyruvate were purchased from Sigma, UK. Lactate dehydrogenase and pyruvate kinase were purchased from Boehringer. All other materials were of reagent grade purchased from Sigma.

6.2.1 ISOLATION OF RABBIT SARCOPLASMIC RETICULUM

Sarcoplasmic reticulum was isolated from the white muscle of New Zealand white rabbits by the method of Nakamura et al., (1976). The animals were killed by cervical dislocation, the white muscle from the back and hind legs removed and placed in ice cold buffer (10mM Tris, 0.1M KCl pH 7.3). After removal of any connective tissue and red muscle the tissue was passed through an electric mincer and homogenised in a domestic blender using four one minute bursts and 2 litres of buffer. All subsequent procedures were conducted at 4^{o}C. The homogenate was centrifuged at 2,000 x g for 10 minutes to sediment cell debris and the supernatant filtered through four layers of muslin to remove any further gross contaminants. The filtrate was centrifuged at 10,000 x g for ten minutes to sediment mitochondria. The resultant supernatant was centrifuged at 30,000 x g for 1 hour to sediment the SR. Actin contaminants in the SR were solubilised by incubation in high salt buffer (10mM Tris, 0.6M KCl pH 7.3) for 1 hour. SR was again sedimented by

centrifugation at 70,000 x g for 25 minutes. The crude SR so prepared was resuspended in sucrose buffer (50mM Tris-HCl, 250mM sucrose, 1M KCL, 2mM DTT, pH 8.0)

6.2.2 PURIFICATION OF SARCOPLASMIC RETICULUM AND THE Ca^{++}-ATPase

The crude SR prepared as above was layered onto continuous sucrose density gradients (15-60% w/v sucrose in 50mM Tris, 1M KCl, 2mM DTT, pH 8.0). These gradients were then centrifuged at 62,000 x g at $4^{o}C$ for 11 hours. Crude SR is fractionated into two bands by this procedure, with different lipid:protein ratios. The upper band contains some contaminants and was discarded. The "heavy" band was washed three times in sucrose buffer by centrifugation at 100,000 x g for 30 minutes , the final pellet resuspended in sucrose buffer and stored deep frozen.

Purification of Ca^{++}-ATPase from SR was according to the method of Warren et al., (1974) or Meissner et al., (1973) . SR was incubated with sodium cholate (0.5mg/mg protein or 0.1mg/mg protein) for 30 minutes at room temperature. The protein/detergent mixture was layered onto continuous sucrose density gradients (20-60%, composition as previously described with the addition of 1mM Mg-ATP) and centrifuged at 200,000 x g for 11 hours. A single white band of protein was removed and washed by centrifugation in 50mM Tris, 1M KCl, 2mM DTT pH 8.0 at 100,000 x g. The pellet was

resuspended in sucrose buffer and stored deep frozen.

6.2.3 FTIR SPECTROSCOPY

Infrared spectra were recorded on a Perkin-Elmer 1750 Fourier transform infrared spectrometer or a Nicolet MX-1 FTIR spectrometer, coupled to a Perkin-Elmer 7300 data station or Nicolet 1200S data station respectively.

Suspensions of Ca^{++}-ATPase were washed in buffer containing 0.1M KCL , 10mM imidazole, 1mM EGTA, 1mM $MgCl_2$ pH 7.4 and resuspended in this buffer to a final concentration of 20mg/ml. Prior to FTIR measurements, concentrated stock solutions of $CaCl_2$, Na_3VO_4, ATP or Na_2HPO_4 were added to the ATPase to give final concentrations of 8μM and 0.1mM Ca^{++} either in H_2O or ^2H_2O, 5mM vanadate, 10μM ATP, 2mM ATP and 5mM phosphate.

Between 30-50μl of protein suspension in each buffer was placed in a Beckman FH-01 thermostated cell fitted with CaF_2 windows separated by a 12μm tin spacer. The spectrometer was continuously purged with dry air to eliminate water vapour absorption from the spectral region of interest. For each sample, 200 scans were co-added at a resolution of $2cm^{-1}$. Buffer spectra were recorded under identical conditions. All spectra were recorded at 20^oC unless otherwise stated.

6.2.4. Ca^{++}-ATPase ACTIVITY MEASUREMENT

Activity was measured using the ATP regenerating system

as described by Gomez-Fernandez et al., (1980). All samples gave an activity measurement of 2-3 I.U.

6.2.5. PROTEIN CONCENTRATION DETERMINATION

Protein concentrations were determined by the method of Lowry et al., as modified by Wang and Smith (1975) and Larson et al., (1986), or from the ATPase molar absorptivity.

6.3 RESULTS

6.3.1 COMPARISON OF THE STRUCTURE OF PURIFIED SR AND PURIFIED Ca^{++}-ATPase IN THE E_1 STATE

The difference spectra of the Ca^{++}-ATPase and sarcoplasmic reticulum, generated by the digital subtraction of a buffer spectrum in H_2O from spectra of protein suspensions, are shown in figure 6.3. In both purified Ca^{++}-ATPAse and SR membranes, in H_2O buffer containing 5mM EGTA the amide I maximum was seen at $1657cm^{-1}$ and the amide II maximum at $1550cm^{-1}$. Second derivative and deconvolution analysis (Fig. 6.4a) reveals the presence of a number of components within the amide I band contour. The major feature in both cases is a component at $1657cm^{-1}$. Additional bands can be seen at $1680\text{-}90cm^{-1}$, $1644cm^{-1}$ and $1630cm^{-1}$.In ^2H_2O buffer, the amide I maxima in difference spectra was shifted some $8cm^{-1}$ to $1649cm^{-1}$ (not shown). A residual amide II band was observed at $1550cm^{-1}$ in both cases, indicating incomplete H-^{2}H exchange.Second derivative analysis revealed the presence of bands at $1680\text{-}90cm^{-1}$, $1657cm^{-1}$,$1644cm^{-1}$ and $1632cm^{-1}$. Bands were seen at similar positions in deconvolved spectra (Fig 6.4b)

6.3.2 THE STRUCTURE OF THE E_1Ca.Ca STATE IN PURIFIED SR AND THE PURIFIED Ca^{++}-ATPase

Derivative analysis of spectra of the Ca^{++}-ATPase recorded in the presence of $8\mu m$ and 0.1mM Ca^{++} revealed a

FIGURE 6.3: Difference spectra of the Ca^{++}-ATPase and SR in H_2O, 5mM EGTA

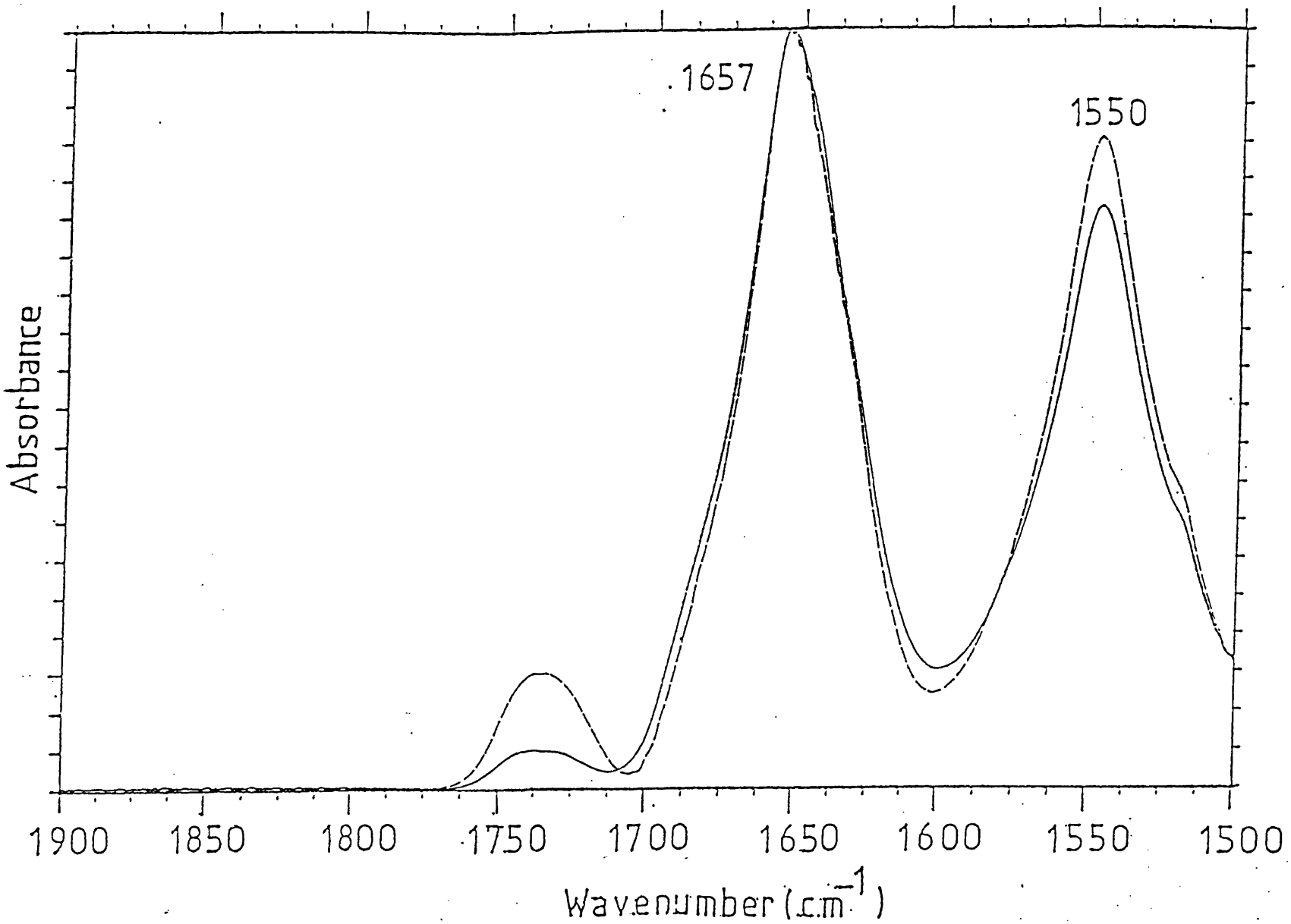
1657
1550
Absorbance
1900
1850
1800
1750
1700
1650
1600
1550
1500
Wavenumber (c.m^{-1})

Figure 6.4: Deconvolved spectra of Ca^{++}ATPase in a) H_2O and b) ^2H_2O in the presence of 5mM EGTA. F=2.1 W=15

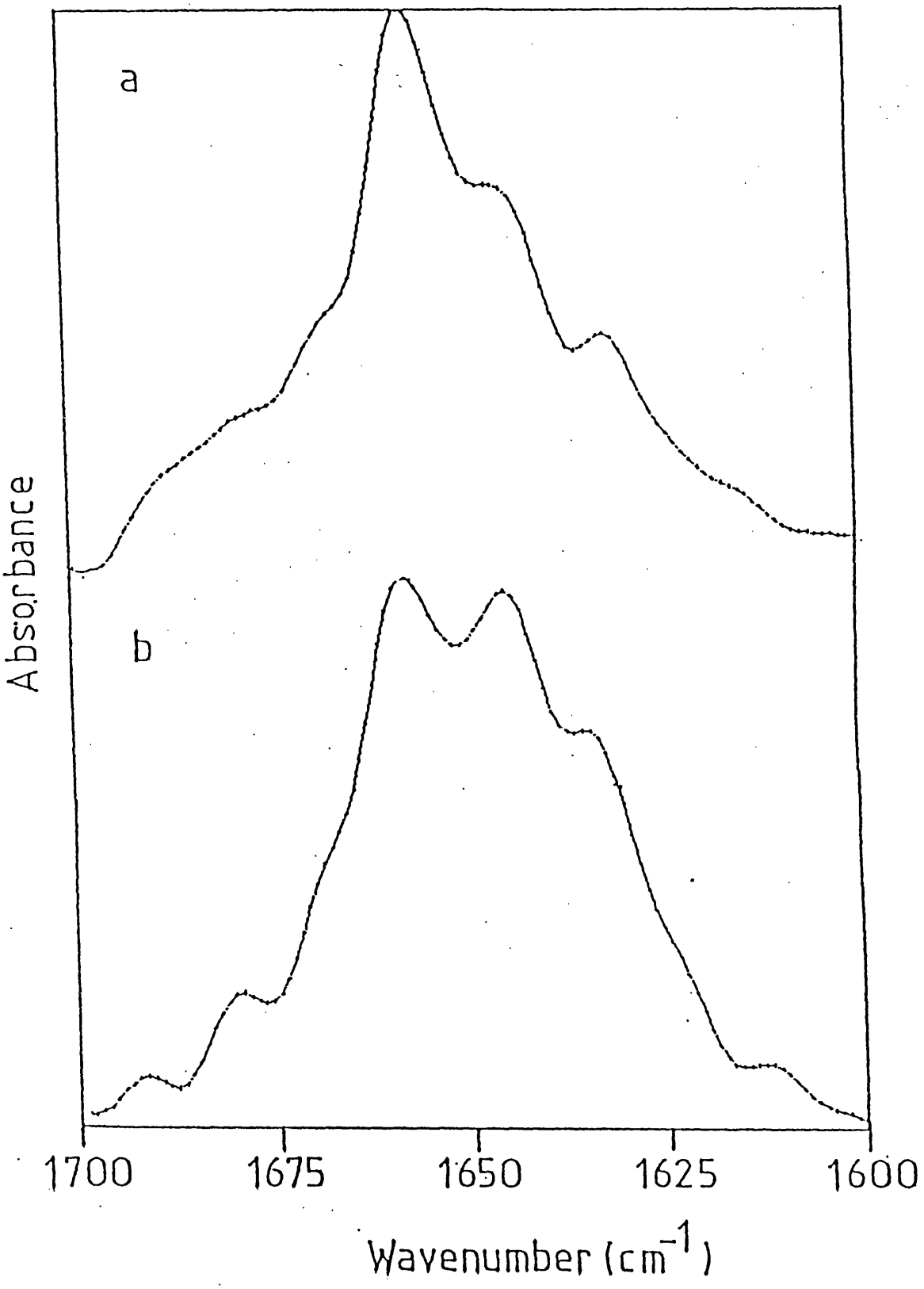
a
b
Absorbance
1700
1675
1650
1625
1600
Wavenumber (cm^{-1})

main component at 1657cm^{-1} in both ^2H_2O and H_2O buffers, together with additional bands at 1680-90cm^{-1}, 1644cm^{-1} and 1632cm^{-1} (Fig. 6.5b,c and 6.6b,c). Similar bands were identified in derivative spectra. Spectra recorded from SR suspensions were identical to those obtained for the purified protein.

6.3.3. STRUCTURE OF THE E_1-P STATE IN PURIFIED SR AND THE PURIFIED Ca^{++}-ATPase

Addition of 10μM or 2mM ATP to protein suspensions produced the deconvolved spectra shown in figure 6.5e and 6.6e. In both cases the major feature in ^2H_2O and H_2O buffers were seen at 1680-90cm^{-1}, 1657cm^{-1}, 1644cm^{-1}, 1630cm^{-} and 1623cm^{-1}. Bands at similar positions were seen after second derivative analysis of the spectrum. Identical results were obtained from SR preparations.

6.3.4 THE STRUCTURE OF THE E_2-V STATE IN SR AND THE PURIFIED Ca^{++}-ATPase

Addition of 5mM vanadate to SR and protein suspensions produces the E_2-V state of the Ca^{++}-ATPase. The deconvolved spectra of this state in the purified protein are shown in figure 6.5f and 6.6f. The major features in derivative and deconvolved spectra appear at 1680-90cm^{-1}, 1657cm^{-1}, 1644cm^{-1}, 1632cm^{-1} and 1623cm^{-1} in both ^2H_2O and H_2O buffers. Identical spectra were recorded for suspensions of SR.

Figure 6.5: Deconvolved spectra of the Ca^{++}-ATPase in H_2O in the presence of a) 5mM EGTA b) 8μM Ca^{++} c) 0.1mM Ca^{++} d) 5mM vanadate e)10μM ATP f) 2mM ATP and g) 5mM phosphate. F=2.1 W=15

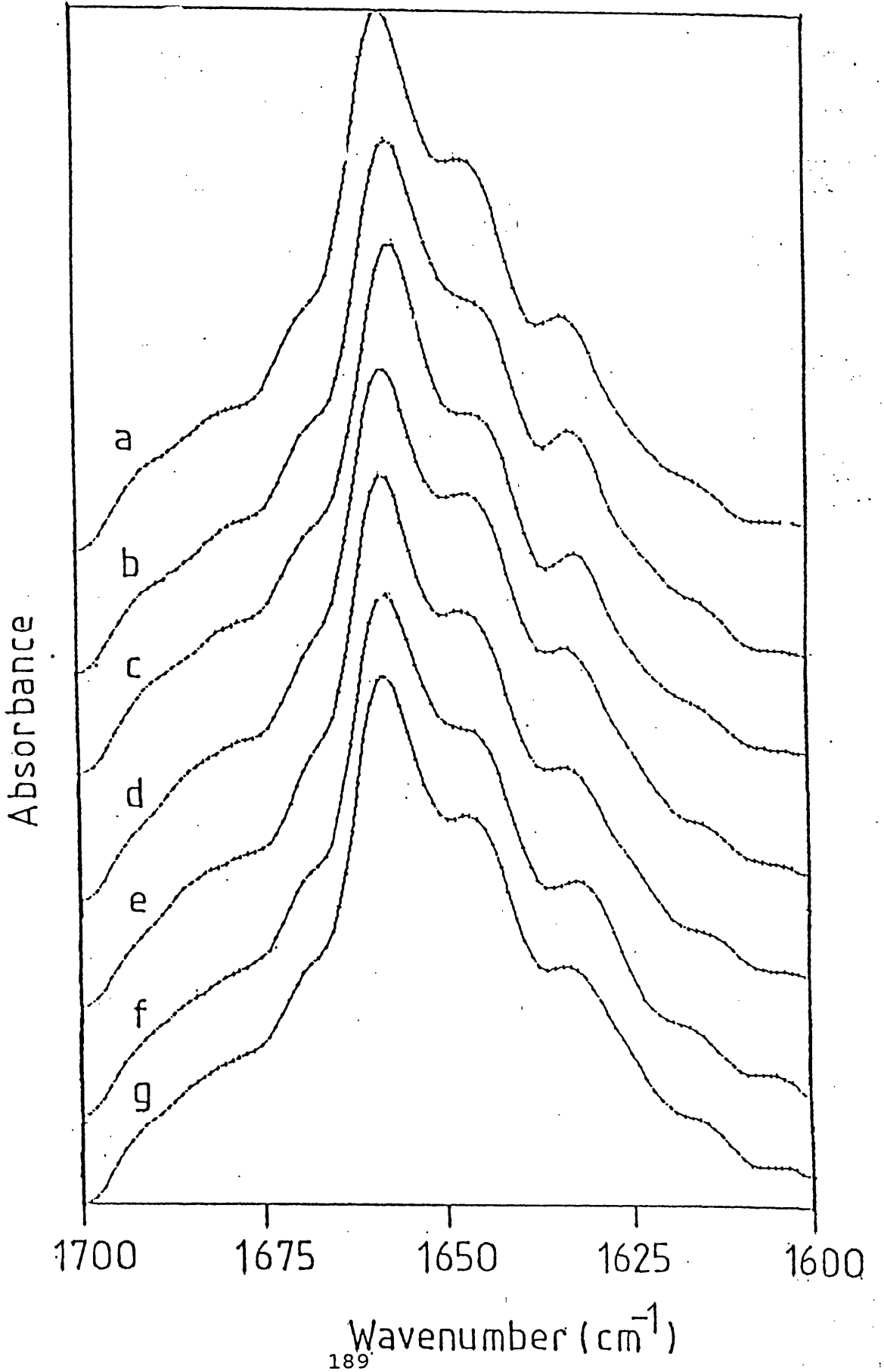
a
b
c
d
e
f
g
Absorbance
1700
1675
1650
1625
1600
Wavenumber (cm^{-1})

Figure 6.6: Deconvolved spectra of the Ca^{++}-ATPase in $^{2}H_{2}O$ in the presence of a) 5mM EGTA b) 8μM Ca^{++} c) 0.1mM Ca^{++} d) 5mM vanadate e) 10μM ATP f) 2mM ATP and g) 5mM phosphate. F=2.1 W=15

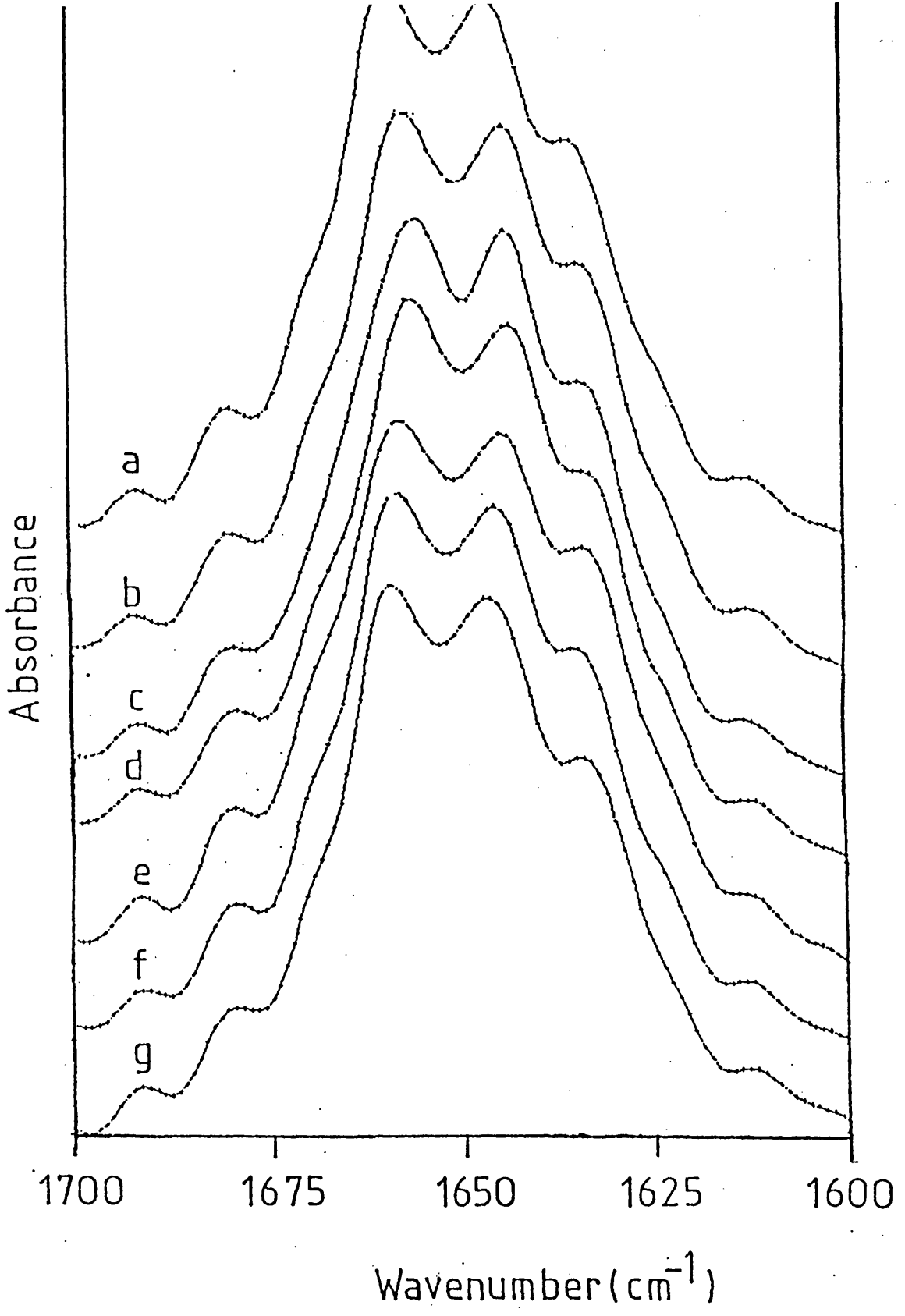
a
b
c
d
e
f
g
Absorbance
1700
1675
1650
1625
1600
Wavenumber (cm⁻¹)

6.3.5 THE STRUCTURE OF THE E_2-P STATE IN SR AND THE PURIFIED Ca^{++}-ATPase

Addition of inorganic phosphate drives the protein into the E_2-P state. The deconvolved spectra of this state are presented in figure 6.5g and 6.6g . The major feature in the the spectra in ^2H_2O and H_2O buffers occur at 1680-90cm^{-1}, 1657cm^{-1}, 1644cm^{-1}, 1630cm^{-1} and 1623cm^{-1}. Bands were observed at similar positions in spectra of SR.

6.3.6 THE EFFECT OF TEMPERATURE UPON CATALYTIC TRANSITIONS WITHIN SR AND THE PURIFIED Ca^{++}-ATPase

Spectra were recorded at 15^oC and 37^oC in each of the above reaction mixtures. In all cases no significant shifts in the bands described above were seen.

6.3.7 QUANTITATIVE ESTIMATE OF THE SECONDARY STRUCTURE OF THE PURIFIED Ca^{++}-ATPase

Quantitative analysis of the secondary structures present within the ATPase under each experimental condition was carried out using the curve fitting routine developed by Fraser and Suzuki (1966). Fig. 6.7 illustrates the best fits that could be obtained when the band shape of the individual components identified by derivative and deconvolution analysis was assumed to be either 90% Lorentzian / 10% Gaussian, 50% Lorentzian / 50% Gaussian or 100% Gaussian. The best fit was obtained when a 100% Gaussian band shape was used, as judged by calculation of

Figure 6.7: Band fitting of the Ca^{++}-ATPase in the presence of 5mM EGTA assuming a) 90% Lorentzian / 10% Gaussian bandshape b) 50% Lorentzian / 50% Gaussian bandshape and c) 100% Gaussian bandshape. GF= goodness of fit (Chi^2) SD= standard deviation.

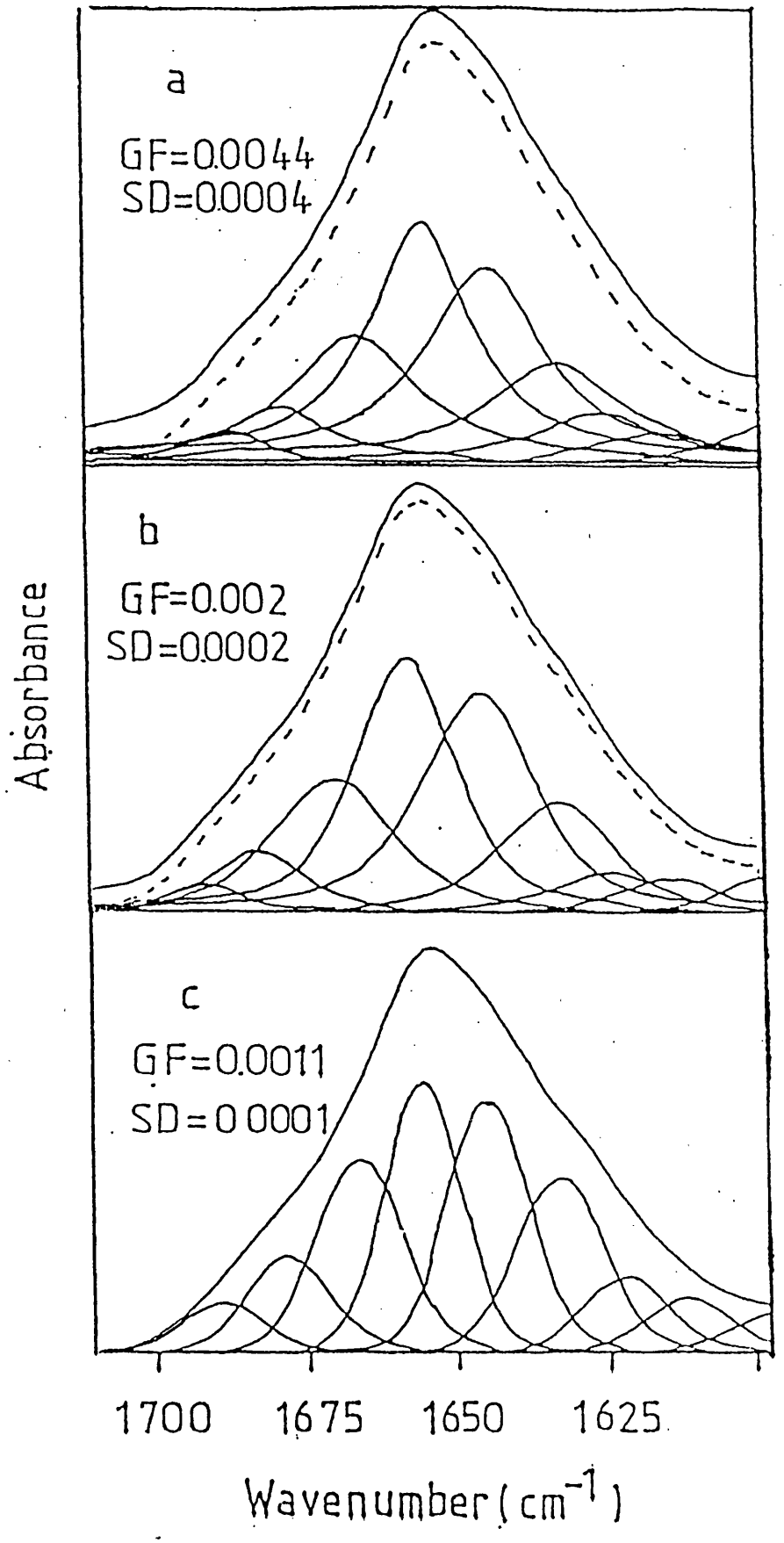
a
GF=0.0044
SD=0.0004
b
GF=0.002
SD=0.0002
c
GF=0.0011
SD=0.0001
Absorbance
1700
1675
1650
1625
Wavenumber (cm⁻¹)

chi^2 values.

The results of such an analysis carried out for the Ca^{++}-ATPase in the presence of 5mM EGTA using 100% Gaussian bandshapes is shown in table 6.I. Assigning the components as described in the Discussion section, the results indicate a structure containing 45% α-helix, 32% β-sheet and 23% turns. This result is compared to those obtained using other techniques in table 6.II.

This analysis was repeated for the Ca^{++}-ATPase in each of the reaction media. In each case the percentage of the various secondary structures was found to vary by no more than 1%.

FREQUENCY (cm^{-1})	%	ASSIGNMENT
1689.5	4.1	TURNS
1678.9	8.8	β-SHEET
1667.3	18.6	TURNS
1656.7	23.1	α-HELIX
1645.7	22.3	α-HELIX
1633.8	16.3	β-SHEET
1623.4	6.8	TURNS

TABLE 6-I: Band fitting analysis of the spectrum of Ca^{++}-ATPase in H_2O, 5mM EGTA

	CD[a]	AA[b]	RAMAN[c]	FTIR
α-HELIX	46%	52%	50%	45%
β-SHEET	8%	12%	21%	32%
TURNS	13%		17%	23%
RANDOM	33%		11%	

TABLE 6-II: Comparison of the quantitative estimation of the secondary structure of the Ca^{++}-ATPase using various techniques. [a]Csermely et al., 1988 [b]Brandl et al., 1985 [c]Williams et al., 1987

6.4 DISCUSSION

As mentioned in the introduction, a number of biophysical techniques (including Raman spectroscopy, CD spectroscopy and FTIR spectroscopy) have been applied to the study of the secondary structure of the Ca^{++}-ATPase of sarcoplasmic reticulum, often with contradictory results. The discrepancies reported may be due partly to the use of two different preparations, one of which, purified sarcoplasmic reticulum, contains other proteins. Of the protein impurities associated with SR, calsequestrin and M_{55} have been shown to bind calcium. Thus it is possible that conformational changes described in SR preparations arise not from the Ca^{++}-ATPase but from protein impurities. With this is mind, the present study was undertaken to assess not only the conformational responses of the Ca^{++}-ATPase to ligands, but also any differences between these responses and those shown by SR preparations.

Inspection of the reaction cycle shown schematically in figure 6.1 reveals that it is possible to drive the Ca^{++}-ATPase through a series of intermediate stages. Examination of the difference deconvolved and second derivative spectra of SR and the purified ATPase in the resting (E_1) state showed these spectra to be identical (fig. 6.3). In H_2O buffer containing EGTA (i.e. no free Ca^{++}) the predominant structures appear to be helices as deduced from the presence

of an amide I maximum at 1657cm^{-1} in difference spectra and the major component of derivative and deconvolved spectra at 1657cm^{-1} (assignment of bands in this work is based on Susi and Byler 1986, Lee and Chapman 1986, Surewicz and Mantsch 1989, Jackson et al., 1990a). It must be born in mind that unordered polypeptide segments also absorb at this position, and contributions from such structures cannot be ruled out. The presence of significant proportions of β-sheet is indicated by the appearance of a band at 1632cm^{-1}. A broad, composite band seen at 1680-90cm^{-1} in derivative spectra can be associated with turns and β-sheet.

The assignment of the band at 1644cm^{-1} is not straight forward. Such a frequency is too low to be associated with a standard helical vibration or to arise from unordered regions of the protein. These two structures In H_2O have been shown to give overlapping absorptions in the region of 1650-1658cm^{-1} in all proteins studied to date, both membrane and water soluble. Unordered polypeptide chains can be demonstrated to absorb at around 1644cm^{-1} upon deuteration, however this band is seen in the Ca^{++}-ATPase even in H_2O. Such an absorption is also inconsistent with β-sheet structures, which generally absorb in the region 1630-1640cm^{-1}. Thus, this absorption can be seen to be rather unusual. It may arise from an unusual β-sheet structure, or from the $3\pi/2$ vibration of helices, as

suggested by Lee et al., (1985). It is interesting to note that this absorption band is not seen in two other ATPases studied by FTIR spectroscopy (Haris et al., 1986b, Mitchell et al., 1988).

Upon suspending the ATPase in ^2H_2O buffer containing EGTA, the amide I maximum in the difference spectrum shifts $8cm^{-1}$ lower to $1649cm^{-1}$. This is consistent with deuteration of unordered polypeptide segments, the absorption arising from these segments shifting from $1657cm^{-1}$, where it overlaps with helical absorptions, to lower frequencies. The increase in absorption at $1644cm^{-1}$ confirms this. This results in a significant downward shift in the peak maximum.

A residual amide II absorption is still seen in ^2H_2O buffer, indicating the presence of significant proportions of non-deuterated protein segments. This can be related to substantial amounts of the helical structure of the protein being situated within the bilayer, where it is inaccessible to solvent. The relatively strong residual amide II band would imply that the Ca^{++}-ATPase does not form an aqueous channel, as suggested by Edmonds (1984), as this would be expected to enhance the extent of hydrogen-deuterium exchange.

Further substates of the E_1 conformation can be induced by the addition of varying amounts of Ca^{++} (de Meis and Vianna 1979) and ATP (Dupont 1977). This results in the

formation of $E_1.Ca^{++}$, $E_1.Ca^{++}Ca^{++}$ and $E_1.P$ substates. Conversion from the E_1 reference state to these states has been shown by tryptophan fluorescence (Dupont 1976) and electron spin resonance (ESR) spectroscopy (Coan and Inesi 1977) to be accompanied by structural rearrangements. Deconvolved spectra of these substates are shown in figure 6.7 and 6.8. It is apparent that not only are these spectra identical to each other, but they are also identical to that obtained for the reference E_1 state. Similar results were obtained with SR. Thus it can be concluded that binding of Ca^{++} or ATP to the Ca^{++}-ATPase or SR membrane fractions produces no major rearrangement of the protein secondary structure.

It is well known that addition of vanadate ions to preparations of the Ca^{++}-ATPase induces the E_2 state of the enzyme (Pick and Karlish 1982), with the formation of 2-dimensional crystalline arrays of protein. Addition of P_i to the reaction medium also stabilises the protein in the E_2 state (Masuda and de Meis 1973), accompanied by structural rearrangements as deduced from low angle X-ray diffraction (Blasie et al., 1985) and TNP-ATP fluorescence (Watanabe and Inesi 1982). Difference, second derivative and deconvolved spectra of these two states proved to be identical in the purified ATPase and SR, and also to be identical to spectra obtained in the presence of EGTA, Ca^{++} and ATP.

Such qualitative results lead to the conclusion that binding of Ca^{++} to the protein and the subsequent translocation of Ca^{++} across the membrane of the sarcoplasmic reticulum are not accompanied by major rearrangements of the protein secondary structure. This is in agreement with results obtained from CD spectroscopy applied to conformational transitions in SR in response to Ca^{++} and vanadate (Csermely et al., 1987) and CD results for the purified ATPase with regards to Ca^{++} binding and phosphoenzyme formation (Nakamoto et al., 1986). It can also be concluded that preparations of the purified protein and SR do not differ significantly from each other in their spectroscopic properties during Ca^{++} translocation.

Structural transitions detected by other spectroscopic techniques probably arise from reorientation of polypeptide chains with respect to each other, that is, sliding or tilting. Such changes, which do not result in a change in the relative proportions of the various secondary structures will not be detected by FTIR spectroscopic analysis of protein suspensions. A particularly fruitful area for future research would be the spectroscopic characterisation of hydrated, oriented layers of Ca^{++}-ATPase using polarisation techniques. Such an analysis would allow estimation of the orientation of the individual secondary structures within the molecule in the various conformational substates.

It has been demonstrated by a number of workers that the activity of the Ca^{+}-ATpase is dependent upon temperature in a manner which suggests that the phase of the lipids in SR and purified protein preparations is important (Inesi et al ., 1973). In this respect, it has been suggested that the gel-liquid crystalline phase transition of DMPC in DMPC-reconstituted ATPase preparations is accompanied by structural rearrangements in the secondary structure of the protein (Merino, 1987). The lack of any demonstrable structural changes accompanying Ca^{++} translocation may possibly be a result of the SR lipids being in a gel state. In light of this, spectra of SR were obtained at temperatures between 10-37^{o}C. No differences in spectra recorded in the reaction media described above were detected. It can therefore be concluded that sub-physiological temperatures are not responsible for the lack of structural rearrangement accompanying Ca^{++} translocation described here. This is as expected, as the Ca^{++}-ATPase can be shown to hydrolyse ATP at the temperatures used in this work, indicating that the protein is functionally normal. This may be a result of the higher lipid:protein ratio and complex lipid composition of SR as compared to reconstituted systems, which will ensure that the lipid is in a liquid crystalline state even at relatively low concentrations.

Although the qualitative information outlined above is

of undoubted use, it would be of immense value to be able to describe the various substates of the Ca^{++} in a quantitative manner. Attempts have recently been made to describe the secondary structure of a number of water soluble proteins in quantitative terms (Susi and Byler 1986, Byler and Susi 1986, Surewicz et al., 1987, Yang et al., 1987). Such studies relied upon the application of curve fitting techniques based upon least squares analysis of the spectra. Briefly, positional data obtained from second derivative and deconvolved spectra together with estimates of the shape (either Lorentzian, Gaussian or mixed) and halfwidth of the bands are used as input parameters for the curve fitting routine. The routine then attempts to match the experimentally obtained amide I band with a synthetic band obtained by varying the widths and relative heights of the components. This iterative procedure continues until the experimental and synthetic amide I bands match to within chosen error limits. The area under each of the components is calculated, and the area of each component as a percentage of the area of the amide I band assumed to represent the percentage of the secondary structure giving rise to the component.

Such a curve fitting analysis was applied to the spectra of the Ca^{++}-ATPase in each of the conformational substates described above. As a preliminary study, the

effect of variations in the assumed band shape was studied. Figure 6.7 illustrates the best analysis that could be achieved assuming a 90% Lorentzian (a), 50% Lorentzian/50% Gaussian (b) and 100% Gaussian band shapes. It can clearly be seen that as the percentage of Gaussian contribution to the band shape is increased the calculated fit improves, the best fit being obtained if 100% Gaussian bandshapes are assumed. It is well known that for simple molecules, infrared bands are close to Lorentzian (Cameron and Moffat 1984). However, the complex nature of the protein chain will significantly increase the Gaussian characteristics of the infrared bands.

Table I lists the fractional areas of the bands calculated for the Ca^{++}-ATPase in the presence of 1mM EGTA in both H_2O and ^2H_2O. In each case the best fit was always obtained assuming a 100% Gaussian band shape. Similar band fittings were made for the ATPase in the other reaction mixtures, and in each case no changes in the area of any band of more than 1% was seen. These results indicate that Ca^{++} translocation across the membrane of the sarcoplasmic reticulum are not accompanied by any major structural rearrangements, in line with the qualitative information discussed above.

The curve fitting analysis described above must be used with extreme caution. A number of important assumptions are

inherent in the method:

1) For each component band, a band shape must be assumed.

2) Each component band is assumed to have the same band shape.

3) Each secondary structure is assumed to have the same molar absorptivity.

Of these assumptions, the last is the most important and also the hardest to justify. It necessitates that the difference in the hydrogen bonding schemes and the different degrees of solvation of the various secondary structures have no effect upon the strength of the infrared absorbance. This has been shown not to be the case (Chirgadze et al., 1973, Jackson et al., 1989, Mantsch et al., 1989, see also chapter 5).

6.5 CONCLUSIONS

Infrared spectra of purified SR and the purified Ca^{++}-ATPase from SR under all conditions studied were found to be identical. Furthermore, we purified the ATPase separately in two laboratories using two different procedures and found no difference in infrared spectra, suggesting that the discrepancy between results obtained using a variety of techniques is not related to the use of different preparations.

Stabilisation of the ATPase or SR in a variety of conformational substates by the use of Ca^{++}, vanadate, ATP or P_i produced identical spectra for each substate. From this we may deduce that translocation of Ca^{++} across the SR membrane is not accompanied by any major changes in the secondary structure of the protein. Any structural rearrangements which occur within the protein are more likely to be due to reorientation or twisting of polypeptide chains with respect to each other, rather than a refolding of the polypeptide chain.

Curve fitting analysis was applied to the spectra of the purified Ca^{++}-ATPase in each of the conformational substates. No significant variations in the area of each computed band was found as the reaction medium was varied, confirming the qualitative results discussed above. However, the curve fitting analysis should be used with caution, as a

number of assumptions in the method are open to question.

CHAPTER 7

THERMAL DENATURATION OF PROTEINS STUDIED USING FTIR SPECTROSCOPY

7.1 INTRODUCTION

One of the most intriguing problems in protein biochemistry is the mechanism by which proteins fold. Whilst our knowledge of protein folding and unfolding pathways is limited, a few points are generally agreed (Anfinsen, 1973; Baldwin, 1975; Creighton, 1978)

1) all of the information necessary for correct folding of a protein is contained in the amino acid sequence of the protein
2) it is accepted that the folding process is spontaneous
3) the folding process cannot occur by a random sampling of all possible conformational states, a process which would take 10^{77} years for a protein of only 100 amino acids. Such rates are not only biologically unfeasible, but are inconsistent with experimental data which suggests that time scales in the subsecond-minute range are relevant.

Important questions which remain to be addressed are;

1) Are proteins synthesised in their entirety before folding is initiated ?

2) Are there common pathways in the folding/unfolding of all proteins ?

3) Are the folding and unfolding processes the same for water soluble and membrane proteins ?

4) What is the nature of the folding intermediates in proteins ?

The nature of folding intermediates is currently being investigated by a number of workers using bovine pancreatic trypsin inhibitor and ribonucleases as model systems (Creighton, 1974; Creighton, 1975; Creighton, 1977). These protein can be reversibly unfolded and intermediates in the refolding process trapped (Creighton, 1975).

Another useful approach to the problem of protein folding is to study the reciprocal process of protein unfolding. The folded states of most proteins are only marginally stable and can be disrupted in many cases by relatively minor changes in temperature, pH, ionic strength, solvent or pressure. Furthermore, agents which disrupt the structure of water (eg. urea, guanidine hydrochloride) can also disrupt protein structure (Tanford, 1964; Hibbard and Tulinsky, 1978).

The unfolding of proteins occurs over a narrow range of denaturing conditions, rather like phase transitions in lipids. Before this point there will be local disruption and increased mobility of the chains but the average conformation of the protein will be unchanged. At the denaturing point the protein will rapidly convert to a non-native form. It should be born in mind that denaturation does not imply conversion of the protein to a completely unordered form, rather conversion to a conformational state different from the native state. Also, denaturation events

induced within the same protein by different mechanisms do not necessarily result in the same protein conformation.

Solvent and salt perturbation of proteins have recently led to the production of so-called " molten-globule " states in a number of proteins (Ohgoshi et al., 1985). This state has a secondary structure similar to the native protein, but has a fluctuating tertiary structure. Molten globule states have properties intermediate between the denatured and native protein states.

Whilst useful information can be obtained from studies of such conformational substates, the number of proteins in which the molten globule state has been demonstrated is limited. It is therefore clear that a more generally applicable technique is needed. In recent years FTIR spectroscopy has been used to probe structural changes associated with solvent, pressure and thermal denaturation of proteins. However, no systematic study of a wide range of water soluble and membrane protein denaturation profiles has yet been undertaken using FTIR spectroscopy. In this chapter results of a study on the thermal denaturation of a wide range of proteins will be presented.

7.2 MATERIALS AND METHODS

Haemoglobin, myoglobin, parvalbumin, fibrinogen, polylysine, cytochrome C, lysosyme, concanavalin A and chymotrypsinogen were purchased from Sigma, UK. Ca^{++}-ATPase was isolated from sarcoplasmic reticulum as described in chapter 6. Calmodulin was the generous gift of Prof. Sarzala Gabriella.

Samples were prepared for infrared spectroscopy by dissolving or suspending the protein in ^2H_2O or ^2H_2O buffer to a final concentration of 3% (w/v). Spectra were recorded by placing 50ul of each sample between a pair of CaF_2 windows separated by a 50um teflon spacer. The windows were mounted in a Beckman FH-01 cell. Temperature was maintained at 20°C or 70°C by a circulating water jacket. For each sample 100scans were recorded at $4cm^{-1}$ resolution and signal averaged. Difference spectra were generated by the digital subtraction of the relevant buffer spectrum recorded under identical conditions.

Polyacrylamide gel electrophoresis was carried out under non-denaturing conditions. Briefly, samples of haemoglobin, myoglobin and BSA were incubated at 80°C for 20 minutes in the absence of SDS. These heat treated samples together with unheated samples and standards were layered onto a 5% stacking gel and run through both the stacking and resolving gel (15%) at constant current (40A).Staining and fixing was with Coomasie blue/isopropanol. Destaining was

achieved with acetic acid/isopropanol.

7.3 RESULTS

7.3.1 FTIR spectroscopy

The difference spectrum of bovine serum albumin recorded at 20° after 1hr incubation in ^2H_2O at 50°C is shown in figure 7.1. The amide I band maximum is seen at 1651cm^{-1}, with no residual amide II band in the 1550cm^{-1} region of the spectrum. Second derivative analysis reveals the presence of additional bands at 1670cm^{-1} and 1630cm^{-1} (fig. 7.2). Elevation of the temperature to 70°C produced the difference spectrum indicated by the broken line in figure 7.1. A slight decrease in the amide I frequency to 1650cm^{-1} is apparent. Two new bands are observed as shoulders at 1615cm^{-1} and 1680cm^{-1}. Derivative analysis highlights these features at 1615cm^{-1} and 1683cm^{-1} (fig. 7.2).

A difference spectrum generated by the subtraction of a spectrum of BSA recorded upon immediate elevation of the temperature to 70°C from a spectrum recorded after 15 minutes at 70°C is shown in figure 7.3. Maxima are observed at 1616m^{-1} and 1681cm^{-1}, with a minimum at 1651cm^{-1}.

Similar spectra were obtained for haemoglobin, myoglobin,troponin C, calmodulin,parvalbumin, poly-L-lysine and fibrinogen and the membrane bound Ca^{++}-ATPase. The major amide I bands seen after second derivative analysis at 20°C and 70°C for all proteins studied are shown in table 7-I.

The difference spectrum of concanavalin A is shown in

Figure 7.1: Difference spectra of BSA recorded at $20^{o}C$ (solid line) and $70^{o}C$ (broken line) in $^{2}H_{2}O$.

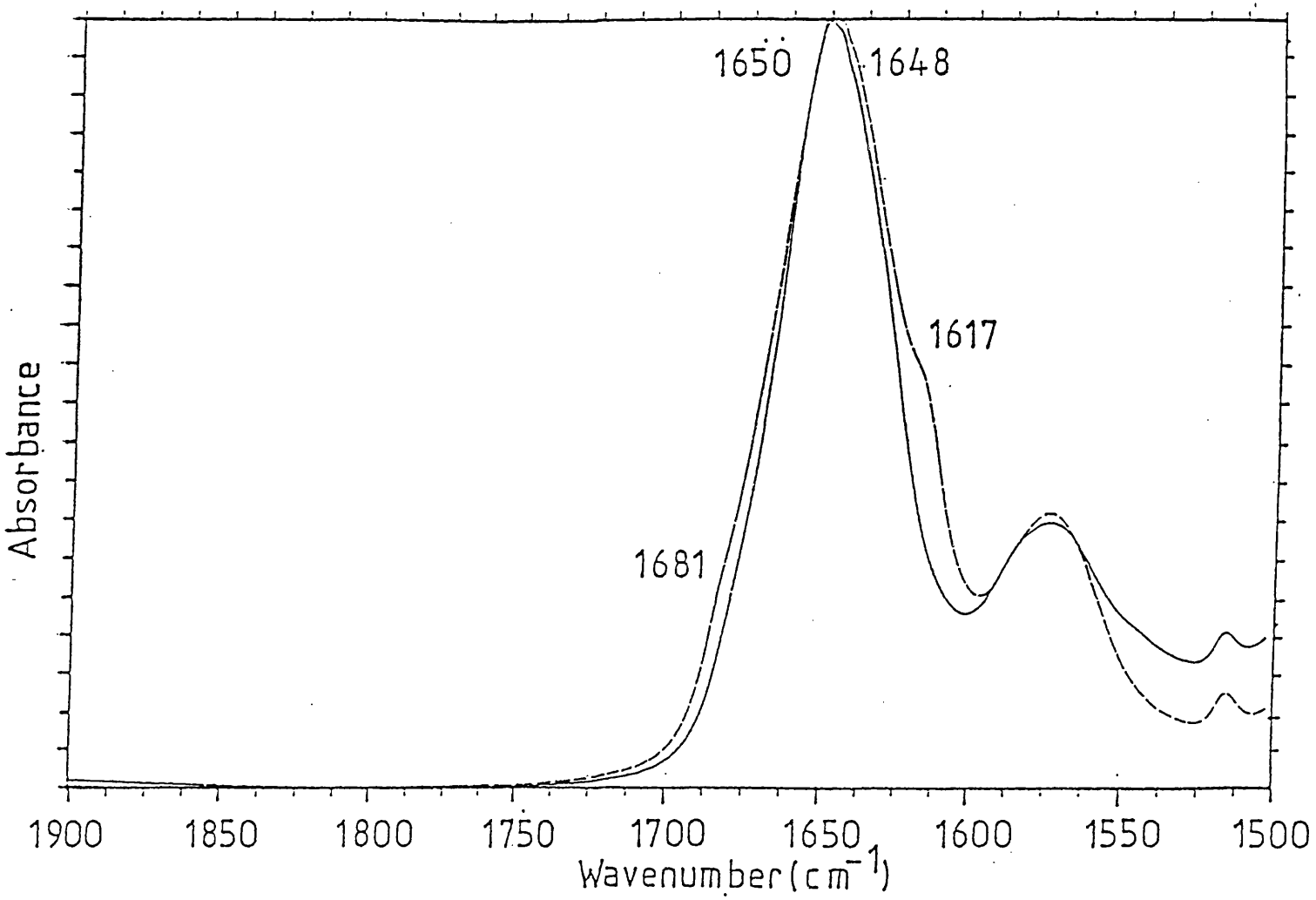
1650
1648
1617
1681
Absorbance
1900
1850
1800
1750
1700
1650
1600
1550
1500
Wavenumber (cm⁻¹)

Figure 7.2: Second derivative spectrum of BSA recorded at 20^{o}C (solid line) and 70^{o}C (broken line). Factor=13

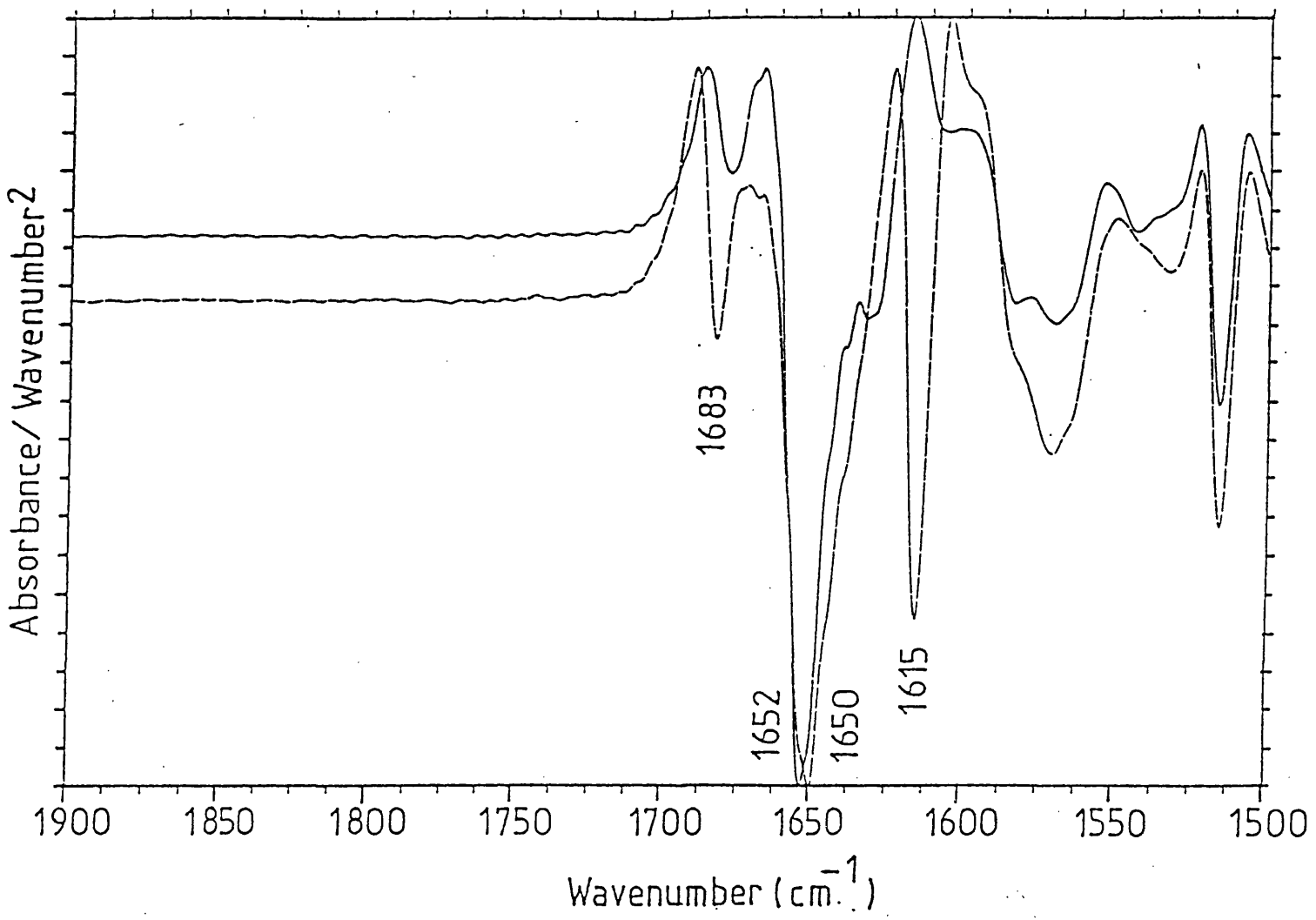
Absorbance/ Wavenumber2
1683
1652
1650
1615
1900
1850
1800
1750
1700
1650
1600
1550
1500
Wavenumber (cm.-1)

Figure 7.3: Difference spectrum of BSA generated by the subtraction of a spevctrum of BSA recorded after 2 minutes at 70^{o}C form a spectrum of BSA recorded after 45 minutes at 7-0^{o}C.

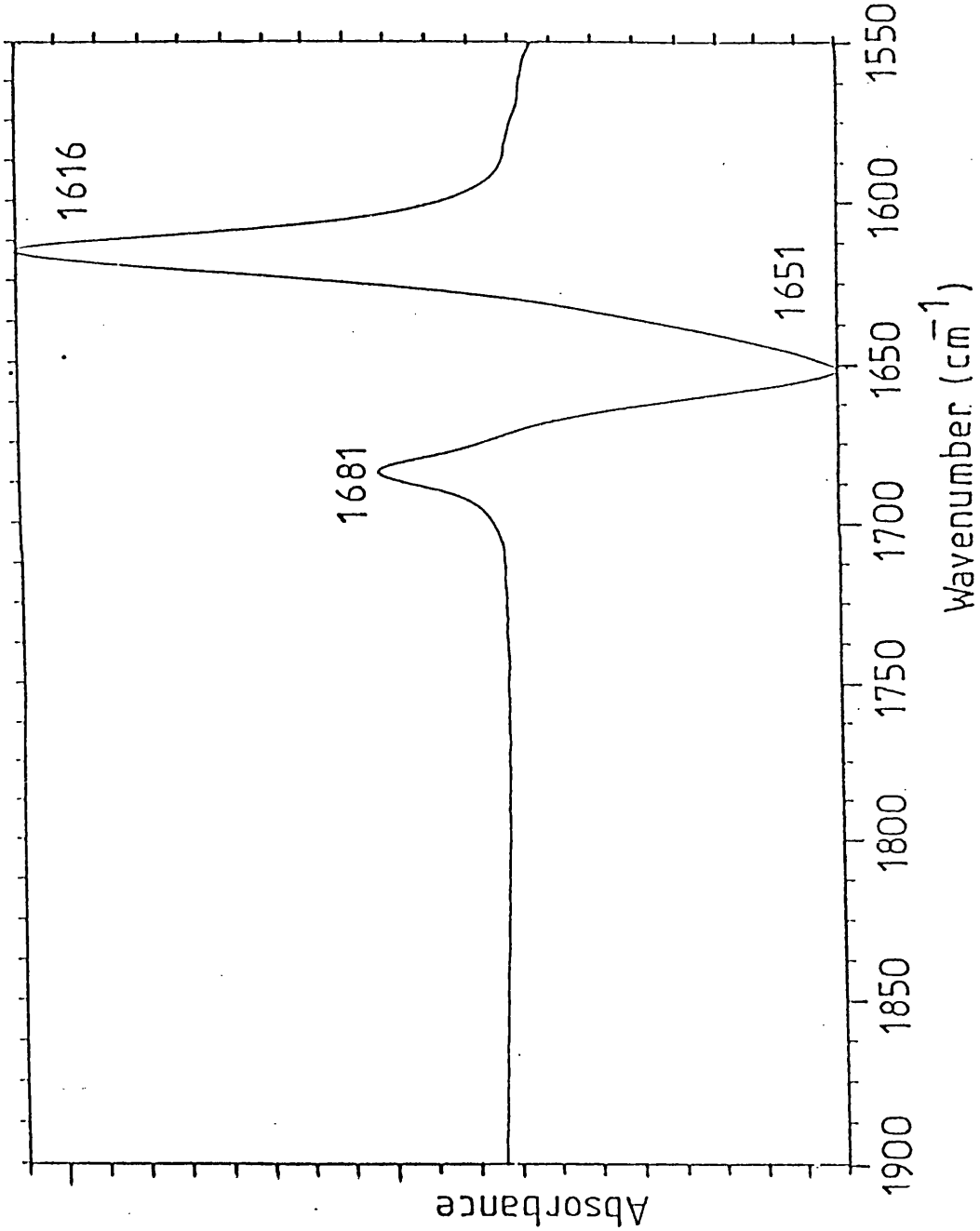
1616
1651
1681
1900
1850
1800
1750
1700
1650
1600
1550
Wavenumber (cm^{-1})
Absorbance

Figure 7.4: Second derivative spectra of cancanavalin A recorded at 20°C (solid line) and 70°C (broken line) in ^2H_2O. Factor=13

Absorbance / Wavenumber2
1900
1850
1800
1750
1700
1650
1600
1550
1500
Wavenumber(cm-1)
1695
1635
1623

figure 7.4. The amide I maximum is observed at 1636cm^{-1}. Derivative analysis reveals the presence of bands at 1690cm^{-1}, at 1650cm^{-1}, 1635cm^{-1} and 1625cm^{-1}. Elevation of the temperature to 70^{o}C produced the derivative spectrum shown in figure 7.4, with bands seen at 1680cm^{-1}, 1650cm^{-1}, 1635cm^{-1} and 1625cm^{-1}.

7.3.2 Polyacrylamide gel electrophoresis

Polyacrylamide gel electrophoresis carried out upon heated and unheated haemoglobin, myoglobin and BSA indicated an apparent large increase in the molecular weight of each heated protein. Little, if any staining was observed in lanes to which heated proteins were added. Heavy staining was seen at the top of the resolving gel in these lanes.

PROTEIN	MAJOR BANDS (cm^{-1})	
	$20^{o}C$	$70^{o}C$
Haemoglobin	1654 1636	1686 1652 1615
Myoglobin	1652 1634	1685 1650 1615
Calmodulin	1670 1644 1630	1686 1644 1615
Parvalbumin	1666 1644 1630	1685 1644 1615
BSA	1678 1650	1683 1650 1616
Fibrinogen	1650 1640 1628	1683 1650(s) 1643 1615
Poly-L-lysine	1638 1623	1685 1610
Ca^{++}-ATPase	1657 1644 1633	1686 1657 1644 1615
PSII complex	1678 1657 1630-8	1686 1652 1624

Table 7-I: Major band positions in second derivative spectra of a range of proteins at $20^{o}C$ and $70^{o}C$. Spectra recorded in $^{2}H_{2}O$, pD 7.5
s=shoulder

7.4 DISCUSSION

The amide I of BSA in ^2H_2O after complete exchange (as judged by the absence of a residual amide II band) was observed at 1651cm^{-1}. Such an absorption is typical of a predominantly α-helical protein. Elevation of the temperature to 70^{o}C results in the production of two strong shoulders in the spectrum at 1615cm^{-1} and in the region 1680-90cm^{-1}. Derivative analysis reveals the presence of two new bands in the spectrum recorded at 70^{o}C, at 1615cm^{-1} and 1685cm^{-1}. The appearance of two such narrow, intense bands (the low frequency band being the most intense) is often taken to indicate the presence of anti-parallel β-sheet structures. However, upon examination of the spectrum of predominantly β-sheet proteins such as chymotrypsinogen and concanavalin A (fig 7.3), the bands generally assigned to β-sheet structures can be seen to occur at 1630-40cm^{-1} and 1680cm^{-1}. The low frequency of the 1615cm^{-1} band compared to bands seen in β-sheet proteins therefore suggests that standard β-sheet structures are not responsible for the new bands. Similar spectra have been reported for solvent induced denaturation of chymotrypsinogen A and β-lactoblobulin (Purcell and Susi, 1984). In this study the unusual frequencies of theses bands was attributed to the presence of an unusual type of β-sheet structure. However, Casal et al (1988) suggested that similar bands appearing in the spectrum of thermally denatured β-lactoglobulin B were

the result of intermolecular association. In this respect they noted that Papiz et al (1986) have previously described the formation of an intermolecular β-sheet between polypeptide strands on neighbouring molecules for this protein.

Results obtained from PAGE tend to confirm the suggestion that the bands at 1615cm^{-1} and 1685cm^{-1} arise from peptide groups involved in intermolecular associations. After heat treatment only minor amounts of protein entered the resolving gel, suggesting a drastic increase in the molecular weight of the materials in each of the relevant lanes. In fact, much of the material was observed to remain in the wells of the stacking gel as particulate matter. Furthermore, in many cases heat treatment was observed to be accompanied by a concomitant increase in the viscosity and turbidity of the solutions.

Examination of the spectrum generated by the subtraction of a spectrum recorded after 30 seconds at 70^{o}C from that obtained after 45 minutes at 80^{o}C reveals a decrease in absorbance at 1650cm^{-1} which parallels the increase in absorbance at 1616cm^{-1} and 1683cm^{-1}, suggesting the formation of these new structures is at the expense of α-helical polypeptide segments.It appears that the new bands which appear in the spectrum of BSA following heat treatment can be related to the formation of an intermolecular β-sheet. As the temperature is increased, regions of α-helix

appear to unfold and become involved in hydrogen bonding to adjacent molecules.

Similar spectra were obtained for all of the predominantly α-helical proteins studied here. Thus the unfolding of helical polypeptide strands and the formation of intermolecular β-sheets appears to be a general phenomenon for helical proteins, whether fibrous (eg. fibrinogen), globular (eg. haemoglobin) or membrane bound (eg. Ca^{++}-ATPAse). However, it must be born in mind that the Ca^{++}-ATPase forms highly ordered arrays within the sarcoplasmic reticulum membrane and protein-protein contacts between the cytoplasmic domains are probably extensive. Other membrane proteins which do not have such extensive intermolecular interactions may not be able to form this intermolecular β-sheet.

Studies of the time dependence of the spectral changes indicate a progressive alteration of the protein structure, that is, this interconversion is not a rapid event. The rearrangement appears in most cases to be incomplete, not all helical regions are unfolded. In fact, in almost all proteins studied so far the helix still remains the dominant structural motif. The one exception to this generalisation is poly-l-lysine, which appears to convert almost completely to an intermolecular β-sheet form (see Chapter 4).

The spectroscopic changes detailed above are not observed for the predominantly β-sheet protein concanavalin

A. Spectra recorded at 20°C and 70°C are identical (see fig. 7.5). This is presumably related to the greater stability of the β-sheet secondary structure as compared to the α-helix. In this respect it is interesting to compare the thermal profiles of the two forms of antitrypsin. This protein exists as a single (uncleaved) polypeptide chain and also in a form in which the chain has been cleaved. Both forms are believed to be predominantly β-sheet (Haris et al., 1990). The cleaved form can be shown to undergo proton-deuteron exchange at a reduced rate compared to the uncleaved form, indicating a more compact and possibly more stable structure (Haris et al 1990). This form of antitrypsin does not show the bands associated with the intermolecular β-sheet structure described above. However, the uncleaved antitrypsin does exhibit these bands. Thus, the formation of intermolecular aggregates upon unfolding of native structures may be a property common to all proteins. This phenomenon is not apparent for concanavalin A as it does not unfold at the temperatures used here.

It must be born in mind that the protein concentrations required for FTIR spectroscopy are significantly higher than those used for most other biophysical measurement techniques. Thus, the spectral phenomena described in this chapter may not be apparent using other techniques. This does not imply that the results reported here have no biological relevance. Indeed, this phenomenon may allow us

to establish the existence of intermolecular associations within multi-protein complexes.

7.5 CONCLUSIONS

FTIR spectroscopy has been applied to the study of the thermal denaturation of a range of proteins. For all of the α-helical proteins studied, elevation of the temperature to 80^{o}C resulted in the appearance of two new bands in the region 1690-89cm^{-1} and at 1616cm^{-1}. Results from PAGE and the visible increases in turbidity and viscosity of many of the solutions suggested aggregation occurred after heat treatment. The FTIR spectra could thus be interpreted as being the result of a decrease in the helical structure of the protein accompanied by the formation of an intermolecular β-sheet. This appears to be widespread phenomenon for α-helical proteins, being demonstrated for polylysine, haemoglobin, myoglobin, BSA,Ca^{++}-ATPase, PSII reaction centre,calmodulin, parvalbumin and fibrinogen. Predominantly β-sheet proteins such as concanavalin A do not show this unusual behaviour. This is presumably related to the greater stability of the β-sheet secondary structure compared to α-helices. It may be that elevation of the temperature above that used in this study will result in the appearence of the low frequency band in the spectra of β-sheet proteins.

CHAPTER 8

FUTURE WORK

Whilst a great deal of useful information has been obtained from FTIR spectroscopic studies, much work remains to be done. The most fundamental problem lies in the assignment of amide I bands in deconvolved and second derivative spectra. The assignment of bands to turn structures is not always straight forward, as contributions from β-sheet occur in the same region. As many β-sheet structures also contain turns, bands arising from both structures are seen in most spectra. Thus, it is difficult to definitively assign these bands. Studies on model compounds and proteolytic cleavage of β-sheets at the positions where the direction of the polypeptide chain reverses will be useful in this respect.

An important but much neglected aspect of the FTIR spectrum of proteins is the sensitivity of the amide I band to the strength of solvent interactions. This has been shown in Chapter 5 to play a dominant role in determining the amide I band position and has led to incorrect structural determination in the past (Trewhella et al., 1989). The effect of protein hydration upon the FTIR spectrum will be assessed by relating existing protein-solvent interaction data (eg. the number of molecules of water present in crystals, charge/surface area ratio etc.) to the position of the amide I band maximum for a wide range of proteins.

With the development of FTIR microscopy, it is now possible to obtain spectra of proteins in the crystalline

state. The technique of choice for structural characterisation of proteins for many years has been X-ray diffraction. However, the extent to which the structure of a crystallised protein resembles that of the protein in the native environment is not known. This problem can now be addressed using FTIR spectroscopy. To this end a collaboration has been undertaken with Dr. David Stokes of the National Institute for Medical Research to produce crystals of the Ca^{++}-ATPase of sarcoplasmic reticulum. These crystals will be examined using FTIR microscopy and the structure of the protein compared to that of the protein in aqueous solution.

Examination of the Ca^{++}-ATPase by electron microscopy is already in progress in Dr. Stokes' laboratory. The relevance of the structure determined in this manner (at $-186^{o}C$) will be assessed by comparing infrared spectra of the crystals recorded at $-186^{o}C$ and $20^{o}C$.

Polarisation studies of proteins and peptides are frequently carried using the technique of attenuated total reflectance (ATR) spectroscopy. Deposition of ordered films onto infrared-transmitting crystalline materials (such as germanium) is followed by exposure of the sample to polarised infrared radiation. Variation in the polarisation of the radiation allows estimations of the orientation of secondary structures to be made. Orientation of Ca^{++}-ATPase on germanium crystals has not been successful to date. However, the use of crystals of the protein may overcome

this problem allowing, estimation of the relative orientation of the secondary structures present.

Work is about to be undertaken by Dr B. M. Charalambos in this department to produce mutants of the Ca^{++}-ATPase. Over expression of the protein will generate sufficient material for spectroscopic analysis. It is intended to introduce tryptic cleavage sites into the protein to allow the complete removal of cytoplasmic polypeptide strands. Polarisation studies will then be carried out on the membrane fragment to estimate the orientation of the membrane-spanning helices.

Production of mutant proteins will allow spectroscopic characterisation of the effects of particular amino acids upon the secondary structure of peptides and small proteins.

REFERENCES

Allen, J. P., Feher, G., Yeates, T., Komiya, M. and Rees, D. C. (1987) Proc. Natl. Acad. Sci. U.S.A. **84**, 5730

Alvarez, J., Haris, P. I., Lee, D. C. and Chapman, D. (1987) Biocmim. Biophys. Acta **916**, 5-12

Anfinsen, C. B. (1973) Science **181**, 223-230

Arrondo, J. L. R., Mantsch, H. H., Mullner, N., Pikula, S. and Martonosi, A. (1987) J. Biol. Chem. **262**, 9037-9043

Asher, I. M. and Levin, I. W. (1977) Biochim. Biophys. Acta **468**, 63

Babu, Y. S., Sack, J. S., Greenhough,T. J.,Bugg, C. E., Means, A. R. and Cook, W. J. (1985) Nature **315**, 37

Babu, Y. S., Bugg, C. E. and Cook, W. J. (1987) Methods Enzymol. **139**, 632-42

Baldwin, R. L. (1975) Ann. Rev. Biochem. **44**, 453-475

Baker, P. F. and Knight, D. E. (1986) Br. Med. Bull **42**, 399-404

Baudier, J., Glasser, N. and Gerard, D. (1986) J. Biol. Chem. **261** 8192-8203

Blasie, J. K., Herbette, L., Pascolini, D., Skita, V., Pierce, D. and Scarpa, A. (1985) Biophys. J **48**, 9-18

Blume, A., Hubner, W. and Messner, G. (1988) Biochemistry **27**, 8239-8249

Bush, S. F., Levin, H. and Levin, I.R (1980) Chem. Phys. Lipids **27**, 101-111

Byler, D. M. and Susi, H. (1986) Biopolymers **25**, 469-487

Cameron, D. G., Casal, H. L. and Mantsch, H. H. (1980) Biochemistry **19**, 3655

Cameron, D. G. and Moffat, D. J. (1984) J. Testing Evaluation **12**, 78-85

Casal, H. L., Kohler, U. and Mantsch, H. H. (1988) Biochim. Biophys. Acta **957**, 11-20

Case, R. M. (1980) Cell Calcium **1**, 1-5

Chapman, D., Owen, N. F., Phillips, M. C. and Walker, D. A. (1969) Biochim. Biophys. Acta **183**, 458-465

Chapman, D. and Salsbury, N. K. (1966) Trans. Farad. Soc. **62**, 2607-26021

Chapman, D., Williams, R. M. and Ladbrooke, B. D. (1967) Chem. Phys. Lipids **1**, 445-475

Chiba, K. and Mohri, T. (1989) Biochemistry **28**, 2995-2999

Chirgadze, Y. N., Shestopalov, B. V. and Venyaminov, S. Y. (1973) Biopolymers **12**, 1337-1351

Clarke, D. M., Loo, T. W., Inesi, G. and MacLennan, D. H. (1989) Nature **339**, 476-478

Closset, J. and Gerday, C. (1975) Biochim. Biophys. Acta **405** 228-235

Coan, C. and Inesi, G. (1977) J. Biol. Chem **252**, 3044-3049

Collins, J. H., Potter, J. D., Horn, M.J., Wilshire, G. and Jackman, N. (1973) FEBS Lett **36**, 268

Cortijo, M., Alonso, A., Gomez-Fernandez, J.-C. and Chapman, D. (1982) J. Mol. Biol. **157**, 597

Cortijo, M. and Chapman, D. (1981) FEBS Letts **131**, 245

Creighton, T. E. (1974) J. Mol. Biol. **78**, 579-602

Creighton, T. E. (1975) J. Mol. Biol **95**, 167-199

Creighton, T. E. (1977) J. Mol. Biol **113**, 295-312

Creighton, T. E. (1978) Prog. Biophys. Mol. Biol. **33**, 231-297

Creighton, T. E. (1984) in "Proteins: Structures and Molecular Principles" W. H. Freeman and Co. New York, p.235

Csermely, P., Katopis, C., Wallace, B. A. and Martonosi, A. (1987) Biochem. J. **241**, 663-669

Curatolo, W. (1982) Biochemistry **21**, 1761

Curatolo, W. (1985) Biochim. Biophys. Acta **817**,134-138

Danielli, J. F. and Davson, H. (1935) J. Cell. Comp. Physiol. **5**, 459

Danielli, J. F. (1954) Symp. Soc. Exp. Biol. **8**, 502-516

Davson, H. and Danielli, J. F. (1952) in "The Permeability of Natural Membranes", Cambridge University Press, London

Dedman, J. R., Jackson, R. L.,Schreiber, W. E. and Means, A. R. (1978) J. Biol. Chem **253**, 343

Deisenhofer, J., Epp, O., Miki, K., Huber,R. and Michel, H. (1985) Natute **318**, 618-624

de Meis, L. and Vianna, (1979) Annu. Rev. Biochem. **48**, 275-292

Dev, S. B. (1987) J. Biol. Phys. **15**, 57-61

Dickens, B. F. and Thompson, G. A. (1982) Biochemistry **21**, 3604-3611

Dupont, Y. (1976) Biochem. Biophys. Res. Commun. **71**, 544-550

Dupont, Y. (1977) Eur. J. Biochem. **72**, 185-190

Ebashi, S., Endo, M. and Ohtsuki, I. (1969) Q. Rev. Biophys. **2**, 351

Edmonds, D. T. (1984) in "Biological Membranes vol. 5" (D. Chapman ed.) Academic Press, London 350-387

Epand, R. M., Wheeler, G. E. and Moscarello, R. M. (1974) Biopolymers **13**, 359-369

Fraser, R. D. B., and Suzuki, E. (1966) Anal. Chem. **38**, 1770-1773

Freire,E., Bach, D., Correa-Freire, M.m Miller, I R. and Barenholz, Y (1980) Biochemistry **19**, 3662-3665

Gomez-Fernandez, J.-C., Goni, F. M., Bach, D., Restall, C. J. and Chapman, D. (1980) Biochim. Biophys. Acta **598**, 502-516

Gorter, E. and Grendel, F. (1925) J. Exp. Med. **41**, 439

Haris, P. I., Lee, D. C. and Chapman, D. (1986a) Biochim. Biophys. Acta **874**, 255-265

Haris, P. I., Mitchell, R. C., Fallowfield, C., Keelig, D. J., and Chapman, D. (1986b) Biochem. Soc. Trans. **15**, 1126-1127

Haris, P. I., Lee, D. C., Gabriella, S. and Chapman, D. (1987) British Biophysical Society Meeting, Cambridge, Abstract no. 4

Haris, P. I. and Chapman, D. (1989) Biochem. Soc. Trans. **17**, 161

Haris, P.I., Chapman, D., Harrison, R., Smith, K. F. and Perkins, S. J. (1990) in press

Heidorn, D. B. and Trewhella, J. (1988) Biochemistry **27**, 909-915

Hertzberg, O. and James, M. N. G. (1985) Nature **313**, 653

Hibbard, L. S. and Tulinski, A (1978) Biochemistry **17**, 5460-5468

Hoffman, T., Kawakami, M., Morris, H., Hitchman, A. J. W., Harrison, J. E. and Dorrington, K. J. (1977) in " Calcium Binding Proteins and Calcium Function" (R. H. Wasserman, R. Corradino, E. Carafoli, R. H. Kretsinger, D. H. MacLennan and F. Siegel, eds.) North-Holland, New York p.373

Ikemoto, N., Bhantnagar, G. M., Nagy, B. and Gergly, J. (1972) J. Biol. Chem. **247**, 7835-7837

Inesi, G., Millmar, M and Eltr, S. (1973) J. Mol. Biol **81**, 483

Inesi, G. (1985) Annu. Rev. Physiol. **47**, 573-601

Jackson, M., Haris, P. I. and Chapman, D. (1989) Biochim. Biophys. Acta **998**, 75-78

Jackson, M., Haris, P. I. and Chapman, D. (1990) J. Mol. Struct. **214**, 329-355

Jackson, M., Davies, G. H., Haris, P. I. and Chapman, D. (1990) in press

Jackson, M., Johnston, D. S. and Chapman, D. (1988) Biochim. Biophys. Acta **944**, 497-506

Johnston, D. S. and Chapman, D (1988) Biochim. Biophys. Acta

838, 603-614

Kauppinen, J. K., Moffat, D. J., Mantsch, H. H. and Cameron, D. G. (1981) Anal. Chem **53**, 1454-1457

Kendrew, J. C., Bodo, G., Dintzis, H. M., Parrish, R. G., Wyckoff, H. W. anf Phillips, D. C. (1958) Nature **181**, 662

Kennedy, D. F., Crisma, M., Toniolo, C. and Chapman, D. manuscript in preparation.

Kobayashi, M. and Kobayashi, M. (1980) J. Phys. Chem. **84**, 781-785

Koenig, J. L. and Tabb, D. L. (1980) in "Analytical Applications of FTIR to Molecular and Biological systems" (J. R. Durig ed.) Reidel, Dordrecht p.241

Krebs, H. A. and Johnson, W. A. (1937) Enzymologia **4**, 148-156

Kretsinger, R. H. (1980) CRC Crit. Rev. Biochem. **8**, 118-174

Kretsinger, R. H. and Nockolds, C. E. (1973) J. Biol. Chem. **248**, 3313-3321

Krimm, S. and Bandekar, J. (1986) Adv. Prot.Chem. **38**, 181-364

Ladbrooke, B. D., Williams, R. M. and Chapman, D. (1968) Biochim. Biphys. Acta. **150**, 333-340

Larson, E., Howlett, B. and Jagendorf, A. (1986) Anal. Biochem. **155**, 243-248

Lee, D. C., Hayward, J. A., Restall, C. J. and Chapman, D. (1985) Biochemistry **24**, 4364-4373

Lee, D. C., Miller, I. R. and Chapman, D. (1986) Biochim. Biophys. Acta **859**, 266-270

Lee, D. C. and Chapman, D. (1986) Biosci. Rep. **6**, 235-256

Lippert, J. L., Lindsay, R. M. and Schultz, R. (1981) J. Biol. Chem. **256**, 12411-12416

Lowry, O. H., Rosebrough, N.J., Farr, A. L. and Randall, R. J. (1951) J. Biol. Chem **193**,265-275

MacLennan, D. H., Brandl, C. J., Korczac, B. and Green, N.

M. (1985) Nature **316**, 597-607

Mantsch, H. H. and Casal, H. L. (1989) Proceedings of the 3rd international conference on FTIR spectroscopy, Fairfax.

Merino, C. G. (1987) Archives of Biochem. Biophys. **252** 303-314

Masuda, H. and de Meis, L. (1973) Biochemistyr **12**, 4581-4585

Mauger,J.-P., Poggioli, J. and Claret, M. (1985) J. Biol. Chem. **260**, 11635-11642

Meisner, G., Cooner, G. and Fleischer, S. (1973) Biochim. Biophys. Acta **298**, 246-269

Metcalfe, J. C., Moore, J. P., Smith, G. A. and Hesketh, T. R. (1986) Br. Med. Bull. **42**, 405-412

Metz, C. B. and Morroy, A. (1985) Biology of Fertilization, vol. 3, Academic Press, New York

Michelson, A. A. (1891) Phil. Mag. **31**, 256

Miller, A. (1982) Trends Biochem. Sci. **7**, 13-18

Miller, I. R. and Bach, D. (1986) Biochim. Biphys. Acta, **863**, 121-127

Miller, J. B. and Koshland, D. E. (1977) J. Mol. Biol. **111**, 183

Mitchell, R. C., Haris, P. I., Fallowfield, C., Keelig, D. J. and Chapman, D (1988) Biochim. Biophys. Acta **941**, 31-38

Miyazawa, T. (1960) J. Chem. Phys. **32**, 1647-1652

Moews, P. C. and Kretsinger, R. H. (1975) J. Mol. Biol. **91**, 201-228

Nakamoto, R. K. and Inesi, G. (1986) FEBS Lett. **194**, 258-262

Nakamura, H., Jilka, R. L., Boland, R. and Martonosi, A. (1976) J. Biol. Chem **251**, 5414-5423

Ohgushi, M and Wada, A (1983) FEBS Lett. **164**, 21-24

Oldfield, E. and Chapman, D. (1972) FEBS Lett. **23**, 285-97

Oldfield, E., Keough, K. and Chapman, D. (1972) FEBS Lett**20**,

344-346

Painter, P. C. and Koenig, J. C. (1976) Biopolymers **15**, 229-240

Papiz, M. Z. Sawyer, L., Eliopoulos, E. E., North, A. C. T., Findlay, J. B. C., Sivaprasadarao, R., Jones, T. A., Newcomer, M. E. and Kraulis, P. J. (1986) Nature **324**, 383

Pauling, L and Corey, R. B. (1951) Proc. Natl. Acad. Sci. USA **37**, 729-740

Pauling, L., Corey, R. B. and Branson, H. R. (1951) Proc. Natl. Acad. Sci. USA **37**, 205-211

Perutz, M. F. and Lehmann, H. (1968) Nature **219**, 902-909

Pick, U. and Karlish, J. D. (1982) J. Biol. Chem **257**, 6120-6126

Picton, C., Klee, C. B. and Cohen, P. (1981) Cell Calcium **2**, 281-294

Purcell, J. M. and Susi, H. (1984) J. Biochem. Biophys. Methods **9**, 193-199

Rasmussen, H. and Barrett, P. Q. (1988) In: "Hormones And Their Actions, Part II" (B. A. Cooke, R. J. B. King and H. J. van der Molen eds.) Elsevier Science Publishers, BV

Reed, R. A. and Shipley, G. G. (1987) Biochim. Biophys. Acta **896**, 153-164

Rubin, R. P. (1982) Fed. Proc. **41**, 2181-2187

Ruocco, M. J., Atkinson, D., Small, D. M., Skarjune, R. P., Oldfield, E. and Shipley, G. G. (1981) Biochemistry **20**, 5957-5966

Ruocco, M. J., Shipley, G. G. and Oldfield, E. (1983) Biophys. J. **43**, 91-101

Ruocco, M. J. and Shipley, G. G. (1984) Biophys. J. **46**, 695-707

Sanger, F. (1952) Adv. Prot. Chem. **7**, 1-67

Schroeder, W. A. (1968) in "The Primary Structure of Proteins" Harper and Row, New York

Singer, S. J. and Nicholson, G. L. (1972) Science **175**, 720-731

Skarjune, R. P. and Oldfield, E. (1982) Biochemistry **21**, 3154-3160

Snyder, R. G., Strauss, H. L. and Elliger, C. A. (1982) J. Phys. Chem. **86**, 5145

Squier, T. C., Hughes, S. E. and Thomas, D. D. (1988) J. Biol. Chem. **263** 9162-9170

Steim, J. M., Tourtello, M. E., reinert, J. C., McElhaney, R. N. and Radar, R. L. (1969) Proc. Natl. Acad. Sci. USA **63**, 104-109

Surewicz. W.K. and Mantsch, H. H. (1980) in "Protein Engineering: Approaches From the Classical to the Genetic" Butterworths

Surewicz, W. K., Szabo, A. G. and Mantsch, H. H. (1987) Eur. J. Biochem. **167**, 519-523

Susi, H. and Byler, D. M. (1986) Methods in Enzymology **130**, 290-311

Susi, H., Timasheff, S. N. and Stevens, L. (1967) J. Biol. Chem **242**, 5460-5466

Tanford, C. (1964) J. Am. Chem. Soc. **86**, 2050-2059

Taylor, K. A., Dux, L. and Martonosi, A. (1986) J. Mol. Biol. **187**, 412-427

Townend, R., Kumosinski, T. F. and Timasheff, S. N. (1966) Biochem. Biophys. Res. Commun. **32**, 163-169

Tiffany, M. L. and Krimm, S. (1969) Biopolymers **8**, 347-359

Tooke, P. B. (1988) Trends in Analytical Chem. **7**, 130-136

Trewhella, J., Liddle, W. K., Heidorn, D. B. and Strynadka, N. (1989) Biochemistry **28** 1294-

Tyler, A. (1941) Biol. Rev. **16**, 291-305

Villalain, J., Gomez-Fernandez, J. C., Jackson, M and Chapman, D. (1989) Biochim. Biophys. Acta **978**, 305-312

Wang, C.-S. and Smith, R. L. (1975) Anal. Biochem. **63**, 414-

Warren, G. B., Toon, P. A., Birdsall, N. J. M., Lee, A. G. and Metcalfe, J. C. (1974) Proc. Natl. Acad. Sci. USA **71**, 622-626

Watanabe, T. and Inesi, G. (1982) J. Biol. Chem. **257**, 11903-11907

Watson,, J. D. and Crick, F. H. C. (1953a) Nature **171**, 737-738

Watson, J. D. and Crick, F. H. C. (1953b) Nature **171**, 964-967

Weeds, A. G. and McLachlan (1974) Nature **252**, 646

Yang, P. W., Mantsch, H. H., Arrondo, J. L. R., Saint-Girons,I., Guillon, Y., Cohen, G. N. and Barzu, O. (1987) Biochemistry **26**, 2706-2711

Yasui, S. C., Keiderling, T. A., Bonora, G. M. and Toniolo, C. (1986) Biopolymers **25**, 79-89

PUBLICATIONS

1. Jackson, M., Johnston, D. S. and Chapman, D. (1988) Biochim. Biophys. Acta **944**, 497-506 " Differential scanning calorimetric and Fourier transform infrared spectroscopic investigations of cerebroside polymorphism"

2. Villalain, J., Gomez-Fernandez, J. C., Jackson, M. and Chapman, D. (1989) Biochim. Biophys. Acta **978**, 305-312 "Fourier transform infrared spectroscopic studies on the secondary structure of the Ca^{++}-ATPase of sarcoplasmic reticulum"

3. Chapman, D., Hall, B., Bird, R., Haris, P. I. and Jackson, M. in "Biomembranes; Basic Science and New Technology"

4. Chapman, D., Jackson, M. and Haris, P. I. (1989) Biochem. Soc. Trans. **17**, 1-3 "Investigation of membrane protein structure using Fourier transform infrared spectroscopy"

5. Jackson, M., Haris, P. I. and Chapman, D. (1989) Biochim. Biophys. Acta. **998**, 75-79 "Conformational transitions in Poly-L-Lysine: Studied using Fourier transform infrared spectroscopy"

6. Jackson, M., Haris, P. I. and Chapman, D. (1989) J. Mol. Struc. **204**, 329-355 "Fourier transform infrared spectroscopic studies of lipids, peptides and proteins " (review)

7. Jackson, M., Davies, G. H., Haris, P. I. and Chapman, D. (1990) in press "Thermal denaturation of proteins in aqueous solution studied by FTIR spectroscopy"

8. Jackson, M., Haris, P. I., Martin, S., Bailey, P. and Chapman, D. manuscript in preparation "Solution conformation of parvalbumin, calmodulin and troponin C studied using FTIR and CD spectroscopy"

Biochimica et Biophysica Acta, 944 (1988) 497–506
Elsevier

BBA 74171

Differential scanning calorimetric and Fourier transform infrared spectroscopic investigations of cerebroside polymorphism

Michael Jackson, David S. Johnston and Dennis Chapman

Department of Protein & Molecular Biology, Royal Free Hospital School of Medicine, University of London, London (U.K.)

(Received 21 December 1987)
(Revised manuscript received 26 July 1988)

Key words: Cerebroside; Cholesterol; Dipalmitoylphosphatidylcholine; Polymorphism; Fourier transform infrared spectroscopy; Differential scanning calorimetry; (Bovine brain)

Calorimetric and Fourier transform infrared (FTIR) spectroscopic studies have been made of the polymorphism exhibited by bovine brain cerebroside–water systems, and the effect of cholesterol and dipalmitoylphosphatidylcholine (DPPC) upon this polymorphism was investigated. The conversion of the cerebroside from the thermodynamically stable to the metastable form is found to be accompanied by spectral changes, indicating a decrease in cerebroside headgroup hydration and a rearrangement of the hydrogen-bond network. The incorporation of low concentrations of cholesterol and DPPC into cerebroside bilayers broadens the thermal transitions associated with the cerebroside as a result of the disruption of cerebroside–cerebroside interactions. This disruption is evident in the spectra of cerebroside/cholesterol mixtures.

Introduction

Cerebrosides belong to a class of lipid known as glycosphingolipids. These lipids, composed of a sphingosine backbone, a fatty acid (either hydroxy-substituted or unsubstituted), and one or more hexose sugar residues, are found in most, if not all, animal cell membranes, albeit in relatively small amounts. Appreciable amounts are found in certain severe pathological conditions (Gaucher's disease, Krabbe's disease, metachromic leucodystrophy) and in certain specialised tissues under normal circumstances. A good example of the latter is the myelin sheath, which contains high level of cerebrosides. The function of cerebrosides in such tissues is not clear, but it is likely that they are involved in maintaining membrane integrity.

Cerebrosides and many other glycosphingolipids exhibit complex polymorphic phase behaviour. The structure and polymorphism of non-hydroxy fatty acid galactocerebrosides (type II galactocerebrosides) have been the subject of a number of studies in recent years, using such techniques as DSC [1,2], X-ray diffraction [3] and spectroscopy [4–6]. At present, the thermotropic mesomorphism is believed to be due to rearrangement of hydrogen-bond networks [3] and changes in hydration [3,7].

Upon heating type II galactocerebrosides in excess water, the main gel-liquid crystalline phase transition occurs at around 80 °C. Rapid cooling of this phase produces a gel state with an X-ray

Abbreviations: FTIRS, Fourier transform infrared; DPPC, 1,2-dipalmitoyl-1-*sn*-glycero-3-phosphorylcholine; DSC, differential scanning calorimetry.

Correspondence: D. Chapman, Department of Protein and Molecular Biology, Royal Free Hospital, Rowland Hill Street, London, NW3 2PF, U.K.

diffraction pattern identical to that of an anhydrous sample [3]. Subsequent heating of this phase results in an exothermic transition over the range 50–60 °C followed by the main endotherm at 80 °C. The exothermic nature of the first transition indicates conversion from a high-energy metastable state to a lower-energy stable state.

As cerebrosides are the major polar lipid in central and peripheral nervous system myelin, it is apparent that a more complete understanding of this polymorphism and how other myelin components affect it is desirable.

Materials and Methods

Type II bovine brain cerebrosides (98% non-hydroxy fatty acids, 99% pure) and cholesterol (5(6)-cholesten-3β-ol, 99% pure) were purchased from Sigma. 1,2-Dipalmitoyl-1-*sn*-glycero-3-phosphorylcholine (DPPC, 99% pure) was purchased from Fluka. All solvents were of spectrophotometric grade.

DSC thermograms were recorded on a Perkin-Elmer DSC7 at heating and cooling rates of 2.5 C°/min over the range 0–100 °C. Lipid mixtures were prepared as below and anhydrous material weighed into a stainless steel pan. Each sample (15–20 mg) was then hydrated by introducing excess water via a microsyringe and the pans were then sealed. To ensure that the samples were homogeneous and at equilibrium they were taken through several heating and cooling cycles and left to stand for 24 h before being scanned.

IR spectra were recorded on a Perkin-Elmer 1750 FTIR spectrometer continuously purged with dry air at a flow rate of 100 l/min. Samples were mounted in a Beckman FH-01 CFT cell fitted with CaF_2 windows separated by a 6 μm tin spacer. Temperature was maintained at 20 °C using a circulating water jacket. For each sample, 200 scans were recorded at 4 cm^{-1} resolution and were signal averaged. Difference spectra were generated by digital subtraction of a suitable background spectrum on a Perkin-Elmer computer.

Samples were prepared for FTIR spectroscopy as follows. Stock solutions of galactocerebroside, cholesterol and DPPC were made up in chloroform/methanol (2 : 1). Cerebroside/cholesterol and cerebroside/DPPC dispersions were formed by mixing the appropriate volumes of each solution to produce the ratios required. The solvent was then evaporated under N_2 and the samples stored under vacuum to remove any final traces of solvent.

Hydration of samples was achieved by heating lipid and water (cerebroside concentration = 10 mg/ml) at 90 °C and agitating with a vortex mixer. Metastable samples were produced by quenching hydrated mixtures from 90 to 0 °C in an ice bath. Stable samples were produced by incubation of metastable samples at 70 °C for 10 min.

Spectra of anhydrous galactocerebrosides were obtained from a KBr disc containing 1% galactocerebrosides by weight.

Results

Differential scanning calorimetry

Calorimetric thermograms of hydrated galactocerebrosides and galactocerebroside/cholesterol mixtures are presented in Fig. 1. Upon heating the pure cerebrosides, the main gel-liquid crystalline phase transition occurs at 79 °C, with an enthalpy change of 90 J/g. Cooling scans show two exothermal transitions, at 58.4 °C and 36.2 °C with enthalpy changes of −26.2 J/g and −7.61 J/g, respectively, indicating formation of two gel states. The disparity in enthalpy changes of the heating and cooling scans demonstrates that at least one of the gel forms is metastable. A further heating scan (Fig. 1c) shows a distinct exotherm centered at 51.8 °C which has an enthalpy change of −12 J/g. This is followed by a split endotherm, with peaks at 74.8 and 78.7 °C and a combined enthalpy change of 85 J/g. A second cooling scan was identical to the first.

Addition of 9 mol% cholesterol has little effect upon the first heating scan but produces a complex exotherm in the cooling scan with an enthalpy change of −40 J/g and a peak at 57.3 °C (Fig. 1e). A subsequent heating scan (Fig. 1f) shows the characteristic exotherm, reduced in peak temperature to 46.6 °C but of comparable enthalpy to the pure cerebroside. Again, a split endotherm is seen, with peaks at 73.6 °C and 79 °C and an enthalpy change of 70 J/g. This reduction in enthalpy change upon addition of

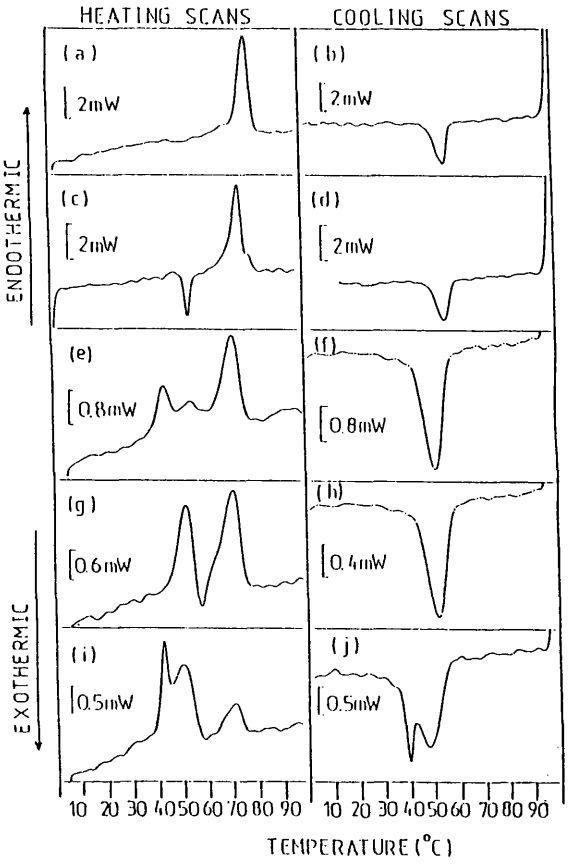

Fig. 2. DSC thermograms of hydrated type II galactocerebrosides containing (a–d) 9; (e–h) 33 and (i–j) 50 mol% DPPC. Heating and cooling rate = 2.5 C°/min. See text for equilibration protocol.

atures of the first two transitions. The final endotherm is observed to have a peak temperature of 71.6°C.

Further elevation of the concentration of DPPC to 50 mol% produces the thermograms shown in Fig. 2i–j. Multiple peaks are seen in heating scans, centred at 42.9, 51.4 and 70.9°C, the combined enthalpy change of the three endotherms being 48.6 J/g. A cooling scan produces a complex thermogram consisting of a broad exotherm at 47.7°C with a shoulder at 52°C and a sharp peak at 39.6°C, the combined enthalpy change being −43 J/g. The observation of three transitions in the cooling scans suggests that phase separation into three domains is occurring. The similarity between the enthalpies of heating and cooling curves demonstrates that no metastable state is formed. A subsequent heating scan confirms this, since it is identical to the first heating scan.

FTIR spectroscopy

Pure galactocerebrosides containing non-hydroxy fatty acids show marked spectral differences between metastable and stable forms [6]. The most notable differences are seen in the amide I and II regions of the spectrum which occur between 1700 cm^{-1} and 1500 cm^{-1}. The amide I region consists of absorptions due to C=O stretching vibrations weakly coupled to N–H bending and C–N stretching vibrations. The amide II region, on the other hand, consists of absorptions due to N–H bending vibrations strongly coupled to C–N stretching vibrations [10].

Fig. 3 shows difference spectra obtained by subtraction of the aqueous background from the spectra of hydrated quenched (metastable) and reheated (stable) galactocerebrosides. In the metastable form, the amide I band consists of a major absorption at 1646 cm^{-1} and a shoulder at 1630 cm^{-1}, whilst the amide II band is at 1546 cm^{-1}. Upon formation of the stable form, the lower amide I band in the metastable form decreases in frequency from 1630 cm^{-1} to 1615 cm^{-1}, and increases in intensity. This decrease in frequency is a result of the formation of hydrogen bonds which draw electrons from the C=O bond. The amide II band increases in frequency upon conversion to the stable form as a result of the formation of hydrogen bonds involving N–H groups in a plane perpendicular to the N–H bending [10,11].

Spectral differences are apparent in the 1200–1000 cm^{-1} region associated with C–O stretching vibrations of the galactose and sphingosine hydroxyl groups (Fig. 3b). It is not possible to assign the peaks in this region to specific C–O bonds, but decreases in frequency of the peaks at 1072, 1053 and 1023 cm^{-1} (metastable form) to 1064, 1045 and 1018 cm^{-1} (stable form) are apparent, due to a weakening of the C–O bond caused by an increase in the degree or strength of hydrogen bonding. These shifts suggest that the galactose and/or the sphingosine hydroxyl groups play a role in the formation of the polymorphic forms of the cerebroside.

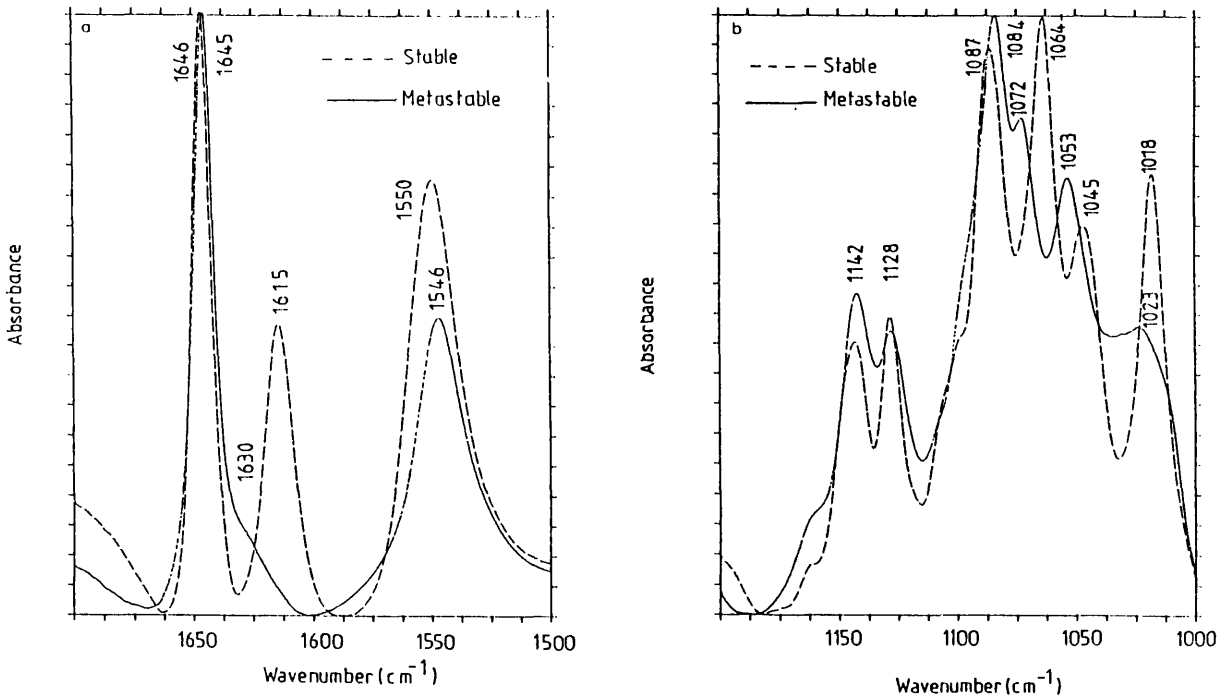

Fig. 3. FTIR difference spectra of amide region (a) and C–O stretching region (b) of type II galactocerebrosides in the metastable (———) and stable states (— — —). Absorbance scales in arbitrary units.

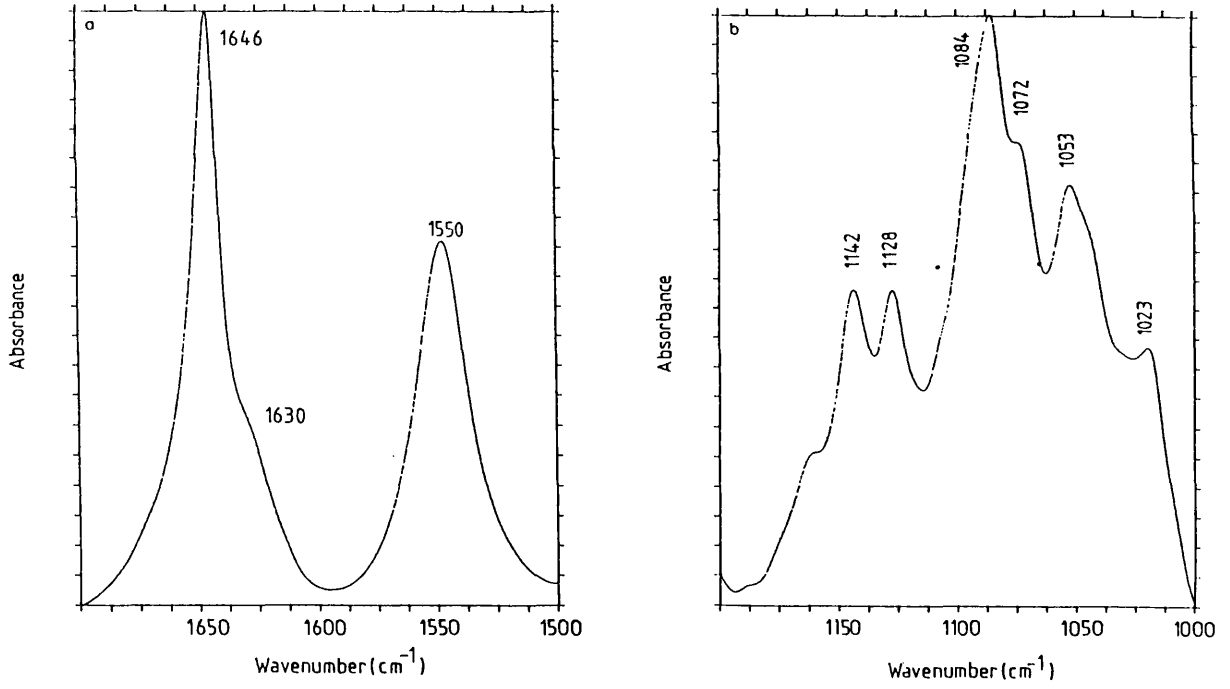

Fig. 4. FTIR spectrum of the amide region (a) and C–O stretching region (b) of anhydrous, type II galactocerebrosides. Absorbance scale in arbitrary units.

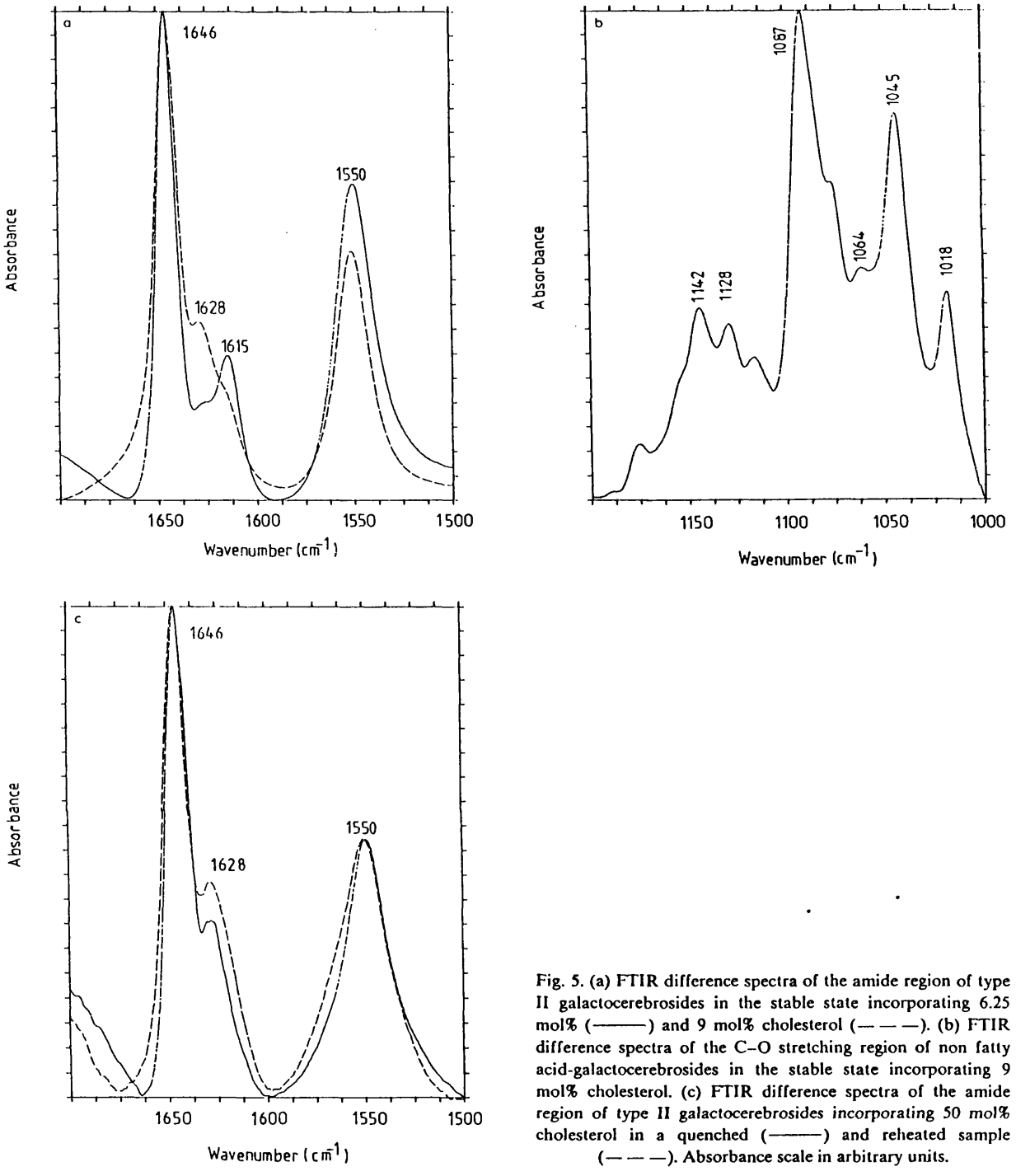

Fig. 5. (a) FTIR difference spectra of the amide region of type II galactocerebrosides in the stable state incorporating 6.25 mol% (———) and 9 mol% cholesterol (— — —). (b) FTIR difference spectra of the C–O stretching region of non fatty acid-galactocerebrosides in the stable state incorporating 9 mol% cholesterol. (c) FTIR difference spectra of the amide region of type II galactocerebrosides incorporating 50 mol% cholesterol in a quenched (———) and reheated sample (— — —). Absorbance scale in arbitrary units.

The spectra obtained from a sample of anhydrous galactocerebrosides are shown in Figs. 4a and b. The method of sample preparation did not affect the spectra. The amide II absorption of the anhydrous form occurs at 1550 cm^{-1}, the same frequency as that of the stable polymorphic

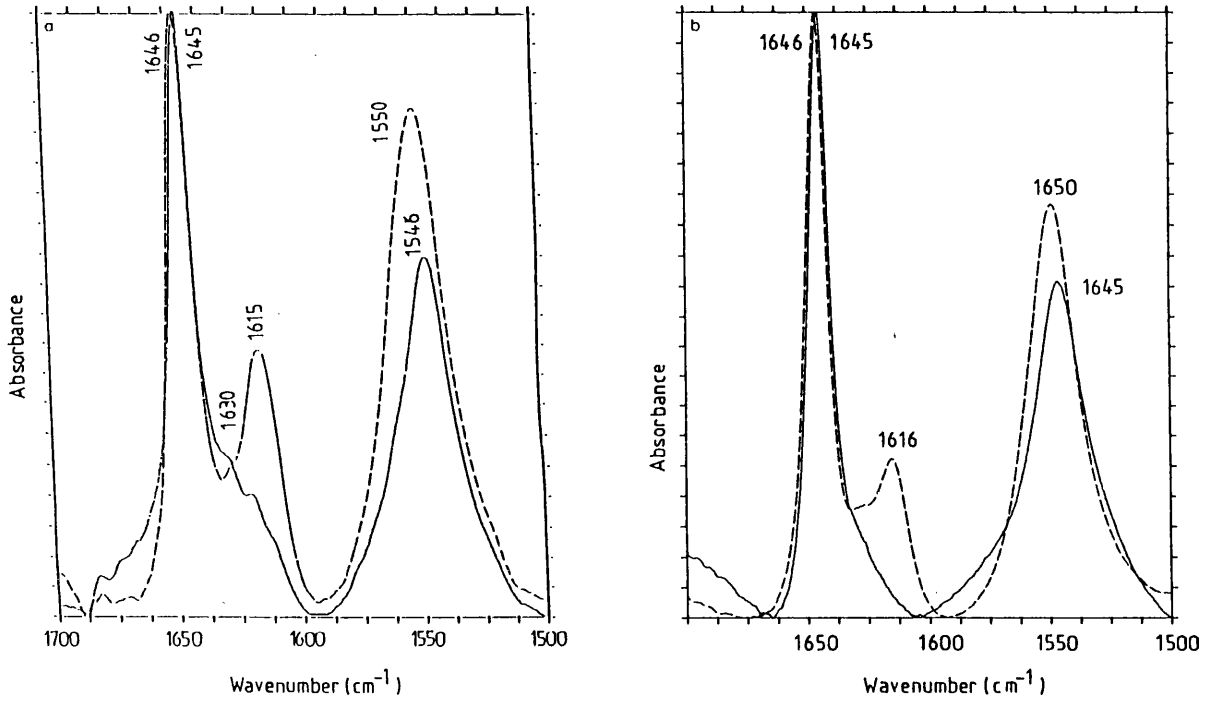

Fig. 6. FTIR difference spectra of the amide region of type II galactocerebrosides incorporating 9 mol% (a) and 33 mol% (b) DPPC in a quenched (———) and a reheated (— — —) sample. Absorbance scale in arbitrary units.

form. The spectrum of the anhydrous galactocerebroside in the amide I region and the C–O stretching region is identical to that of the metastable polymorph.

Incorporation of cholesterol into galactocerebroside bilayers has a significant effect upon the spectrum (Fig. 5). The intense amide I peak at 1615 cm^{-1} in the stable state is progressively reduced in intensity and increased in frequency as the proportion of cholesterol incorporated into the bilayer is increased. At 9 mol% cholesterol, only a shoulder at 1628–30 cm^{-1} occurs. In the C–O stretching region of the spectrum the peak occurring at 1064 cm^{-1} in the stable state is also progressively reduced in intensity with increasing cholesterol content (Fig. 5b). The effect of addition of 50 mol% cholesterol to cerebroside bilayers is shown in Fig. 5c. The amide I and II peaks occur at 1646 cm^{-1} and 1550 cm^{-1}, respectively, in both quenched and reheated samples.

The effect upon spectra of incorporating varying amounts of DPPC into cerebroside bilayers is shown in Fig. 6. At 9 and 33 mol% DPPC the amide I peaks in reheated samples occur at 1646 cm^{-1} and 1615 cm^{-1} and the amide II band occurs at 1550 cm^{-1}. At 33 mol% DPPC a slight reduction of the second amide I peak at 1615 cm^{-1} takes place. Addition of 50 mol% DPPC (not shown) results in the disappearance of the second amide I band. The amide I and II band peak positions are at 1646 cm^{-1} and 1550 cm^{-1}, respectively, in both quenched and reheated samples.

Discussion

Cerebrosides exhibit complex polymorphic phase behaviour. Earlier studies (Refs. 1–3,12,13 and references therein) and our results (in Fig. 1) show the existence of a metastable as well as a stable polymorphic form. The occurrence of one high-temperature melting endotherm at 80 °C on the first heating scan and two peaks at 74.8 °C and 78.7 °C in the subsequent heating scan must be due to phase separation occurring, associated with the heterogeneous character of the acyl chains of type II galactocerebrosides.

The FTIR difference spectra provide evidence concerning the hydrogen bonding of the stable and metastable forms. The spectra presented in Figs. 3a and b show pronounced spectral changes upon conversion from the stable to the metastable polymorphic form. In the stable cerebroside form, two distinct amide I peaks are seen. It is possible that one of the components arises from water of hydration. However, upon deuteration, both bands shift by about 15 cm^{-1} (not shown). If either band were due to water, it would be found some 400 cm^{-1} lower in ^2H_2O than in H_2O. Furthermore, in spectra recorded at 70°C, no change in either band position is seen (not shown). We therefore conclude that these two bands represent two different populations of C=O groups. The low frequency of the band at 1616 cm^{-1} suggests this population of C=O groups is more strongly hydrogen-bonded than the other population. In the spectrum of the metastable form, the second amide I absorption is only observed as a weak shoulder at around 1630 cm^{-1}.

The similarity between the spectra of the anhydrous cerebroside and the metastable cerebroside indicates that the cerebroside headgroups in the metastable and anhydrous states are in a similar hydrogen-bonding and perhaps conformational state. X-ray diffraction patterns of anhydrous and metastable galactocerebrosides have been found to be identical [3]. In addition, hydration of cerebrosides in the presence of ethylene glycol produces a state with thermotropic properties intermediate between the metastable and stable states [7,14]. This was taken as evidence of dehydration, due to decreased water activity, producing a state with thermotropic properties tending towards those of the metastable state.

Our calorimetric studies show that addition of 9 mol% cholesterol to the cerebroside has little effect upon thermograms (Fig. 1d–f). The enthalpy changes, peak temperatures and cooperativity of the phase transitions are slightly reduced due to disruption of the chain packing. In cooling scans, two peaks are seen in a complex exotherm as a cerebroside/cholesterol phase and a pure cerebroside phase solidify. The presence of an heating exotherm in a subsequent heating scan indicates that the metastable state is still formed in the presence of 9 mol% cholesterol.

Heating scans of mixtures containing 34 mol% cholesterol show the behaviour characteristic of metastability (Fig. 1i). Initial heating scans show four endotherms, the result of phase separation of cerebroside/cholesterol mixtures into four domains. The basis of this separation into so many domains is presumably related to the heterogeneity of the cerebroside sample.

The high temperature of the fourth transition suggests that the phase responsible for this endotherm does not contain cholesterol, but is pure cerebroside, perhaps of uniform cerebroside chain length and saturation. Presumably, in the presence of cerebrosides of different composition the onset temperature of chain melting of this cerebroside phase is reduced to 79°C. This phase separates almost immediately upon cooling, and gives rise to an exotherm centered at 80.6°C. However, the enthalpy change associated with this transition is small and therefore only a very small fraction of the cerebroside solidifies at this temperature. Most of the cerebroside solidifies, still mixed with cholesterol in a transition with a reduced cooperativity, such that no enthalpy change can be detected. The phase separation of this mixture is not immediate, allowing us to assume that in our FTIR experiments we have only one major phase. A minor phase contains the relatively small amount of pure cerebroside which solidified immediately upon cooling, whilst the major phase contains most of the cerebrosides and cholesterol in a homogeneous mixture. It is this second phase which dominates the spectrum.

The thermotropic behaviour of a full range of cholesterol/cerebroside mixtures have been studied [15] and no metastable transition was detected at 50 mol% cholesterol.

We can see from Fig. 6 that incorporation of cholesterol into galactocerebroside bilayers in the stable state produces marked spectral changes (these changes are not due to absorption bands arising from cholesterol). The intensity of the second amide I peak of the stable state decreases as the concentration of cholesterol increases, until at 9 mol% cholesterol only a shoulder at 1628 cm^{-1} is seen. This reduction in intensity and increase in frequency is due to disruption of hydrogen bonds involving one of the C=O group populations.

In the C–O stretching region the peak at 1064

cm^{-1} of the stable state is also progressively reduced in intensity until at 9 mol% cholesterol it is no longer seen (Fig. 5b). Cholesterol appears to disrupt hydrogen bonding involving either the galactose hydroxyls or the sphingosine hydroxyl group. The fact that only one vibrational mode of the headgroup is affected is striking and suggests that the interaction between cerebrosides and cholesterol is highly specific in nature.

Increasing cholesterol content further to 50 mol% resulted in identical spectra after quenching and reheating. The rearrangements in the hydrogen-bonding network associated with the changes in band frequency, which occurred in previous samples upon quenching, no longer occur at this cholesterol concentration.

Fig. 2 illustrates thermograms obtained from an galactocerebroside bilayers incorporating 9, 33 and 50 mol% DPPC. At 9 mol%, DPPC thermograms show endotherms with reduced enthalpy changes due to disruption of cerebroside–cerebroside interactions by DPPC. Cooling scans exhibit a much lower enthalpy change than that of heating scans due to formation of a metastable cerebroside form. The phase separation of cerebroside molecules observed in the pure lipid and in the presence of cholesterol is much reduced in the presence of 9 mol% DPPC.

Increasing the DPPC concentration to 33 mol% produced three endothermic transitions, with a further reduction in enthalpy change due to a further decrease in the cooperativity of the cerebroside transitions. As cerebrosides and DPPC exhibit gel-state immiscibility [9], it is likely that the lower of the three peaks represents the melting of a DPPC phase containing only a small amount of cerebroside, and the remaining transitions arise from processes involving two cerebroside phases, each of which contains a small amount of DPPC. A heating scan subsequent to a cooling scan shows thermotropic behaviour characteristic of a metastable cerebroside form.

The disruption by cholesterol of the cerebroside–cerebroside interactions causing a reduction in the cooperativity of the cerebroside thermal transitions was apparent from the increase in frequency and decrease in intensity of the second amide I band and the C–O band at 1064 cm^{-1} in the stable form with increasing cholesterol concentration. Due to the rapid nature of the phase separation of cerebroside and DPPC upon cooling from the liquid crystalline state, these spectral changes are not observed at 9 mol% DPPC and are barely noticeable at 33 mol% DPPC. The amount of DPPC required to disrupt the highly cooperative nature of the cerebroside thermal transitions would therefore appear to be quite low. This phase separation of cerebrosides and DPPC has also been described in studies of mixtures of DPPC and excess *N*-palmitoylgalactosylsphingosine [9], although the time-course of the phase separation in the present study is much reduced. This may be related to the use of a heterogeneous cerebroside mixture in this study.

At 50 mol% DPPC, thermograms demonstrate that no metastable form is produced by quenching. The enthalpy changes associated with heating and cooling scans were similar and no exotherms was seen in heating scans. Cooling scans indicate immediate separation of the lipids into three phases. This phase separation does not result in DPPC-free cerebroside phases, as indicated by the very low peak temperature and degree of cooperativity of heating endotherms in thermograms, and the absence of the second amide I band in spectra (not shown). The absence of metastability may be due to the presence of DPPC in the cerebroside domains and/or interfacial effects.

Conclusions

Cerebroside polymorphism is a well-documented phenomenon. It has been demonstrated by X-ray diffraction [3], DSC [1,2], Raman spectroscopy [5] and FTIR spectroscopy [6]. Our results are in general agreement with these studies, although we note formation of multiple cerebroside domains in pure cerebrosides, cerebroside/cholesterol and cerebroside/DPPC mixtures. The basis for this separation of cerebroside into multiple domains presumably lies in the heterogeneous nature of our sample, and may be a function of fatty acid chain length, fatty acid chain unsaturation, position of the double bond in unsaturated chains.

The FTIR difference spectra presented in Figs. 3 and 4 support an involvement of hydration changes and hydrogen bond network re-arrange-

Elsevier

BBAPRO 33447

Conformational transitions in poly(L-lysine): studies using Fourier transform infrared spectroscopy

Michael Jackson, Parvez I. Haris and Dennis Chapman *

Department of Protein and Molecular Biology, Division of Basic Medical Science, Royal Free Hospital School of Medicine, London (U.K.)

(Received 23 December 1988)
(Revised manuscript received 28 April 1989)

Key words: Polypeptide conformation; poly(L-lysine); FT-IR; Molar absorptivity

FT-IR spectroscopy has been applied to the study of the pH-induced conformational transitions which occur with poly(L-lysines) of varying molecular weight. The studies were performed in aqueous media under conditions believed from previous CD studies to induce the polypeptide to adopt a particular type of secondary structure. Each different type of secondary structure gives amide I bands with different frequencies. The α-helix secondary structure shows a strong band at 1638 cm^{-1}, random structures a strong band at 1644 cm^{-1} and the β-sheet arrangement a strong absorption at 1610 cm^{-1} with a weaker band at 1680 cm^{-1}. The low band frequency of the polypeptide when in an α-helical conformation compared to the band characteristic of α-helical structures in proteins is discussed. Additional components are observed when second derivative analysis is applied to the spectra corresponding to the random and helical conformations. The number of these additional components increases with the α-helical conformation as the molecular weight of the polymer increases. Estimations of the area of the amide I band in the various conformations are made.

Introduction

Fourier transform infrared (FT-IR) spectroscopy is becoming increasingly popular with experimentalists seeking to gain information concerning the secondary structure of proteins. The bands most frequently used for secondary structural analysis are the amide I and amide II bands. In principle it is possible to obtain both qualitative and quantitative information from analysis of the amide I band. Qualitative secondary structure predictions are usually based upon the frequency of this band. The asignment of the amide I components to specific secondary structures then relies upon correlations with band positions observed for homopolypeptides and proteins which are known to adopt a particular secondary structure under specific experimental conditions [1]. For example, alteration of the pH of polylysine solutions has been shown by Circular Dichroism (CD) techniques [2–4] to produce interconversion between various structural forms. As the pH is increased it is possible to induce the polypeptide to adopt random, α-helical or β-sheet structures.

In the present paper we examine the effects of manipulation of pD upon the conformation of polylysine of varying molecular weight, using the more sophisticated instrumentation and data-processing techniques associated with FT-IR spectroscopy. Previous studies of this polypeptide, using infrared spectroscopy, used little or no data processing [5].

Quantitative determination of the various secondary structures present is also possible. For this it is usually assumed that each different secondary structural arrangement has equal molar absorptivity. The ease of interconversion of polylysine between its structural forms provides a model system which allows us to assess the validity of this assumption.

Materials and Methods

Deuterium oxide (98 atom%), poly(L-lysine) (molecular weight as determined by viscometry = 3300, 24 000 and 27 100, all 98% pure) and poly(L-glutamate) (molecular weight = 43 000) were purchased from Sigma Chemicals. Infrared spectra were recorded on a Perkin-Elmer 1750 FT-IR spectrometer continuously purged

Abbreviations: FT-IR, Fourier transform infrared; CD, circular dichroism.

Correspondence: D. Chapman, Department of Protein and Molecular Biology, Division of Basic Medical Science; Royal Free Hospital School of Medicine, Rowland Hill St., London, NW3 2PF, U.K.

with dry air. Samples were injected into a sealed cell (Specac Ltd.) with constant path length (50 μm). Temperature was maintained with a circulating water bath. For each sample, 100 scans were recorded and the signal averaged at a resolution of 4 cm^{-1} and 20 °C. Difference spectra were generated by digital subtraction of a spectrum of D_2O recorded under the same conditions as the sample spectra.

Samples were prepared for infrared spectroscopy as follows. Poly(L-lysine) was dissolved in D_2O to give a 2% solution by weight, with the pD (pD = pH meter reading + 0.4) adjusted to 8.3 with NaOD. The pD of the solution was adjusted to 11.2 and spectra recorded. The solution was adjusted to pD 11.9, and heated at 60 °C for 30 min, then cooled to 20 °C and the spectra recorded. For comparison purposes, spectra of polyglutamate (2% by weight) were recorded at pD 7 and 4.3.

Results

Fig. 1 shows the difference spectrum of polylysine (M_r = 24000) in D_2O and pD 8.3. A broad band contour with band maximum at 1644 cm^{-1} is seen. Application of second derivative routines reveals the presence of two bands, at 1666 and 1641 cm^{-1} (Fig. 1b). Spectra obtained in H_2O exhibited bands at 1677, 1648, and near 1620 cm^{-1}. A band due to carboxylate groups at the C-terminus of the polypeptide chain is seen at 1590 cm^{-1}. This band is reduced in intensity as chain length is increased.

The difference spectrum of polylysine (M_r = 3300 recorded at pD 11.2 is shown in Fig. 2a. The amide I maximum is observed at 1638 cm^{-1}. Higher molecular weight polymers also gave a band maximum at 1638 cm^{-1}. Second derivative analysis of polylysine of molecular weight 3300 (Fig. 2b) reveals the presence of two bands, at 1662 and 1638 cm^{-1}. The band seen at 1590 cm^{-1} is from the carboxylate groups at the C-terminus of the helices. This is reduced in relative intensity as the polymer weight is increased. When the polypeptide molecular weight is increased to 24000, bands are observed at 1670, 1644, 1638 and 1623 cm^{-1} with a shoulder at 1644 cm^{-1} (Fig. 3a). Further increase of the molecular weight of the polypeptide to 271000 (Fig. 3b) gives rise to bands at 1670, 1644, 1638 and 1623 cm^{-1}.

Fig. 4a and b shows the difference and second derivative spectra of polylysine (M_r = 24000) in D_2O at pD 11.9 after 30 min at 60 °C. Further heating does not alter the spectrum. In the difference spectrum, two bands are observed at 1680 and 1610 cm^{-1}. The low frequency band is asymmetric, suggesting the presence of an additional component between 1630–40 cm^{-1}. Second derivative analysis reveals only two bands at 1680 and 1610 cm^{-1}. Even after extensive heating and further elevation of the pD, the lowest molecular weight

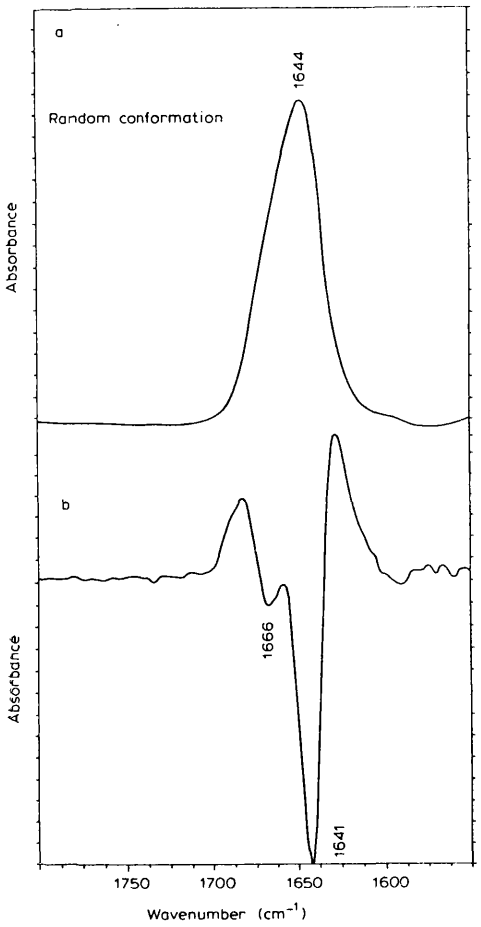

Fig. 1. FT-IR difference (a) and second derivative (b) spectra of polylysine (M_r = 24000) recorded at pD 8.3.

polylysine gave a spectrum identical to that shown in Fig. 2a, and so had not converted to β-sheet. The M_r 271000 polypeptide converted to β-sheet spontaneously upon increasing the pD to 11.9 and required no heating (spectrum identical to Fig. 4).

The second derivative spectra of polyglutamate are shown in Fig. 5. At pD 7 (Fig. 5a) two bands are seen, at 1670 and 1644 cm^{-1}. A band which we assign to ionised carboxylate side-chains is seen at 1565 cm^{-1}. A decrease in the pD to 4.3 gives a spectrum with bands at

TABLE I

Integrated area of the amide I band of 2% solutions of polylysine in D_2O in random, helical and β-sheet forms

Results are the mean of four observations normalised to the random conformation.

Structure	Area
Random	1.0
α-Helix	1.13 ± 0.04
β-Sheet	1.31 ± 0.11

1673, 1651, 1642 and 1623 cm^{-1}. A group of bands assigned to unionised carboxylic acid side-chains occurs in the region 1740–1700 cm^{-1}.

The area of the amide I band for polylysine (a 2% solution of M_r 24000) was calculated for the spectrum recorded at each pD using the AREA routine supplied with the Perkin-Elmer data station. This was not possible for polyglutamate, due to the presence of the strong absorptions from the glutamate side-chains. The results of these calculations are presented in Table I, normalised to values for the random conformation to account for any variation in pathlength and concentration in repeat experiments. The integrated area of the amide I band is the product of path length (l) molar absorptivity (ε) and concentration (c) in accordance with the Beer-Lambert law:

$$\text{absorbance} = \varepsilon lc \qquad (1)$$

As the pathlength and concentration are identical for each sample, this value is proportional to the molar absorptivity (ε). Thus any change in the integrated absorbance can be used to assess changes in molar absorptivity of the different structures.

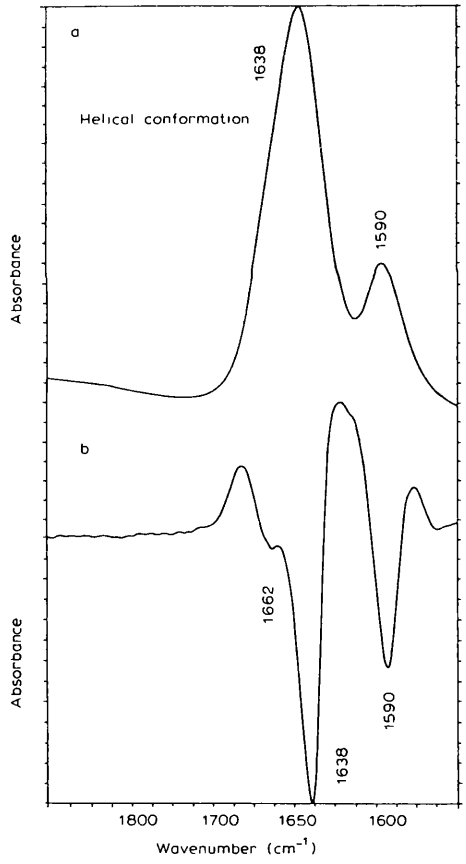

Fig. 2. FT-IR difference (a) and second derivative (b) spectra of polylysine (M_r = 3300) recorded at pD 11.2.

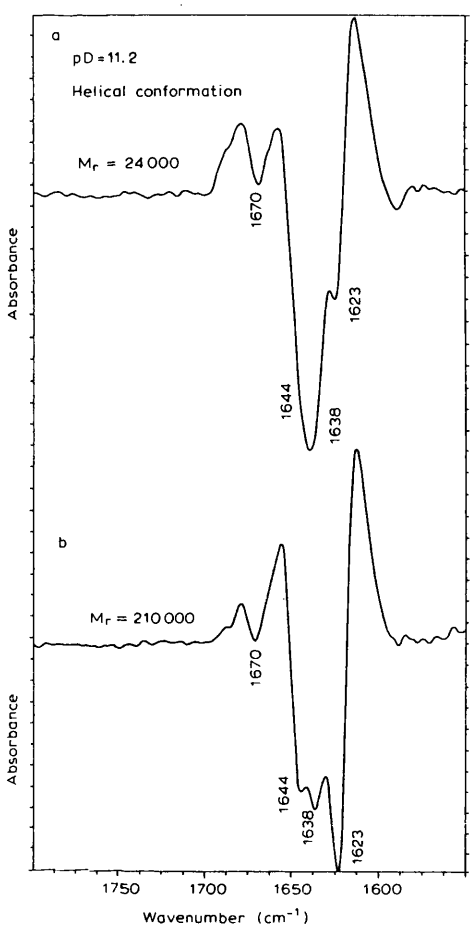

Fig. 3. FT-IR second derivative spectra of polylysine recorded at pD 11.2, (a) M_r = 24000 and (b) 210000.

Comparison of the integrated absorbances (Table I) indicates that random polylysine has a lower molar absorptivity (by about 13%) than α-helical polylysine, which in turn has a molar absorptivity 18% lower than that of β-sheet polylysine. Similar changes were observed in experiments conducted with 1 and 0.5% polylysine solutions.

Discussion

Previous CD studies [2–4] with polylysine have shown that a variation in pH can induce different conformational states of the polypeptide. Our FT-IR spectroscopic studies show that as the pH or pD is varied, marked spectral changes occur. Under conditions reported to favour the formation of a random structure, the absorbance spectrum of polylysine in D_2O exhibits a strong absorption at 1644 cm^{-1}. Existing correlation tables [5] are in agreement that a band at this frequency is indicative of a random conformation of the polypeptide chain. However, with the calculation of the

second derivative, the broad band contour is resolved into two components (see Fig. 1b). The main band at 1641 cm^{-1} can be assigned to the presence of random structures, but the assignment of the band at 1666 cm^{-1} is uncertain. An examination of the derivative spectrum of polyglutamate under conditions considered to favour the production of a random structure [2] shows two bands at similar frequencies. One possible conclusion from this is that the random structure of this polypeptide is characterized by two bands. However, an alternative explanation is that some kind of additional ordered structure is present in the system at this pD. Both turns and 3_{10} helices have been reported to absorb in this spectral range [6,7]. Some workers have suggested, based upon (a) Raman band widths, (b) the difference in amide I maxima in Raman and infrared spectra, and (c) comparison of the effects upon CD spectra of various salts and the incorporation of D-amino acids into the polypeptide chain [8] that the random chains of polylysine and polyglutamate are interupted

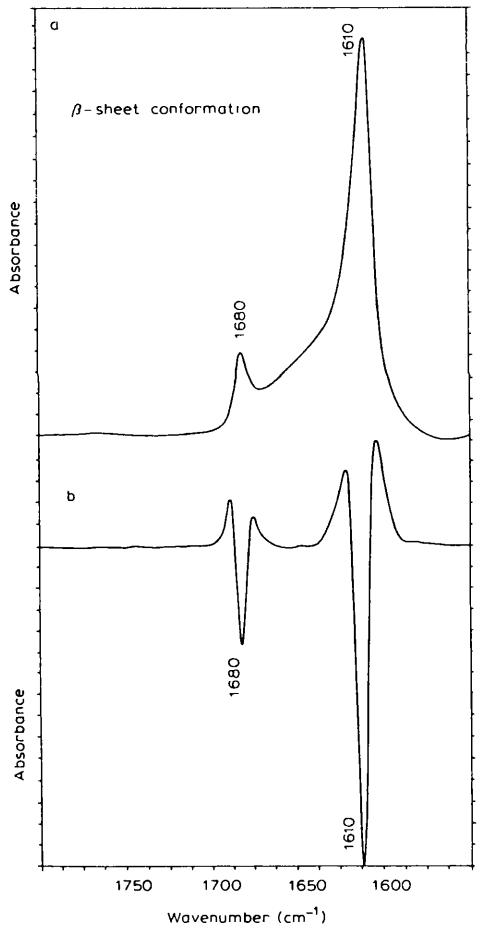

Fig. 4. FT-IR difference (a) and second derivative (b) spectra of polylysine (M_r = 24000) recorded at pD 11.9 after heating for 10 min at 60 °C.

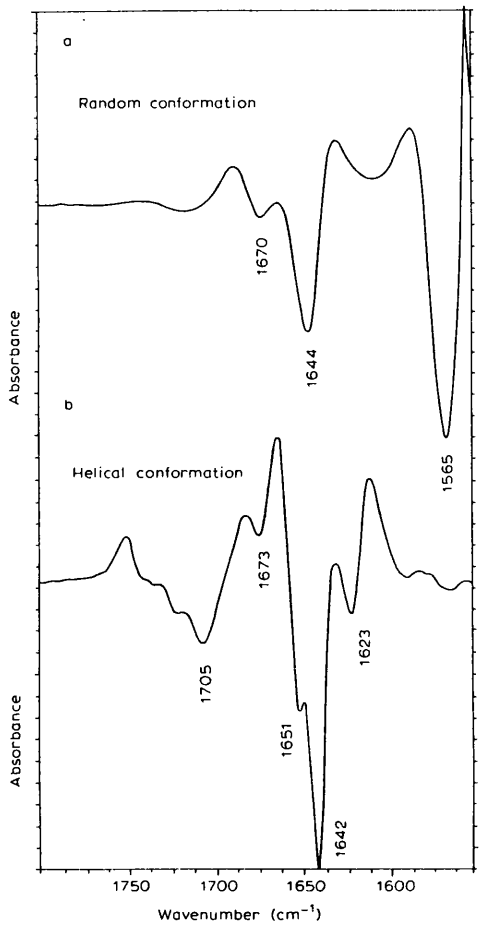

Fig. 5. FT-IR second derivative spectra of polyglutamate recorded at (a) pD 7 and (b) pD 4.3.

by regions of extended or 3_1 helices. However, we note that the spectrum of polyglycine II (which exists as a 3_1 helix) shows little similarity with spectra of random polylysine and polyglutamate (not shown).

Under conditions which are reported to favour the formation of a helical structure as deduced from CD spectroscopy [2–4], the FT-IR difference spectrum shows an amide I maximum at 1638 cm^{-1}. This amide I band maximum is at a lower frequency than the amide I band usually associated with proteins known from X-ray diffraction to contain α-helical structures (1650–1657 cm^{-1}). It may be suggested that this may reflect the presence of an unusual helical structure e.g. α_{II} or 3_{10} type structures. However, polypeptides which contain such unusual helical structures are found [7] to show significantly higher amide I maxima (1660–1663 cm^{-1}). The rather low band frequency observed with polylysine may reflect a higher degree of regularity in polylysine helices as compared to α-helical structures in proteins. Furthermore, the heterogeneous amino acid composition of a protein is likely to disrupt the inter- and

Biochimica et Biophysica Acta, 978 (1989) 305–312
Elsevier

BBA 74297

Fourier transform infrared spectroscopic studies on the secondary structure of the Ca^{2+}-ATPase of sarcoplasmic reticulum

J. Villalain [1], J.C. Gomez-Fernandez [1], M. Jackson [2] and D. Chapman [2]

[1] *Departamento de Bioquimica, Universidad de Murcia, Murcia (Spain) and* [2] *Department of Protein and Molecular Biology, Royal Free Hospital School of Medicine, London (U.K.)*

(Received 15 July 1988)

Key words: Fourier transform infrared spectroscopy; ATPase, Ca^{2+}-; Sarcoplasmic reticulum; Secondary structure; (Rabbit)

Fourier transform infrared spectroscopy has been applied to the study of the secondary structure of the Ca^{2+}-ATPase of sarcoplasmic reticulum. An attempt is made to quantitatively assess the various secondary structures present. Values of 45% α-helix, 32% β-sheet and 23% turns were obtained. A comparison is made of these results and those obtained using other techniques such as CD and Raman spectroscopy. The various assumptions inherent in the present procedure are discussed. The effect of various ligands, e.g. Ca^{2+}, vanadate, ATP and phosphate, upon the structure were investigated. Upon binding these ligands no marked spectral changes were observed.

Introduction

The Ca^{2+}-transporting ATPase of sarcoplasmic reticulum (EC 3.6.1.38) is one of the best characterized membrane ion transport systems. This enzyme catalyzes the active transport of two moles of Ca^{2+} ions per mole of ATP hydrolyzed (see Ref. 1 for a review on this system).

The primary structure of this protein has been recently deduced from its cDNA sequence and from this data predictions of its secondary structure have been made [2,3]. It has been deduced from electron microscopy studies [4] and from X-ray and neutron diffraction data [5,6] that about 40% of the protein volume lies inside the lipid bilayer whilst the remainder of the protein lies on the outside of the lipid bilayer on the cytoplasmic surface. Combining all of these results [3] the picture which emerges is that the Ca^{2+}-ATPase consists of a major globular part in the cytolasm formed by three domains of β-structure, where these domains are linked between them and to the membrane by α-helical and random elements. The portion of the protein situated inside the membrane is considered to be predominantly α-helical in character.

During the ATP-dependent Ca^{2+} transport cycle, the Ca^{2+}-ATPase undergoes several conformational transitions, characterized by different affinities for Ca^{2+}, ATP and other ligands [1]. During this cycle the calcium-enzyme complex is destabilized by enzyme phosphorylation at the catalytic site [7,1]. These conformational transitions are to be expected for vectorial transport of Ca^{2+}. To attempt to follow such structural changes in the protein it is necessary to use physical techniques that can give information on the spatial organization of this protein. For example, the secondary structure of the Ca^{2+}-ATPase has been probed by spectroscopic techniques, including circular dichroism [8–10] and Raman [11,12] and Fourier transform infrared spectroscopy [13–18]. From the bands in the Amide I region it is possible to detect the presence of α-helical, β-sheet and random coil structures. Application of these and other techniques to the study of the structural implications of ligand binding to the Ca^{2+}-ATPase have however to date resulted in a body of contradictory reports. Thus, no change in protein secondary structure is detected by circular dichroism [9,10]. However a recent FTIR study is reported to show a significant increase in the spectral contribution associated with the α-helical structures [18], whilst laser Raman spectroscopy is reported to show a slight decrease in α-helical conformation [11]. In some of these studies different preparations were used (i.e. some authors have examined sarcoplasmic reticulum membranes [18] whilst others have studied purified Ca^{2+}-ATPase [9]) and this may partly explain the confusion.

Abbreviations: S/N ratio, signal-to-noise ratio; FTIR, Fourier transform infrared spectroscopy; CD, circular dichroism.

Correspondence: D. Chapman, Department of Protein and Molecular Biology, Royal Free Hospital School of Medicine, Rowland Hill Street, London NW3 2PF, U.K.

It is apparent that clarification of the structural basis of Ca^{2+} translocation is required. We have therefore undertaken a study of the possible conformational changes in the secondary structure of the Ca^{2+}-ATPase in the presence and absence of a number of ligands, such as Ca^{2+}, vanadate, ATP and phosphate using FTIR spectroscopy. We use established curve fitting procedures to quantify the secondary structure of the protein. We discuss the problems which arise in the application of such procedures.

Experimental Procedures

Materials

Deuterium oxide (99.8%), ATP and phospho*enol*-pyruvate were obtained from Sigma, UK, and lactate dehydrogenase and pyruvate kinase from Boehringer. All other chemicals used throughout this work were analytical grade also from Sigma.

Preparation of purified Ca^{2+}-ATPase for FTIR measurements

Sarcoplasmic reticulum was prepared from rabbit back and leg white muscles according to the method of Nakamura et al. [19]. Ca^{2+}-ATPase was purified from these membranes by the method of Warren et al. [20] using 0.5 mg of sodium cholate per mg of protein (purified ATPase in H_2O) and procedure 2 of Meissner et al. [21] using 0.2 mg of sodium cholate per mg of protein (purified ATPase in ^2H_2O). Protein was estimated by the method of Lowry et al. [22] as modified by Wang and Smith [23], and Larson et al. [24] using bovine serum albumin as standard or from the ATPase molar absorption [8].

Preparations of purified ATPase were stored before use at $-40\,^\circ C$ in 50 mM sucrose, 10 mM Tris-maleate (pH 7.0) at a protein concentration of 25–50 mg/ml. Within four days of purification and before measurements, the preparations were thawed, centrifuged and the pellet resuspended in buffer containing 0.1 M KCl, 10 mM imidazole, 1 mM EGTA, 1 mM $MgCl_2$ (pH 7.4), either in H_2O or in ^2H_2O. This last step was repeated once more, obtaining a final protein concentration of 20 mg/ml. Before FTIR measurements were made, concentrated stock solutions of $CaCl_2$, Na_3VO_4, ATP or Na_2HPO_4, either in H_2O or ^2H_2O buffer were added to the purified Ca^{2+}-ATPase solutions giving final concentrations of 8 μM and 0.1 mM free Ca^{2+}, 5 mM vanadate, 10 μM ATP, 2 mM ATP and 5 mM phosphate. The concentration of free Ca^{2+} was calculated using a computer program that takes into account the concentration of the different molecules in solution [25].

ATPase activity was assayed at $25\,^\circ C$ with an ATP regenerating system essentially as described by Gomez-Fernandez et al. [26]. All samples gave an activity between 2 and 3 mmol ATP/mg of protein per min.

FTIR spectroscopy

Infrared spectra of purified ATPase suspensions in ^2H_2O were recorded on a Nicolet MX-1 FT-IR spectrometer assisted by a Nicolet 1200S data station and in H_2O with a Perkin-Elmer 1750 FTIR spectrometer assisted by a Perkin-Elmer 7300 data station. Samples were examined in a Beckman FH-01 CFT thermostated cell equipped with CaF_2 windows separated by a 25 μm Teflon spacer for samples in ^2H_2O and 6 μm tin spacer for samples in H_2O. The spectrometers were continuously purged with dry air to eliminate water vapour absorptions from the spectral region of interest. Either 216 scans for ATPase in ^2H_2O or 200 scans for ATPase in H_2O were recorded at $20\,^\circ C$, 2 cm^{-1} resolution and signal averaged. For the ATPase in H_2O a sample shuttle was used to record spectra ratioed against the background over the scanning period. Buffer spectra, either in H_2O or in ^2H_2O, were recorded under the same temperature and scanning conditions as the corresponding protein spectra. Each sample was equilibrated at the chosen temperature and conditions for at least 10 min before data aquisition. Subtracted spectra were digitized (0.9645 cm^{-1} and 1 cm^{-1} data point increment for the Nicolet and Perkin-Elmer spectrometers, respectively) and transferred to an Olivetti M-24 computer were all data analysis was made. Overlapping infrared bands were resolved by Fourier deconvolution and Fourier derivation [27] and band-fitting analysis was performed using established procedures [28,29].

Results

Infrared spectra of Ca^{2+}-ATPase in H_2O and ^2H_2O media

The most useful band in the infrared spectra of proteins for structural analysis is the Amide I band. This band, however, usually has a very broad band contour. This is because it consists of several overlapping components which are assigned to specific secondary structures, such as α-helix, β-sheet, turns, non-ordered segments. Bands corresponding to amino acid side chains also appear. The Amide I and Amide II regions of the infrared spectra of purified ATPase in H_2O and ^2H_2O buffer are shown in Figs. 1A and 1D, respectively. Due to the hydrogen-deuterium exchange of the amide groups, the maximum of the Amide I band shifts from 1655 cm^{-1} in H_2O to 1648 cm^{-1} in ^2H_2O and the Amide II band shifts from 1547 cm^{-1} in H_2O to 1460 cm^{-1} in ^2H_2O. The region from 1600 to 1520 cm^{-1} in ^2H_2O contains residual bands due to slowly exchanging amide hydrogens.

Due to the large intrinsic widths of the individual components present they cannot be resolved by increasing instrumental resolution. For this it is necessary to

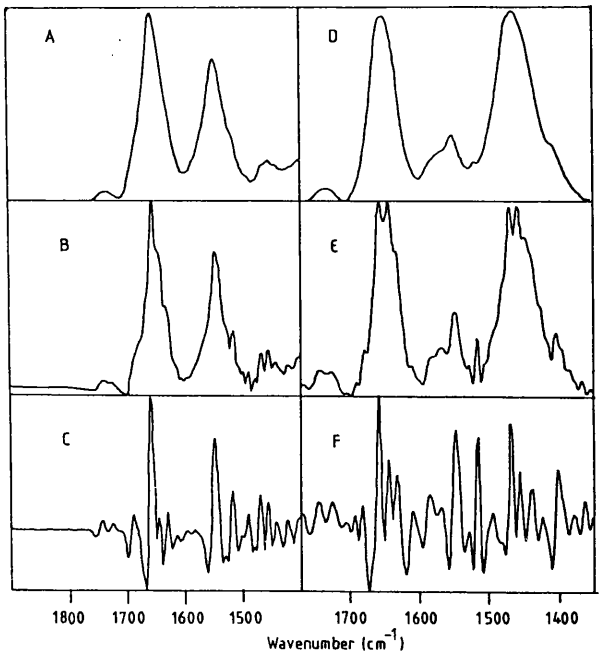

Fig. 1. Amide I and Amide II regions of the infrared spectra of the purified Ca^{2+}-ATPase from sarcoplasmic reticulum in H_2O buffer (A, B and C) and ^2H_2O buffer (D, E and F). (A, D) Original spectra, (B, E) Fourier deconvolved spectra (90% Lorentzian bandshape, resolution enhancement factor of 2.1 and bandwidth of 15 cm^{-1}), and (C, F) Fourier derivative spectra (power of 3 and breakpoint of 0.25). See text for more details. Redrawn from originals.

rely upon application of several qualitative and quantitative methods which recently have been developed. The qualitative computational methods which have been recently introduced for band narrowing are Fourier deconvolution and Fourier derivation (Refs. 27, 30 and references therein). These methods, given the correct input parameters and working on spectra of good resolution and signal-to-noise ratio (S/N ratio), provide the number and frequencies of the component bands which form the original band contour.

Fourier deconvolution is an iterative procedure controlled by three adjustable parameters, i.e., band-width, resolution enhancement factor and bandshape (Lorentzian, Gaussian or mixed), whereas Fourier derivation is controlled by one adjustable parameter, the breakpoint, which controls the resolution enhancement. The limits of the resolution enhancement factor are determined by the S/N ratio, resolution of the spectrometer and the lineshape (the resolution enhancement factor is always higher for Lorentzian bandshapes than for Gaussian bandshapes).

In order to choose the best parameters for Fourier deconvolution and Fourier derivation we monitored the S/N ratio of the 1900–1800 cm^{-1} region of the spectrum which is free of any absorption (see for example Fig. 1A). For Fourier deconvolution we have used 90% Lorentzian/10% Gaussian[30] bandwidth of 15 cm^{-1} and a resolution enhancement factor of 2.1, which gives a final S/N ratio of 150 and minimal negative lobes (see Figs. 1B and 1E), whereas four Fourier derivation we have used a power of 3 [27] and a breakpoint of 0.25, which corresponds to a smoothed fourth derivative, giving a final S/N ratio of 110 (Figs. 1C and 1F). Much care has to be taken in the use of these procedures. It is not possible to rely on peak heights of the enhanced spectra as a measure of the relative proportion of protein secondary structure as bandshapes can be severely distorted depending on the parameters used for the band-narrowing process as well as upon the bandwidths of the component bands.

Figs. 1 and 2 show the result of Fourier derivation and deconvolution carried out on the spectra of the Ca^{2+}-ATPase in H_2O and ^2H_2O. The component bands of the Amide I band can be attributed, in accordance with the classical correlations in the literature, to the different types of secondary structures present. The major components in the Amide I region of the purified Ca^{2+}-ATPase appear at 1657 and 1646 cm^{-1}. The band at 1656 cm^{-1} in H_2O can be assigned to α-helical segments of protein. The band at 1646 cm^{-1} has previously been assigned to random structures [31]. However, no shift is seen in the frequency of this band upon deuteration. We therefore suggest that this band may be attributed to α-helices as suggested by Lee et al. [15]. Two other bands which appear at 1667 and 1634 cm^{-1}, have been assigned to turns and β-sheet secondary structure, respectively. All assingments made in this work are taken from Refs. 31–33. The simultaneous appearance of two bands, a relatively strong band at 1630 cm^{-1} and a weaker band at 1675 cm^{-1}, are often assigned to antiparallel β-sheet structures. Recent studies [34] however suggest that it is not possible to distinguish between parallel and antiparallel β-sheets. We have therefore assigned the bands which appear at 1679 and 1634 cm^{-1} to β-sheet structures without further definition. The remaining bands are weak ones which have been assigned to turns (band at 1689 cm^{-1}), β-structure (band at 1623 cm^{-1}) and amino acid side chains (band at 1613 cm^{-1}). The band appearing at 1657 cm^{-1} has been assigned to α-helix. However, the reduction in the frequency of the Amide I maximum upon deuteration suggests that random structures are also absorbing in this region in H_2O.

Search for ligand-induced conformational changes in the Ca^{2+}-ATPase

In order to detect conformational changes in the Ca^{2+}-ATPase, spectra were taken first in the presence of 1 mM EGTA. It is assumed that as no free Ca^{2+} is left in this case, the protein will be present in the so called E_1 conformation [35]. Other additions were 8 μM and 0.1 mM free Ca^{2+}, so that the high affinity sites of

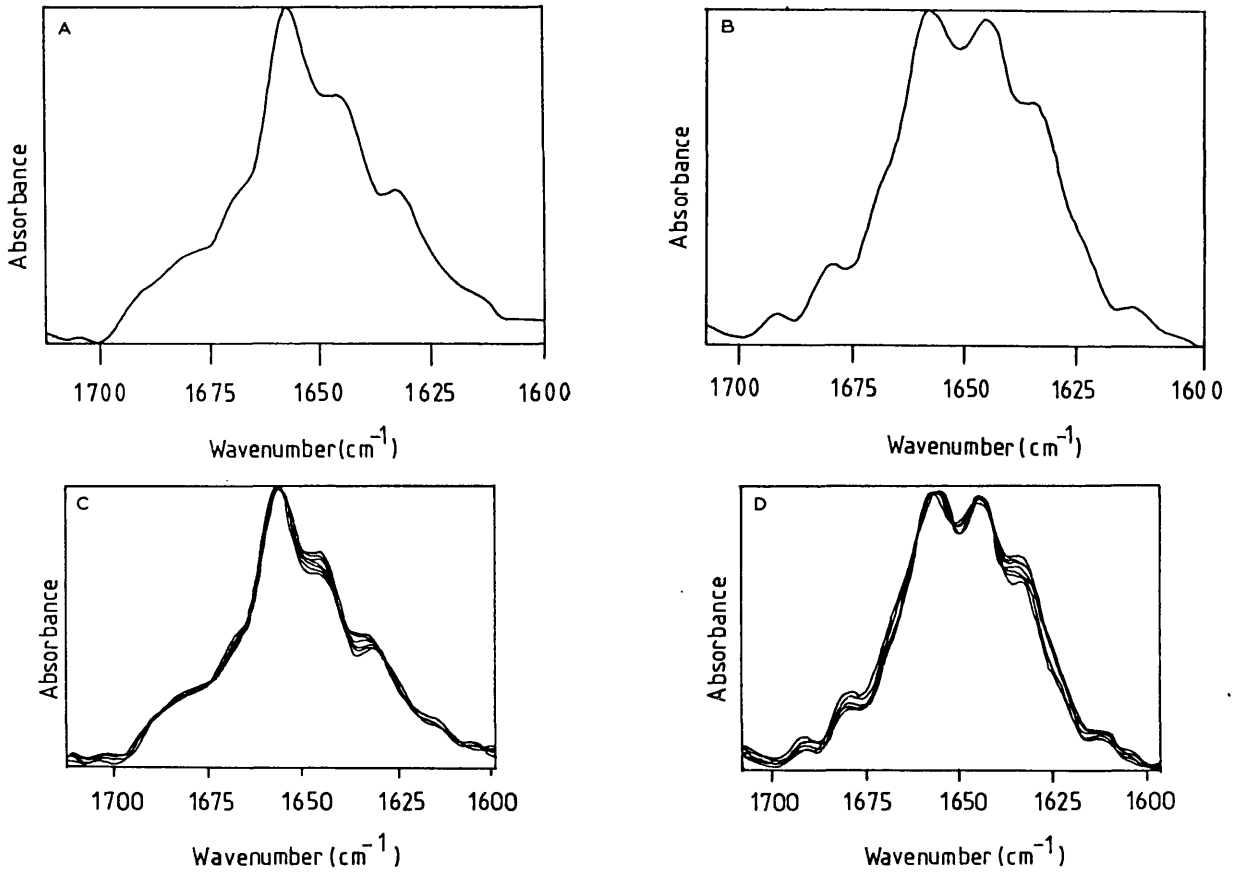

Fig. 2. Fourier deconvolved spectra (90% lorentzian band shape, resolution enhancement factor of 2.1 and bandwidth of 15 cm^{-1}) of the purified Ca^{2+}-ATPase in (A) H_2O buffer containing 1 mM EGTA (B) ^2H_2O buffer containing 1 mM EGTA (C) deconvolved spectra of the Ca^{2+}-ATPase in each of the reaction mixtures (in H_2O) superimposed (D) deconvolved spectra of the Ca^{2+}-ATPase in each of the reaction mixtures (in ^2H_2O) superimposed (see text for more details). Redrawn from originals.

Ca^{2+} will be then occupied and the enzyme will be in the E_1-Ca conformation [35]. Vanadate and inorganic phosphate, which in a calcium-free medium stabilize the E_2 conformation, giving the E_2-P and E_2-V forms, respectively [36,37], were also studied. The addition of ATP was also studied at low (10 μM) and high (2 mM) concentrations. It has been proposed that ATP may bind to the enzyme with different affinities in the absence of free Ca^{2+}: low (μM) and high (mM) affinities [38]. The addition of ATP is therefore to ascertain whether the binding of ATP to the enzyme at different concentrations induces any detectable conformational change.

Fig. 2C shows the superimposed deconvolved spectrum of the Amide I region of samples of the Ca^{2+}-ATPase in H_2O buffer to which the various ligands were added. It is evident that only very minor changes in frequency and intensity occur. Similar results were obtained when the experiments were performed in ^2H_2O media (Fig. 2D). Comparisons were also made using Fourier derivation of the spectra, both in ^2H_2O and H_2O, (spectra not shown). No significant changes were detected in the presence of the various ligands.

Quantification of the secondary structure of the Ca^{2+}-ATPase

It is well known that infrared bands are close to Lorentzian [30] at least for simple molecules, so in order to obtain meaningful results either by Fourier deconvolution or band-fitting analysis Lorentzian bandshapes or bandshapes with a small percentage of Gaussian contribution are generally used. Throughout this work Fourier deconvolution with 90% Lorentzian bandshapes has been applied, The results of such an analysis is illustrated in Fig. 2A. The best band-fitting analysis which can be made with the information obtained from the deconvolution shown in Fig. 2A can be seen in Fig. 3A. Ideally the band-shapes used for the band-fitting analysis should be the same as those used for the Fourier deconvolution. It can be seen however from Fig. 3A that the band-fitting obtained is very poor (partly due to the fact that Lorentzian bandshapes have

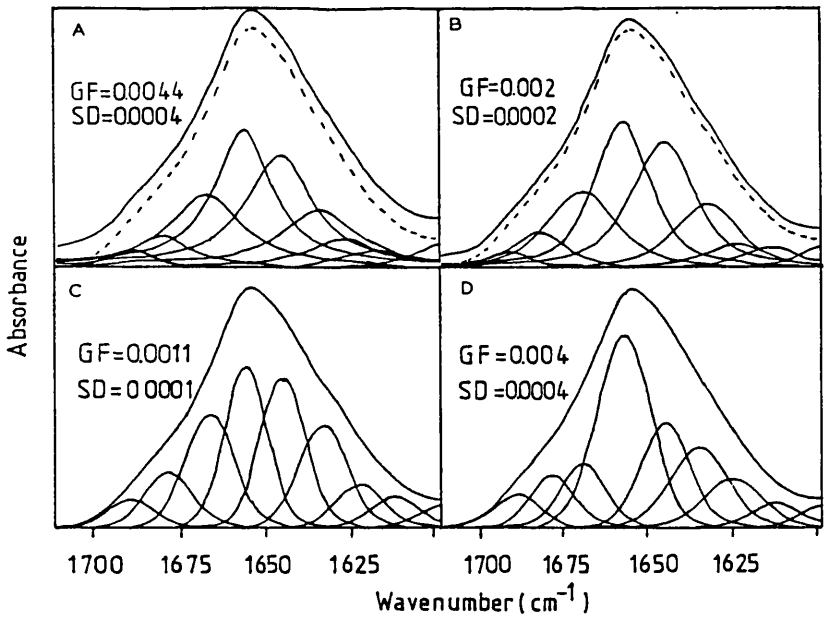

Fig. 3. Band-fitting of the purified Ca^{2+}-ATPase in the presence of 1 mM EGTA, assuming (A) 90% Lorentzian bandshape (B) 50% Lorentzian/50% Gaussian bandshapes (C) 100% Gaussian band shape (D) 100% Gaussian bandshape, with the band at 1657 cm^{-1} arranged to be 32% in area. Solid lines are synthetic curves generated from the individual bands, broken lines are the original spectra (indistinguishable in C and D). Redrawn from originals. GF, goodness of fit; SD, standard deviation of the fit.

large wings). Increasing the Gaussian contribution to the band shapes greatly improves the band-fitting results. This is clearly seen in Fig. 3B, assuming the bands have 50% Gaussian character. In fact the best results are obtained if the bands are assumed to be 100% Gaussian (Fig. 3C). It can be seen from Fig. 3C that a very good curve fit has been obtained, with minimal differences between the experimental and the synthetic spectra. The use of 100% Gaussian shaped bands for band-fitting is a procedure used by a number of authors to fit the 100% Lorentzian deconvolution of the original spectrum [31,33,34]. Some authors do not mention the bandshape used for making the band-fitting analysis of the original spectrum [39–42].

It should be stressed that a good fit cannot be judged by visual inspection. Fig. 3D shows the result of a band fitting in which the area under one of the component curves (centered at 1657 cm^{-1}) was arranged to increase from 23% to 32%. Visually, the fit appears as good as that obtained in Fig. 3C. However, calculation of the goodness of fit (chi^2) reveals that the fit is actually much worse, and is in fact similar to that obtained assuming 10% Gausian bands.

The component bands derived from the band fitting analysis are shown in Fig. 3C. Referring to this figure, eight components can be seen and the percentage of each one over the total area (excluding the amino acid side chain band) are shown in Table I. In order to assess the relative contribution of each type of secondary structure present it is assumed that all of the component bands have the same molar absorption coefficient.

Similar band-fittings were also made for the purified Ca^{2+}-ATPase in the presence of the various ligands, with the protein in H_2O and in ^2H_2O (only the E_1 conformation), always beginning with the deconvolved spectrum as shown in Fig. 2. In all the cases the best band-fitting was always obtained using 100% Gaussian bandshapes and the same number of bands were identified in each experiment. In all cases the frequencies of the various components did not change by more than 0.5 cm^{-1}. Some band frequency changes were observed in the presence of ATP but no significant changes in area occurred. The meaning of this changes in frequency is not clear. Nevertheless, if the addition of ATP causes a conformational change in the protein, it is not a major one.

TABLE I

Band-fitting analysis of purified Ca^{2+}-ATPase in 1 mM EGTA

H_2O media		^2H_2O media		Assignment
frequency (cm^{-1})	%	frequency (cm^{-1})	%	
1689.5	4.1	1692.5	0.7	turns
1678.9	8.8	1679.4	7.4	β-sheet
1667.3	18.6	1666.8	14.9	turns
1656.7	23.1	1656.3	25.6	α-helices
1645.7	22.3	1645.1	23.8	α-helices
1633.8	16.3	1634.2	19.7	β-sheet
1623.4	6.8	1623.7	7.9	β-turns

The area contributed to the band envelope by each individual component in the presence of each ligand does not change by more than 1%. These results indicate that there are no appreciable changes in the protein secondary structure upon ligand binding.

Discussion

Quantitative estimation of the secondary structure of the Ca^{2+}-ATPase

During the past two years a number of studies have been reported which analyse quantitatively the secondary structure of various proteins using FTIR spectroscopy [31,33,34,39–44]. The procedures used are based on band-narrowing techniques such as Fourier deconvolution and Fourier derivation techniques which identify the number and position of component bands. This information is then used as the input parameters for band-fitting analysis of the original or, in some cases, the deconvolved spectrum. The integrated intensities obtained for the different fitted bands are then related to the relative population of the conformational structures represented by these bands (α-helix, β-sheet, etc.). For water soluble proteins agreement with X-ray crystallography data has been good with predictions agreeing to within 4% (see Ref. 31 for a brief review). We will compare results obtained using this method for our membrane protein with results obtained using other techniques.

The secondary structures present in the Ca^{2+}-ATPase has been estimated using different approaches (see Table II). On the basis of the aminoacid sequence, it has been predicted that the Ca^{2+}-ATPase consist of an intramembranous, primarily helical domain, and several cytoplasmic domains composed of α-helical, β-sheet, β-turn and random elements [2,3]. In accordance with these predictions, the α-helix content will amount to 52%, β-sheet, 12%, and β-turns and random elements, 36%. Circular dichroism studies of sarcoplasmic reticulum vesicles give the following composition: 46% α-helix, 8% β-sheet, 13% β-turn and 33% random coil [10]. Raman spectroscopic studies made with light sarcoplasmic reticulum and reconstituted ATPase also agreed with the predominantly α-helical structure of the protein: 50% α-helix, 21% β-sheet, 17% β-turns and 12% random elements [12]. It should be noted that Williams et al. use a completely different way of band-fitting to that normally used for vibrational infrared spectroscopy and their Raman spectra had a very poor S/N ratio.

TABLE II

Quantitative estimation of secondary structure

	CD [a]	AA [b]	Raman [c]	FTIR [d]
α-Helix	46%	52%	50%	45%
β-Sheet	8%	12%	21%	32%
turns	13%		17%	23%
Random	33%		11%	

[a] From Ref. 10.
[b] From Ref. 3, amino acid analysis (AA).
[c] From Ref. 12.
[d] Present communication.

Our results (Table II), show the percentage of α-helical structures of the purified Ca^{2+}-ATPase, assuming 100% Gaussian shaped bands. There is some ambiguity in the assignment of the bands. If we assign the band at 1646 cm^{-1} to random structures the α-helical content would be only 23% of the secondary structure. This is much lower than the other estimations.

Furthermore, when we deliberately arrange the band fitting so as to increase the relative importance of the band centered at 1657 cm^{-1} (assigned to α-helix), so as to increase the α-helix content the resultant curve fitting becomes inadequate. See for example Fig. 3D, where the band at 1656 cm^{-1} accounts for 32% of the total area. If we assign the band at 1646 cm^{-1} also to α-helical structures the α-helical content becomes 45%. In deconvolved and fourth derivative spectra of the protein in ^2H_2O we see no shift in this band, which suggests that the more common assignment of this band to random structures is incorrect. We assign this band to α-helices as previously suggested [15]. The amount of β-sheet predicted from our study amounts to 32% of the secondary structure. This is more than has been calculated by other procedures (see Table II). Finally, β-turns, account for 23% of the secondary structure.

The application of FTIR spectroscopy to the quantitative analysis of the secondary structure of membrane proteins must be approached with caution. The technique used at the present time requires a number of assumptions. These are (a) the band assignments are based primarily upon studies of water soluble proteins, (b) application of curve fitting and deconvolution require assumption of a band shape, e.g. Gaussian, Lorentzian or mixed, (c) it is assumed that all component bands have the same shape and (d) the assumption that all protein secondary structures have equal molar absortivities.

Other techniques of course have their limitations. Circular dichroism, for example, is known to be seriously limited for the study of membrane proteins due to light scattering effects. Raman spectroscopy is limited as the spectra obtained normally have poor S/N ratio, which makes accurate resolution of individual components within the Amide I band envelope impossible. The method used for the band-fitting analysis of Raman data is also somewhat limited. The band-fitting analysis which is currently used fits the spectrum by comparison with the composite data of a number of water-soluble proteins. Application of this technique to membrane proteins assumes that the main band frequencies are the same for water-soluble and membrane

proteins. The FTIR and Raman spectra of bacteriorhodopsin, however, show that at least for this protein the main α-helical band is anomalously high compared to that which is observed for the water-soluble proteins. The general application of water-soluble protein data to membrane proteins is therefore unreliable. Finally, predictions made on the bases of amino acid sequence can be taken only as rough approximations.

Retention of secondary structure between enzymatic states of the Ca^{2+}-ATPase

From our results obtained with purified Ca^{2+}-ATPase, it is apparent that the transitions involved in the enzyme mechanism are not accompanied by major reorganizations of the protein secondary structure. We have considered seven different enzyme states by manipulations of the reaction mixture. The ligand-free enzyme which is obtained here in the presence of 1 mM EGTA, is taken as the reference state. This form is proposed to undergo a structural rearrangement upon cooperative binding of calcium to high-affinity transport sites [45]. This rearrangement has been observed using techniques such as tryptophan fluorescence [46] and electron spin resonance (ESR) spectroscopy [47]. Another transition in the enzyme structure is proposed upon formation of the phosphoenzyme by addition of P_i deduced from low-angle X-ray diffraction [6] or TNP-ATP fluorescence [48]. Vanadate will produce an enzyme-vanadate complex, similar to the phosphoenzyme, with formation of two-dimensional crystals [49]. The binding of ATP at different concentrations to the enzyme depleted of calcium may also produce a conformational change upon binding to the nucleotide binding site, as seen by tryptophan fluorescence [50].

Our studies show that it is not possible, using FTIR spectroscopy, to detect any major change in the secondary structure of the purified ATPase in the presence of various ligands (see Fig. 2). This conclusion agrees with results obtained from circular dichroism using sarcoplasmic reticulum preparations applied to Ca^{2+} binding or formation of vanadate complex [10]. They also agree with circular dichroism experiments performed on the purified Ca^{2+}-ATPase, with respect to calcium-binding and phosphoenzyme formation [9]. Our results differ from previous conclusions obtained by FTIR spectroscoy [18]. However, Arrondo et al. studied sarcoplasmic reticulum vesicles where other proteins present may also contribute to the IR spectrum, and we have studied the purified Ca^{2+}-ATPase. Our band fitting analysis shows that it is possible to measure frequency changes in the presence of ATP (but not in the presence of calcium, vanadate or phosphate) in those bands which we assign to β-structure and aminoacid side chains.

It has been predicted from the amino acid sequence [3] that the nucleotide binding, phosphorylation and transduction domains of the Ca^{2+}-ATPase are composed of predominantly β-sheet secondary structure and are separated from the calcium binding domain (α-helix). Since the calcium and phosphorylation sites of the enzyme are located in different regions of the enzyme and separated by about 40 Å [51], a coordinated conformational change of the Ca^{2+}-ATPase must take place during the catalytic cycle, in order to facilitate the reciprocal influence of calcium binding and phosphorylation [1]. If significant secondary structure changes are not taking place in these domains during this process (as shown here) it must be assumed that twisting and reorientation of polypeptide segments are responsible for the protein conformational changes which accompany the catalytic cycle.

Acknowledgements

This work was supported by CAICYT (Spain), grant No. 0822/84 (to J.C.G.-F.) NATO grant No. 8610712 (to J.C.G.-F. and D.C.) and the Wellcome Trust (M.J.) We also thank Dr. Hector L. Casal for providing the computer programs used in this work as well as his many useful suggestions.

References

1 Inesi, G. (1985) Annu. Rev. Physiol. 47, 573–601.
2 MacLennan, D.H., Brandl, C.J., Korczak, B. and Green, N.M. (1985) Nature 316, 696–700.
3 Brandl, C.J., Green, N.M., Korczak, B. and MacLennan, D.H. (1986) Cell 44, 597–607.
4 Taylor, K.A., Dux, L. and Martonosi, A. (1986) J. Mol. Biol. 187, 417–427.
5 Herbette, L., Defoor, P., Fleischer, S., Pascolini, D., Scarpa, A. and Blasie, J.K. (1985) Biochim. Biophys. Acta 817, 103–122.
6 Blasie, J.K., Herbette, L., Pascolini, D., Skita, V., Pierce, D. and Scarpa, A. (1985) Biophys. J. 48, 9–18.
7 Jenks, W. (1980) Adv. Enzymol. 51, 75–106.
8 Hardwicke, P.M.D. and Green, N.M. (1974) Eur. J. Biochem. 42, 183–193.
9 Nakamoto, R.K. and Inesi, G. (1986) FEBS Lett. 194, 258–262.
10 Csermely, P., Katopis, C., Wallace, B.A. and Martonosi, A. (1987) Biochem. J. 241, 663–669.
11 Lippert, J.L., Lindsay, R.M. and Schultz, R. (1981) J. Biol. Chem. 256, 12411–12416.
12 Williams, R.W., McIntyre, J.D., Gaber, B.P. and Fleischer, S. (1986) J. Biol. Chem. 261, 14520–14524.
13 Cortijo, M., Alonso, A., Gomez-Fernandez, J.C. and Chapman, D. (1982) J. Mol. Biol. 157, 597–618.
14 Mendelsohn, R., Anderle, G., Jaworsky, M., Mantsch, H.H. and Dluhy, R.A. (1984) Biochim. Biophys. Acta 775, 215–224.
15 Lee, D.C., Hayward, J.A., Restall, C.J. and Chapman, D. (1985) Biochemistry 24, 4364–4373.
16 Arrondo, J.L.R., Urbaneja, M.A., Goni, F.M., Macarulla, J.M. and Sarzala, G. (1985) Biochem. Biophys. Res. Commun. 128, 1159–1163.
17 Jaworsky, M. (1985) Biochemistry 24, 3422–3428.
18 Arrondo, J.L.R., Mantsch, H.H., Mullner, N., Pikula, S. and Martonosi, A. (1987) J. Biol. Chem. 262, 9037–9043.

19 Nakamura, H., Jilka, R.L., Boland, R. and Martonosi, A. (1976) J. Biol. Chem. 251, 5414–5423.
20 Warren, G.B., Toon, P.A., Birdstall, N.J.M., Lee, A.G. and Metcalfe, J.C. (1974) Proc. Natl. Acad. Sci. USA 71, 622–626.
21 Meissner, G., Cooner, G. and Fleischer, S. (1973) Biochim. Biophys. Acta 298, 246–269.
22 Lowry, O.H., Rosebrough, N.J., Farr, A.L. and Randall, R.J. (1951) J. Biol. Chem. 193, 265–275.
23 Wang, C.-S. and Smith, R.L. (1975) Anal. Biochem. 63, 414–417.
24 Larson, E., Howlett, B. and Jagendorf, A. (1986) Anal. Biochem. 155, 243–248.
25 Fabiato, A. and Fabiato, F. (1979) J. Physiol. (Paris) 75, 463–505.
26 Gomez-Fernandez, J.C., Goni, F.M., Bach, D., Restall, C.J. and Chapman, D. (1980) Biochim. Biophys. Acta 598, 502–516.
27 Moffatt, D.J., Kauppinen, J.C., Cameron, D.G., Mantsch, H.H. and Jones, R.N. (1986) Computer Programs for Infrared Spectrophotometry, N.R.C.C. Bulletin No. 18, Ottawa, Canada.
28 Fraser, R.D.B. and Suzuki, E. (1966) Anal. Chem. 38, 1770–1773.
29 Fraser, R.D.B. and Suzuki, E. (1969) Anal. Chem. 41, 37–39.
30 Cameron, D.G. and Moffatt, D.J. (1984) J. Testing Evaluation 12, 78–85.
31 Susi, H. and Byler, D.M. (1986) Methods Enzymol. 130, 290–311.
32 Chirgadze, Y.N., Fedorov, O.V. and Trushina, N.P. (1975) Biopolymers 14, 679–694.
33 Byler, D.M. and Susi, H. (1986) Biopolymers 25, 469–487.
34 Susi, H. and Byler, D.M. (1987) Arch. Biochem. Biophys. 258, 465–469.
35 De Meis, L. and Vianna, V. (1979) Annu. Rev. Biochem. 48, 275–292.
36 Masuda, H. and de Meis, L. (1973) Biochemistry 12, 4581–4585.
37 Pick, U. and Karlish, J.D. (1982) J. Biol. Chem. 257, 6120–6126.
38 Dupont, Y. (1977) Eur. J. Biochem. 72, 185–190.
39 Surewicz, W.K., Moscarello, M.A. and Mantsch, H.H. (1987) Biochemistry 26, 3881–3886.
40 Surewicz, W.K., Mantsch, H.H., Stahl, G.L. and Epand, R.M. (1987) Proc. Natl. Acad. Sci. USA 84, 7028–7030.
41 Surewicz, W.K., Moscarello, M.A. and Mantsch, H.H. (1987) J. Biol. Chem. 262, 8598–8602.
42 Surewicz, W.K., Szabo, A.G. and Mantsch, H.H. (1987) Eur. J. Biochem. 167, 519–523.
43 Yang, P.W., Mantsch, H.H., Arrondo, J.L.R., Saint-Girons, I., Guillon, Y., Cohen, G.N. and Barzu, O. (1987) Biochemistry 26, 2706–2711.
44 Surewicz, W.K., Stepanik, T.M., Szabo, A.G. and Mantsch, H.H. (1988) J. Biol. Chem. 263, 786–790.
45 Inesi, G., Kurzmack, M., Coan, C. and Lewis, D. (1980) J. Biol. Chem. 255, 3025–3031.
46 Dupont, Y. (1976) Biochem. Biophys. Res. Commun. 71, 544–550.
47 Coan, C. and Inesi, G. (1977) J. Biol. Chem. 252, 3044–3049.
48 Watanabe, T. and Inesi, G. (1982) J. Biol. Chem. 257, 11510–11516.
49 Dux, L. and Martonosi, A. (1983) J. Biol. Chem. 258, 11903–11907.
50 Dupont, Y., Bennett, N. and Lacapere, J.J. (1982) Ann. N.Y. Acad. Sci. USA 402, 569–572.
51 Scott, T.C. (1985) J. Biol. Chem. 260, 14421–14423.